Exploring the non-equilibrium dynamics of kinetically constrained spin systems: Rydberg quantum simulation and artificial dissipation

Dissertation

der Mathematisch-Naturwissenschaftlichen Fakultät

der Eberhard Karls Universität Tübingen

zur Erlangung des Grades eines

Doktors der Naturwissenschaften

(Dr. rer. nat.)

vorgelegt von

Matteo Magoni

aus Alzano Lombardo (Italien)

Tübingen

2023

Gedruckt mit Genehmigung der Mathematisch-Naturwissenschaftlichen Fakultät der Eberhard Karls Universität Tübingen.

Tag der mündlichen Qualifikation: 17/07/2023

Dekan:	Prof. Dr. Thilo Stehle
1. Berichterstatter:	Prof. Dr. Igor Lesanovsky
2. Berichterstatter:	Prof. Dr. Christian Groß
3. Berichterstatter:	Prof. Dr. Hossein R. Sadeghpour

Abstract

This thesis discusses the non-equilibrium dynamics of one-dimensional quantum many-body systems. In particular, we investigate two distinct situations in which interesting dynamical properties arise, i.e., when the quantum evolution is subject to kinetic constraints or competes with an artificial dissipation through stochastic resets. Both topics have attracted considerable interest in the last decade, as they offer a playground to theoretically investigate the long-standing question of how isolated quantum systems evolve under non-equilibrium conditions. From the experimental point of view, the recent technological progress in the control and manipulation of ultracold atomic gases has led to new breakthroughs in the domains of quantum simulation and quantum computation. Key for the latter applications is the utilization of atomic Rydberg states in which atoms, trapped in optical tweezers, interact via state-dependent electrostatic dipolar forces. These strong interactions make Rydberg systems ideal for the realization of kinetic constraints, which cause a restriction of the connectivity between many-body states in the Hilbert space.

A prominent example of a kinetic constraint is the Rydberg blockade, in which an excited Rydberg atom prevents the surrounding atoms to be excited to the Rydberg state. This effect has been largely exploited to implement controlled gates and complex many-body dynamics. Much less explored is the opposite situation, called the facilitation (or anti-blockade) constraint, where the interactions shift the otherwise detuned laser in resonance. In this case only atoms at the correct distance to an already excited atom are resonantly driven by the laser, thereby creating an "avalanche" of excitations.

The first part of the thesis is devoted to the study of the facilitation dynamics in Rydberg chains. The facilitation constraint favours the dynamical creation of

contiguous Rydberg excitations. We find that the resulting Rydberg excitation "cluster" develops long-range interactions that cause the onset of Bloch oscillations, preventing the system from reaching an ergodic stationary state. Contrary to the blockade constraint, facilitation is more challenging to implement in current Rydberg quantum simulators. The reason for this difficulty is that facilitation is particularly affected by mechanical effects and position disorder. These two problems originate respectively from the mechanical forces that displace the atoms from their initial positions and the spreading of the atomic wave functions in the optical traps. The interplay between the electronic degrees of freedom and the vibrational ones leads to a coupling between the (internal) Rydberg dynamics and the (external) atomic motion. We find that such spin-phonon coupling inhibits the facilitation mechanism, suppressing the expansion of the excitation cluster. This vibronic interaction can be also exploited to explore molecular physics in Rydberg atom arrays. We show this by considering a system composed of three atoms trapped in optical tweezers that form an equilateral triangle. We find that the atomic vibrations in the traps break the electronic degeneracy and generate a structural Jahn-Teller distortion, paving the way towards the exploration of molecular physics at the exaggerated length scales typical of Rydberg systems.

The second part of the thesis investigates the effects of stochastic resetting on the stationary properties of quantum many-body spin systems. Stochastic resetting is a process that interrupts the dynamics of a system at random times and resets it to a certain state. Then the dynamics restarts again. This process leads very generally to a non-equilibrium stationary state. When the choice of the reset state is determined by the outcome of a measurement taken immediately before resetting, we find that resetting induces an emergent non-Markovian open dynamics, described by a generalized Lindblad equation. We also show that stochastic resetting can generate quantum correlation and collective behaviour even in a non-

interacting system, showing its potential for quantum sensing applications.

The structure of the thesis is as follows. In the first chapter we introduce the topics covered in the thesis and provide useful references for the reader. In the second chapter we review the physics of Rydberg systems, including their single-body properties and their interactions. We also explain how Rydberg quantum simulators are used for the implementation of kinetic constraints. In the third chapter we review the physics of stochastic resetting and the main mathematical techniques used in the thesis. In the fourth chapter we summarize the original results contained in the thesis. The fifth chapter is dedicated to the conclusions and an outlook on possible future research directions.

Zusammenfassung

Thema diese Dissertation ist die Untersuchung der Nichtgleichgewichtsdynamik eindimensionaler quantenmechanischer Vielteilchensysteme. Insbesondere studieren wir zwei verschiedene Situationen, in denen interessante dynamische Eigenschaften zutage treten. Dies sind auf der einen Seite quantenmechanische Systeme, die kinetischen Zwangsbedingungen unterliegen und, auf der anderen Seite, Systeme, in denen künstliche Dissipation durch stochastische Resets realisiert wird. Beide Szenarien haben in den letzten zehn Jahren erhebliches Interesse geweckt, da sie es erlauben zu untersuchen, wie isolierte quantenmechanische Systeme unter Nichtgleichgewichtsbedingungen evolvieren.

Aus experimenteller Sicht hat der jüngste technologische Fortschritt bei der Kontrolle und Manipulation von ultrakalten atomaren Gasen zu Durchbrüchen auf den Gebieten der Quantensimulation und Quantencomputing geführt. Eine Schlüsselrolle für diese Anwendungen spielt die Nutzung elektronisch hochangeregter Rydberg-Zustände, in denen Atome über zustandsabhängige elektrostatische dipolare Kräfte miteinander wechselwirken. Diese starken Wechselwirkungen machen Rydbergsysteme ideal zur Realisierung kinetischer Zwangsbedingungen, die eine Einschränkung der Konnektivität zwischen Vielteilchenzuständen im Hilbertraum bewirken.

Ein prominentes Beispiel für eine kinetische Zwangsbedingung ist die sogenannte Rydbergblockade, bei der ein angeregtes Rydberg-Atom verhindert, dass die es umgebenden Atome auch in den Rydbergzustand angeregt werden. Dieser Effekt wurde bisher weitgehend genutzt, um kontrollierte Gatter und komplexe Vielteilchendynamiken zu implementieren. Viel weniger erforscht ist die umgekehrte Situation, die als Facilitation (oder Anti-Blockade) bezeichnet wird. Hier schieben die Wechselwirkungen zwischen den Rydbergatomen einen verstimmten Laser erst in Resonanz. In diesem Fall werden nur Atome in der richtigen Entfernung von

bereits angeregten Atomen resonant durch den Laser angeregt und erzeugen dabei eine “Lawine” von Anregungen.

Der erste Teil der Arbeit widmet sich der Untersuchung der Facilitation-Dynamik in Rydbergketten. Die Facilitation-Zwangsbedingung begünstigt die dynamische Erzeugung zusammenhängender Rydberganregungen. Langreichweitige Anteile der Rydbergwechselwirkung innerhalb dieser Cluster verursachen das Auftreten sogenannter Bloch-Oszillationen und hindern damit das System daran, einen ergodischen stationären Zustand zu erreichen. Im Gegensatz zur Blockade-Zwangsbedingung ist die Implementierung von Facilitation in aktuellen Rydbergquantensimulatoren deutlich anspruchsvoller. Der Grund dafür liegt darin, dass Facilitation besonders von mechanischen Effekten und Positionsfluktuationen beeinflusst wird. Diese beiden Effekte entstehen einerseits durch mechanische Kräfte, die die Atome von ihren ursprünglichen Positionen verschieben, und andererseits durch die endliche Ausdehnung der atomaren Wellenfunktionen in den Atomfallen, aus denen Rydbergatome angeregt werden. Das Zusammenspiel zwischen den elektronischen Freiheitsgraden und den Vibrationsfreiheitsgraden der Atomfallen führt zu einer Kopplung zwischen der (inneren) Rydberg-Dynamik und der (äußeren) atomaren Bewegung. Diese sogenannte Spin-Phonon-Kopplung, bzw. vibronische Wechselwirkung, hemmt den Facilitationmechanismus und unterdrückt die Ausbreitung der Rydbergcluster.

Die vibronische Wechselwirkung kann auch dazu genutzt werden, Prozesse der Molekülphysik in Rydberggittern zu erforschen. Wir zeigen dies anhand eines Systems, das aus drei separat gefangenen Atomen besteht, die ein gleichseitiges Dreieck bilden. Dabei stellt sich heraus, dass die atomaren Schwingungen in den Fallen die elektronische Entartung aufheben und einen strukturellen Jahn-Teller-Effekt erzeugen, der den Weg zur Erforschung molekularer Prozesse auf den für

Rydbergsysteme typischen großen Längenmaßstäben ebnet.

Der zweite Teil der Arbeit untersucht die Auswirkungen stochastischer Resets auf die stationären Eigenschaften von quantenmechanischen Vielteilchenspinsystemen. Stochastisches Resetting ist ein Prozess, der die Dynamik eines Systems zu zufälligen Zeitpunkten unterbricht und auf einen bestimmten Zustand zurücksetzt. Anschließend startet die Dynamik erneut. Dieser Prozess führt im Allgemeinen auf einen stationäre Nichtgleichgewichtszustand. Wenn die Wahl des Reset-Zustands durch das Ergebnis einer unmittelbar vor dem Resetting durchgeführten Messung bestimmt wird, findet man, dass das Resetting eine emergente nicht-markovsche offene Dynamik erzeugt, die durch eine verallgemeinerte Lindblad-Gleichung beschrieben wird. Weiterhin zeigen wir, dass stochastisches Resetting selbst in einem nicht wechselwirkenden System Quantenkorrelationen und kollektives Verhalten erzeugen kann, was das Potenzial dieser künstlich erzeugten Dynamik für Anwendungen in der Quantensensorik zeigt.

Die Arbeit ist wie folgt aufgebaut. Im ersten Kapitel führen wir die in der Arbeit behandelten Themen ein und geben dem Leser nützliche Referenzen. Im zweiten Kapitel erläutern wir die Physik der Rydbergatome, einschließlich ihrer Einteilcheneigenschaften und ihrer Wechselwirkungen. Wir erklären auch, wie Rydbergquantensimulatoren zur Implementierung kinetischer Zwangsbedingungen verwendet werden können. Im dritten Kapitel geben wir einen Überblick über die Physik des stochastischen Resettings und die wichtigsten mathematischen Techniken, die in der Arbeit verwendet werden. Im vierten Kapitel fassen wir die in der Arbeit enthaltenen Forschungsergebnisse zusammen. Das fünfte Kapitel widmet sich den Schlussfolgerungen und einem Ausblick auf mögliche zukünftige Forschungsrichtungen.

List of publications and personal contribution

List of publications

1. M. Magoni, P. P. Mazza and I. Lesanovsky, *Emergent Bloch oscillations in a kinetically constrained Rydberg spin lattice*, Phys. Rev. Lett. **126**, 103002 (2021).

2. M. Magoni, P. P. Mazza and I. Lesanovsky, *Phonon dressing of a facilitated one-dimensional Rydberg lattice gas*, SciPost Phys. Core **5**, 041 (2022).

3. M. Magoni, R Joshi and I. Lesanovsky, *Rydberg tweezer molecules: Spin-phonon entanglement and Jahn-Teller effect*, arXiv:2303.08861 (2023).

4. G. Perfetto, F. Carollo, M. Magoni and I. Lesanovsky, *Designing nonequilibrium states of quantum matter through stochastic resetting*, Phys. Rev. B **104**, L180302 (2021).

5. M. Magoni, F. Carollo, G. Perfetto and I. Lesanovsky, *Emergent quantum correlations and collective behavior in noninteracting quantum systems subject to stochastic resetting*, Phys. Rev. A **106**, 052210 (2022).

Personal contribution of the candidate

No.	Author position	Scientific ideas (%)	Data generation (%)	Analysis and interpretation (%)	Paper writing (%)	Status
1	1	50	100	70	80	Published
2	1	50	90	70	80	Published
3	1	50	80	70	70	Preprint
4	3	30	10	30	10	Published
5	1	50	100	70	80	Published

Acknowledgements

Although the PhD years are an individual path towards the doctoral degree, team working inside and outside the university is very important, and I must say that I have been lucky to have so many great people around me in these years.

First of all, I want to thank my supervisor, Prof. Igor Lesanovsky, for his great guidance and supportive mentorship during my PhD research. His dedication and passion for physics gave me a lot of positive energy and his availability to discuss and openly consider new ideas created a fruitful and collaborative environment. I am also grateful for the great opportunity he gave me to go to the USA, and for the advice and support I could benefit from throughout my PhD.

I also want to thank my second supervisor, Prof. Christian Groß, for the nice discussions about the experimental applications of my works and his constant support during these years. I also want to thank his group, Philip, Lea, Arno, Roxana and Ludwig, for the exchange of ideas about our works and the many visits in the lab.

I thank Prof. Hossein Sadeghpour, for his kind availability to be a reviewer of my thesis and for making my visit at ITAMP possible. I really enjoyed the scientific and human environment there and I hope to come back in the future.

I want to thank Federico Carollo, Paolo P. Mazza, Gabriele Perfetto and Radhika Joshi, for their helpful collaboration that led to our joint works.

I thank all my colleagues and members of the group: Priv.-Doz. Beatriz Olmos Sanchez, Albert, Gabriele, Joe, Mario, Marc, Paulo, Wilson, Mathias and all the master and bachelor students that have been part of our group, for the many discussions about our projects and the great time we have spent together. Special thanks to Federico, who has been my office mate since I moved to Tübingen: I

enjoyed every discussion we had and learnt a lot from them. And to Francesco, for the great time discussing about physics, riding by bike and many other activities. I finally want to remember Romanos, and our months spent together: you will never be forgotten.

I would like to thank our secretary, Frau Ingrid Estiry, for the great job she has been doing since I moved in Tübingen. She really helped me to set the contract up during the hard times of Covid and she has been always available to assist me throughout these years.

In physics only four fundamental forces are known, but I actually believe there is a hidden fifth one that is responsible for agglomerating Italian people while they are abroad. And, being a fundamental force, I was also subject to that. I want to thank the Italian crew I had to pleasure to be with, Enza, Martina, Nadia, Gabriele and Francesco B., for the nice dinners during the sad nights in Covid time and the great time we spent together. I also want to thank my colleagues during my first year, Beppe, for his unlimited imagination, and Paolo, for the awesome dinners together (and delicious wine).

I thank Johanna and Ingemar, with whom I lived for three years in our shared flat, for the entertaining time together. I also want to thank Sahel, Berit, Anne H., Rohana, Anne, Mona, Ria and Bernat and all the new friends I met in Tübingen that I could not include here. I thank my friends from Collegio Ghislieri with whom, despite the distance, I have a very close bond of friendship, and my friends and colleagues from the Master degree.

Finally, I want to thank my parents, Oriana and Ferruccio, and my sister Elena for being such a great family. You have been supporting me during these years and helped me to accomplish all the results I have achieved, and I am sure that this will continue. The best is yet to come!

Contents

1 Introduction **1**

1.1 Kinetically constrained systems 3

1.2 Thermalization in isolated quantum systems 5

1.3 Slow quantum relaxation due to kinetic constraints 7

1.4 Implementation of kinetic constraints with Rydberg atoms 9

1.5 Stochastic resetting 15

2 The physics of Rydberg atoms **21**

2.1 Single-body properties of Rydberg atoms 21

2.1.1 The hydrogen atom 21

2.1.2 Alkali atoms and quantum defect theory 25

2.1.3 Dipole matrix elements 26

2.1.4 Rydberg excitation and transitions between Rydberg states . 27

2.1.5 Rydberg lifetime 28

2.2 Many-body properties of Rydberg atoms 29

2.2.1 Electrostatic interactions 29

2.2.2 Van der Waals interaction 30

2.2.3 Förster resonances and dipolar exchange interaction 32

2.3 Rydberg blockade 33

2.4 Rydberg facilitation 35

2.4.1 Effective model for Rydberg facilitation 37

2.5 Engineering interaction potentials via microwave driving 39

3 The physics of stochastic resetting **45**

3.1 Diffusion with stochastic resetting 45

3.1.1 Renewal equation approach 47

3.1.2 Non-equilibrium stationary state . . . 48
3.2 Generalization of the resetting dynamics . . . 49
3.2.1 Multiple reset states and spatially dependent resetting . . . 49
3.2.2 Non-Poissonian resetting . . . 50
3.3 Quantum dynamics subject to resetting . . . 52

4 Results and discussion **55**
4.1 Bloch oscillations of Rydberg clusters . . . 57
4.2 Phonon dressing of a facilitated Rydberg lattice gas . . . 58
4.3 Rydberg tweezer molecules . . . 59
4.4 Designing non-equilibrium states of quantum matter through stochastic resetting . . . 60
4.5 Collective behavior in non-interacting systems subject to stochastic resetting . . . 61

5 Conclusion and outlook **65**
5.1 Future directions . . . 67
5.1.1 Localization phenomena in Rydberg quantum simulators . . . 67
5.1.2 Self-organized criticality in quantum many-body systems . . . 69

6 Bibliography **71**

7 Appendix: publications **98**

1 Introduction

Despite being older than 150 years, the concepts of ergodicity and thermalization are still intriguing the current scientific community. Since the seminal works by Ludwig Boltzmann [1, 2], the question on under which conditions a physical system reaches a well defined equilibrium state has sparked the interest of physicists of any generation. Several approaches have been developed to address this fundamental question that led to the formalization of modern statistical physics. In classical physics, a system is described through canonical coordinates that define a point in the phase space. Given a Hamiltonian, the microscopic dynamics of the system is dictated by the Hamilton's equations of motion, whose solution gives a trajectory of points in the phase space. Although such solution is in principle obtainable, it is practically extremely complicated to find an explicit solution for systems with a large number of particles. These difficulties motivated the fathers of statistical physics to formulate a *macroscopic* description of such complicated systems that would capture the relevant aspects of the *microscopic* physics. The idea is to fill the disconnection between the laws of classical mechanics and the practical experience of incomplete knowledge, by adding some uncertainty about which microscopic state the system is in. This is also motivated from an experimental point of view, since the tracking of each particle's motion is infeasible. This led to the definition of statistical ensembles [3], which consist of sets that contain all the possible microscopic configurations (microstates) that a system can assume. A probability measure is then assigned to each of these microstates. The expression of this probability distribution only depends on macroscopic quantities that can be controlled experimentally, like the temperature, volume or particle number. It is then evident that the introduction of statistical ensembles brings a fundamental simplification in that the system is no more described in terms of a large number of

microscopic coordinates, but only of few macroscopic variables. While the particles of the system evolve in time according to the Hamilton's equations, the probability distribution defining the statistical ensemble evolves according to the Liouville's equation. In particular, the Liouville theorem states that the local density of microstates following a point trajectory through phase space is constant as viewed by an observer moving with the ensemble.

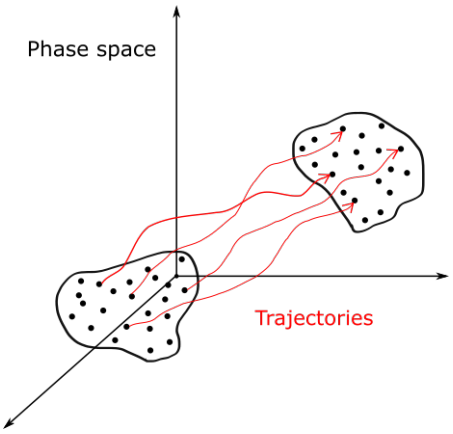

Figure 1: **Evolution of an ensemble of classical systems in phase space.** Each point represents a different microstate of the system, which evolves in time according to the Hamilton's equations. The ensemble, which contains the points, evolves according to the Liouville's equation.

An important class of statistical ensembles is given by so called *stationary ensembles*. They are ensembles that do not evolve in time and describe systems that are in thermodynamic equilibrium. Their probability measure (equilibrium distribution) only depends on the conserved quantities of the system and therefore does not depend on time. This formalism allows to analytically compute the aforementioned average values of quantities that, when measured in experiments, are found to be time-independent. In fact, these quantities, which are in principle functions of the microscopic coordinates of the particles, can be more easily computed as averages over the equilibrium distribution. One then may think that this aver-

aged observable can be equally obtained by averaging the value that it acquires over the experimental time, during which the microstate of the system is evolving in phase space through the Hamilton's equations. When the results of the two expectation values coincide, then the system is said to be *ergodic* [4, 5]. While this seems a rather natural assumption, some classical systems, called *integrable* systems [6], defy this paradigm, being therefore a notable example of nonergodic systems. The intuitive reason is that integrable systems are characterized by an extensive set of conserved charges that strongly constrain the trajectories in phase space, preventing the system from exploring the entirety of phase space. These systems are also described by a different stationary distribution called *generalized Gibbs ensemble* [7, 8], that depends on the conserved charges.

The same concepts can be adopted also for quantum many-body systems. In this case the full many-body wave function evolves according to the Schrödinger equation, while the statistical ensemble evolves according to the von Neumann equation. In the quantum case, the statistical ensemble is given by a density matrix. Similarly to the classical counterpart, the stationary ensemble is given by a diagonal matrix in the orthogonal basis of states that simultaneously diagonalize each conserved charge. However, a full understanding of the concepts of ergodicity and thermalization in isolated quantum systems is still lacking. The study of these topics is also important from the practical point of view, because the precise control of low-dimensional quantum systems is expected to be necessary for the future development of quantum technologies.

1.1 Kinetically constrained systems

The first topic of this thesis is about kinetically constrained systems, which are prototypical models that are used to understand thermalization and ergodicity [9, 10].

This type of systems was originally introduced to understand the glass transition problem. Glasses are amorphous solid-like materials that are typically created when a viscous fluid is cooled or compressed sufficiently fast [11]. Generally, a glass exists in a structurally metastable state with respect to its crystalline form and as such constitutes a paradigmatic example of non-equilibrium matter. Indeed, the liquid-glass transition is not believed to be a transition between equilibrium states, as the true equilibrium state is supposed to be always crystalline [12]. Glass is believed to exist in a kinetically locked state subject to dynamical arrest and, therefore, the glass transition is considered to be a dynamic phenomenon. Despite extensive efforts, a full understanding of the glass transition is still lacking, making it one of the remarkable problems in condensed matter physics, as already outlined in 1995 by P. W. Anderson [13]:

The deepest and most interesting unsolved problem in solid state theory is probably the theory of the nature of glass and the glass transition. This could be the next breakthrough in the coming decade. [...] The solution of the more important and puzzling glass problem may also have a substantial intellectual spin-off. Whether it will help make better glass is questionable.

The key features of glassy systems are their dynamical heterogeneity, i.e., the existence of local regions in a material with very different relaxation timescales [14]. These are typically accompanied by an absence of evident structural changes in contrast to conventional condensed matter systems. Simply speaking, there are two main theoretical approaches to investigate this peculiar behavior, as sketched in Fig 2. One is *thermodynamic* [15], in the sense that it tries to explain the observed dynamics on the basis of an underlying thermodynamic potential possessing a large number of local minima. This theory, known as random first-order transition theory [16], shares some ideas with the ones developed in spin-glasses [17], which are

however systems with quenched disorder and, therefore, fundamentally different from ordinary glasses that are not disordered. The other approach is purely *dynamical* and is formalized within the framework of kinetically constrained models (KCMs). The idea is that the dynamics of the system is constraint to satisfy a set of rules which eventually gives rise to glassy slowing down if the system is in a state for which these rules are hardly satisfied. These models, which are often characterized by simple thermodynamics, propose to ascribe dynamical arrest to scarse dynamical connectivity between different states.

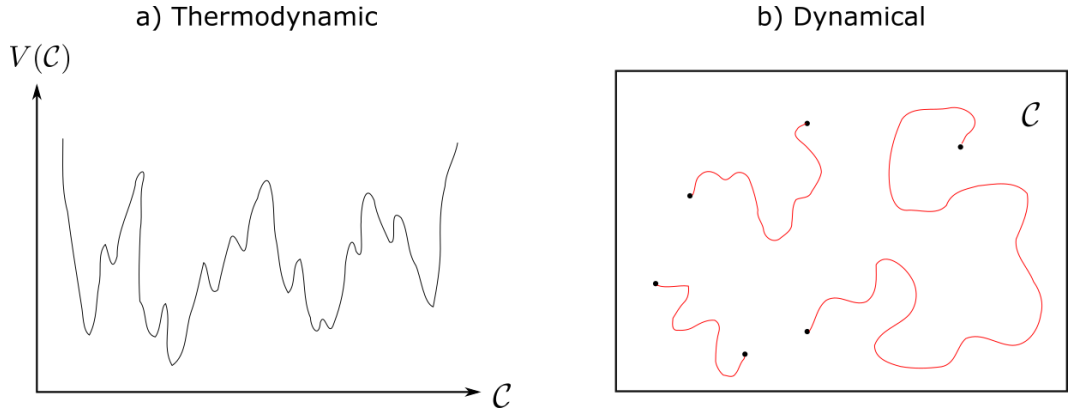

Figure 2: **Sketch of the approaches to the glass transition problem.** a) Thermodynamic approach: the dynamical heterogeneity of glassy systems is explained by a rugged potential landscape in the configuration space $\mathcal{C}$. b) Dynamical approach: the glass behavior is explained by complex dynamical features of the trajectories in the configuration space.

1.2 Thermalization in isolated quantum systems

Thinking about the properties of classical KCMs, it appears very natural to extend them to the quantum world. In particular, it is interesting to see whether the dynamical constraints induce some peculiar effects in the equilibration process of a quantum system. This is especially relevant since the field of non-equilibrium

quantum physics has recently attracted a lot of interest and the relation between the dynamical properties of quantum KCMs and the ones featured by other quantum many-body systems is not fully understood. Generic quantum many-body systems are said to *equilibrate* when their state, in the long-time limit, is indistinguishable from the time-integrated state, as fas as expectation values of observables are concerned [18, 19, 20]. In other words, observations of the state in the long-time limit are stationary. This is caused by the dephasing of the state of the system due to rapidly rotating terms in the off-diagonal elements of the density matrix when written in the energy eigenbasis. Besides equilibration, most isolated quantum many-body systems are also believed to *thermalize* [21]. The notion of thermalization in quantum mechanics is similar to what is meant by equilibration in classical physics in the following sense. Consider for example a certain quantum many-body system and separate it in two subsystems A and B. Now consider the long-time expectation value of an observable of subsystem A: if it can be computed by averaging the observable over a thermal distribution, then the system is said to thermalize. Thermalization is therefore the general framework for *quantum ergodicity*, where the system acts as its own thermal reservoir [22, 7]. Quantum thermalization can be seen as a consequence of the energy eigenstates obeying the eigenstate thermalization hypothesis (ETH), which states that the energy eigenfunctions behave as if they were Gaussian random variables [23, 24, 25, 26]. More precisely, the spectrum is similar, in the large size limit, to the one of a random matrix that has the same symmetries of the Hamiltonian [19]. Therefore, it displays level repulsion and the bipartite entanglement entropy scales linearly with the size of the smaller subsystem, thus providing the characteristic thermodynamic feature of entropy.

An exception to this situation is given by integrable systems which equilibrate to the generalized Gibbs ensemble [27, 8, 28, 29]. Quantum ergodicity can be

also broken by a different mechanism, originating from the presence of special eigenstates in the spectrum called *quantum many-body scars* [30, 31] that, despite being embedded in an otherwise thermalizing spectrum, are responsible for the periodic revivals observed in certain experimental platforms [32]. A third notable exception to quantum thermalization is given by quantum many-body systems with quenched disorder that display *many-body localization* (MBL) [33, 34, 35, 36, 37]. Typically, in those systems, there exists a critical value for the disorder strength that separates two phases: an ergodic one, characterized by the system acting as its own thermal bath, and a localized one, where the system does not relax to thermal equilibrium under the dynamics of its Hamiltonian but instead retains memory of the initial state. This is believed to be due to an extensive number of emergent local conservation laws. If on the one hand MBL shares this property with quantum integrability, on the other, an important difference with quantum integrable systems is that MBL persists also in the presence of a small perturbation. In this sense, MBL is so far the only known robust mechanism that prevents thermalization in isolated quantum systems. However, there is still a debate whether MBL is a phase or only a metastable state of matter that emerges as a finite size effect [38, 39]. Furthermore, the connection of MBL phenomenology to the slow dynamics in quantum spin glasses has been recently questioned [40].

1.3 Slow quantum relaxation due to kinetic constraints

There is a key distinction between systems displaying MBL and kinetically constrained systems: the former require the presence of quenched disorder, while the latter do not. An interesting question to ask is then whether the slow dynamics experienced by glasses can be translated in the quantum framework, i.e., whether kinetic constraints induce slow relaxation in isolated quantum systems. This can

be seen as a consequence of the reduced connectivity between many body states induced by kinetic constraints, which causes a splitting of the Hilbert space into many disconnected sectors [41]. Several recent papers [42, 43, 44, 45, 46, 47, 48, 49] have indeed shown indications of this. For example, Ref. [41] considers hard-core particles hopping on a 1D strip of a triangular lattice, where hopping between two sites is constrained to the state of the neighboring sites (see Fig. 3). This situation mimics the excluded volume interaction that is present in models describing classical glasses. The authors find two regimes: when kinetic energy dominates over the potential energy, thermalization is fast. On the contrary, when the potential terms dominate over the kinetic terms, the system displays an emergent separation of timescales characterized by a slow dynamics in which memory of the initial conditions is retained before eventually thermalizing, in close analogy with what occurs in glasses.

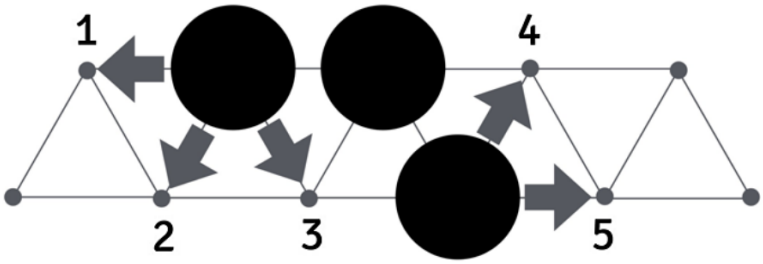

Figure 3: **Example of a kinetically constrained quantum model**. Particle can hop only if at least one common neighbor of the initial and final sites is empty, mimicking the excluded volume interaction that is present in models describing classical glasses. Figure from Ref. [41].

1.4 Implementation of kinetic constraints with Rydberg atoms

The interest in kinetically constrained quantum systems has experienced a substantial rise in the last decade [50], due to the concomitant technological advances in the field of quantum simulation [51]. The development of quantum simulators has been motivated by difficulties encountered in the theoretical and computational studies of the physics of interacting quantum many-body systems [52]. From the theoretical side, the interactions between constituents create quantum correlations, like entanglement, that make the full wave function of the system so complicated that exact analytical calculations become impractical. From the computational side, exact numerical simulations are extremely challenging as the required computational resources scale exponentially with the number of particles. Standard methods to overcome these difficulties employ various approximations in a way that either analytical treatment becomes feasible or numerical simulations tractable. An alternative way to tackle these difficulties that has recently attracted a lot of interest is indeed based on the use of quantum simulators. The basic idea is to directly exploit the quantum properties of real particles, like atoms, ions or superconducting circuits, to solve problems that are difficult to simulate on classical computers and to simulate complex quantum phenomena in a controllable way. This idea, originated from two seminal works by Y. Manin [53] and R. Feynman [54], has been extremely successful with numerous applications in disparate fields of modern quantum science, ranging from material science to chemical physics, quantum information and condensed matter physics.

Quantum simulators can be realized in different ways, including highly tunable "analog" systems that naturally implement the problem of interest, or more "digital" methods that employ external control fields, thus mimicking classical com-

puters, to implement Hamiltonian evolution through a sequence of quantum gates. Early implementations of controllable quantum simulators based on ultracold atoms started in the early 2000s and since then these platforms have provided the first observations of several quantum phenomena, like quantum phase transitions induced by microscopic quantum fluctuations [55], strong correlations in quantum fluids [56] and ultracold fermionic matter [57, 58], novel many-body dynamical phenomena [59] and artificial physical systems without natural analogs like hyperbolic spaces [60] and synthetic dimensions [61]. Other quantum simulators have been recently implemented, like programmable superconducting circuits demonstrating quantum supremacy [62], trapped ion based simulators displaying dynamical phase transitions [63], ultracold molecules trapped in optical tweezers [64], semiconductor quantum dots simulating the Fermi–Hubbard model [65], cavity QED systems with photon-mediated atomic interactions [66] and two-dimensional material heterostructures hosting long-lived excitons [67].

In the last decade, tremendous experimental progress has been achieved in another class of quantum simulators, called *Rydberg quantum simulators* and based on neutral atoms excited to high-lying Rydberg states through an external laser field [70]. The large electric dipole moment of the atoms when excited to the Rydberg state leads to strong dipole-dipole interactions between them. These atoms, either trapped in an optical lattice [71] or in configurable tweezers [72] (see Fig. 4), feature strong state-dependent interactions that make them a versatile model system for condensed matter physics capable to realize generic many-body quantum Hamiltonians [73]. In particular, thanks to their versatility in terms of interaction energy scales and lattice geometries, they constitute the natural setting to simulate quantum Ising models, which are the prototypical models for quantum magnetism. Among the recent experimental achievements using this platform for quantum simulation are the observation of strongly correlated many-

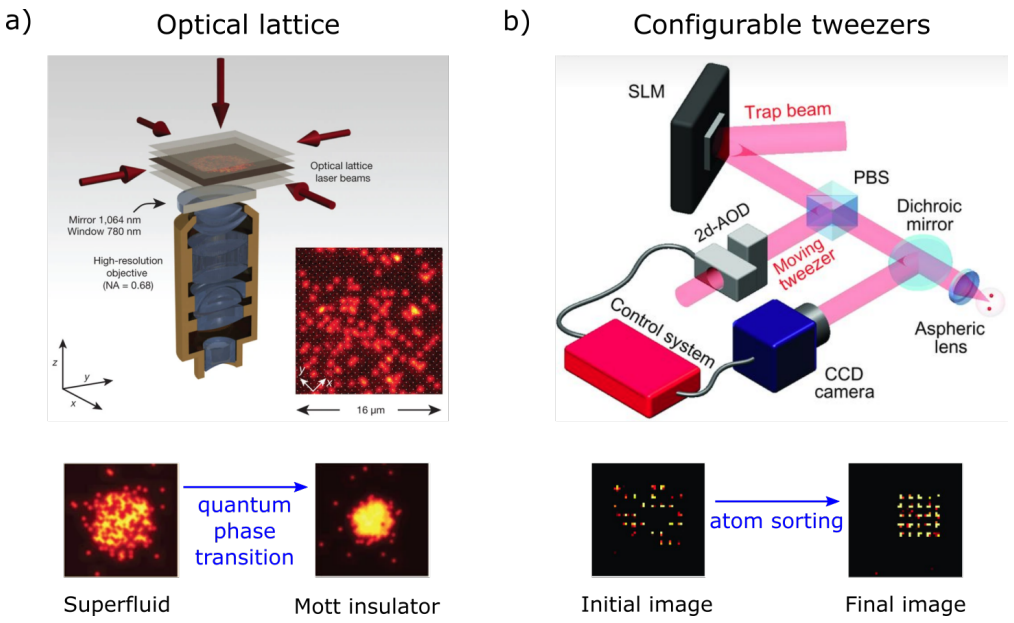

Figure 4: **Experimental platforms for realizing arrays of individually controlled neutral atoms.** a) Atoms are trapped in an optical lattice by interfering several laser beams and observed by fluorescence in a quantum gas microscope. To obtain unit filling, a quantum phase transition from the superfluid phase to the Mott insulator phase is driven. b) In a tweezer platform, laser-cooled atoms are loaded from a magneto-optical trap into the optical tweezers, in an arbitrary lattice geometry thanks to a spatial light modulator. The atoms can then be ordered in a unit filling lattice by moving the tweezers. Figures adapted from [68, 69].

body states [74, 75, 76], enhanced coherent light-matter coupling [77], quantum many-body dynamics after a sudden quench [78, 79], non-trivial long-lived collective oscillations [32], crystallization in Ising quantum magnets [80] and critical behavior near quantum phase transitions [81]. Very recently, various topological systems have also been successfully observed in Rydberg experiments, like the SSH model for hardcore bosons [82], Laughlin states made of Rydberg polaritons [83], density-dependent Peierls phases [84] and quantum spin liquid [85]. Most of these experiments exploit a crucial property that characterize Rydberg systems, that is

the presence of a kinetic constraint, called *Rydberg blockade*. It is naturally implemented in those situations in which the Rydberg-Rydberg interaction prevents the simultaneous Rydberg excitation of two nearby atoms, as shown in Fig. 5a. In the language of kinetically constrained systems, this means that many-body states with two nearby excited atoms cannot be reached dynamically. The Rydberg blockade has been originally introduced as a tool to implement fast and robust quantum gates between neutral atoms [86, 87], which eventually led to a plethora of quantum information protocols for conditional logic [88].

Much less explored is the opposite situation, dubbed the *facilitation* (or anti-blockade) constraint [89], where the interactions shift the otherwise detuned laser in resonance. In this case only atoms at the correct distance to an already excited atom are resonantly driven by the external laser, thereby creating an "avalanche" of excitations, as shown in Fig. 5b. In fact, as the name suggests, an atom that is excited to the Rydberg state "facilitates" the neighboring atoms to be also excited to the Rydberg state. This kinetic constraint has attracted a lot of attention as it allows to model certain types of complex non-equilibrium dynamics, also in many phenomena outside of physics like epidemics, population dynamics or spreading of information in social media [90, 91]. The possibility to implement the facilitation constraint with Rydberg atoms opens the possibility to study unexplored non-equilibrium phenomena in quantum systems and investigate how the effects of dynamical constraints impact on the relaxation of a quantum many-body system.

Introduced in 2007 by Ref. [92], the facilitation constraint has since then been studied extensively. For example, its application in quantum computation tasks has been proposed [93, 94, 95], as well as for the exploration of non-equilibrium phase transitions [96], the emergence of quantum glassy dynamics [97] and self-organized criticality [98, 99]. The first experimental signatures of the facilitation

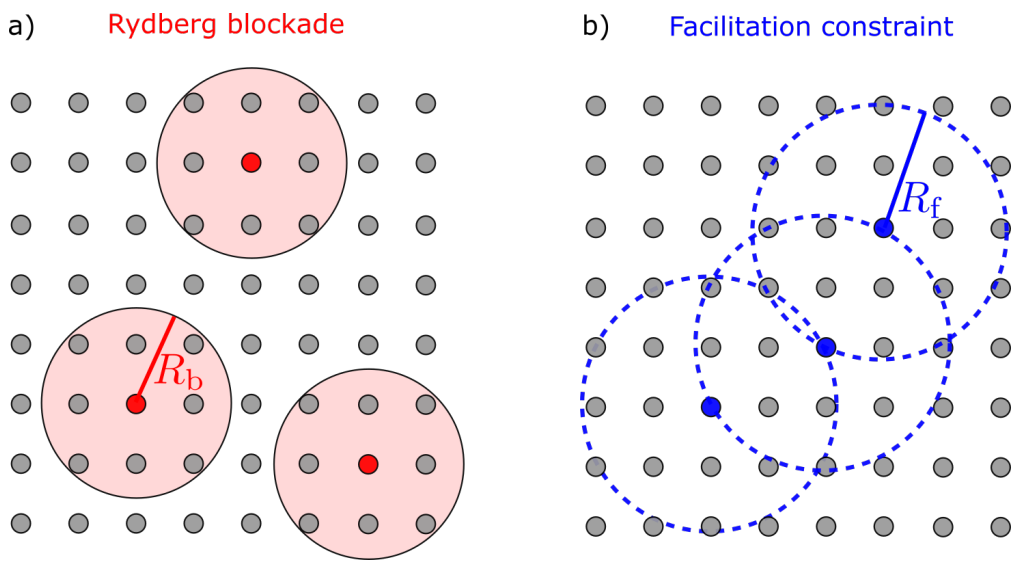

Figure 5: **Kinetic constraints in Rydberg lattice gases.** a) Rydberg blockade: a Rydberg excitation (red circle) prevents other ground state atoms from being excited to the Rydberg state if they are closer than the blockade radius R_b. b) Facilitation constraint: by canceling the Rydberg-Rydberg interaction with the laser detuning, ground state atoms that are at the distance R_f from an already excited atom (blue circle) are facilitated to be excited.

constraint have been measured in 2010 in Ref. [100], in which variations in the Rydberg pair distribution in an ultracold gas were detected by time-resolved spectroscopic measurements. The "Rydberg aggregates" [101] that are expected to form under the facilitation constraint have been measured and characterized in various subsequent experiments [102, 103, 104]. Facilitation is also responsible for unwanted atom losses [105, 106] that originate from a contaminant Rydberg excitation uncontrollably facilitating neighboring ground state atoms and thus introducing undesired dephasing in the system [107, 108].

The aforementioned experiments have successfully shown clear indications of facilitation dynamics in Rydberg gases. However, in these platforms one has no

control on the individual atoms: it seems therefore promising to implement these ideas in Rydberg quantum simulators, where atoms, trapped in harmonic traps, form a discrete lattice with potentially arbitrary geometry. Some attempts have indeed been made, notably in Ref. [109], where a linear chain of atoms was driven by an external detuned laser to implement the facilitation condition. However, because of the finite temperature of the system, the position of the atoms inside the traps could not be kept fixed, failing the required fine-tuning of the relative interatomic distance. The position fluctuations, acting as a quenched disorder, dramatically inhibited the expected creation of facilitated Rydberg excitations, and only a model that explicitly considered the randomness in the positions could qualitatively explain the experimental results. Other works have investigated the impact that the position disorder has on the facilitation dynamics [110, 111, 112], by treating the position of the atoms inside traps as Gaussian random variables. This generates position disorder that hinders the spreading of Rydberg excitations, similar to what happens in MBL systems. This treatment, however, only models the position fluctuations that are induced by the finite temperature of the system. To also model the position disorder induced by the quantum fluctuations one has to fully consider the quantum nature of the harmonic traps holding the atoms, whose effect becomes even dominant at low temperature. The quantum fluctuations of the atomic positions can be indeed modeled in terms of the creation and annihilation operators that typically describe the quantum harmonic oscillator.

Contrary to the Rydberg blockade, facilitation is more challenging to implement in current Rydberg quantum simulators for an additional reason. Indeed, while the blockade constraint restricts the evolution to states with approximately zero interaction energy, the facilitation constraint relies on canceling the interaction energy with single-atom energy shifts. The resulting Rydberg aggregates are thus subject to mechanical forces that displace the atoms, preventing the perfect cancellation

of the interaction energy. This effect gives rise to a spin-boson coupling in the model, since the displacement, which is described in terms of bosonic operators, takes place only when two neighboring atoms, which are described in terms of spin operators, are excited to the Rydberg state. This spin-boson coupling in Rydberg quantum simulators has been theoretically studied in some recent works. For example, Ref. [113] shows the possibility to engineer long-range phonon-mediated interactions between atoms thanks to this spin-boson coupling, while in Ref. [114] the Rydberg aggregates originating from facilitation get vibrationally dressed by phonons, showing polaronic behavior.

1.5 Stochastic resetting

A second topic of this thesis lies on an emergent field closer to statistical physics and stochastic processes, which has attracted a lot of interest in the past decade. Consider a system that evolves with a certain dynamics (either stochastic or deterministic) and impose the condition that at random times the system interrupts the dynamics and is reinitialized to a certain state before restarting the dynamics again. This process is called *stochastic resetting* (see [115] for an extensive review on the topic). It has two main properties: *i*) at long times the system generally reaches a nontrivial non-equilibrium stationary state (NESS); *ii*) it models generic search algorithms and can provide optimal search strategies. The concept of stochastic resetting was introduced in 2011 by M. R. Evans and S. N. Majumdar in Ref. [116], where they consider the situation in which a diffusive particle is subject to stochastic resetting, as shown in Fig. 6. Despite its simplicity, this model shows both the aforementioned properties. Indeed, resetting changes the long-time position distribution of the particle from being a Gaussian with time-dependent variance to a stationary distribution with a completely different functional form.

Moreover, if a target is introduced at a fixed position, one finds an optimal value for the resetting rate that minimizes the average time needed for the diffusing particle to reach the target.

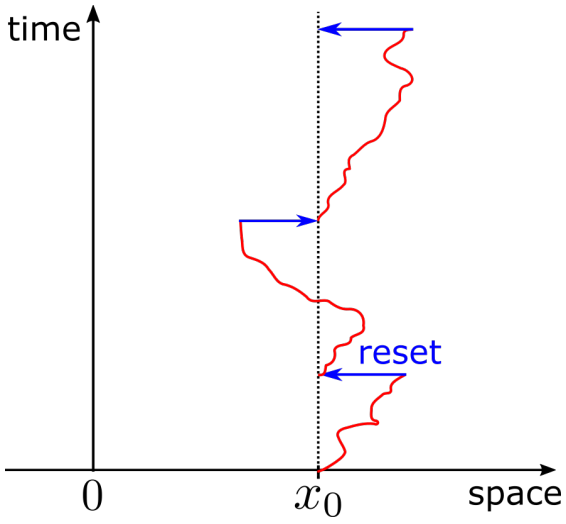

Figure 6: **Trajectory of a diffusive particle subject to stochastic resetting.** The particle is reset to its initial position x_0 at rate r.

Characterizing such emerging NESS and the possible optimal search strategies has recently become a problem of central interest in classical statistical physics with many applications across disciplines, like biology, chemistry and computer science. For example, stochastic resetting brings many similarities with the ideas behind simulated annealing [117]. Here one usually starts from a specific initial state in the configuration space and attempts to locate the minimum of a complex potential landscape. One often encounters the situation in which the algorithm gets stuck for a long time at a local minimum. To speed up the search, restarting the algorithm all the way from the initial state proves to be a good strategy to explore alternative pathways on the landscape towards the global minimum [118]. Notions of resetting are also found in human and animal behavior: for instance, rhesus macaques, during the foraging period, perform stochastic resetting to previously visited sites

and the effects of such memory-induced resetting have been modeled [119]. Similar aspects are also found in biology, for example with the stochastic interruption of RNA polymerization, which is responsible for the synthesis of RNA from a DNA template [120]. Stochastic resetting has been also studied in several contexts ranging from chemical processes like the Michaelis-Menton reaction scheme [121], to run-and-tumble particles [122], effects of catastrophes in population dynamics [123], biological traffic models [124] and population genetics [125].

In addition to these applications, stochastic resetting is an interesting process by its own nature, since it is a very general problem that can be applied to any dynamics and leads to an emergent non-equilibrium stationary state. For this reason, it has been indeed studied in many different contexts in classical physics. For instance, in addition to the aforementioned case of a diffusive process, the effects induced by stochastic resetting have been investigated in various single-particle problems, including diffusion in an external potential [126] and in arbitrary spatial dimension [127], discrete-time random walks [128] and multiparticle diffusive systems [129]. Furthermore, generic properties regarding the transient dynamics before relaxing to the stationary state [130], as well as settings with spatially dependent resetting [131] and generic reset time distribution [132] have been studied.

Resetting dynamics can be also generalised to extended systems with interacting degrees of freedom. Examples in the literature are fluctuating interfaces [133], reaction-diffusion systems [134], exclusion processes [135] and Ising model [136]. Other generic processes have been studies, like resetting with memory of history, i.e., at each reset event the process is reset to its value at some randomly selected time from the past. Examples of this include the preferential visit model [137], used to model animal mobility, and resetting to the past maximum of a random walk [138]. More recently, new developments that further extend the resetting

paradigm have been carried out. One involves the thermodynamics of resetting addressed in [139], in which the authors identify the thermodynamic work done by resetting to obtain a first law of thermodynamics. By further identifying the entropy change due to resetting, Ref. [140] analyzes how integral fluctuation theorems apply to resetting problems. Recent developments also involve the derivation of large deviation theory for stochastic processes subject to stochastic resetting [141, 142].

All the works mentioned in the previous paragraphs regard problems of classical physics. Indeed, only very recently physicists have started to study quantum systems subject to stochastic resetting, while evolving unitarily according to the Schrödinger equation. A notable example is given by Ref. [143], where the authors find that the stationary density matrix possesses nonzero off-diagonal elements in the energy eigenbasis, thus maintaining quantum coherence and giving rise to a novel non-diagonal ensemble. The spectral properties of quantum Markov processes have been studied in Ref. [144], where stochastic resetting is shown to have the effect of accelerating or even inducing relaxation to a stationary state. Resetting also plays an important role in the study of quantum systems that are subject to repeated measurements. Some works have investigated this in the context of quantum random walks [145, 146] and first passage time statistics for quantum dynamics [147, 148]. In the context of open quantum systems, resetting to some initial state is shown to be a useful source to contrast decoherence and obtain an entangled stationary state [149]. Resetting in open quantum systems has been also analysed in Ref. [150], in which the finite-time probability of a certain state is computed through large deviation methods and in Ref. [151], where the statistics of quantum-jumps are exactly derived. Connections to measurement-induced phase transitions have been also recently made [152, 153].

We conclude this section by mentioning that there are some recent developments to explore the physics of stochastic resetting from the experimental point of view. Ref. [154] has implemented experimentally a setting in which a diffusing colloidal particle is subject to stochastic resetting, finding excellent agreement with theoretical predictions [155]. Resetting is done by transporting the particle back to its initial position with holographic optical tweezers. This experiment has also provided the first measure of the energetic cost of resetting in steady-state and first-passage scenarios. A different group has studied experimentally the optimal strategy for a diffusing particle to reach a target in the presence of stochastic resetting [156, 157], finding excellent agreement with theoretical predictions [158]. The experiment is performed using a micrometer-sized silica microsphere immersed in pure water. The reset is performed by turning an optical tweezer on to restore the position of the microsphere to the initial one. Despite these experimental successes, performing the resetting of the position poses some experimental challenges. First of all, resetting the particle to its initial position requires some finite time, contrary to the approximation of instantaneous resetting assumed in most theoretical works. Furthermore, by turning the harmonic tweezer on, the particle position is not exactly reset to the initial position as the particle relaxes to a Gaussian distribution with a temperature dependent variance.

2 The physics of Rydberg atoms

The goal of this chapter is to provide the theoretical framework describing the physics of Rydberg atoms. We first describe the main single-body properties of Rydberg atoms, including their energy spectrum, their coupling with the light field and their lifetime. We then present the many-body properties of Rydberg systems, with a focus on their interactions and the emergence of kinetic constraints. We conclude this chapter with the derivation of the effective model for the facilitation constraint, which constitutes the starting point of some of the original works presented in this thesis.

2.1 Single-body properties of Rydberg atoms

Rydberg atoms are highly-excited atoms whose valence electron is in a state with high principal quantum number n [70]. They are important from the historical point of view, as the observation of the Rydberg series helped the understanding of atomic spectroscopy in the early days of quantum mechanics [159]. More recently, these atoms have received a renovated interest mainly for two reasons. The first is that a Rydberg state, being at the boundary between a bound state and a state in the continuum, can be produced in any physical process that results in either excited bound states or free electrons and the ion core. The second and more recent reason is owed to the exaggerated properties of Rydberg atoms that allow the realization of experiments that would be prohibitive with normal atoms.

2.1.1 The hydrogen atom

Many properties of Rydberg atoms can be understood by starting studying the hydrogen atom. The reason is that the Rydberg electron, being far from the

nucleus, feels an effective attractive potential from the ionic core made of the nucleus and the remaining electrons. The Hamiltonian of the hydrogen atom is

$$H_{\mathrm{H}} = \frac{\boldsymbol{p}_p^2}{2m_p} + \frac{\boldsymbol{p}_e^2}{2m_e} - \frac{e^2}{|\boldsymbol{r}_p - \boldsymbol{r}_e|}, \tag{1}$$

where $\boldsymbol{p}_p, m_p, \boldsymbol{r}_p$ and $\boldsymbol{p}_e, m_e, \boldsymbol{r}_e$ are the momentum, mass and position of the proton and the electron. The first two terms describe the kinetic energy of the proton and the electron and the third term is the electrostatic Coulomb interaction between the two particles. By introducing the center of mass and relative coordinates as

$$\boldsymbol{R} = \frac{m_p\boldsymbol{r}_p + m_e\boldsymbol{r}_e}{m_p + m_e}, \qquad \boldsymbol{r} = \boldsymbol{r}_e - \boldsymbol{r}_p,$$

we can rewrite Eq. (1) as

$$H_{\mathrm{H}} = \frac{\boldsymbol{P}^2}{2(m_p + m_e)} + \frac{\boldsymbol{p}^2}{2\mu} - \frac{e^2}{r},$$

where

$$\boldsymbol{P} = \boldsymbol{p}_p + \boldsymbol{p}_e, \qquad \frac{\boldsymbol{p}}{\mu} = \frac{\boldsymbol{p}_e}{m_e} - \frac{\boldsymbol{p}_p}{m_p}, \qquad \mu = \frac{m_e m_p}{m_e + m_p}$$

are the total momentum, the relative momentum and the reduced mass of the two-body problem. Thus the Hamiltonian H_{H} consists of a part describing the free motion of the center of mass and one part

$$H = \frac{\boldsymbol{p}^2}{2\mu} - \frac{e^2}{r} \tag{2}$$

describing a single particle in an attractive Coulomb potential. The eigenvalues and eigenfunctions of this problem are very well known and read

$$H\psi_{nlm}(\boldsymbol{r}) = E_n\psi_{nlm}(\boldsymbol{r}),$$

where

$$E_n = -\frac{\mathrm{Ry}}{n^2} \tag{3}$$

are the energy levels of the hydrogen atom and

$$\psi_{nlm}(\boldsymbol{r}) = \frac{\phi_{nl}(r)}{r} Y_{lm}(\theta, \phi),$$

with

$$\phi_{nl}(r) = \frac{1}{n}\left[\frac{(n-l-1)!}{a(n+l)!}\right]^{\frac{1}{2}} \left(\frac{2r}{na}\right)^{l+1} L_{n-l-1}^{2l+1}\left(\frac{2r}{na}\right) e^{-r/(na)}$$

being the radial part of the wave function, L_ν^α standing for the generalized Laguerre polynomial, $Y_{lm}(\theta, \phi)$ being spherical harmonics and $a = \hbar^2/(\mu e^2) \simeq 5 \cdot 10^{-11} m$ being the Bohr radius. The eigenfunctions are labelled by three quantum numbers: n is called the principal quantum number and only takes positive integer values, l follows from the eigenvalue, $\hbar^2 l(l+1)$, of the operator $\boldsymbol{L}^2$ and takes integer values between 0 and $n-1$, m corresponds to the projection of the angular momentum operator onto the z-axis, L_z, and acquires integer values between $-l$ and $+l$. The binding energies in Eq. (3) contain the Rydberg energy Ry, whose value is $\mathrm{Ry} = \mu e^4/(2\hbar^2) \simeq 13.6\,\mathrm{eV}$. Importantly, they depend on n, but not on l or m. The degeneracy with respect to m is the consequence of the spherical symmetry of the problem, while the degeneracy with respect to l is more subtle and is due to the conservation of the Laplace–Runge–Lenz (LRL) vector [160]. More generally, the LRL vector is conserved in any Kepler problem, i.e., in all problems in which two bodies interact with a central force that varies as the inverse square of the distance between them. For atoms with more than one electron, the LRL vector is no more a conserved quantity and the spectrum deviates from the one of hydrogen, as we will see later.

A more complete treatment requires the inclusion of relativistic effects, which turn out to be important in order to understand the properties of Rydberg atoms. Indeed, the electron is subject to the spin-orbit interaction which couples its spin $\boldsymbol{S}$ to the orbital angular momentum $\boldsymbol{L}$ as

$$V_{LS} = \frac{e^2}{2m_0^2 c^2}\frac{1}{r^3}\boldsymbol{L}\cdot\boldsymbol{S},$$

where m_0 is the rest mass of the electron and c is the speed of light. After adding this interaction to Hamiltonian (2), the orbital angular momentum is no more conserved. The binding energies are now given by

$$E_{nj} = m_0 c^2 \left[1 + \frac{\alpha^2}{(n-\eta_j)^2}\right]^{-\frac{1}{2}}, \tag{4}$$

with

$$\eta_j = j + \frac{1}{2} - \sqrt{(j+1/2)^2 - \alpha^2}.$$

Here $\alpha = e^2/(\hbar c) \simeq 1/137$ is the dimensionless fine-structure constant and j is the total angular momentum quantum number, that follows from the eigenvalue, $\hbar^2 j(j+1)$, of $\boldsymbol{J}^2$, with $\boldsymbol{J} = \boldsymbol{L} + \boldsymbol{S}$ being the total angular momentum operator. The energies (4) depend not only on n, but also on j, which, for a given n, can take the values $j = 1/2, 3/2, \ldots, n-1/2$. Indeed, in the presence of the spin-orbit interaction, the LRL vector is no more conserved. Expanding Eq. (4) in powers of α yields

$$E_{nj} = m_0 c^2 \left[1 - \frac{\alpha^2}{2n^2} - \frac{\alpha^4}{2n^3}\left(\frac{1}{j+1/2} - \frac{3}{4n}\right) + \ldots\right].$$

The first term is the rest energy of the electron and the second term is the non-relativistic binding energy $-\mathrm{Ry}/n^2$. The third is the first relativistic correction which is smaller than the non-relativistic energies by a factor of α^2/n. This fine structure lowers all the energy levels by an n and l-dependent shift. For this reason, the standard nomenclature for the energy states of the hydrogen atom is nl_j. The low-l orbitals also have an alternative notation, where $l = 0$ is denoted by S, $l = 1$ by P, $l = 2$ by D etc. This same notation is also used to indicate energy levels of Rydberg atoms.

We conclude the section by mentioning that it is possible to go beyond the presented treatment by additionally considering the vacuum quantum fluctuations giving rise to the Lamb shift and the hyperfine interaction, which would provide additional corrections to the binding energies.

2.1.2 Alkali atoms and quantum defect theory

Alkali atoms are atoms that belong to the first column of the periodic table. They have a positive nuclear charge Ze and a single valence electron orbiting around a core of $Z-1$ electrons that occupy close orbitals. Examples of alkali metals are Potassium ($Z=19$), Rubidium ($Z=37$) and Caesium ($Z=55$). The effects of the core electrons can be described by an effective potential introduced in [161]

$$V_{\text{eff}}(r) = -\frac{Z_l(r)}{r} - \frac{\alpha_c}{2r^4}\left[1 - e^{-(r/r_c)^6}\right]$$

that replaces the Coulomb potential. Here α_c is the static polarizability of the ion core, r_c is the cut-off radius, a_1, a_2, a_3, a_4 are four l-dependent parameters that define the effective nuclear charge

$$Z_l(r) = 1 + (Z-1)e^{-a_1 r} - r(a_3 + a_4 r)e^{-a_2 r}.$$

These expressions formalize the quantum defect theory, which provides the corrections of the atom's binding energies that are due to the electronic cloud. As a result, the binding energies also depend on the orbital quantum numbers l and j and are given by the Rydberg-Ritz formula [162, 163]

$$E_{nlj} = -\frac{\text{Ry}}{(n-\delta_{nlj})^2} = -\frac{\text{Ry}}{n^{*2}}, \tag{5}$$

where δ_{nlj} is the quantum defect and $n^* = n - \delta_{nlj}$ is called the effective quantum number. Quantum defects strongly depend on l, and only weakly on n and j. The effective reduction of the principal quantum number can be intuitively explained. When the valence electron penetrates the cloud formed by the other electrons, it feels a stronger attractive potential due to the reduced shielding of the positive nuclear charge. As a result, the radial wave function of the valence electron is pulled into the ionic core more than in the hydrogen atom. This effect is more pronounced for low-l states of the electron which are indeed characterized by a

quantum defect that can exceed unity. These states feel a small centrifugal force that make them have a finite probability to occupy the vicinity of the ionic core. High-l state also have a slightly smaller energy than the corresponding hydrogen level. However, this effect is not due to core penetration, but rather on the polarization of the ionic core induced by the valence electron, which results in a shift of the levels to lower energies that is typically very small, not exceeding 10^{-2} [164].

In general, Rydberg wave functions are characterized by quantum numbers n, l, j, m_j, where m_j corresponds to the projection of the total angular momentum onto the z-axis and takes integer values between $-j$ and $+j$. These wave functions can be separated in radial and angular components as

$$|n, l, j, m_j\rangle = |R_{nlj}\rangle \otimes |l j m_j\rangle \,.$$

2.1.3 Dipole matrix elements

In the previous section we have described the properties of alkali atoms and how they differ from the ones of the hydrogen atom. Alkali atoms can be excited from the ground state ($|4S\rangle$ in the case of Potassium) to a Rydberg state with large value of n (typically $n \in (15, 100)$) through an external laser source. The coupling strength of this transition, as well as other important properties of such Rydberg state, including its radiative lifetime, the response to electric fields and interactions between Rydberg atoms, are linked to the electric dipole matrix elements. The electric dipole operator is defined as $\boldsymbol{d} = e\boldsymbol{r}$, where $\boldsymbol{r} = (x, y, z)$ is the position operator of the valence electron. Correspondingly, the dipole matrix element between two states, $|i\rangle = |n, l, j, m_j\rangle$ and $|f\rangle = |n', l', j', m'_j\rangle$ is given by $\boldsymbol{d}_{fi} = \langle f|\boldsymbol{d}|i\rangle$. Generally, the dipole operator couples states with a difference $\Delta l = \pm 1$, due to the selection rules. For this reason, to compute the dipole matrix elements, it is useful to perform a change of basis as $|n, l, j, m_j\rangle = \sum_{m_l, m_s} \mathcal{C}^{1/2\, j\, l}_{m_s\, m_j\, m_l} |n, l, m_l\rangle\, |\frac{1}{2}, m_s\rangle$,

where $\mathcal{C}^{1/2\,j\,l}_{m_s\,m_j\,m_l} = \langle \frac{1}{2}, m_s, l, m_l | j, m_j \rangle$ are Clebsch–Gordan coefficients. Typically, the matrix elements $\boldsymbol{d}_{fi}$ are computed in the spherical basis $\boldsymbol{r} = (r_{-1}, r_0, r_{+1})$, with $r_0 = z$ and $r_{\pm 1} = \mp \frac{1}{\sqrt{2}}(x \pm iy)$. Thanks to the fact that r_0 couples states with $\Delta m_j = 0$ and $r_{\pm 1}$ states with $\Delta m_j = \pm 1$, one can then obtain the explicit values of the dipole matrix elements.

2.1.4 Rydberg excitation and transitions between Rydberg states

Due to the small spatial overlap between the atomic ground state and a Rydberg state, dipole matrix elements between these two states are smaller by several orders of magnitude compared to stronger transitions at lower n. This results in small Rabi frequencies and long radiative lifetimes. A laser field $\boldsymbol{E} = E_0 \boldsymbol{\epsilon}$ with amplitude E_0 and polarization $\boldsymbol{\epsilon}$ driving a transition between the atomic ground state $|\mathrm{GS}\rangle$ and a Rydberg state induces a Rabi frequency

$$\Omega = \frac{eE_0}{\hbar} \langle n, l, j, m_j | \boldsymbol{\epsilon} \cdot \boldsymbol{r} | \mathrm{GS} \rangle \,,$$

whose order of magnitude is given by the reduced matrix element which scales as $\langle R_{nlj} || \boldsymbol{r} || R_{\mathrm{GS}} \rangle \propto (n^*)^{-\frac{3}{2}}$.

On the contrary, the dipole matrix element between two neighboring Rydberg states $|n, l, j, m_j\rangle$ and $|n', l', j', m'_j\rangle$, coupled through a microwave field $\boldsymbol{E}$, can be very large. Indeed, for states that have $n \simeq n'$ and $l = l' \pm 1$, the reduced matrix element scales as

$$\langle n', l', j', m'_j || \boldsymbol{r} || n, l, j, m_j \rangle \propto (n^*)^2. \tag{6}$$

This scaling is at the origin of the strong electrostatic interactions between atoms in the Rydberg state, as we will see later. Moreover, the large dipole coupling between Rydberg states may be exploited to implement microwave field sensors [165].

2.1.5 Rydberg lifetime

The success of platforms based on Rydberg atoms is also due to their long lifetimes that allow them to implement long coherent dynamics. The total lifetime τ_{nlj} of a Rydberg state $|n, l, j, m_j\rangle$ is mostly limited by two independent process, a spontaneous decay to the ground state and a black-body induced transition to other Rydberg states.

The spontaneous decay rate Γ_{sp} to the ground state $|\text{GS}\rangle$ can be described by Fermi's golden rule and reads

$$\Gamma_{\text{sp}} = \frac{|\langle n, l, j, m_j|\boldsymbol{d}|\text{GS}\rangle|^2(\omega_{nlj} - \omega_{\text{GS}})^3}{3\pi\epsilon_0\hbar c^3} \propto (n^*)^{-3},$$

where $\omega_{nj} - \omega_{\text{GS}}$ is the transition frequency between the Rydberg state and the ground state and ϵ_0 is the vacuum permittivity. This gives a spontaneous decay time $\tau_{\text{sp}} = \Gamma_{\text{sp}}^{-1} \propto (n^*)^3$, which makes high-$n$ Rydberg states ideal for simulating long coherent quantum dynamics.

The second source of decay from a Rydberg state is due to black-body induced transition to neighboring Rydberg states. At finite temperature T black-body photons, whose spectrum follows the Planck's law

$$B(\nu, T) = \frac{2h\nu^3}{c^2}\frac{1}{e^{\frac{h\nu}{k_B T}} - 1},$$

can trigger transitions between energetically adjacent Rydberg states. By multiplying this factor with the corresponding transition rate given by Fermi's golden rule and summing over all possible final states, one finds the approximate expression [70]

$$\tau_{\text{bb}} \propto (n^*)^2.$$

As a result, black-body induced transitions constitute the major limitation for the lifetime, as n increases. While this source of decoherence is a limiting factor for

the simulation of quantum dynamics, since it populates Rydberg states that are not coupled by the driving laser, it can be suppressed in cryogenic environments, as shown experimentally in Refs. [166, 167].

2.2 Many-body properties of Rydberg atoms

The first experimental signatures of interactions between Rydberg atoms have been detected as broadening mechanisms of energy transfer resonances [168, 169]. The strong interactions between atoms in the Rydberg state constitute the main reason why Rydberg platforms are useful tools for the study of quantum science. These interactions originate from the large dipole moment possessed by Rydberg atoms, which scales quadratically with the principal quantum number of the corresponding Rydberg state, as shown by Eq. (6). Strictly speaking, the dipole moment of an isolated Rydberg state is identically zero, due to the selection rules of electric dipole moment transitions. However, an isolated atom can possess large dipole moments by slightly mixing Rydberg states with opposite parity. This mixing can be induced for example by coupling different Rydberg states through a microwave driving or by the presence of a second Rydberg atom nearby creating an induced dipole moment. The mixing induced by a microwave source can be also used to engineer tailored interaction potential between Rydberg states, as we show in the Section 2.5. We proceed now by deriving the expression of the electrostatic interactions between two Rydberg atoms.

2.2.1 Electrostatic interactions

Let us consider two atoms that are in two excited Rydberg states $|e_1\rangle = |n_1, l_1, j_1, m_{j1}\rangle$ and $|e_2\rangle = |n_2, l_2, j_2, m_{j2}\rangle$. At very large distances, the Hamiltonian of the system

is simply given by the sum of the two single-atom Hamiltonians and the product state $|e_1, e_2\rangle$ is an eigenstate with eigenvalue $E_{e_1,e_2} = E_{n_1,l_1,j_1,m_{j1}} + E_{n_2,l_2,j_2,m_{j2}}$, as given by the Rydberg-Ritz formula (5). When the atoms get closer to each other, the interaction term

$$H_{\text{int}}(\boldsymbol{R}, \boldsymbol{r}_1, \boldsymbol{r}_2) = \frac{e^2}{4\pi\epsilon_0}\left(\frac{1}{|\boldsymbol{R}+\boldsymbol{r}_2-\boldsymbol{r}_1|} + \frac{1}{|\boldsymbol{R}|} - \frac{1}{|\boldsymbol{R}-\boldsymbol{r}_1|} - \frac{1}{|\boldsymbol{R}+\boldsymbol{r}_2|}\right)$$

is added to the Hamiltonian, where $\boldsymbol{R}$ is the distance vector between the ionic cores and $\boldsymbol{r}_1$ and $\boldsymbol{r}_2$ are the distance vectors of the electrons from the respective atom, as shown in Fig. 7. The first two terms describe the electrostatic repulsive interaction between the electrons and the ionic cores, respectively, while the last two terms represent the electrostatic attractive interaction between one ionic core and the electron of the other atom. Under the condition $|\boldsymbol{r}_1|, |\boldsymbol{r}_2| \ll |\boldsymbol{R}|$, Eq. (2.2.1) can be rewritten as a multipole expansion [170], which, to leading order, yields the dipole-dipole interaction Hamiltonian

$$V_{\text{dd}}(\boldsymbol{R}) = \frac{\boldsymbol{d}_1 \cdot \boldsymbol{d}_2 - 3(\boldsymbol{d}_1 \cdot \boldsymbol{n}_{\boldsymbol{R}})(\boldsymbol{d}_2 \cdot \boldsymbol{n}_{\boldsymbol{R}})}{4\pi\epsilon_0 R^3}, \tag{7}$$

where $\boldsymbol{d}_i = e\boldsymbol{r}_i$, $i = 1, 2$ are the dipole moment operators of the two atoms and $\boldsymbol{n}_{\boldsymbol{R}} = \boldsymbol{R}/R$ is the unit vector along the interatomic distance. The dipole-dipole interaction general gives rise to different types of interactions that decay algebraically with the interatomic distance. The most relevant ones are the van der Waals interaction (decaying as R^{-6}) and the dipolar exchange interaction (decaying as R^{-3}).

2.2.2 Van der Waals interaction

Two atoms that are excited to the same Rydberg state $|e\rangle$ are energetically detuned from other pair states $|e_i, e_j\rangle$ by the so-called Förster defect $\Delta_{ij} = 2E_e - E_{e_i} - E_{e_j}$, which corresponds to the energy difference between two isolated pair states. The

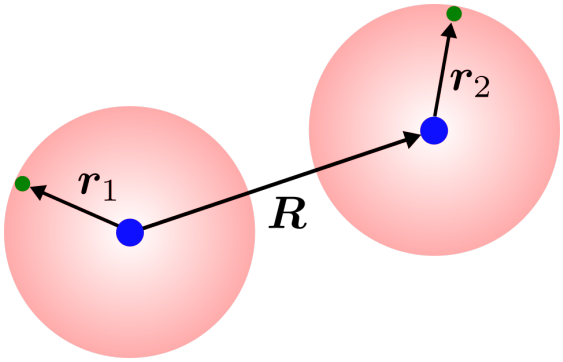

Figure 7: **Illustration of two interacting Rydberg atoms.** Each atom consists of a ionic core (in blue) and a Rydberg electron (in green).

atoms of the pair state $|e, e\rangle$ do not directly interact via the dipole-dipole interaction (7) because of the selection rules of the electric dipole operator. However, by virtually populating other Rydberg states through the dipole-dipole interaction, the pair state $|e, e\rangle$ gets an energy shift given by

$$V_{\mathrm{vdW}}(\boldsymbol{R}) = \sum_{i,j} \frac{|\langle e, e|V_{\mathrm{dd}}\boldsymbol{R})|e_i, e_j\rangle|^2}{\Delta_{ij}} = \frac{C_6(\theta)}{R^6}, \tag{8}$$

which shows the typical R^{-6} dependence of the van der Waals interaction. The coefficient $C_6(\theta)$ results from the sum of the terms contributing to the second-order process that lead to the interaction. In general, it depends on the angle θ, which is the angle between the interatomic axis and the quantization axis of the atoms where the projection of the total angular momentum m_j is defined. In many cases, there is only one pair state $|e', e''\rangle$ that mostly contribute to the sum in Eq.(8), because of the small Förster defect $\Delta_{e',e''}$. In this case the sign of the interaction simply depends on the sign of the contributing Förster defect. Moreover, the energy splitting between states with different total angular momentum J is generally smaller than the Förster defect. As a result, the sum in Eq. (8) typically includes terms with the allowed quantum numbers j and m_j, which leads to an isotropic coefficient $C_6(\theta) \simeq C_6$ [171]. Its scaling with the effective quantum num-

ber is $C_6 \propto (n^*)^{11}$, since the interaction matrix element $\langle e, e|V_{\rm dd}\boldsymbol{R})|e_i, e_j\rangle \propto (n^*)^4$ and the Förster defects $\Delta_{ij} \propto (n^*)^{-3}$. This clearly shows why atoms excited to Rydberg states with large n are subject to strong electrostatic interactions.

2.2.3 Förster resonances and dipolar exchange interaction

When the Förster defects are not much larger than the interaction matrix elements, the perturbative expansion leading to Eq. (8) is no more possible. This typically happens when the atoms are close to each other or when the Förster defects are very small. In the first case, one observes a transition from a R^{-6} scaling of the interaction at large interatomic distance to a R^{-3} scaling when the atoms get closer. In the second case, the perturbative treatment breaks down even at large interatomic distances, leading to a R^{-3} scaling of the interaction. Such condition, called Förster resonance [88], takes place when two distinct pair states, $|e, e\rangle$ and $|e', e''\rangle$, are energetically quasi-degenerate. Förster resonances can also be experimentally realized by applying fine-tuned electric fields that shift the energy levels of Rydberg states [172, 173]. Such situation induces some coherent quantum oscillations between the two states, as observed experimentally in Ref. [174]. Another similar situation is when two atoms are prepared in two states that are coupled through the dipole operator. This is realized when the atoms are in the pair state $|e, e'\rangle$, with non vanishing dipole matrix element $\langle e|\boldsymbol{d}|e'\rangle$. Such state can be experimentally created by preparing an atom in a P-state and the other atom in a S- or D-state. If this pair state is energetically well separated from all the other pair states, the system undergoes coherent quantum oscillations between the states $|e, e'\rangle$ and $|e', e\rangle$ at a frequency proportional to the dipole-dipole interaction between them. The coupling between these two pair states is called dipolar exchange interaction [175] and decays with the interatomic distance as R^{-3}.

Property	Expression	Scaling	Value (for $70P_{1/2}$ of ^{87}Rb)
Binding energy	E_{nlj}	$(n^*)^{-2}$	-725 GHz
Förster defects	Δ_{ij}	$(n^*)^{-3}$	-0.78 GHz
Red. mat. elem. $\|e\rangle \leftrightarrow \|e'\rangle$	$\langle e\|\|\boldsymbol{r}\|\|e'\rangle$	$(n^*)^2$	5162 ea_0
Red. mat. elem. $\|\mathrm{GS}\rangle \leftrightarrow \|e\rangle$	$\langle e\|\|\boldsymbol{r}\|\|\mathrm{GS}\rangle$	$(n^*)^{-\frac{3}{2}}$	-0.0015 ea_0
Spontaneous decay rate	Γ_{sp}	$(n^*)^{-3}$	1.2 ms^{-1}
Black-body ind. decay rate	Γ_{bb}	$(n^*)^{-2}$	3.9 ms^{-1}
Van der Waals coefficient	C_6	$(n^*)^{11}$	-27 GHz μm^6
Blockade radius	R_b	$(n^*)^{\frac{11}{6}}$	3.1 μm

Table 1: **Summary of the main properties of Rydberg atoms.** For each property, the expression used in the text, the scaling with the effective quantum number n^* and its numerical value are given. The latter is computed for ^{87}Rb atoms in the $70P_{1/2}$ state, using the ARC package [176]. The Förster defect is computed with respect to the $70S_{1/2}$ and $71S_{1/2}$ states. The reduced matrix elements are computed with $|e'\rangle = |70S_{1/2}\rangle$ and $|\mathrm{GS}\rangle = |5S_{1/2}\rangle$ respectively. The black-body induced decay rate is computed for a temperature $T = 300$ K. The value of the blockade radius follows from Eq. (11) by choosing a typical value of the Rabi frequency $\Omega = 2\pi \times 5$ MHz.

2.3 Rydberg blockade

In the last decades, the fields of quantum computation and quantum information have experienced an unprecedented development and Rydberg atoms have constituted one of the most promising platforms for these fields, thanks to the strong interactions between them when excited to the Rydberg state [86, 87]. These interactions can be so strong that a single atom excited to the Rydberg state prevents other neighbouring atoms to be excited to the Rydberg state. This blockade effect is known as Rydberg blockade and has been successfully exploited in many

quantum information tasks [88, 177]. In this section we summarize the theoretical framework that describes the Rydberg blockade.

Let us consider an atom in the ground state $|g\rangle$ which is coupled to an excited Rydberg state $|r\rangle$ through a resonant laser with Rabi frequency Ω, as shown in Fig. 8a. In the interacting picture, the system is described by the single-body Hamiltonian ($\hbar = 1$)

$$H_0 = \frac{\Omega}{2}\left(|g\rangle\langle r| + |r\rangle\langle g|\right). \tag{9}$$

The simple model of the atom as a two-level system, which considerably simplifies the calculations, is justified because the laser is highly off-resonant with respect to all the other Rydberg states. The atom, initialized in $|g\rangle$, performs Rabi oscillations between $|g\rangle$ and $|r\rangle$ at a frequency Ω. Adding a second atom in the system introduces an additional term to the Hamiltonian given by the interaction $V(R)$ between the two atoms when both are excited to the Rydberg state. The Hamiltonian then reads

$$H = \frac{\Omega}{2}\left[\left(|g\rangle_1\langle r|_1 \otimes \mathbb{1}_2 + \mathbb{1}_1 \otimes |g\rangle_2\langle r|_2\right) + \text{h.c.}\right] + V(R)\,|r,r\rangle\langle r,r|\,.$$

The dynamics of the two-atom system strongly depends on the interatomic distance R. For large R where $V(R) \simeq 0$, the two atoms perform Rabi oscillations independently on each other and their dynamics is completely described by the single-body Hamiltonian (9). For small interatomic distance where $V(R) \gg |\Omega|$, the state $|r,r\rangle$ is energetically not accessible and the relevant part of the Hilbert space for the system's dynamics is spanned by the remaining three states $\{|g,g\rangle, |g,r\rangle, |r,g\rangle\}$. To show that, we perform a change of basis to $\{|g,g\rangle, |g,r\rangle^+, |r,g\rangle^-, |r,r\rangle\}$, with $|g,r\rangle^\pm = \frac{1}{\sqrt{2}}(|g,r\rangle \pm |r,g\rangle)$. By further moving to the rotating frame defined by $U = e^{-iV(R)|r,r\rangle\langle r,r|t}$, the transformed Hamiltonian $H' = U^\dagger H U + i\dot{U}^\dagger U$ is given by

$$H' = \frac{\sqrt{2}\Omega}{2}\left(|g,g\rangle\langle g,r|^+ + |g,r\rangle^+\langle r,r|\,e^{-iV(R)t} + \text{h.c.}\right). \tag{10}$$

One then immediately realizes that Hamiltonian (10) couples $|g,g\rangle$ only to the state $|g,r\rangle^+$ with an enhanced Rabi frequency $\sqrt{2}\Omega$, while the state $|r,g\rangle^-$ is completely decoupled from the other three states. By employing the rotating wave approximation (RWA) with $V(R) \gg \Omega$, the second term of Eq. (10) can be neglected, and one obtains enhanced Rabi oscillations between $|g,g\rangle$ and $|g,r\rangle^+$. These oscillations, induced by the Rydberg blockade, have been successfully observed experimentally in Ref. [178]. The underlying mechanism can also be generalized to a system of N atoms where the Rabi frequency is enhanced by a factor $\sqrt{N}$ [77, 78]. Furthermore, Rydberg-Rydberg interactions impede the Rydberg excitation of other atoms when they are larger than the bandwidth of the coupling, which is given by the Rabi frequency Ω. In this case, indeed, the complex exponential $e^{-iV(R)t}$ oscillates so fast that it can be safely ignored and, as a result, the doubly excited Rydberg state $|r,r\rangle$ cannot be pumped from $|g,r\rangle^+$: this is known as the Rydberg blockade. The blockade radius is accordingly defined as the distance at which the interaction equals the Rabi frequency, i.e., $V(R_b) = \Omega$, providing, in the case of van der Waals interaction $V(R) = C_6/R^6$,

$$R_b = \left(\frac{|C_6|}{\Omega}\right)^{\frac{1}{6}}. \tag{11}$$

As a result, the atoms that are closer than R_b to a Rydberg excitation cannot be excited to the Rydberg state. This mechanism introduces kinetic constraints in the dynamics and makes strongly interacting Rydberg systems ideal platforms to study kinetically constrained quantum systems [179].

2.4 Rydberg facilitation

The opposite situation to the Rydberg blockade is known as the Rydberg facilitation (or anti-blockade). It has been introduced in 2007 by Ref. [92] and it relies

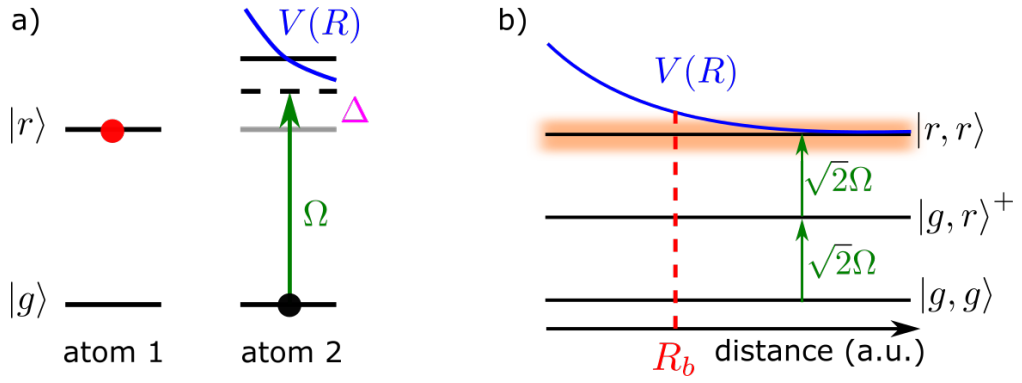

Figure 8: **Rydberg blockade.** a) Atoms can be modeled as two-level systems, where $|g\rangle$ represents the ground state and $|r\rangle$ denotes the Rydberg state. The ground state and the Rydberg state are coupled through a laser with Rabi frequency Ω and detuning Δ. An atom close to a Rydberg excitation is subject to the interaction potential $V(R)$ that shifts the Rydberg state. b) Under the Rydberg blockade condition, the Hilbert space is spanned by the states $\{|g,g\rangle, |g,r\rangle^+, |r,r\rangle\}$, which are coupled with an enhanced Rabi frequency $\sqrt{2}\Omega$. The state $|r,r\rangle$ gets shifted by the Rydberg interaction. The orange, shaded region shows the width of Ω. R_b is the blockade radius, whereby the interaction shift is larger than the broadening mechanism, allowing only one excitation to be present.

on the cancellation of the interaction energy shift by the laser detuning. If the driving laser is off-resonant with detuning $\Delta = \omega_{\text{at}} - \omega_{\text{L}}$, where ω_{at} and ω_{L} are the atomic transition frequency and the laser frequency respectively, Eq. (10) gets modified to

$$H' = \frac{\sqrt{2}\Omega}{2}\left[|g,g\rangle\langle g,r|^+ e^{-i\Delta t} + |g,r\rangle^+\langle r,r| e^{-i(\Delta+V(R))t} + \text{h.c.}\right].$$

If $\Delta = -V(R)/2$ and $|\Delta| \gg |\Omega|$, one employs the RWA to get the effective Hamiltonian [180]

$$H_{\text{eff}} = \frac{\Omega^2}{2\Delta}\left[(|g,g\rangle + |r,r\rangle)(\langle g,g| + \langle r,r|) - 2\,|g,r\rangle^+\langle g,r|^+\right],$$

which shows that the state $|g,g\rangle$ is converted to the state $-|r,r\rangle$ at time $t = \pi|\Delta|/\Omega^2$, thus implementing Rydberg facilitation.

Another approach to get facilitation which is also easily generalizable to multi-atom systems consists in two sequential steps. First, we excite one atom to the Rydberg state by applying a π-pulse with Rabi frequency Ω. Subsequently, we couple the ground state to the Rydberg state of the second atom with an off-resonant laser with detuning Δ and same Rabi frequency. After the π-pulse applied to the first atom, the Hamiltonian of the system, in the interaction picture, is given by

$$H = \frac{\Omega}{2}\left[|rg\rangle\langle rr| e^{-i(\Delta+V(R))t} + \text{h.c.}\right] \tag{12}$$

after moving to the rotating frame defined by $U = e^{-iV(R)|r,r\rangle\langle r,r|t}$. If the facilitation condition $\Delta + V(R) = 0$ is satisfied, the transition $|r,g\rangle \to -i|r,r\rangle$ is generated at time $t = 2\pi/\Omega$, thus achieving Rydberg facilitation.

2.4.1 Effective model for Rydberg facilitation

Generalizing this mechanism to multi-atom systems, Eq. (12) shows that a single Rydberg excitation can trigger the excitation of the neighboring atoms, which in turn can excite their neighbouring atoms etc., leading to an "avalanche" of Rydberg excitations. To be concrete, let us consider a one-dimensional chain of atoms held in harmonic traps and separated by a regular lattice spacing a. Atoms are modeled as two-level systems where the ground state and Rydberg state are denoted by $|\downarrow\rangle$ and $|\uparrow\rangle$ respectively. Thus we identify $|g\rangle = |\downarrow\rangle$ and $|e\rangle = |\uparrow\rangle$. The ground state and the Rydberg state are off-resonantly coupled through a laser with Rabi frequency Ω and detuning Δ, as shown in Fig. 9a. In the interaction picture and neglecting all the interactions beyond the nearest-neighbor ones (V_{NN}), the Hamiltonian of the system is given by

$$H = \sum_{j=1}^{N}\left(\frac{\Omega}{2}\sigma_j^x + \Delta n_j + V_{\text{NN}} n_j n_{j+1}\right).$$

The operator $\sigma^x = |\downarrow\rangle\langle\uparrow| + |\uparrow\rangle\langle\downarrow|$ describes the coupling between the ground and Rydberg state, and $n = |\uparrow\rangle\langle\uparrow|$ is the projector onto the Rydberg state. Periodic boundary transitions are also adopted. Imposing the facilitation condition $V_{\mathrm{NN}} + \Delta = 0$ (see Fig. 9a) yields

$$H = \sum_{j=1}^{N} \left[\frac{\Omega}{2} \sigma_j^x + \Delta n_j (1 - n_{j+1}) \right].$$

We further assume that $|\Delta| \gg \Omega$, so as to energetically suppress spin flips if not in the presence of a single neighboring Rydberg excitation. This means that transitions like $|\downarrow\downarrow\downarrow\rangle \leftrightarrow |\downarrow\uparrow\downarrow\rangle$ or $|\uparrow\downarrow\uparrow\rangle \leftrightarrow |\uparrow\uparrow\uparrow\rangle$ are not allowed. Defining a "cluster" as a sequence of consecutive Rydberg excitations, we get that clusters cannot be created or disappear, nor can they split or merge. In other words, the facilitation dynamics conserves the total number of clusters N_{cl} in the chain. The number of clusters is equal to the number of right kinks $\uparrow\downarrow$, i.e., $N_{\mathrm{cl}} = \sum_j n_j(1 - n_{j+1})$. Then the Hamiltonian can be written as

$$H = \Delta N_{\mathrm{cl}} + \sum_{j=1}^{N} \frac{\Omega}{2} \sigma_j^x P_j,$$

where we define the projector $P_j = n_{j-1} + n_{j+1} - 2n_{j-1}n_{j+1}$. By restricting to the special case $N_{\mathrm{cl}} = 1$, we can express the state of the system with only two coordinates: the center of mass c and the relative coordinate r of the cluster (see Fig. 9b). The first can have integer or half-integer values, $c = \frac{1}{2}, 1, \frac{3}{2}, \ldots, N$, while the second can only have integer values, $r = 1, 2, 3, \ldots, N-1$. Since a cluster only grows and shrinks at its edges, a given state $|c\rangle \otimes |r\rangle$ is coupled to four states, corresponding to the four clusters that can be obtained by expanding or shrinking the cluster at the left or at the right edge, as shown in Fig. 9c. Using this notation, the Hamiltonian can be written in terms of the new coordinates as

$$H_{\mathrm{eff}} = \Omega \sum_{c=\frac{1}{2}}^{N} \sum_{r=1}^{N-2} \left[|c + \tfrac{1}{2}\rangle\langle c| \otimes (|r+1\rangle\langle r| + \mathrm{h.c.}) + \mathrm{h.c.} \right]. \tag{13}$$

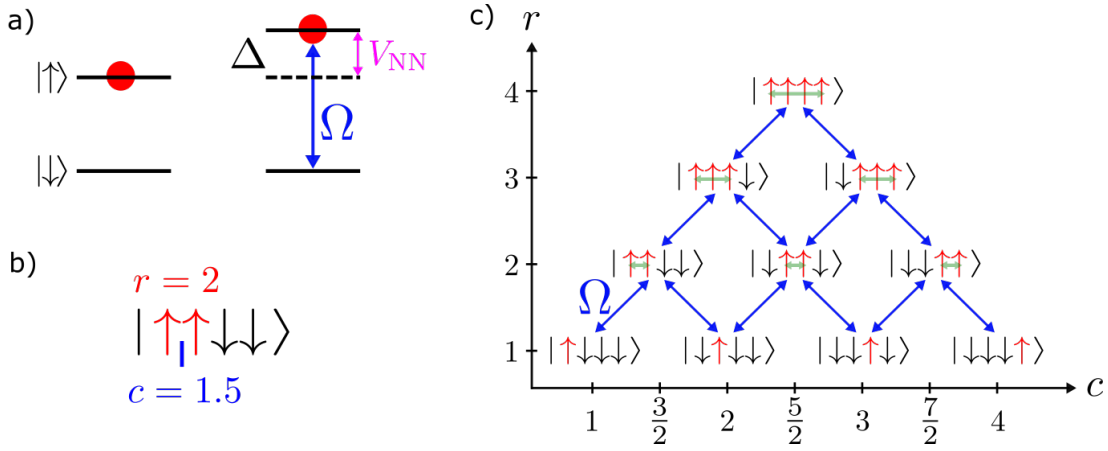

Figure 9: **Rydberg facilitation.** a) Using the spin language, the ground state is denoted with $|\downarrow\rangle$ and the Rydberg state with $|\uparrow\rangle$. They are coupled through a laser with Rabi frequency Ω and detuning Δ. An atom close to a Rydberg excitation is subject to the interaction potential V_{NN} that shifts the Rydberg state. The facilitation constraint is implemented if $\Delta + V_{\mathrm{NN}} = 0$. b) A cluster of Rydberg excitations is described by its center of mass position c and its size r. c) Schematic picture showing how the cluster states are coupled through Hamiltonian (13).

This Hamiltonian is the starting point to investigate the facilitation constraint in a one-dimensional chain. The introduction of the coordinates c, r is particularly advantageous as it allows to reduce the complex many-body problem to a much simpler two-body problem.

2.5 Engineering interaction potentials via microwave driving

In this section we study a system of two atoms subject to a microwave (MW) field that couples Rydberg states with different parity. The resulting mixing between those states can be exploited to engineer interaction potentials that feature a minimum, similar in shape to the Lennard-Jones potential. This potential profile can be convenient for the experimental implementation of the facilitation constraint

with Rydberg atoms. Indeed, if the lattice spacing is designed to coincide with the position of the minimum, then the Rydberg excitations in the cluster do not feel any mechanical force since they are located at a distance where the interaction potential is locally flat. This idea is applicable if one neglects all the interactions beyond the nearest-neighbor ones: for this reason, the lattice spacing needs to be large enough to fulfill this approximation.

To be concrete, let us consider a system composed of two atoms modeled as two-level systems, where the states are labeled as $|s\rangle$ and $|p\rangle$. These represent two Rydberg states with opposite parity, an S-state and a P-state. In contrast to the previous sections, our focus here is on the Rydberg manifold, where non-trivial dynamics occurs through the MW driving coupling the two states. The Hamiltonian of the system reads

$$H = H_{\mathrm{MW}} \otimes \mathbb{1}_2 + \mathbb{1}_1 \otimes H_{\mathrm{MW}} + V_{\mathrm{dd}}, \tag{14}$$

where H_{MW} is the Hamiltonian describing the MW driving and V_{dd} is the dipole-dipole interaction given by Eq. (7).

Under the assumption that the atoms are sufficiently far apart, one can treat V_{dd} as a perturbation. Equation (14) is then written as a sum of an unperturbed Hamiltonian $H_0 = H_{\mathrm{MW}} \otimes \mathbb{1}_2 + \mathbb{1}_1 \otimes H_{\mathrm{MW}}$ and the perturbation V_{dd}:

$$H = H_0 + V_{\mathrm{dd}}.$$

In the basis $\{|ss\rangle, |sp\rangle, |ps\rangle, |pp\rangle\}$, H_0 and V_{dd} can be written in matrix form as

$$H_0 = \begin{pmatrix} 0 & \Omega & \Omega & 0 \\ \Omega & \Delta & 0 & \Omega \\ \Omega & 0 & \Delta & \Omega \\ 0 & \Omega & \Omega & 2\Delta \end{pmatrix},$$

where Ω is the Rabi frequency and Δ is the detuning of the MW field, and

$$V_{\mathrm{dd}} = \begin{pmatrix} 0 & 0 & 0 & \langle pp|V_{\mathrm{dd}}|ss\rangle \\ 0 & 0 & \langle ps|V_{\mathrm{dd}}|sp\rangle & 0 \\ 0 & \langle sp|V_{\mathrm{dd}}|ps\rangle & 0 & 0 \\ \langle ss|V_{\mathrm{dd}}|pp\rangle & 0 & 0 & 0 \end{pmatrix},$$

since terms like $\langle ss|V_{\mathrm{dd}}|ss\rangle$, $\langle ss|V_{\mathrm{dd}}|sp\rangle$, $\langle pp|V_{\mathrm{dd}}|pp\rangle$, ... vanish due to the selection rules. The unperturbed eigenvalues of H_0 are $E_+^{(0)} = \Delta + \sqrt{\Delta^2 + 4\Omega^2}$, $E_-^{(0)} = \Delta - \sqrt{\Delta^2 + 4\Omega^2}$ and $E_{d_1}^{(0)} = E_{d_2}^{(0)} = \Delta$.

We further assume for simplicity that the nonzero matrix elements of V_{dd} are all equal to

$$\langle pp|V_{\mathrm{dd}}|ss\rangle = \langle ps|V_{\mathrm{dd}}|sp\rangle = \langle sp|V_{\mathrm{dd}}|ps\rangle = \langle ss|V_{\mathrm{dd}}|pp\rangle = -\frac{\mu^2}{4\pi\epsilon_0 R^3},$$

where μ is the dipole matrix element coupling the state $|s\rangle$ to the state $|p\rangle$ and R is the distance between the two atoms. Then, by applying degenerate second-order perturbation theory, one finds that, in the dressing regime $\Omega \ll |\Delta|$, the eigenvalue $E_+^{(0)}$ gets modified to

$$E_+(R) = E_+^{(0)} - \frac{C_3}{R^3} + \frac{C_6}{R^6}, \tag{15}$$

where

$$C_3 = 4\frac{\Omega^2}{\Delta^2}\frac{\mu^2}{4\pi\epsilon_0} \qquad \text{and} \qquad C_6 = \frac{\Delta^2 + 6\Omega^2}{2\Delta^3}\left(\frac{\mu^2}{4\pi\epsilon_0}\right)^2$$

are two coefficients that depend on the parameters of the MW field. The energy curve $E_+(R)$ given by Eq. (15) is plotted in Fig. 10, which shows both results obtained from exact diagonalization of Hamiltonian (14) and the perturbative expansion (15). Its functional form, reminiscent of molecular potentials, features a minimum that originates from an avoided crossing between two energy levels due to the dipole-dipole interaction.

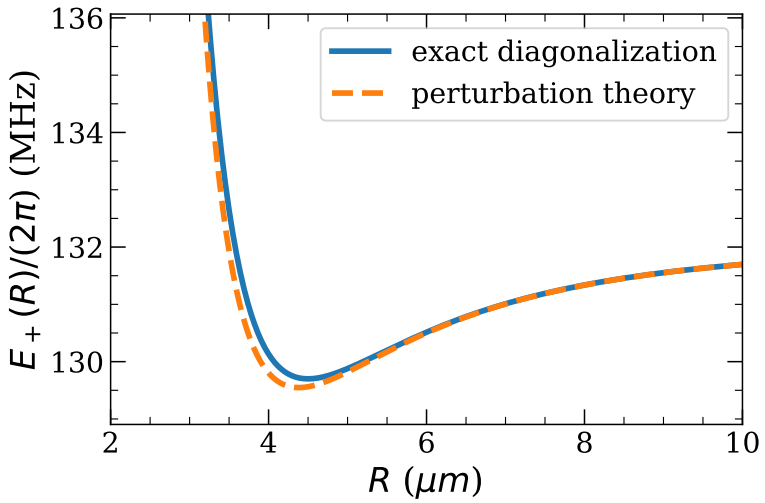

Figure 10: **MW-induced molecular-like potential**. The energy curve $E_+(R)$ features a minimum that emerges from an avoided crossing. The eigenvalue obtained from exact diagonalization of Hamiltonian (14) is well reproduced by the perturbative result (15). The parameters used in this plot are $\Omega = 2\pi \times 20$ MHz and $\Delta = 2\pi \times 60$ MHz, while the states are $|s\rangle = |60S_{\frac{1}{2}}\rangle$ and $|p\rangle = |60P_{\frac{3}{2}}\rangle$ of rubidium atom.

It is also possible to estimate the position of the minimum R_{min} of the potential curve $E_+(R)$. In general, it is given by

$$R_{\text{min}} = \sqrt[3]{\frac{\Delta^2 + 6\Omega^2}{2\Omega^2\Delta}\frac{\mu^2}{4\pi\epsilon_0}},$$

which, in the dressing regime $\Omega \ll \Delta$, can be approximated as

$$R_{\text{min}} \simeq \sqrt[3]{\frac{\Delta}{\Omega}}\sqrt[3]{\frac{1\,\text{GHz}}{\Omega}}\mu m, \tag{16}$$

where we have used a typical value for the dipole moment $\mu = 1.5 \times 10^3 e a_0$ to get the estimate. Since $\Delta/\Omega \gg 1$, R_{min} can take values of few micrometers, corresponding to the order of magnitude of the lattice spacing implemented in modern Rydberg quantum simulators.

The potential depth $\delta E = \left|E_+(R_{\text{min}}) - E_+^0\right|$ at the minimum can be also estimated.

It is given by

$$\delta E \simeq 8\Omega \left(\frac{\Omega}{\Delta}\right)^3, \tag{17}$$

which, in the dressing regime, takes small values, of the order of hundreds kHz. However, the dip also appears for intermediate values of Δ/Ω and its depth can reach values of few MHz, as shown in Fig. 10.

The engineering of molecular-like potentials through MW dressing holds promises for an efficient experimental implementation of the facilitation constraint. For example, if performed on a one-dimensional chain of optical tweezers separated by a lattice spacing equal to R_{min}, two nearest-neighbor atoms excited to the Rydberg state would not be subject to mechanical forces and would remain at the center of the trap throughout the facilitation dynamics. Moreover, if the potential depth reaches values of few MHz, bound states of Rydberg atoms can emerge, providing technological advantage for the implementation of the facilitation dynamics.

3 The physics of stochastic resetting

In this chapter we review the physics of stochastic resetting, which is a topic in statistical physics that has attracted a lot of interest in recent years (for a comprehensive review see [115]). Consider a system evolving with a certain dynamics, either deterministic or stochastic, and add the condition that at random times the system interrupts its dynamics, is reset to a certain state and then restarts the dynamics again. Because of the competition between the underlying dynamics and resetting, the system reaches a nontrivial non-equilibrium stationary state (NESS), exhibiting features that are very general and hold for various dynamics. The aim of this chapter is to review the developments of this topic. We start by presenting the simplest system in which resetting has a nontrivial impact on its stationary properties, i.e., a single particle undergoing diffusion in one dimension which is reset to its initial position at a constant rate. We then proceed with the derivation of the theoretical framework needed to study classical systems subject to stochastic resetting, including notions of renewal theory. We conclude the chapter focusing on the dynamics of quantum systems in presence of stochastic resetting.

3.1 Diffusion with stochastic resetting

The concept of stochastic resetting was introduced in 2011 in Ref. [116], in which the authors considered a particle undergoing diffusion in one dimension and subject to Poissonian resetting. This constitutes an important case study to understand the main properties of the resulting NESS, which generally hold for various stochastic processes. Poissonian resetting means that the diffusion is interrupted at a constant rate r: this assumption simplifies the calculations but more general settings with non-Poissonian resetting have also been studied, as we show later.

Let us consider a particle undergoing diffusion on a line from the initial position x_0 and subject to resetting with rate r to position x_r. In general, x_0 and x_r are distinct positions, although in certain cases it may be useful to set them to be equal. The position of the particle is updated by the stochastic rule

$$x(t+dt) = \begin{cases} x_r & \text{with probability} \quad rdt \\ x(t) + \xi(t)(dt)^{\frac{1}{2}} & \text{with probability} \quad 1 - rdt \end{cases} \tag{18}$$

where $\xi(t)$ is a Gaussian random variable with

$$\langle \xi(t) \rangle = 0 \quad \text{and} \quad \langle \xi(t)^2 \rangle = 2D, \tag{19}$$

where D is the diffusion constant. The resulting dynamics of the particle is therefore a mixture of ordinary diffusion and resetting to position x_r. Denoting the probability density of the particle to be at position x at time t as $p(x,t)$, it is possible to obtain a master equation for it. From the update rule (18) and averaging over events in the infinitesimal time interval $[t, t+dt]$, one gets

$$p(x, t+dt) = rdt\, \delta(x - x_r) + (1 - rdt) \int \mathcal{D}\xi\, p(x - \xi(dt)^{\frac{1}{2}}, t),$$

where the integral $\int \mathcal{D}\xi$ indicates the average over the noise distribution. Expanding in dt, one obtains

$$\begin{aligned} p(x, t+dt) \;\; = \;\; & rdt\, \delta(x - x_r) \\ & + (1 - rdt) \int \mathcal{D}\xi \left[p(x,t) - \xi(dt)^{\frac{1}{2}} \frac{\partial p(x,t)}{\partial x} + \frac{\xi^2}{2} dt \frac{\partial^2 p(x,t)}{\partial x^2} + \dots \right]. \end{aligned}$$

Evaluating the integrals making use of Eq. (19) and taking the limit $dt \to 0$ yields the master equation for $p(x,t)$

$$\frac{\partial p(x,t)}{\partial t} = D \frac{\partial^2 p(x,t)}{\partial x^2} - rp(x,t) + r\delta(x - x_r), \tag{20}$$

with initial condition $p(x,0) = \delta(x - x_0)$. This equation has a very transparent physical interpretation. The first term on the right hand side represents the diffusive expansion of the probability, the second term denotes the loss of probability

from x due to resetting to x_r and the last term expresses the probability gain at x_r due to resetting from position x. For $t \to \infty$, as we see later, the system reaches a non-equilibrium stationary state, where the global balance condition is satisfied, whereas detailed balance is not fulfilled as there is circulation of probability at x_r due to the loss and gain terms in Eq. (20).

3.1.1 Renewal equation approach

Instead of dealing with the master equation, there is an equivalent and intuitive approach that indeed gives the solution to Eq. (20), which is based on a renewal equation. In absence of resetting ($r = 0$), the diffusive Green's function (or propagator), denoted with $G_0(x, t|x_0)$, satisfies the diffusion equation

$$\frac{\partial G_0(x,t|x_0)}{\partial t} = D\frac{\partial^2 G_0(x,t|x_0)}{\partial x^2},$$

with initial condition $G_0(x, 0|x_0) = \delta(x - x_0)$. Its solution provides the well known Gaussian expression

$$G_0(x,t|x_0) = \frac{1}{\sqrt{4\pi D t}} \exp\left(-\frac{|x-x_0|^2}{4Dt}\right), \tag{21}$$

characterized by a variance that increases linearly in time.

In the presence of resetting, the probability density of the particle to be at position x at time t, $p(x, t)$, is the result of two contributions. One is given by ordinary diffusion up to time t, which happens when no reset events take place in $[0, t]$. This occurs with probability e^{-rt}. The second contribution comes from summing over trajectories where the last reset event happens at time $t-\tau$. This occurs with probability density $re^{-r\tau}$. Indeed, it corresponds to the occurrence of a reset event at time $t - \tau$, which happens with probability $rd\tau$, followed by no reset events

in $[t-\tau, t]$, which occurs with probability $e^{-r\tau}$. These considerations lead to the renewal equation

$$p(x,t) = e^{-rt} G_0(x,t|x_0) + r \int_0^t d\tau\, e^{-r\tau} G_0(x,\tau|x_r). \tag{22}$$

The validity of this equation is very general, as it applies to any stochastic process for which the expression of the Green's function is known.

3.1.2 Non-equilibrium stationary state

In the long time limit, the system very generally reaches a non-equilibrium stationary state. Its expression can be straightforwardly derived from Eq. (22) taking the limit $t \to \infty$

$$p_{\rm stat}(x) = r \int_0^\infty d\tau\, e^{-r\tau} G_0(x,\tau|x_r). \tag{23}$$

Mathematically, it is related to the Laplace transform of the Green's function in absence of resetting. In the case of a diffusive particle this integral can be evaluated exactly. Using the identity [181], with $\gamma, \beta > 0$,

$$\int_0^\infty d\tau e^{-\gamma\tau} \tau^{\nu-1} e^{-\beta/\tau} = 2 \left(\frac{\beta}{\nu}\right)^{\nu/2} K_\nu(2\sqrt{\beta\gamma}),$$

where K_ν is the modified Bessel function of the second kind of order ν. In our case, $\nu = 1/2$, which provides $K_{1/2}(z) = (2z/\pi)^{-1/2} e^{-z}$. Using the expression of the diffusive Green's function (21), the stationary probability distribution (23) reads

$$p_{\rm stat}(x) = \frac{\alpha_0}{2} e^{-\alpha_0|x-x_r|}, \tag{24}$$

where $\alpha_0 = \sqrt{r/D}$. One can easily check that this expression is, of course, also the solution of the master equation (20) when the left hand side is set to 0. It shows that resetting changes the functional form of the probability density of the

position of the particle. First of all, the particle turns out to be symmetrically localized around the reset position x_r, as its position probability distribution decays exponentially over the length scale α_0^{-1}. Moreover, it shows a cusp singularity at x_r.

3.2 Generalization of the resetting dynamics

After reviewing perhaps the simplest case of dynamics subject to stochastic resetting, i.e., a diffusive particle in one dimension, we now present some generalizations of the resetting dynamics. We start by analyzing the case of multiple reset positions, which are chosen at every reset event according to a probability distribution. We then study the case when the resetting rate is not a constant number, but a function of the current position of the particle. Finally, we extend the previous results by considering the case of non-Poissonian resetting.

3.2.1 Multiple reset states and spatially dependent resetting

In the presence of multiple reset states, or positions, one can define a resetting distribution $P(x_r)$ such that the particle is reset to $x_r + dx_r$ with probability $P(x_r)dx_r$. The renewal equation (22) becomes

$$p(x,t) = e^{-rt}G_0(x,t|x_0) + r\int_0^t d\tau\, e^{-r\tau} \int dx_r\, P(x_r)G_0(x,\tau|x_r).$$

In the long time limit the stationary probability distribution is

$$p_{\rm stat}(x) = \int dx_r\, P(x_r)p_{\rm stat}(x|x_r),$$

where $p_{\rm stat}(x|x_r)$ denotes the stationary distribution in the presence of resetting to the fixed position x_r. The interpretation of this equation is very intuitive, as the

stationary state is given by averaging over the different stationary distributions with fixed positions according to the probability $P(x_r)$.

We now consider the case in which the resetting rate is not a constant number, but a function of the particle's position. This means that the particle at position x at time t is reset to x_r in the infinitesimal time interval $[t, t+dt]$ with probability $r(x)dt$. The master equation is generalized from (20) to

$$\frac{\partial p(x,t)}{\partial t} = D\frac{\partial^2 p(x,t)}{\partial x^2} - r(x)p(x,t) + \int dx' r(x')p(x',t)\delta(x-x_r),$$

where the last term represents the gain of probability at x_r due to resetting from all the other points x'. This equation is in general difficult to solve, but explicit solutions have been nevertheless found in some specific cases, like in the presence of a non-resetting window of width a around x_r ($r(x) = 0$ for $|x - x_r| < a$ and $r(x) = r$ for $|x - x_r| \geq a$) [155]. Analytical results have also been obtained using a path integral approach [182].

3.2.2 Non-Poissonian resetting

We now extend the formalism presented in the previous sections to the case of non-Poissonian resetting. This means that reset events do not occur at a constant rate r, but are characterized by a generic time-dependent waiting time distribution $w(t)$, that is after a reset the next reset happens in the infinitesimal time interval $[t, t + dt]$ with probability $w(t)dt$. Accordingly, the probability, $q(t)$, that no reset happens for time t, also called the survival probability, is given by

$$q(t) = \int_t^\infty d\tau\, w(\tau).$$

For Poissonian resetting at constant rate r, we recover $w(t) = re^{-rt}$ and $q(t) = e^{-rt}$. In the case of a time-dependent resetting rate $r(t)$, which constitutes an example

of non-Poissonian resetting, we have $w(t) = r(t)e^{-R(t)}$, with $R(t) = \int_0^t r(\tau)d\tau$, and $q(t) = e^{-R(t)}$ [158]. It is important to note that, at each reset event, the resetting rate is also reset: this means that the function $r(t)$ depends on the time elapsed since the last reset event, and not on the absolute time [183]. In this case, the process is still Markovian, as the system forgets the whole history before the last reset. In particular, as it is necessary to keep track of the time elapsed since the last reset, one generally obtains a generalized master equation [132], which extends Eq. (20). Another approach, which we now present, is based on the renewal approach [184, 185, 122].

Let us consider a particle that starts its dynamics from the position x_0. We want to find the expression for $p(x,t)$, that is the probability density that the particle is at position x at time t. In the time interval $[0,t]$ any number of resets may occur, i.e., no resetting at all, one reset, two resets, and so on. Let us first focus on the situation with no resets. This event happens with probability $q(t)$ and, therefore, its contribution to $p(x,t)$ is $q(t)G_0(x,t|x_0)$. In the case of one reset event at time τ_1, the contribution to $p(x,t)$ is

$$\int_0^t d\tau_1\, w(\tau_1)q(t-\tau_1)G_0(x,t-\tau_1|x_r),$$

where $w(\tau_1)d\tau_1$ represents the probability that a reset event happens in the infinitesimal time interval $[\tau_1, \tau_1 + d\tau_1]$, followed by no resets up to time t, which occurs with probability $q(t-\tau_1)$. Analogously, in the case of two reset events, say at times τ_1 and τ_2, the contribution to $p(x,t)$ is

$$\int_0^t d\tau_1 \int_0^{t-\tau_1} d\tau_2\, w(\tau_1)w(\tau_2)q(t-\tau_1-\tau_2)G_0(x,t-\tau_1-\tau_2|x_r).$$

Iterating the procedure for $n > 2$ resets and summing over n, one obtains the probability distribution $p(x,t)$. Thanks to the convolution structure of these ex-

pressions, it is convenient to work in the Laplace space. Defining

$$\tilde{p}(x,s) = \int_0^\infty dt\, e^{-st} p(x,t)$$

as the Laplace transform of $p(x,t)$, one obtains, after applying the Laplace transform and using the geometric series to perform the sum over all possible reset events,

$$\tilde{p}(x,s) = \int_0^\infty dt\, e^{-st} q(t) G_0(x,t|x_0) + \frac{\tilde{w}(s)}{1-\tilde{w}(s)} \int_0^\infty dt\, e^{-st} q(t) G_0(x,t|x_r),$$

where $\tilde{w}(s)$ is the Laplace transform of the waiting time distribution. This equation gets simplified by taking $x_r = x_0$, yielding

$$\tilde{p}(x,s) = \frac{1}{s\tilde{q}(s)} \int_0^\infty dt\, e^{-st} q(t) G_0(x,t|x_0), \tag{25}$$

where we use the identity $\tilde{q}(s) = [1-\tilde{w}(s)]/s$, with $\tilde{q}(s)$ being the Laplace transform of the survival probability.

The stationary state, which is provided by the coefficient of $1/s$ in Eq. (25) in the $s \to 0$ limit according to the final value theorem, is thus given by

$$p_{\rm stat}(x) = \frac{\int_0^\infty dt\, q(t) G_0(x,t|x_0)}{\int_0^\infty dt\, q(t)}, \tag{26}$$

which exists only if the denominator does not diverge. This condition requires the waiting time distribution $w(t)$ to decay faster than $1/t^2$. If this does not occur, then the system does not relax to a stationary state [186].

3.3 Quantum dynamics subject to resetting

The impact of stochastic resetting on a system's dynamics can be also generalized to the quantum case. To be concrete, let us consider a quantum system evolving with a time independent Hamiltonian H from the initial state $|\psi_0\rangle$ as

$$|\psi(t)\rangle = e^{-iHt} |\psi_0\rangle ,$$

where we set $\hbar = 1$. The density matrix $\rho(t) = |\psi(t)\rangle \langle\psi(t)|$ evolves accordingly as

$$\rho(t) = e^{-iHt}\rho_0 e^{iHt},$$

where $\rho_0 = |\psi_0\rangle \langle\psi_0|$. Introducing Poissonian resetting to the initial state, one obtains an update rule analogous to Eq. (18)

$$|\psi(t+dt)\rangle = \begin{cases} |\psi_0\rangle & \text{with probability} \quad rdt \\ (1 - iHdt)\,|\psi(t)\rangle & \text{with probability} \quad 1 - rdt \end{cases}.$$

The dynamics is a mixture of unitary quantum evolution and stochastic resetting to the initial state. In presence of resetting, the density matrix, denoted as

$$\rho_r(t) = |\psi(t)\rangle \langle\psi(t)|\,,$$

becomes stochastic, in the sense that it changes depending on the realization of the reset process. The density matrix observed at time t, given by $\mathbb{E}[\rho_r(t)]$, is obtained by averaging over all the possible reset realizations and satisfies the renewal equation

$$\mathbb{E}[\rho_r(t)] = e^{-rt}e^{-iHt}\rho_0 e^{iHt} + r\int_0^t d\tau\, e^{-r\tau}e^{-iH\tau}\rho_0 e^{iH\tau},$$

where the first term represents absence of resetting in the time interval $[0, t]$ and the second term considers the time evolution from the last reset event that occurs at time $t - \tau$. The stationary density matrix, obtained in the limit $t \to \infty$, is given by

$$\rho_{\text{stat}} = r\int_0^\infty d\tau\, e^{-r\tau}e^{-iH\tau}\rho_0 e^{iH\tau}.$$

As pointed out in Ref. [143], this stationary density matrix maintains nonzero off-diagonal matrix elements in the energy eigenbasis. This is in stark contrast with the reset-free ($r = 0$) time evolution, where the density matrix is diagonal in the eigenbasis of H.

We conclude this section by mentioning that the interruption of the unitary quantum evolution due to stochastic resetting is related to the application of repeated measurements on a quantum system [187]. Moreover, the stationary properties originating from the interplay between unitary evolution and stochastic resetting bear some similarities with dynamical phases of many-body systems undergoing measurement-induced phase transitions [188, 189].

4 Results and discussion

Neutral atoms, trapped in optical lattices or tweezers, constitute a versatile tool to simulate complex many-body phenomena. The concomitant possibility to realize arbitrary lattice geometries and tailor strong electrostatic interactions when they are excited to the Rydberg states make Rydberg quantum simulators ideal to implement generic quantum many-body Hamiltonians. These interactions also enable high-fidelity qubit entanglement through the Rydberg blockade, which prevents the simultaneous excitation of nearby atoms and therefore constitutes an example of a kinetic constraint. Less explored is the opposite situation, called the facilitation (or anti-blockade) constraint, where the interactions shift the otherwise detuned laser in resonance. In this case, only atoms at the correct distance to an already excited atom are resonantly driven by the laser, thereby creating a cluster of excitations. These are subject to strong electrostatic interactions, whose influence on the long-time properties of the system is investigated in our **first work** [190]. We indeed find that the relaxation to an ergodic state is prevented by the onset of Bloch oscillations in the cluster size.

Contrary to the blockade constraint, facilitation is more challenging to implement in current Rydberg quantum simulators. The reason for this difficulty is that facilitation is particularly affected by mechanical effects and position disorder. While the blockade constraint restricts the evolution to states with approximately zero interaction energy, the facilitation constraint relies on canceling the interaction energy with single-atom energy shifts. The resulting Rydberg aggregates are thus subject to mechanical forces that displace the atoms, preventing the perfect cancellation of the interaction energy. Furthermore, the position disorder induced by the spreading of the atomic wave functions in the optical traps introduces an additional obstacle to implement facilitation dynamics. In experiments atoms are

typically trapped in optical tweezers and an accurate theoretical description of the facilitation dynamics needs to consider atoms as extended objects, beyond the frozen gas approximation. This approach has two major consequences. First, the interatomic distance is no more equal to the lattice spacing, but becomes a stochastic quantity, due to the atom position uncertainties in the traps caused by quantum fluctuations. This position disorder in turn impacts on the facilitation dynamics since the latter strongly depends on the interatomic distance. Second, the mechanical forces between Rydberg excitations displace the atoms from the center of the traps. This results in a coupling between the (internal) Rydberg dynamics and the (external) vibrational degrees of freedom. Both aspects are addressed in our **second work** [191], in which we derive an effective Hamiltonian that describes the vibrational dressing of the Rydberg excitations. This spin-phonon coupling can be also exploited to study molecular physics at the exaggerated length scales that characterize Rydberg systems. In our **third work** [192] we indeed show how the atomic vibrations in the traps can lead to structural transitions typical of molecules with electronic degeneracy. This phenomenon, known as the Jahn-Teller effect, can be readily explored in artificial Rydberg tweezer molecules at length scales much larger that the ones present in conventional molecules.

The remaining part of our thesis is devoted to the investigation of the interplay between quantum unitary evolution and stochastic resetting in quantum many-body systems. The influence of stochastic resetting on the evolution of closed quantum systems has been analyzed in Ref. [143] using the renewal equation approach. However, a complete characterization of the resulting open system dynamics describing the time evolution of closed quantum systems subject to stochastic resetting is missing. In particular, the impact of resetting on systems displaying a quantum phase transition is not fully understood. In our **fourth work** [193] we establish this connection developing a general theory based on semi-Markov processes [194].

By averaging the unitary time evolution over the reset realizations, we derive an effective non-Markovian open dynamics, described by a generalized Lindblad equation. Furthermore, the resulting non-equilibrium stationary state (NESS) displays signatures of the underlying equilibrium quantum phase transition.

Another interesting question to ask is how resetting impacts on the stationary properties of non-interacting quantum systems. We address this question in our **fifth work** [195], where we consider a system composed of spins that evolve independently with the same single-body Hamiltonian. The system is also subject to stochastic resetting with two distinct reset states. At each reset event, the reset state is chosen according to the outcome of the measurement of the magnetization taken immediately before resetting. We find that the global character of the reset mechanism induces quantum correlation in the NESS despite the system being non-interacting. The NESS also shows critical behavior, which makes this resetting protocol promising for quantum sensing applications.

In the next sections we present in more detail the main results of the thesis.

4.1 Bloch oscillations of Rydberg clusters

The facilitation constraint features interesting dynamical properties that we analyse in our first work [190]. Here we consider a one-dimensional lattice model, where each lattice site hosts an atom modeled as a two-level system. The detuning of the laser that couples the ground state to the Rydberg state is tuned such that the presence of a Rydberg excitation facilitates the nearest-neighbouring (NN) atoms to be coherently excited to the Rydberg state. This leads to the formation of a compact cluster of consecutive Rydberg excitations, which can be labeled by two coordinates, c and r, corresponding to the center of mass position and the size

of the cluster. The system evolves according to Hamiltonian (13) and its dynamics is characterized by freely propagating domain walls (cluster edges). However, residual interactions between Rydberg excitations beyond the NN ones provide an additional linear potential in the cluster size which opposes to its expansion. The new Hamiltonian can then be related to the one of a hopping particle in a tilted lattice, which is a classic problem in condensed matter physics [196, 197, 198] that displays the emergence of so-called Bloch oscillations [199]. We analogously find that the Rydberg cluster undergoes Bloch oscillations which inhibit the relaxation towards an ergodic stationary state. These oscillations, which have shown to signal non-ergodicity in the absence of disorder in other contexts, e.g., when external fields are imposed [200, 201, 202, 203], can be observed in the dynamics of the (Rydberg atom) density and thus are in principle directly accessible in experiments. Using realistic experimental parameters, we estimate their period to be about 20 times smaller than the typical lifetime of the Rydberg states. We also argue that these oscillations lead to an emergent "Hilbert space fragmentation" [204, 205] in many disconnected Hilbert subspaces, reminiscent of fractonic systems [206, 207].

4.2 Phonon dressing of a facilitated Rydberg lattice gas

Contrary to the Rydberg blockade, the facilitation constraint is more challenging to implement in current Rydberg experiments. The reason for this difficulty is that facilitation is particularly affected by mechanical effects and position disorder. Indeed, the resulting Rydberg aggregates are subject to strong mechanical forces that displace the atoms from the center of the traps or even eject them out of the lattice potential, thereby limiting the potential of the experiments. Furthermore, the quantum uncertainty of the atomic position in the trap introduces an additional obstacle to implement the facilitation constraint. These features have been

analyzed in our second work [191], where we model the atoms as extended objects confined in the traps and subject to forces that displace them from the trap centers when they are in the Rydberg state. This results in a nontrivial coupling between the (internal) Rydberg dynamics and the (external) atomic motion. Treating such spin-boson coupling within a perturbative approach, we analytically obtain an effective model that describes the dynamics of the resulting phonon-dressed Rydberg cluster. We find that the avalanche of Rydberg excitations spreading from a single Rydberg excitation under the facilitation condition is strongly suppressed, while for other initial states the expansion is only slowed down. The fact that the single excitation cluster is the only state that is not subject to mechanical forces makes it effectively off resonant from the other states, thereby preventing its expansion. Using Fano resonance theory [208], we derive an expression for the survival probability of the single excitation cluster, finding excellent agreement with numerical simulations based on exact diagonalization.

4.3 Rydberg tweezer molecules

We further explore the spin-phonon coupling arising in Rydberg quantum simulators in our third work [192], where we consider a simple system of three atoms held in harmonic traps and driven by an external laser under the facilitation constraint. The traps are placed at the vertices of an equilateral triangle. We find that the system displays a geometric transition to a deformed configuration given by an equal-weighted quantum superposition of distorted triangular states. We identify this structural change as due to the Jahn-Teller effect, a mechanism of spontaneous symmetry breaking, first studied by H. A. Jahn and E. Teller [209, 210]. This effect is typically found in molecular and solid-state systems in presence of electronic degeneracy, which is spontaneously broken by the geometrical dis-

tortion that minimizes the total energy of the system. Moreover, we find that such distorted triangular configuration exhibits spin-phonon entanglement at the micrometer length scales, which can be experimentally detected through field ionization [211] or via reconstruction of the Wigner function [212, 213]. Such platform highlights the potential of Rydberg tweezer arrays for the exploration of molecular phenomena at the exaggerated length scales [214, 215] typical of Rydberg systems that are not attainable in conventional molecules.

4.4 Designing non-equilibrium states of quantum matter through stochastic resetting

Stochastic resetting, i.e., the halting of a process which is then restarted from a certain configuration, has attracted substantial interest in the last decade for both its conceptual and practical implications. In the realm of classical stochastic dynamics, it has been shown [116] that stochastic resetting has dramatic effects on the long-time properties of a system, which very generally relaxes into a non-equilibrium stationary state (NESS). For closed many-body quantum systems, a full understanding of the emergence of this NESS is, however, still lacking. Attempts to tackle this problem have only started recently [143], and it has been shown that the NESS emerging from the reset dynamics is of genuine non-equilibrium nature also in quantum systems. In a complementary approach, one can consider open quantum systems interacting with the surrounding environment. Within such a setting, stochastic resetting has been recently described via a Markovian master equation in the Lindblad form [144, 150, 216]. Despite this recent progress, efforts are still required in order to develop a framework that bridges the gap between the open quantum systems formulation of stochastic resetting and the one available for closed quantum systems. Related to that,

whether signatures of quantum phase transitions can be generated in the NESS from the effective open dynamics induced by the resetting mechanism is still an open question. In our work [193] we provide a unified analytical understanding of the above-mentioned phenomena. We analytically show that the averaging of the microscopic unitary dynamics over all the possible reset realizations leads to an effective open system dynamics, which generalizes the Lindblad form. As an example, we consider the paradigmatic quantum Ising chain in a transverse field, that, while evolving unitarily after a quench, is subject to stochastic resetting. The possible reset states are the two states corresponding to the fully-polarized states along the z-direction. The choice between the two reset states at each reset event is determined by the outcome of the measurement of the magnetization taken immediately before resetting. Under this conditional reset, we show that the ensuing NESS displays signatures of the equilibrium quantum phase transition in terms of a sharp crossover. To prove this, we make use of techniques available from quantum quenches in closed systems and the mathematical formalism of semi-Markov processes. Our results further indicate that stochastic resetting may find practical application as a protocol to design collective non-equilibrium stationary states with a sharp crossover, which can be exploited, e.g., for sensing applications. Furthermore, in our analysis, upon controlling the timescale of the resetting, we can hinder uncontrolled dissipative effects such as heating.

4.5 Collective behavior in non-interacting systems subject to stochastic resetting

Since the early days of quantum mechanics there has been an intense research activity on the interplay between coherent quantum evolution and measurement. This topic is currently receiving much attention in the context of open quantum

systems, where the coupling to the environment competes with the internal interactions in the system [217]. Such open system dynamics can also be artificially engineered in modern experiments, e.g., through the use of so-called feedback protocols [218], which generate non-trivial quantum correlations due to the external continuous monitoring and subsequent operation on the system. Another mechanism which realizes an effective open system dynamics is constituted by stochastic resetting. The NESS resulting from this process has been investigated in a variety of physical scenarios. However, whether resetting can lead to a non-trivial NESS that displays emergent quantum correlations or non-equilibrium phase transition behavior remains an open question. In our work [195], we explore the interplay between stochastic resetting and many-body quantum coherent evolution in the simplest — yet surprisingly non-trivial — case of non-interacting spin systems. In particular, we consider a set of N qubits undergoing Rabi oscillations independently on each other. We devise three reset protocols: the first is the simple stochastic resetting of the system to a fixed state, while the remaining two protocols include an additional measurement step whose outcome determines to which state the system is reset. In all the three protocols, we find that, despite the absence of interactions in the coherent dynamics, the global character of the resetting induces long-range correlations, that are not only of statistical nature, but also have a quantum origin. Quantum correlations are quantified through the quantum discord [219], which isolates the fluctuations that are caused only by the coherence of the state and not by its mixedness. Furthermore, resetting is shown to introduce non-analytic behavior, reminiscent of standard non-equilibrium phase transitions. Our approach for engineering NESS can thus be useful for high-density quantum sensing, where the collectively enhanced response of the system to external parameter variations may be exploited for quantum metrology applications. The proposed protocols create correlated many-body states even in non-interacting sys-

tems, which can be implemented in state-of-the-art quantum simulators without the need to create strong coherent interactions.

5 Conclusion and outlook

This thesis collects original results in two distinct, yet connected, topics. The first part is devoted to the study of non-equilibrium properties of Rydberg systems under the facilitation condition [92], also known as Rydberg antiblockade. When performed on a one-dimensional chain of individually trapped atoms, the facilitation condition implements a kinetic constraint, consisting in facilitating the excitation of ground state atoms that are neighbors of one Rydberg excitation. This mechanism leads to the formation of extended clusters of excitations, subject to long-range interactions that are extensive in the cluster size. By developing an effective model, we map this system to a hopping particle subject to a linear potential and find that the cluster undergoes Bloch oscillations that hinder its expansion and, more generally, its relaxation toward equilibrium.

In order to improve the theoretical description of the facilitation dynamics, it is necessary to go beyond the frozen gas approximation and consider the quantum position fluctuations of the atoms in the traps. We develop a model that captures the resulting coupling of the (internal) electronic degrees of freedom to the (external) vibrational ones, whose strength is proportional to the mechanical forces induced by the Rydberg interactions that displace the atoms from the center of the trap. We analytically find that this spin-phonon coupling is responsible for the suppression of the otherwise ballistic expansion of the Rydberg cluster under the facilitation constraint.

The mechanical forces induced by the Rydberg interactions often cause decoherence in the internal dynamics of the atomic ensemble. However, the resulting spin-phonon coupling may be exploited to investigate novel phenomena. We show this by introducing an artificial molecular system, a Rydberg tweezer molecule, and find that it features a controllable transition in its geometric structure. This

phenomenon, known as the Jahn-Teller effect, originates from the breaking of the electronic degeneracy due to the atomic vibrations. With this result, we establish a new connection between Rydberg physics and molecular physics, allowing the probing of novel molecular phenomena at the exaggerated length scales typical of Rydberg systems.

The second part of the thesis investigates the influence of stochastic resetting on the dynamics of quantum many-body systems. We find that the action of resetting introduces an effective non-Markovian open dynamics, governed by a generalized Lindblad equation. We apply the formalism to the one-dimensional transverse field Ising model, where the unitary evolution after a quantum quench is interrupted at random times and the system is reset to one of the two fully polarized states depending on the outcome of a measurement taken immediately before resetting. We show that signatures of the equilibrium quantum phase transition are also present in the non-equilibrium stationary state. Furthermore, we show that resetting can be exploited to mitigate incoherent effects, such as heating, thereby allowing for the design of stationary states that can be used in quantum simulator platforms for sensing applications.

We further study the impact of resetting on the stationary properties of a non-interacting system. In particular, we consider a one dimensional chain of non-interacting atoms undergoing Rabi oscillations. In the three considered reset protocols we find that the system develops long-range correlations that are not only of statistical nature, but also have a quantum origin. We quantify such non-classical correlations through the quantum discord and find, in the thermodynamic limit, a collective behaviour reminiscent of that occurring in non-equilibrium phase transitions. The resulting large sensitivity of the order parameter on external parameters may be useful for potential applications in quantum-enhanced metrology.

5.1 Future directions

In our works we assume that atoms in both their ground state and Rydberg state are trapped in the lattice potential. Although its feasibility has been demonstrated in [220], this is not yet standard technology in Rydberg quantum simulator platforms. This feature can be inserted in our model by making the trap frequency dependent on the internal state of the atom. Another improvement would be to consider the finite lifetime of the Rydberg state, as well as other decoherence sources from the surrounding environment. Furthermore, a strategy to mitigate the effect of mechanical forces in experiments can be through the engineering of specific interaction potentials between Rydberg states. It is indeed possible to go beyond the bare dipole-dipole or van der Waals potential, e.g., through microwave dressing [221, 222], as outlined in Section 2.5. The resulting mixing of different dipole-coupled Rydberg states allows to engineer interaction potentials that feature local minima at interatomic distances of few micrometers, preventing the onset of mechanical forces between Rydberg atoms. We plan to address these topics in future studies.

5.1.1 Localization phenomena in Rydberg quantum simulators

The capability of Rydberg quantum simulators to implement generic quantum Hamiltonians has been proven on many occasions. However, for a successful functionality, several experimental challenges are required to be overcome and a complementary effort from the theoretical side is necessary. The fact that the interactions between Rydberg atoms are very strong is certainly an advantage, as it allows to efficiently simulate long-range interacting Hamiltonians. However, for the same reason, atoms in the Rydberg state are subject to strong mechanical forces that displace them from the center of the trap or even eject them

out of the lattice potential, thereby limiting the potential of these experiments. It is therefore necessary to go beyond the simple frozen-gas approximation and consider the vibrational degrees of freedom of the atoms to understand how the real-space motion affects the (internal) Rydberg spin dynamics. In one of our works [191], we have studied analytically this situation in the context of a facilitated Rydberg dynamics and found that the avalanche process that would arise under the frozen gas approximation gets hindered by such lattice vibrations. An interesting question is whether there is some connection between this obstruction of the facilitation dynamics and the phenomenon of Anderson localization [223]. The nature of the relationship between the two models is not clear because the Rydberg-boson coupling resulting from the vibrations of the atoms contrasts with the concept of quenched disorder that underlies the Anderson model. Indeed, the vibrational degrees of freedom get influenced by the internal Rydberg dynamics because the strong interactions between Rydberg atoms displace the atoms from the center of the trap. The randomness of the atom positions becomes effectively a fully dynamical quantity. It is therefore interesting to understand the influence of this dynamically induced disorder on the Rydberg dynamics and investigate its connection with other recent theoretical and experimental works that have studied localization phenomena in a disorder-free setting [224, 225], which include the notions of Wannier-Stark localization [202] and Hilbert space fragmentation [204]. At the same time, the versatility offered by Rydberg platforms allows to tune parameters in the Hamiltonian in a way that a crossover from dynamical to quenched disorder may be possible, for example by changing the trapping frequency. This study may establish a connection between novel localization phenomena induced by classical or quantum dynamical fluctuations and the well known paradigm given by Anderson or many-body localization stemming from disorder.

5.1.2 Self-organized criticality in quantum many-body systems

Self-organized criticality (SOC) is the property of dynamical systems to evolve towards a stationary critical state without tuning an external control parameter. It is therefore fundamentally different from critical points at (non)-equilibrium phase transitions which can be reached only by tuning the parameters of the phase diagram. Being introduced in 1987 [226], it is considered to be one of the mechanisms by which complexity arises in nature and has explained the emergence of scaling and power laws across fields as diverse as biology, ecology, economics and neuroscience. So far the great majority of SOC systems lies in the field of classical physics. It is therefore intriguing to identify quantum systems that exhibit a phase transition in a self-organized way and understand whether self-organization can also manifest in quantum properties, like entanglement. One of the key requirements to have SOC in classical systems is a competition between an avalanche dynamics and sources of dissipation. For this reason, Rydberg systems subject to the facilitation constraint appear to be the natural setting to study quantum SOC, thanks to their dynamics and state-dependent dissipative effects. Recent experiments [98, 99] have indeed shown signatures of SOC in facilitated Rydberg gases subject to dissipation. However, the adopted theoretical models are based on semiclassical rate equations that rely on variants of mean-field approximations. The much higher controllability and versatility of Rydberg atoms trapped in optical lattices or tweezers offer new perspectives to study unexplored aspects of SOC, such as its dependence on the lattice geometry, the influence of frustration and its relation with quantum cellular automata. The idea is to extend our works on the facilitation constraint to the two-dimensional case and additionally consider state-dependent dissipative processes. One can then characterize various properties of the resulting stationary state, like the Rydberg cluster size distribution and

the Rydberg density correlation function. This model may constitute the natural setting to study SOC in quantum physics in an unprecedented, monitored way, and help to shed light on how SOC manifests in quantities that are quantum in nature, like entanglement and quantum fluctuations.

6 Bibliography

References

[1] L. Boltzmann, "Weitere Studien über das Wärmegleichgewicht unter Gasmolekülen," *Sitzungsberichte Akademie der Wissenschaften*, vol. 66, pp. 275–370, 1872.

[2] L. Boltzmann, "Über die beziehung dem zweiten Hauptsatze der mechanischen Wärmetheorie und der Wahrscheinlichkeitsrechnung respektive den Sätzen über das Wärmegleichgewicht," *Wien. Ber.*, vol. 76, pp. 373–435, 1877.

[3] J. Gibbs, *Elementary Principles in Statistical Mechanics*. Elementary Principles in Statistical Mechanics: Developed with Especial Reference to the Rational Foundation of Thermodynamics, C. Scribner's sons, 1902.

[4] G. D. Birkhoff, "Proof of the ergodic theorem," *Proc. Natl. Acad. Sci. U.S.A.*, vol. 17, no. 12, pp. 656–660, 1931.

[5] J. v. Neumann, "Proof of the quasi-ergodic hypothesis," *Proc. Natl. Acad. Sci. U.S.A.*, vol. 18, no. 1, pp. 70–82, 1932.

[6] K. Vogtmann, A. Weinstein, and V. Arnol'd, *Mathematical Methods of Classical Mechanics*. Graduate Texts in Mathematics, Springer New York, 1997.

[7] F. H. L. Essler and M. Fagotti, "Quench dynamics and relaxation in isolated integrable quantum spin chains," *J. Stat. Mech.*, vol. 2016, no. 6, p. 064002, 2016.

[8] L. Vidmar and M. Rigol, "Generalized Gibbs ensemble in integrable lattice models," *J. Stat. Mech.*, vol. 2016, p. 064007, jun 2016.

[9] F. Ritort and P. Sollich, "Glassy dynamics of kinetically constrained models," *Adv. Phys.*, vol. 52, no. 4, pp. 219–342, 2003.

[10] D. Chandler and J. P. Garrahan, "Dynamics on the Way to Forming Glass: Bubbles in Space-Time," *Annu. Rev. Phys. Chem.*, vol. 61, no. 1, pp. 191–217, 2010. PMID: 20055676.

[11] J.-P. Hansen and I. R. McDonald, *Theory of Simple Liquids*. Oxford: Academic Press, fourth edition ed., 2013.

[12] S. Nemilov, *Thermodynamic and Kinetic Aspects of the Vitreous State*. CRC Press, 1995.

[13] P. W. Anderson, "Through the Glass Lightly," *Science*, vol. 267, no. 5204, pp. 1615–1616, 1995.

[14] G. Biroli and J. P. Garrahan, "Perspective: The glass transition," *J. Chem. Phys.*, vol. 138, 03 2013. 12A301.

[15] V. Lubchenko and P. G. Wolynes, "Theory of Structural Glasses and Supercooled Liquids," *Annu. Rev. Phys. Chem.*, vol. 58, no. 1, pp. 235–266, 2007. PMID: 17067282.

[16] G. Biroli and J.-P. Bouchaud, *The Random First-Order Transition Theory of Glasses: A Critical Assessment*, ch. 2, pp. 31–113. John Wiley & Sons, Ltd, 2012.

[17] M. Mezard, G. Parisi, and M. Virasoro, *Spin Glass Theory And Beyond: An Introduction To The Replica Method And Its Applications*. World Scientific Lecture Notes In Physics, World Scientific Publishing Company, 1987.

[18] L. D'Alessio, Y. Kafri, A. Polkovnikov, and M. Rigol, "From quantum chaos and eigenstate thermalization to statistical mechanics and thermodynamics," *Adv. Phys.*, vol. 65, no. 3, pp. 239–362, 2016.

[19] M. Rigol, V. Dunjko, and M. Olshanii, "Thermalization and its mechanism for generic isolated quantum systems," *Nature*, vol. 452, pp. 854–8, 05 2008.

[20] F. Borgonovi, F. Izrailev, L. Santos, and V. Zelevinsky, "Quantum chaos and thermalization in isolated systems of interacting particles," *Phys. Rep.*, vol. 626, pp. 1–58, 2016.

[21] C. Gogolin and J. Eisert, "Equilibration, thermalisation, and the emergence of statistical mechanics in closed quantum systems," *Rep. Prog. Phys.*, vol. 79, no. 5, p. 056001, 2016.

[22] M. Cramer, C. M. Dawson, J. Eisert, and T. J. Osborne, "Exact Relaxation in a Class of Nonequilibrium Quantum Lattice Systems," *Phys. Rev. Lett.*, vol. 100, p. 030602, 2008.

[23] J. M. Deutsch, "Quantum statistical mechanics in a closed system," *Phys. Rev. A*, vol. 43, pp. 2046–2049, Feb 1991.

[24] M. Srednicki, "Chaos and quantum thermalization," *Phys. Rev. E*, vol. 50, pp. 888–901, Aug 1994.

[25] H. Tasaki, "From Quantum Dynamics to the Canonical Distribution: General Picture and a Rigorous Example," *Phys. Rev. Lett.*, vol. 80, pp. 1373–1376, Feb 1998.

[26] M. Srednicki, "The approach to thermal equilibrium in quantized chaotic systems," *J. Phys. A: Math. Gen.*, vol. 32, pp. 1163–1175, jan 1999.

[27] M. Rigol, V. Dunjko, V. Yurovsky, and M. Olshanii, "Relaxation in a Completely Integrable Many-Body Quantum System: An Ab Initio Study of the Dynamics of the Highly Excited States of 1D Lattice Hard-Core Bosons," *Phys. Rev. Lett.*, vol. 98, p. 050405, Feb 2007.

[28] P. Calabrese, F. H. L. Essler, and G. Mussardo, "Introduction to 'Quantum Integrability in Out of Equilibrium Systems'," *J. Stat. Mech.*, vol. 2016, p. 064001, jun 2016.

[29] E. Ilievski, M. Medenjak, T. Prosen, and L. Zadnik, "Quasilocal charges in integrable lattice systems," *J. Stat. Mech.*, vol. 2016, p. 064008, jun 2016.

[30] C. Turner, A. Michailidis, D. Abanin, M. Serbyn, and Z. Papić, "Weak ergodicity breaking from quantum many-body scars," *Nat. Phys.*, vol. 14, p. 745, 05 2018.

[31] M. Serbyn, D. A. Abanin, and Z. Papić, "Quantum many-body scars and weak breaking of ergodicity," *Nat. Phys.*, vol. 17, pp. 675–685, Jun 2021.

[32] H. Bernien, S. Schwartz, A. Keesling, H. Levine, A. Omran, H. Pichler, S. Choi, A. S. Zibrov, M. Endres, M. Greiner, *et al.*, "Probing many-body dynamics on a 51-atom quantum simulator," *Nature*, vol. 551, no. 7682, p. 579, 2017.

[33] D. Basko, I. Aleiner, and B. Altshuler, "Metal-insulator transition in a weakly interacting many-electron system with localized single-particle states," *Ann. Phys.*, vol. 321, no. 5, pp. 1126 – 1205, 2006.

[34] V. Oganesyan and D. A. Huse, "Localization of interacting fermions at high temperature," *Phys. Rev. B*, vol. 75, p. 155111, Apr 2007.

[35] D. A. Abanin, E. Altman, I. Bloch, and M. Serbyn, "Colloquium: Many-body localization, thermalization, and entanglement," *Rev. Mod. Phys.*, vol. 91, p. 021001, May 2019.

[36] R. Nandkishore and D. A. Huse, "Many body localization and thermalization in quantum statistical mechanics," *Annu. Rev. Condens. Matter Phys.*, vol. 6, p. 15, June 2015.

[37] E. Altman and R. Vosk, "Universal dynamics and renormalization in many body localized systems," *Annu. Rev. Condens. Matter Phys.*, vol. 6, p. 383, Aug. 2015.

[38] J. Šuntajs, J. Bonča, T. c. v. Prosen, and L. Vidmar, "Quantum chaos challenges many-body localization," *Phys. Rev. E*, vol. 102, p. 062144, Dec 2020.

[39] D. Abanin, J. Bardarson, G. De Tomasi, S. Gopalakrishnan, V. Khemani, S. Parameswaran, F. Pollmann, A. Potter, M. Serbyn, and R. Vasseur, "Distinguishing localization from chaos: Challenges in finite-size systems," *Ann. Phys.*, vol. 427, p. 168415, 2021.

[40] L. Rademaker and D. A. Abanin, "Slow Nonthermalizing Dynamics in a Quantum Spin Glass," *Phys. Rev. Lett.*, vol. 125, p. 260405, Dec 2020.

[41] Z. Lan, M. van Horssen, S. Powell, and J. P. Garrahan, "Quantum Slow Relaxation and Metastability due to Dynamical Constraints," *Phys. Rev. Lett.*, vol. 121, p. 040603, Jul 2018.

[42] C.-J. Lin and O. I. Motrunich, "Exact Quantum Many-Body Scar States in the Rydberg-Blockaded Atom Chain," *Phys. Rev. Lett.*, vol. 122, p. 173401, Apr 2019.

[43] W. W. Ho, S. Choi, H. Pichler, and M. D. Lukin, "Periodic orbits, entanglement and quantum many-body scars in constrained models: matrix product state approach," *Phys. Rev. Lett.*, vol. 122, p. 040603, 2019.

[44] T. Iadecola and M. Schecter, "Quantum many-body scar states with emergent kinetic constraints and finite-entanglement revivals," *Phys. Rev. B*, vol. 101, p. 024306, Jan 2020.

[45] H. Zhao, J. Vovrosh, F. Mintert, and J. Knolle, "Quantum Many-Body Scars in Optical Lattices," *Phys. Rev. Lett.*, vol. 124, p. 160604, Apr 2020.

[46] N. Pancotti, G. Giudice, J. I. Cirac, J. P. Garrahan, and M. C. Bañuls, "Quantum East Model: Localization, Nonthermal Eigenstates, and Slow Dynamics," *Phys. Rev. X*, vol. 10, p. 021051, Jun 2020.

[47] A. Morningstar, V. Khemani, and D. A. Huse, "Kinetically constrained freezing transition in a dipole-conserving system," *Phys. Rev. B*, vol. 101, p. 214205, Jun 2020.

[48] R. J. Valencia-Tortora, N. Pancotti, and J. Marino, "Kinetically Constrained Quantum Dynamics in Superconducting Circuits," *PRX Quantum*, vol. 3, p. 020346, Jun 2022.

[49] M. Ljubotina, J.-Y. Desaules, M. Serbyn, and Z. Papić, "Superdiffusive Energy Transport in Kinetically Constrained Models," *Phys. Rev. X*, vol. 13, p. 011033, Mar 2023.

[50] J. P. Garrahan, "Aspects of non-equilibrium in classical and quantum systems: Slow relaxation and glasses, dynamical large deviations, quantum non-ergodicity, and open quantum dynamics," *Physica A*, vol. 504, pp. 130 – 154, 2018.

[51] I. Bloch, J. Dalibard, and S. Nascimbène, "Quantum simulations with ultracold quantum gases," *Nat. Phys.*, vol. 8, p. 267, 2012.

[52] J. Eisert, M. Friesdorf, and C. Gogolin, "Quantum many-body systems out of equilibrium," *Nat. Phys.*, vol. 11, pp. 124–130, Feb 2015.

[53] Y. I. Manin, *Vychislimoe i nevychislimoe*. Sov. Radio., 1980.

[54] R. P. Feynman, "Simulating physics with computers," *Int. J. Theor. Phys*, vol. 21, pp. 467–488, 1982.

[55] M. Greiner, O. Mandel, T. Esslinger, T. W. Hänsch, and I. Bloch, "Quantum phase transition from a superfluid to a Mott insulator in a gas of ultracold atoms," *Nature*, vol. 415, pp. 39–44, Jan 2002.

[56] A. Adams, L. D. Carr, T. Schäfer, P. Steinberg, and J. E. Thomas, "Strongly correlated quantum fluids: ultracold quantum gases, quantum chromodynamic plasmas and holographic duality," *New J. Phys.*, vol. 14, p. 115009, nov 2012.

[57] M. J. H. Ku, A. T. Sommer, L. W. Cheuk, and M. W. Zwierlein, "Revealing the Superfluid Lambda Transition in the Universal Thermodynamics of a Unitary Fermi Gas," *Science*, vol. 335, no. 6068, pp. 563–567, 2012.

[58] P. T. Brown, D. Mitra, E. Guardado-Sanchez, R. Nourafkan, A. Reymbaut, C.-D. Hébert, S. Bergeron, A.-M. S. Tremblay, J. Kokalj, D. A. Huse, P. Schauß, and W. S. Bakr, "Bad metallic transport in a cold atom Fermi-Hubbard system," *Science*, vol. 363, no. 6425, pp. 379–382, 2019.

[59] M. Schreiber, S. S. Hodgman, P. Bordia, H. P. Lüschen, M. H. Fischer, R. Vosk, E. Altman, U. Schneider, and I. Bloch, "Observation of many-

body localization of interacting fermions in a quasirandom optical lattice," *Science*, vol. 349, no. 6250, pp. 842–845, 2015.

[60] A. J. Kollár, M. Fitzpatrick, and A. A. Houck, "Hyperbolic lattices in circuit quantum electrodynamics," *Nature*, vol. 571, pp. 45–50, Jul 2019.

[61] Y.-J. Lin, K. Jiménez-García, and I. B. Spielman, "Spin–orbit-coupled Bose–Einstein condensates," *Nature*, vol. 471, pp. 83–86, Mar 2011.

[62] F. Arute *et al.*, "Quantum supremacy using a programmable superconducting processor," *Nature*, vol. 574, pp. 505–510, Oct 2019.

[63] J. Zhang, G. Pagano, P. W. Hess, A. Kyprianidis, P. Becker, H. Kaplan, A. V. Gorshkov, Z.-X. Gong, and C. Monroe, "Observation of a many-body dynamical phase transition with a 53-qubit quantum simulator," *Nature*, vol. 551, pp. 601–604, Nov 2017.

[64] L. Anderegg, L. W. Cheuk, Y. Bao, S. Burchesky, W. Ketterle, K.-K. Ni, and J. M. Doyle, "An optical tweezer array of ultracold molecules," *Science*, vol. 365, no. 6458, pp. 1156–1158, 2019.

[65] T. Hensgens, T. Fujita, L. Janssen, X. Li, C. J. Van Diepen, C. Reichl, W. Wegscheider, S. Das Sarma, and L. M. K. Vandersypen, "Quantum simulation of a Fermi–Hubbard model using a semiconductor quantum dot array," *Nature*, vol. 548, pp. 70–73, Aug 2017.

[66] V. D. Vaidya, Y. Guo, R. M. Kroeze, K. E. Ballantine, A. J. Kollár, J. Keeling, and B. L. Lev, "Tunable-Range, Photon-Mediated Atomic Interactions in Multimode Cavity QED," *Phys. Rev. X*, vol. 8, p. 011002, Jan 2018.

[67] G. Wang, A. Chernikov, M. M. Glazov, T. F. Heinz, X. Marie, T. Amand,

and B. Urbaszek, "Colloquium: Excitons in atomically thin transition metal dichalcogenides," *Rev. Mod. Phys.*, vol. 90, p. 021001, Apr 2018.

[68] J. F. Sherson, C. Weitenberg, M. Endres, M. Cheneau, I. Bloch, and S. Kuhr, "Single-atom-resolved fluorescence imaging of an atomic Mott insulator," *Nature*, vol. 467, pp. 68–72, Sep 2010.

[69] D. Barredo, S. de Léséleuc, V. Lienhard, T. Lahaye, and A. Browaeys, "An atom-by-atom assembler of defect-free arbitrary two-dimensional atomic arrays," *Science*, vol. 354, no. 6315, pp. 1021–1023, 2016.

[70] T. F. Gallagher, *Rydberg Atoms*. Cambridge Monographs on Atomic, Molecular and Chemical Physics, Cambridge University Press, 1994.

[71] C. Gross and I. Bloch, "Quantum simulations with ultracold atoms in optical lattices," *Science*, vol. 357, no. 6355, pp. 995–1001, 2017.

[72] Y. Miroshnychenko, W. Alt, I. Dotsenko, L. Förster, M. Khudaverdyan, D. Meschede, D. Schrader, and A. Rauschenbeutel, "An atom-sorting machine," *Nature*, vol. 442, pp. 151–151, Jul 2006.

[73] L.-M. Steinert, P. Osterholz, R. Eberhard, L. Festa, N. Lorenz, Z. Chen, A. Trautmann, and C. Gross, "Spatially tunable spin interactions in neutral atom arrays," *arXiv:2206.12385*, 2022.

[74] P. Schauß, M. Cheneau, M. Endres, T. Fukuhara, S. Hild, A. Omran, T. Pohl, C. Gross, S. Kuhr, and I. Bloch, "Observation of spatially ordered structures in a two-dimensional Rydberg gas," *Nature*, vol. 491, pp. 87–91, Nov 2012.

[75] V. Lienhard, S. de Léséleuc, D. Barredo, T. Lahaye, A. Browaeys, M. Schuler, L.-P. Henry, and A. M. Läuchli, "Observing the Space- and Time-Dependent

Growth of Correlations in Dynamically Tuned Synthetic Ising Models with Antiferromagnetic Interactions," *Phys. Rev. X*, vol. 8, p. 021070, Jun 2018.

[76] E. Guardado-Sanchez, P. T. Brown, D. Mitra, T. Devakul, D. A. Huse, P. Schauß, and W. S. Bakr, "Probing the Quench Dynamics of Antiferromagnetic Correlations in a 2D Quantum Ising Spin System," *Phys. Rev. X*, vol. 8, p. 021069, Jun 2018.

[77] J. Zeiher, P. Schauß, S. Hild, T. Macrì, I. Bloch, and C. Gross, "Microscopic Characterization of Scalable Coherent Rydberg Superatoms," *Phys. Rev. X*, vol. 5, p. 031015, Aug 2015.

[78] H. Labuhn, D. Barredo, S. Ravets, S. de Léséleuc, T. Macrì, T. Lahaye, and A. Browaeys, "Tunable two-dimensional arrays of single Rydberg atoms for realizing quantum Ising models," *Nature*, vol. 534, pp. 667–670, Jun 2016.

[79] H. Kim, Y. Park, K. Kim, H.-S. Sim, and J. Ahn, "Detailed Balance of Thermalization Dynamics in Rydberg-Atom Quantum Simulators," *Phys. Rev. Lett.*, vol. 120, p. 180502, May 2018.

[80] P. Schauß, J. Zeiher, T. Fukuhara, S. Hild, M. Cheneau, T. Macrì, T. Pohl, I. Bloch, and C. Gross, "Crystallization in Ising quantum magnets," *Science*, vol. 347, no. 6229, pp. 1455–1458, 2015.

[81] A. Keesling, A. Omran, H. Levine, H. Bernien, H. Pichler, S. Choi, R. Samajdar, S. Schwartz, P. Silvi, S. Sachdev, P. Zoller, M. Endres, M. Greiner, V. Vuletić, and M. D. Lukin, "Quantum Kibble–Zurek mechanism and critical dynamics on a programmable Rydberg simulator," *Nature*, vol. 568, pp. 207–211, Apr 2019.

[82] S. de Léséleuc, V. Lienhard, P. Scholl, D. Barredo, S. Weber, N. Lang, H. P. Büchler, T. Lahaye, and A. Browaeys, "Observation of a symmetry-

protected topological phase of interacting bosons with Rydberg atoms," *Science*, vol. 365, no. 6455, pp. 775–780, 2019.

[83] L. W. Clark, N. Schine, C. Baum, N. Jia, and J. Simon, "Observation of Laughlin states made of light," *Nature*, vol. 582, pp. 41–45, Jun 2020.

[84] V. Lienhard, P. Scholl, S. Weber, D. Barredo, S. de Léséleuc, R. Bai, N. Lang, M. Fleischhauer, H. P. Büchler, T. Lahaye, and A. Browaeys, "Realization of a Density-Dependent Peierls Phase in a Synthetic, Spin-Orbit Coupled Rydberg System," *Phys. Rev. X*, vol. 10, p. 021031, May 2020.

[85] G. Semeghini, H. Levine, A. Keesling, S. Ebadi, T. T. Wang, D. Bluvstein, R. Verresen, H. Pichler, M. Kalinowski, R. Samajdar, A. Omran, S. Sachdev, A. Vishwanath, M. Greiner, V. Vuletić, and M. D. Lukin, "Probing topological spin liquids on a programmable quantum simulator," *Science*, vol. 374, no. 6572, pp. 1242–1247, 2021.

[86] D. Jaksch, J. I. Cirac, P. Zoller, S. L. Rolston, R. Côté, and M. D. Lukin, "Fast Quantum Gates for Neutral Atoms," *Phys. Rev. Lett.*, vol. 85, pp. 2208–2211, Sep 2000.

[87] M. D. Lukin, M. Fleischhauer, R. Cote, L. M. Duan, D. Jaksch, J. I. Cirac, and P. Zoller, "Dipole Blockade and Quantum Information Processing in Mesoscopic Atomic Ensembles," *Phys. Rev. Lett.*, vol. 87, p. 037901, Jun 2001.

[88] M. Saffman, T. G. Walker, and K. Molmer, "Quantum information with Rydberg atoms," *Rev. Mod. Phys.*, vol. 82, p. 2313, 2010.

[89] S.-L. Su, F.-Q. Guo, J.-L. Wu, Z. Jin, X. Q. Shao, and S. Zhang, "Rydberg antiblockade regimes: Dynamics and applications," *Europhys. Lett.*, vol. 131, p. 53001, sep 2020.

[90] C. Pérez-Espigares, M. Marcuzzi, R. Gutiérrez, and I. Lesanovsky, "Epidemic Dynamics in Open Quantum Spin Systems," *Phys. Rev. Lett.*, vol. 119, p. 140401, Oct 2017.

[91] T. M. Wintermantel, M. Buchhold, S. Shevate, M. Morgado, Y. Wang, G. Lochead, S. Diehl, and S. Whitlock, "Epidemic growth and Griffiths effects on an emergent network of excited atoms," *Nat. Commun.*, vol. 12, p. 103, Jan 2021.

[92] C. Ates, T. Pohl, T. Pattard, and J. M. Rost, "Antiblockade in Rydberg Excitation of an Ultracold Lattice Gas," *Phys. Rev. Lett.*, vol. 98, p. 023002, Jan 2007.

[93] M. Gärttner, K. P. Heeg, T. Gasenzer, and J. Evers, "Dynamic formation of rydberg aggregates at off-resonant excitation," *Phys. Rev. A*, vol. 88, p. 043410, Oct 2013.

[94] S.-L. Su, Y. Gao, E. Liang, and S. Zhang, "Fast Rydberg antiblockade regime and its applications in quantum logic gates," *Phys. Rev. A*, vol. 95, p. 022319, Feb 2017.

[95] J.-L. Wu, Y. Wang, J.-X. Han, Y.-K. Feng, S.-L. Su, Y. Xia, Y. Jiang, and J. Song, "One-step implementation of Rydberg-antiblockade SWAP and controlled-SWAP gates with modified robustness," *Photon. Res.*, vol. 9, pp. 814–821, May 2021.

[96] M. Marcuzzi, M. Buchhold, S. Diehl, and I. Lesanovsky, "Absorbing State Phase Transition with Competing Quantum and Classical Fluctuations," *Phys. Rev. Lett.*, vol. 116, p. 245701, Jun 2016.

[97] M. Mattioli, A. W. Glätzle, and W. Lechner, "From classical to quantum

non-equilibrium dynamics of Rydberg excitations in optical lattices," *New J. Phys.*, vol. 17, p. 113039, nov 2015.

[98] S. Helmrich, A. Arias, G. Lochead, T. M. Wintermantel, M. Buchhold, S. Diehl, and S. Whitlock, "Signatures of self-organized criticality in an ultracold atomic gas," *Nature*, vol. 577, no. 7791, pp. 481–486, 2020.

[99] D.-S. Ding, H. Busche, B.-S. Shi, G.-C. Guo, and C. S. Adams, "Phase Diagram and Self-Organizing Dynamics in a Thermal Ensemble of Strongly Interacting Rydberg Atoms," *Phys. Rev. X*, vol. 10, p. 021023, Apr 2020.

[100] T. Amthor, C. Giese, C. S. Hofmann, and M. Weidemüller, "Evidence of Antiblockade in an Ultracold Rydberg Gas," *Phys. Rev. Lett.*, vol. 104, p. 013001, Jan 2010.

[101] S. Wüster and J.-M. Rost, "Rydberg aggregates," *J. Phys. B*, vol. 51, p. 032001, jan 2018.

[102] H. Schempp, G. Günter, M. Robert-de Saint-Vincent, C. S. Hofmann, D. Breyel, A. Komnik, D. W. Schönleber, M. Gärttner, J. Evers, S. Whitlock, and M. Weidemüller, "Full Counting Statistics of Laser Excited Rydberg Aggregates in a One-Dimensional Geometry," *Phys. Rev. Lett.*, vol. 112, p. 013002, Jan 2014.

[103] A. Urvoy, F. Ripka, I. Lesanovsky, D. Booth, J. P. Shaffer, T. Pfau, and R. Löw, "Strongly Correlated Growth of Rydberg Aggregates in a Vapor Cell," *Phys. Rev. Lett.*, vol. 114, p. 203002, May 2015.

[104] M. M. Valado, C. Simonelli, M. D. Hoogerland, I. Lesanovsky, J. P. Garrahan, E. Arimondo, D. Ciampini, and O. Morsch, "Experimental observation of controllable kinetic constraints in a cold atomic gas," *Phys. Rev. A*, vol. 93, p. 040701, Apr 2016.

[105] J. A. Aman, B. J. DeSalvo, F. B. Dunning, T. C. Killian, S. Yoshida, and J. Burgdörfer, "Trap losses induced by near-resonant Rydberg dressing of cold atomic gases," *Phys. Rev. A*, vol. 93, p. 043425, Apr 2016.

[106] L. Festa, N. Lorenz, L.-M. Steinert, Z. Chen, P. Osterholz, R. Eberhard, and C. Gross, "Blackbody-radiation-induced facilitated excitation of Rydberg atoms in optical tweezers," *Phys. Rev. A*, vol. 105, p. 013109, Jan 2022.

[107] E. A. Goldschmidt, T. Boulier, R. C. Brown, S. B. Koller, J. T. Young, A. V. Gorshkov, S. L. Rolston, and J. V. Porto, "Anomalous Broadening in Driven Dissipative Rydberg Systems," *Phys. Rev. Lett.*, vol. 116, p. 113001, Mar 2016.

[108] J. T. Young, T. Boulier, E. Magnan, E. A. Goldschmidt, R. M. Wilson, S. L. Rolston, J. V. Porto, and A. V. Gorshkov, "Dissipation-induced dipole blockade and antiblockade in driven Rydberg systems," *Phys. Rev. A*, vol. 97, p. 023424, Feb 2018.

[109] M. Marcuzzi, J. Minar, D. Barredo, S. de Léséleuc, H. Labuhn, T. Lahaye, A. Browaeys, E. Levi, and I. Lesanovsky, "Facilitation Dynamics and Localization Phenomena in Rydberg Lattice Gases with Position Disorder," *Phys. Rev. Lett.*, vol. 118, p. 063606, Feb 2017.

[110] M. Ostmann, M. Marcuzzi, J. P. Garrahan, and I. Lesanovsky, "Localization in spin chains with facilitation constraints and disordered interactions," *Phys. Rev. A*, vol. 99, p. 060101, Jun 2019.

[111] M. Ostmann, M. Marcuzzi, J. Minar, and I. Lesanovsky, "Synthetic lattices, flat bands and localization in Rydberg quantum simulators," *Quantum Sci. Technol.*, vol. 4, p. 02LT01, jan 2019.

[112] F. Liu, Z.-C. Yang, P. Bienias, T. Iadecola, and A. V. Gorshkov, "Localization and Criticality in Antiblockaded Two-Dimensional Rydberg Atom Arrays," *Phys. Rev. Lett.*, vol. 128, p. 013603, Jan 2022.

[113] F. M. Gambetta, W. Li, F. Schmidt-Kaler, and I. Lesanovsky, "Engineering NonBinary Rydberg Interactions via Phonons in an Optical Lattice," *Phys. Rev. Lett.*, vol. 124, p. 043402, Jan 2020.

[114] P. P. Mazza, R. Schmidt, and I. Lesanovsky, "Vibrational Dressing in Kinetically Constrained Rydberg Spin Systems," *Phys. Rev. Lett.*, vol. 125, p. 033602, Jul 2020.

[115] M. R. Evans, S. N. Majumdar, and G. Schehr, "Stochastic resetting and applications," *J. Phys. A: Math. Theor.*, vol. 53, p. 193001, apr 2020.

[116] M. R. Evans and S. N. Majumdar, "Diffusion with Stochastic Resetting," *Phys. Rev. Lett.*, vol. 106, p. 160601, Apr 2011.

[117] S. Kirkpatrick, C. D. Gelatt, and M. P. Vecchi, "Optimization by Simulated Annealing," *Science*, vol. 220, no. 4598, pp. 671–680, 1983.

[118] M. Luby, A. Sinclair, and D. Zuckerman, "Optimal speedup of Las Vegas algorithms," *Inf. Proc. Lett.*, vol. 47, no. 4, pp. 173–180, 1993.

[119] D. Boyer and C. Solis-Salas, "Random Walks with Preferential Relocations to Places Visited in the Past and their Application to Biology," *Phys. Rev. Lett.*, vol. 112, p. 240601, Jun 2014.

[120] A. Lisica, C. Engel, M. Jahnel, Édgar Roldán, E. A. Galburt, P. Cramer, and S. W. Grill, "Mechanisms of backtrack recovery by RNA polymerases I and II," *Proc. Natl. Acad. Sci. U.S.A.*, vol. 113, no. 11, pp. 2946–2951, 2016.

[121] S. Reuveni, M. Urbakh, and J. Klafter, "Role of substrate unbinding in Michaelis–Menten enzymatic reactions," *Proc. Natl. Acad. Sci. U.S.A.*, vol. 111, no. 12, pp. 4391–4396, 2014.

[122] M. R. Evans and S. N. Majumdar, "Run and tumble particle under resetting: a renewal approach," *J. Phys. A: Math. Theor.*, vol. 51, p. 475003, oct 2018.

[123] E. Kyriakidis, "Stationary probabilities for a simple immigration-birth-death process under the influence of total catastrophes," *Stat. Probab. Lett.*, vol. 20, no. 3, pp. 239–240, 1994.

[124] S. Ghosh, B. Mishra, A. B. Kolomeisky, and D. Chowdhury, "First-passage processes on a filamentous track in a dense traffic: optimizing diffusive search for a target in crowding conditions," *J. Stat. Mech.*, vol. 2018, p. 123209, dec 2018.

[125] T. T. da Silva and M. D. Fragoso, "The interplay between population genetics and diffusion with stochastic resetting," *J. Phys. A: Math. Theor.*, vol. 51, p. 505002, nov 2018.

[126] A. Pal, "Diffusion in a potential landscape with stochastic resetting," *Phys. Rev. E*, vol. 91, p. 012113, Jan 2015.

[127] M. R. Evans and S. N. Majumdar, "Diffusion with resetting in arbitrary spatial dimension," *J. Phys. A: Math. Theor.*, vol. 47, no. 28, p. 285001, 2014.

[128] L. Kusmierz, S. N. Majumdar, S. Sabhapandit, and G. Schehr, "First Order Transition for the Optimal Search Time of Lévy Flights with Resetting," *Phys. Rev. Lett.*, vol. 113, p. 220602, Nov 2014.

[129] C. D. Bello, A. K. Hartmann, S. N. Majumdar, F. Mori, A. Rosso, and G. Schehr, "Current fluctuations in stochastically resetting particle systems," *arXiv:2302.06696*, 2023.

[130] S. N. Majumdar, S. Sabhapandit, and G. Schehr, "Dynamical transition in the temporal relaxation of stochastic processes under resetting," *Phys. Rev. E*, vol. 91, p. 052131, 5 2015.

[131] R. G. Pinsky, "Diffusive search with spatially dependent resetting," *Stoch. Proc. Appl.*, vol. 130, no. 5, pp. 2954–2973, 2020.

[132] S. Eule and J. J. Metzger, "Non-equilibrium steady states of stochastic processes with intermittent resetting," *New J. Phys.*, vol. 18, p. 033006, mar 2016.

[133] S. Gupta, S. N. Majumdar, and G. Schehr, "Fluctuating Interfaces Subject to Stochastic Resetting," *Phys. Rev. Lett.*, vol. 112, p. 220601, Jun 2014.

[134] X. Durang, M. Henkel, and H. Park, "The statistical mechanics of the coagulation–diffusion process with a stochastic reset," *J. Phys. A: Math. Theor.*, vol. 47, p. 045002, jan 2014.

[135] U. Basu, A. Kundu, and A. Pal, "Symmetric exclusion process under stochastic resetting," *Phys. Rev. E*, vol. 100, p. 032136, Sep 2019.

[136] M. Magoni, S. N. Majumdar, and G. Schehr, "Ising model with stochastic resetting," *Phys. Rev. Res.*, vol. 2, p. 033182, Aug 2020.

[137] D. Boyer and J. C. R. Romo-Cruz, "Solvable random-walk model with memory and its relations with Markovian models of anomalous diffusion," *Phys. Rev. E*, vol. 90, p. 042136, Oct 2014.

[138] S. N. Majumdar, S. Sabhapandit, and G. Schehr, "Random walk with random resetting to the maximum position," *Phys. Rev. E*, vol. 92, p. 052126, Nov 2015.

[139] J. Fuchs, S. Goldt, and U. Seifert, "Stochastic thermodynamics of resetting," *Europhys. Lett.*, vol. 113, p. 60009, apr 2016.

[140] A. Pal and S. Rahav, "Integral fluctuation theorems for stochastic resetting systems," *Phys. Rev. E*, vol. 96, p. 062135, Dec 2017.

[141] J. M. Meylahn, S. Sabhapandit, and H. Touchette, "Large deviations for Markov processes with resetting," *Phys. Rev. E*, vol. 92, p. 062148, Dec 2015.

[142] F. Mori, K. S. Olsen, and S. Krishnamurthy, "Entropy production of resetting processes," *Phys. Rev. Res.*, vol. 5, p. 023103, May 2023.

[143] B. Mukherjee, K. Sengupta, and S. N. Majumdar, "Quantum dynamics with stochastic reset," *Phys. Rev. B*, vol. 98, p. 104309, Sep 2018.

[144] D. C. Rose, H. Touchette, I. Lesanovsky, and J. P. Garrahan, "Spectral properties of simple classical and quantum reset processes," *Phys. Rev. E*, vol. 98, p. 022129, Aug 2018.

[145] S. Dhar, S. Dasgupta, and A. Dhar, "Quantum time of arrival distribution in a simple lattice model," *J. Phys. A: Math. Theor.*, vol. 48, p. 115304, feb 2015.

[146] D. Das, S. Dattagupta, and S. Gupta, "Quantum unitary evolution interspersed with repeated non-unitary interactions at random times: the method of stochastic Liouville equation, and two examples of interactions in the context of a tight-binding chain," *J. Stat. Mech.*, vol. 2022, p. 053101, may 2022.

[147] H. Friedman, D. A. Kessler, and E. Barkai, "Quantum walks: The first detected passage time problem," *Phys. Rev. E*, vol. 95, p. 032141, Mar 2017.

[148] F. Thiel, E. Barkai, and D. A. Kessler, "First Detected Arrival of a Quantum Walker on an Infinite Line," *Phys. Rev. Lett.*, vol. 120, p. 040502, Jan 2018.

[149] L. Hartmann, W. Dür, and H.-J. Briegel, "Steady-state entanglement in open and noisy quantum systems," *Phys. Rev. A*, vol. 74, p. 052304, 11 2006.

[150] F. Carollo, R. L. Jack, and J. P. Garrahan, "Unraveling the Large Deviation Statistics of Markovian Open Quantum Systems," *Phys. Rev. Lett.*, vol. 122, p. 130605, 4 2019.

[151] G. Perfetto, F. Carollo, and I. Lesanovsky, "Thermodynamics of quantum-jump trajectories of open quantum systems subject to stochastic resetting," *SciPost Phys.*, vol. 13, p. 079, 2022.

[152] A. Riera-Campeny, J. Ollé, and A. Masó-Puigdellosas, "Measurement-induced resetting in open quantum systems," *arXiv:2011.04403*, 2020.

[153] V. Dubey, R. Chetrite, and A. Dhar, "Quantum resetting in continuous measurement induced dynamics of a qubit," *J. Phys. A: Math. Theor.*, vol. 56, p. 154001, mar 2023.

[154] O. Tal-Friedman, A. Pal, A. Sekhon, S. Reuveni, and Y. Roichman, "Experimental Realization of Diffusion with Stochastic Resetting," *J. Phys. Chem. Lett.*, vol. 11, pp. 7350–7355, Sep 2020.

[155] M. R. Evans and S. N. Majumdar, "Diffusion with optimal resetting," *J. Phys. A: Math. Theor.*, vol. 44, p. 435001, oct 2011.

[156] B. Besga, A. Bovon, A. Petrosyan, S. N. Majumdar, and S. Ciliberto, "Optimal mean first-passage time for a Brownian searcher subjected to resetting:

Experimental and theoretical results," *Phys. Rev. Res.*, vol. 2, p. 032029, Jul 2020.

[157] F. Faisant, B. Besga, A. Petrosyan, S. Ciliberto, and S. N. Majumdar, "Optimal mean first-passage time of a Brownian searcher with resetting in one and two dimensions: experiments, theory and numerical tests," *J. Stat. Mech.*, vol. 2021, p. 113203, nov 2021.

[158] A. Pal, A. Kundu, and M. R. Evans, "Diffusion under time-dependent resetting," *J. Phys. A: Math. Theor.*, vol. 49, p. 225001, apr 2016.

[159] H. E. White *et al.*, *Introduction to atomic spectra*. McGraw-Hill book Co., Inc., 1934.

[160] H. Goldstein, *Classical Mechanics*. Addison-Wesley, 1980.

[161] M. Marinescu, H. R. Sadeghpour, and A. Dalgarno, "Dispersion coefficients for alkali-metal dimers," *Phys. Rev. A*, vol. 49, pp. 982–988, Feb 1994.

[162] J. R. Rydberg, "Recherches sur la constitution des spectres d'emission des elements chimique," *Den Kungliga Svenska Vetenskapsakademiens Handlingar*, vol. 23, p. 11, 1889.

[163] W. Ritz, "Magnetische Atomfelder und Serienspektren," *Ann. Phys. (Berlin)*, vol. 330, no. 4, pp. 660–696, 1908.

[164] J. E. Mayer and M. G. Mayer, "The Polarizabilities of Ions from Spectra," *Phys. Rev.*, vol. 43, pp. 605–611, Apr 1933.

[165] Y. Cui *et al.*, "Extending bandwidth sensitivity of Rydberg-atom-based microwave electrometry using an auxiliary microwave field," *Phys. Rev. A*, vol. 107, p. 043102, Apr 2023.

[166] M. Mack, J. Grimmel, F. Karlewski, L. m. H. Sárkány, H. Hattermann, and J. Fortágh, "All-optical measurement of Rydberg-state lifetimes," *Phys. Rev. A*, vol. 92, p. 012517, Jul 2015.

[167] T. Cantat-Moltrecht, R. Cortiñas, B. Ravon, P. Méhaignerie, S. Haroche, J. M. Raimond, M. Favier, M. Brune, and C. Sayrin, "Long-lived circular Rydberg states of laser-cooled rubidium atoms in a cryostat," *Phys. Rev. Res.*, vol. 2, p. 022032, May 2020.

[168] W. R. Anderson, J. R. Veale, and T. F. Gallagher, "Resonant Dipole-Dipole Energy Transfer in a Nearly Frozen Rydberg Gas," *Phys. Rev. Lett.*, vol. 80, pp. 249–252, Jan 1998.

[169] I. Mourachko, D. Comparat, F. de Tomasi, A. Fioretti, P. Nosbaum, V. M. Akulin, and P. Pillet, "Many-Body Effects in a Frozen Rydberg Gas," *Phys. Rev. Lett.*, vol. 80, pp. 253–256, Jan 1998.

[170] D. Griffiths, *Introduction to Electrodynamics*. Pearson Education, 2014.

[171] T. G. Walker and M. Saffman, "Consequences of Zeeman degeneracy for the van der Waals blockade between Rydberg atoms," *Phys. Rev. A*, vol. 77, p. 032723, Mar 2008.

[172] K. A. Safinya, J. F. Delpech, F. Gounand, W. Sandner, and T. F. Gallagher, "Resonant Rydberg-Atom-Rydberg-Atom Collisions," *Phys. Rev. Lett.*, vol. 47, pp. 405–408, Aug 1981.

[173] T. Vogt, M. Viteau, J. Zhao, A. Chotia, D. Comparat, and P. Pillet, "Dipole Blockade at Förster Resonances in High Resolution Laser Excitation of Rydberg States of Cesium Atoms," *Phys. Rev. Lett.*, vol. 97, p. 083003, Aug 2006.

[174] S. Ravets, H. Labuhn, D. Barredo, L. Béguin, T. Lahaye, and A. Browaeys, "Coherent dipole–dipole coupling between two single Rydberg atoms at an electrically-tuned Förster resonance," *Nat. Phys.*, vol. 10, pp. 914–917, Dec 2014.

[175] D. Barredo, H. Labuhn, S. Ravets, T. Lahaye, A. Browaeys, and C. S. Adams, "Coherent Excitation Transfer in a Spin Chain of Three Rydberg Atoms," *Phys. Rev. Lett.*, vol. 114, p. 113002, Mar 2015.

[176] N. Šibalić, J. Pritchard, C. Adams, and K. Weatherill, "ARC: An open-source library for calculating properties of alkali Rydberg atoms," *Comput. Phys. Commun.*, vol. 220, pp. 319–331, 2017.

[177] L. Henriet, L. Beguin, A. Signoles, T. Lahaye, A. Browaeys, G.-O. Reymond, and C. Jurczak, "Quantum computing with neutral atoms," *Quantum*, vol. 4, p. 327, Sept. 2020.

[178] A. Gaëtan, Y. Miroshnychenko, T. Wilk, A. Chotia, M. Viteau, D. Comparat, P. Pillet, A. Browaeys, and P. Grangier, "Observation of collective excitation of two individual atoms in the Rydberg blockade regime," *Nat. Phys.*, vol. 5, pp. 115–118, Feb 2009.

[179] I. Lesanovsky and J. P. Garrahan, "Kinetic Constraints, Hierarchical Relaxation, and Onset of Glassiness in Strongly Interacting and Dissipative Rydberg Gases," *Phys. Rev. Lett.*, vol. 111, p. 215305, Nov 2013.

[180] D. F. James and J. Jerke, "Effective Hamiltonian theory and its applications in quantum information," *Can. J. Phys.*, vol. 85, no. 6, pp. 625–632, 2007.

[181] I. S. Gradshteyn and I. M. Ryzhik, *Table of integrals, series, and products.* Elsevier/Academic Press, Amsterdam, seventh ed., 2007. Translated from the Russian.

[182] E. Roldán and S. Gupta, "Path-integral formalism for stochastic resetting: Exactly solved examples and shortcuts to confinement," *Phys. Rev. E*, vol. 96, p. 022130, Aug 2017.

[183] L. Kuśmierz and T. Toyoizumi, "Robust random search with scale-free stochastic resetting," *Phys. Rev. E*, vol. 100, p. 032110, Sep 2019.

[184] A. G. Pakes, "Killing and resurrection of markov processes," *Commun. Stat. Stoch. Model.*, vol. 13, no. 2, pp. 255–269, 1997.

[185] A. Chechkin and I. M. Sokolov, "Random Search with Resetting: A Unified Renewal Approach," *Phys. Rev. Lett.*, vol. 121, p. 050601, Aug 2018.

[186] A. Nagar and S. Gupta, "Diffusion with stochastic resetting at power-law times," *Phys. Rev. E*, vol. 93, p. 060102, Jun 2016.

[187] M. Kulkarni and S. N. Majumdar, "First detection probability in quantum resetting via random projective measurements," *arXiv:2305.15123*, 2023.

[188] B. Skinner, J. Ruhman, and A. Nahum, "Measurement-Induced Phase Transitions in the Dynamics of Entanglement," *Phys. Rev. X*, vol. 9, p. 031009, Jul 2019.

[189] S. Choi, Y. Bao, X.-L. Qi, and E. Altman, "Quantum Error Correction in Scrambling Dynamics and Measurement-Induced Phase Transition," *Phys. Rev. Lett.*, vol. 125, p. 030505, Jul 2020.

[190] M. Magoni, P. P. Mazza, and I. Lesanovsky, "Emergent Bloch Oscillations in a Kinetically Constrained Rydberg Spin Lattice," *Phys. Rev. Lett.*, vol. 126, p. 103002, Mar 2021.

[191] M. Magoni, P. P. Mazza, and I. Lesanovsky, "Phonon dressing of a facilitated one-dimensional Rydberg lattice gas," *SciPost Phys. Core*, vol. 5, p. 041, 2022.

[192] M. Magoni, R. Joshi, and I. Lesanovsky, "Rydberg tweezer molecules: Spin-phonon entanglement and Jahn-Teller effect," *arXiv:2303.08861*, 2023.

[193] G. Perfetto, F. Carollo, M. Magoni, and I. Lesanovsky, "Designing nonequilibrium states of quantum matter through stochastic resetting," *Phys. Rev. B*, vol. 104, p. L180302, Nov 2021.

[194] J. Janssen and R. Manca, *Applied Semi-Markov Processes*. SpringerLink: Springer e-Books, Springer US, 2006.

[195] M. Magoni, F. Carollo, G. Perfetto, and I. Lesanovsky, "Emergent quantum correlations and collective behavior in noninteracting quantum systems subject to stochastic resetting," *Phys. Rev. A*, vol. 106, p. 052210, Nov 2022.

[196] F. Bloch, "Über die Quantenmechanik der Elektronen in Kristallgittern," *Z. Phys.*, vol. 52, pp. 555–600, Jul 1929.

[197] C. Zener, "A Theory of the Electrical Breakdown of Solid Dielectrics," *Proc. R. Soc. London A*, vol. 145, pp. 523–529, July 1934.

[198] G. H. Wannier, "Wave Functions and Effective Hamiltonian for Bloch Electrons in an Electric Field," *Phys. Rev.*, vol. 117, pp. 432–439, Jan 1960.

[199] T. Hartmann, F. Keck, H. J. Korsch, and S. Mossmann, "Dynamics of Bloch oscillations," *New J. Phys.*, vol. 6, pp. 2–2, jan 2004.

[200] M. Kormos, M. Collura, G. Takács, and P. Calabrese, "Real-time confinement following a quantum quench to a non-integrable model," *Nat. Phys.*, vol. 13, pp. 246–249, Mar 2017.

[201] A. Lerose, F. M. Surace, P. P. Mazza, G. Perfetto, M. Collura, and A. Gambassi, "Quasilocalized dynamics from confinement of quantum excitations," *Phys. Rev. B*, vol. 102, p. 041118, Jul 2020.

[202] E. van Nieuwenburg, Y. Baum, and G. Refael, "From Bloch oscillations to many-body localization in clean interacting systems," *Proc. Natl. Acad. Sci. U.S.A.*, vol. 116, no. 19, pp. 9269–9274, 2019.

[203] M. Schulz, C. A. Hooley, R. Moessner, and F. Pollmann, "Stark Many-Body Localization," *Phys. Rev. Lett.*, vol. 122, p. 040606, Jan 2019.

[204] P. Sala, T. Rakovszky, R. Verresen, M. Knap, and F. Pollmann, "Ergodicity Breaking Arising from Hilbert Space Fragmentation in Dipole-Conserving Hamiltonians," *Phys. Rev. X*, vol. 10, p. 011047, Feb 2020.

[205] V. Khemani, M. Hermele, and R. Nandkishore, "Localization from Hilbert space shattering: From theory to physical realizations," *Phys. Rev. B*, vol. 101, p. 174204, May 2020.

[206] R. M. Nandkishore and M. Hermele, "Fractons," *Annu. Rev. Condens. Matter Phys.*, vol. 10, no. 1, pp. 295–313, 2019.

[207] S. Pai and M. Pretko, "Fractons from confinement in one dimension," *Phys. Rev. Res.*, vol. 2, p. 013094, Jan 2020.

[208] U. Fano, "Effects of Configuration Interaction on Intensities and Phase Shifts," *Phys. Rev.*, vol. 124, pp. 1866–1878, Dec 1961.

[209] H. A. Jahn and E. Teller, "Stability of Polyatomic Molecules in Degenerate Electronic States. I. Orbital Degeneracy," *Proc. Roy. Soc. A*, vol. 161, no. 905, pp. 220–235, 1937.

[210] H. A. Jahn, "Stability of Polyatomic Molecules in Degenerate Electronic States. II. Spin Degeneracy," *Proc. Roy. Soc. A*, vol. 164, no. 916, pp. 117–131, 1938.

[211] Y.-Q. Zou, M. Berngruber, V. S. V. Anasuri, N. Zuber, F. Meinert, R. Löw, and T. Pfau, "Observation of Vibrational Dynamics of Orientated Rydberg-Atom-Ion Molecules," *Phys. Rev. Lett.*, vol. 130, p. 023002, Jan 2023.

[212] F.-R. Winkelmann, C. A. Weidner, G. Ramola, W. Alt, D. Meschede, and A. Alberti, "Direct measurement of the Wigner function of atoms in an optical trap," *J. Phys. B: At. Mol. Opt. Phys.*, vol. 55, p. 194004, sep 2022.

[213] M. O. Brown, S. R. Muleady, W. J. Dworschack, R. J. Lewis-Swan, A. M. Rey, O. Romero-Isart, and C. A. Regal, "Time-of-flight quantum tomography of an atom in an optical tweezer," *Nat. Phys.*, vol. 19, pp. 569–573, Apr 2023.

[214] H. Saßmannshausen and J. Deiglmayr, "Observation of Rydberg-Atom Macrodimers: Micrometer-Sized Diatomic Molecules," *Phys. Rev. Lett.*, vol. 117, p. 083401, Aug 2016.

[215] S. Hollerith, J. Zeiher, J. Rui, A. Rubio-Abadal, V. Walther, T. Pohl, D. M. Stamper-Kurn, I. Bloch, and C. Gross, "Quantum gas microscopy of Rydberg macrodimers," *Science*, vol. 364, no. 6441, pp. 664–667, 2019.

[216] A. Tavakoli, G. Haack, N. Brunner, and J. B. Brask, "Autonomous multipartite entanglement engines," *Phys. Rev. A*, vol. 101, p. 012315, 1 2020.

[217] X. Cao, A. Tilloy, and A. D. Luca, "Entanglement in a fermion chain under continuous monitoring," *SciPost Phys.*, vol. 7, p. 024, 2019.

[218] H. M. Wiseman and G. J. Milburn, *Quantum Measurement and Control*. Cambridge University Press, 2009.

[219] D. Girolami, T. Tufarelli, and G. Adesso, "Characterizing Nonclassical Correlations via Local Quantum Uncertainty," *Phys. Rev. Lett.*, vol. 110, p. 240402, Jun 2013.

[220] D. Barredo, V. Lienhard, P. Scholl, S. de Léséleuc, T. Boulier, A. Browaeys, and T. Lahaye, "Three-Dimensional Trapping of Individual Rydberg Atoms in Ponderomotive Bottle Beam Traps," *Phys. Rev. Lett.*, vol. 124, p. 023201, Jan 2020.

[221] D. Petrosyan and K. Mølmer, "Binding Potentials and Interaction Gates between Microwave-Dressed Rydberg Atoms," *Phys. Rev. Lett.*, vol. 113, p. 123003, Sep 2014.

[222] S. Sevinçli and T. Pohl, "Microwave control of Rydberg atom interactions," *New J. Phys.*, vol. 16, p. 123036, dec 2014.

[223] P. W. Anderson, "Absence of Diffusion in Certain Random Lattices," *Phys. Rev.*, vol. 109, pp. 1492–1505, Mar 1958.

[224] A. Smith, J. Knolle, D. L. Kovrizhin, and R. Moessner, "Disorder-Free Localization," *Phys. Rev. Lett.*, vol. 118, p. 266601, Jun 2017.

[225] S. Scherg, T. Kohlert, P. Sala, F. Pollmann, B. Hebbe Madhusudhana, I. Bloch, and M. Aidelsburger, "Observing non-ergodicity due to kinetic constraints in tilted Fermi-Hubbard chains," *Nat. Commun.*, vol. 12, p. 4490, Jul 2021.

[226] P. Bak, C. Tang, and K. Wiesenfeld, "Self-organized criticality: An explanation of the 1/f noise," *Phys. Rev. Lett.*, vol. 59, pp. 381–384, Jul 1987.

7 Appendix: publications

First Publication

Emergent Bloch Oscillations in a Kinetically Constrained Rydberg Spin Lattice

Matteo Magoni,[1] Paolo P. Mazza,[1] and Igor Lesanovsky[1,2]
[1]*Institut für Theoretische Physik, Eberhard Karls Universität Tübingen, Auf der Morgenstelle 14, 72076 Tübingen, Germany*
[2]*School of Physics and Astronomy and Centre for the Mathematics and Theoretical Physics of Quantum Non-Equilibrium Systems, The University of Nottingham, Nottingham NG7 2RD, United Kingdom*

(Received 27 October 2020; accepted 17 February 2021; published 12 March 2021)

We explore the relaxation dynamics of elementary spin clusters in a kinetically constrained spin system. Inspired by experiments with Rydberg lattice gases, we focus on the situation in which an excited spin leads to a "facilitated" excitation of a neighboring spin. We show that even weak interactions that extend beyond nearest neighbors can have a dramatic impact on the relaxation behavior: they generate a linear potential, which under certain conditions leads to the onset of Bloch oscillations of spin clusters. These hinder the expansion of a cluster and, more generally, the relaxation of many-body states toward equilibrium. This shows that nonergodic behavior in kinetically constrained systems may occur as a consequence of the interplay between reduced connectivity of many-body states and weak interparticle interactions. We furthermore show that the emergent Bloch oscillations identified here can be detected in experiment through measurements of the Rydberg atom density and discuss how spin-orbit coupling between internal and external degrees of freedom of spin clusters can be used to control their relaxation behavior.

DOI: 10.1103/PhysRevLett.126.103002

Introduction.—Kinetically constrained quantum systems have become an important setting for the investigation of complex dynamical many-body phenomena, both from the theoretical and the experimental point of view. In particular, constrained spin systems have turned out to constitute useful models for the study of slow relaxation, ergodicity breaking, and the emergence of glassy physics [1–16]. In terms of experimental platforms, a significant role is currently being played by Rydberg gases, in which atoms are excited to high-lying and strongly interacting states. This allows one to implement effective quantum spin models with highly controllable state-dependent interactions that pave the way toward realizing a host of kinetic constraints [17–28].

Kinetic constraints impose restrictions on the connectivity between many-body states that break the Hilbert space into disconnected sectors [29–32]. Ultimately, this may lead to the absence of thermalization and the emergence of nonergodic behavior. This mechanism is different to ergodicity breaking stemming from disorder, occurring in many-body localized systems where it is caused by the emergence of local conservation laws [33]. Ergodicity breaking (in a disorder-free setting) may also occur when imposing externals fields: Refs. [34–42] show that for the case of a transverse field quantum Ising model, where an additionally applied longitudinal field leads to the confinement of excitations. This inhibits propagation of quasiparticles and thus prevents relaxation toward an ergodic steady state.

In this Letter, we investigate the dynamics of a disorder-free, translationally invariant many-body quantum spin system under a so-called facilitation constraint. As shown in Fig. 1, this can be realized with Rydberg atoms held in a lattice. We show that relaxation toward an ergodic stationary state is inhibited by the onset of Bloch oscillations of spin clusters—composite states of domain wall quasiparticles—which are caused by an emerging internal potential linear in the cluster size. These oscillations, which also have shown to herald nonergodicity in the absence of disorder in different contexts, e.g., when external fields are imposed [36,38,43,44], can be observed in the dynamics of the (Rydberg atom) density and thus are directly accessible in experiments. We argue that Bloch oscillations lead to an emergent "Hilbert space fragmentation" [45–47], reminiscent of fractonic systems [48,49]. We furthermore show that there is a strong (spin-orbit) coupling between the internal dynamics of spin clusters and their external motion, which allows one to construct either confined or propagating wave packets. Our Letter shows that constraints in conjunction with weak interactions offer new mechanisms for localization that go beyond merely breaking the Hilbert space connectivity of many-body states.

Rydberg gas under facilitation conditions.—We consider a one-dimensional chain of N atoms as depicted in Fig. 1(a). For each atom, we employ a two-level description in terms of a fictitious spin-$\frac{1}{2}$ particle, which can be either in the up state $|\uparrow\rangle$ (excited Rydberg state) or in the down state $|\downarrow\rangle$ (ground state). Two atoms in the Rydberg state at neighboring sites have interaction energy $V_{\mathrm{NN}} > 0$ (repulsive interactions). Including interactions up to next-nearest neighbors (V_{NNN}), the Hamiltonian of the system is given by

 © 2021 American Physical Society

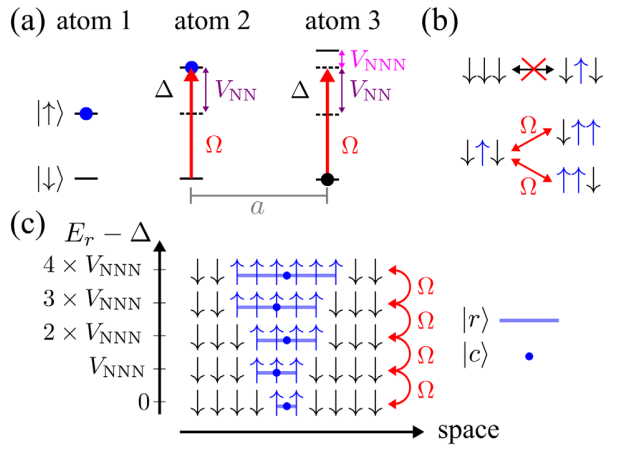

FIG. 1. Facilitated spin dynamics in a Rydberg lattice. (a) Each atom is modeled as a two-level system, in which the states $|\uparrow\rangle$ and $|\downarrow\rangle$ represent the (excited) Rydberg state and the ground state, respectively. Atoms are separated by the distance a. Ω is the Rabi frequency of the excitation laser, which is detuned from the atomic transition by an energy Δ. V_{NN} and V_{NNN} are the nearest neighbor and the next-nearest neighbor interaction strength between excited atoms. (b) In the facilitation regime a spin next to an excited spin is facilitated to (de)excite. This is achieved by setting $V_{\mathrm{NN}} + \Delta = 0$. Each cluster can expand and shrink, but can neither merge with another cluster nor split. (c) Each cluster is parametrized by two coordinates: $|c\rangle$ (labeling the center of mass position) and $|r\rangle$ (labeling the number of excitations). The internal energy of a cluster of extension r is given by $E_r = (r-2)V_{\mathrm{NNN}} + \Delta$, generating a linear potential for spin clusters.

$$H = \sum_{j=1}^{N} \left(\frac{\Omega}{2} \hat{\sigma}_j^x + \Delta \hat{n}_j + V_{\mathrm{NN}} \hat{n}_j \hat{n}_{j+1} + V_{\mathrm{NNN}} \hat{n}_j \hat{n}_{j+2} \right), \quad (1)$$

where Ω is the Rabi frequency and Δ is the laser detuning from the atomic transition energy. The operator $\hat{\sigma}^x = |\uparrow\rangle\langle\downarrow| + |\downarrow\rangle\langle\uparrow|$ effectuates transitions between the ground and Rydberg state, and $\hat{n} = |\uparrow\rangle\langle\uparrow|$ projects on the Rydberg state. Periodic boundary conditions are also adopted.

We consider so-called facilitation conditions as depicted in Fig. 1(b). This means that the detuning cancels out the interaction between two adjacent atoms, i.e., $\Delta + V_{\mathrm{NN}} = 0$. Moreover, we assume that the next-nearest neighbor interaction is small, i.e., $|V_{\mathrm{NNN}}| \ll |\Delta|$. Under these conditions, clusters of consecutive Rydberg excitations expand or shrink, but cannot (dis)appear, i.e., can neither split in two different clusters nor merge with another cluster. Hence, the total number of clusters is a conserved quantity. Note that this is rigorously true only when $\Delta \to \infty$ [38,50], and consequently, we assume Δ to be the largest energy scale (see Supplemental Material [51]). For a single spin cluster, a typical sequence of (near-)resonant transitions is, e.g., given by $|\downarrow\uparrow\downarrow\downarrow\downarrow\ldots\rangle \Leftrightarrow |\downarrow\uparrow\uparrow\downarrow\downarrow\ldots\rangle \Leftrightarrow |\downarrow\uparrow\uparrow\uparrow\downarrow\ldots\rangle \Leftrightarrow |\downarrow\downarrow\uparrow\uparrow\downarrow\ldots\rangle \Leftrightarrow |\downarrow\downarrow\uparrow\downarrow\downarrow\ldots\rangle$ [31]. It is thus convenient to describe the state of each cluster using two coordinates: the position of the center of mass (c.m.) c and the number of excitations r [see Fig. 1(c)]. The internal energy of a cluster composed of r excitations is then $E_r = r\Delta + (r-1)V_{\mathrm{NN}} + (r-2)V_{\mathrm{NNN}} = \Delta + (r-2)V_{\mathrm{NNN}}$, where the facilitation condition was used in the last step.

Quasiparticle excitation spectrum.—Let us begin from the situation in which a single cluster is present in a lattice of length N (with the lattice spacing expressed in units of a) and assume periodic boundary conditions. It is then convenient to write the generic state of the cluster as a tensor product of the c.m. coordinate and the relative coordinate $|\psi\rangle = |c\rangle \otimes |r\rangle$, where c is an index that labels the position of the c.m. of the cluster and r denotes the number of excitations. The total number of possible values of the c.m. coordinate is thus $2N$: $c \in \{\frac{1}{2}, 1, 3/2, \ldots, N\}$. Integer values of c refer to on-site centers of mass, while the half-integer values correspond to centers of mass located at the midpoints between two lattice sites. The coordinate r is instead an integer number between 1 and $N-1$, since a cluster with N excitations is not allowed. Thus, for instance, $|2\rangle|3\rangle = |\uparrow\uparrow\uparrow\downarrow\downarrow\ldots\rangle$ and $|5/2\rangle|2\rangle = |\downarrow\uparrow\uparrow\downarrow\downarrow\ldots\rangle$.

Given this representation, there are four possible transitions that a state $|c\rangle|r\rangle$ can undertake (at rate Ω), provided that $1 < r < N-1$ (when $r = 1$ the cluster can only increase; when $r = N-1$ the cluster can only decrease). Possible target states are (see Fig. 1) $|c + \frac{1}{2}\rangle|r+1\rangle$ (the spin to the right of the rightmost excitation flips up), $|c - \frac{1}{2}\rangle|r+1\rangle$ (the spin to the left of the leftmost excitation flips up), $|c - \frac{1}{2}\rangle|r-1\rangle$ (the rightmost excitation flips down), or $|c + \frac{1}{2}\rangle|r-1\rangle$ (the leftmost excitation flips down). Note that these transitions rules, which determine the kinetic energy of a spin cluster, imply a spin-orbit coupling, i.e., a coupling between the (internal) relative coordinate of the cluster and the (external) c.m. dynamics. This is because a cluster cannot shrink or expand without changing its c.m. position. Taking, furthermore, into account the internal energy E_r, which only depends on the cluster length r, the effective Hamiltonian describing a single spin cluster reads

$$H = \Omega \sum_{c=\frac{1}{2}}^{N} \sum_{r=1}^{N-2} \left[\left| c + \frac{1}{2} \right\rangle \langle c| \otimes (|r+1\rangle\langle r| + \mathrm{H.c.}) + \mathrm{H.c.} \right] + V_{\mathrm{NNN}} \sum_{c=\frac{1}{2}}^{N} \sum_{r=2}^{N-1} (r-2)|c\rangle\langle c| \otimes |r\rangle\langle r|. \quad (2)$$

Taking the Fourier transform of the c.m. coordinate $|c\rangle = 1/\sqrt{2N} \sum_q e^{iqc}|q\rangle$, where $q = -2\pi + (2\pi/N)k$ with $k = 0, 1, \ldots, 2N-1$, simplifies the Hamiltonian to $H = \sum_q H_q |q\rangle\langle q|$, with

$$H_q = 2\Omega \cos\left(\frac{q}{2}\right) \sum_{r=1}^{N-2} (|r+1\rangle\langle r| + \mathrm{H.c.}) + V_{\mathrm{NNN}} \sum_{r=2}^{N-1} (r-2)|r\rangle\langle r|. \quad (3)$$

Note, that the c.m. momentum quantum number q takes on values between -2π and 2π because of the $2N$ lattice sites that make up the c.m. lattice. The Hamiltonian H_q of each c.m. momentum sector can be interpreted as that of a particle hopping with a rate $J_q = 2\Omega\cos(q/2)$ through a semi-infinite lattice, subject to a linear potential of slope V_{NNN}. This potential, however, affects only "sites" with coordinate $r > 2$.

Spin cluster Bloch oscillations.—Evidently, there is a close connection between the spin cluster dynamics and that of a hopping particle in a tilted lattice. The latter is a classic problem in condensed matter physics [57–62], and one of its most striking dynamical features is the emergence of so-called Bloch oscillations. Our situation bears some differences, though, such as the semi-infinite lattice and the fact that spin clusters are composite objects that have an internal and an external structure. In the following, we consider the dynamics of a spin cluster that is initially prepared (time $t = 0$) in a state with c.m. position c_0 and contains r_0 consecutive excitations: $|\psi(0)\rangle = |c_0\rangle \otimes |r_0\rangle$ (note, that c_0 and r_0 have to be compatible, e.g., when r_0 is odd, c_0 has to be an integer). This state evolves according to

$$|\psi(t)\rangle = e^{-iHt}|\psi(0)\rangle = \frac{1}{\sqrt{2N}}\sum_q e^{iqc_0}|q\rangle \otimes e^{-iH_q t}|r_0\rangle. \quad (4)$$

In Fig. 2 we show the site-resolved Rydberg excitation density—a quantity that can be experimentally measured [19]—for a spin cluster of initial size $r_0 = 6$. In the absence of next-nearest neighbor interactions, this cluster expands linearly in time and the density shows the expected light cone structure. For large V_{NNN}, however, we see unambiguously Bloch oscillations of the spin cluster size, whose period is given by $T_{\mathrm{Bloch}} = 2\pi/V_{\mathrm{NNN}}$. At intermediate values of V_{NNN}, we observe that Bloch oscillations and ballistic expansion coexist. The reason for this behavior is the composite nature of the spin domain excitation together with the fact that the tilted lattice is actually semi-infinite. As can be seen from the Hamiltonian (3) each q component is governed by a different "hopping rate" J_q. For a given hopping rate, the amplitude of the Bloch oscillations is then $l_{\mathrm{Bloch}} \simeq J_q/V_{\mathrm{NNN}}$. This relation, however, holds only in case of an infinite lattice. For a spin cluster to effectively experience such infinite lattice, its initial size r_0 must be larger than l_{Bloch}, so that Bloch oscillations never reach its boundary. For the parameters chosen for Fig. 2(b) this is, however, true only for certain values of the c.m. momentum q on which the initial state has support. Therefore, these components perform Bloch oscillations, while the others expand ballistically. This results in the coexistence behavior displayed in the panel.

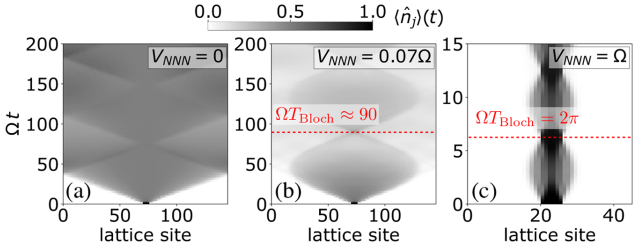

FIG. 2. Time evolution of a spin cluster. Shown is the local Rydberg excitation density $\langle\hat{n}_j\rangle(t)$. (a) Ballistic expansion of spin cluster. (b) Coexistence of Bloch oscillations and ballistic expansion. (c) Bloch oscillations with period $T_{\mathrm{Bloch}} = 2\pi/V_{\mathrm{NNN}}$. The initial state is $|\psi(0)\rangle = |c_0\rangle \otimes |r_0\rangle$ with $r_0 = 6$ and c_0 chosen appropriately for each panel.

Requiring that the initial cluster size r_0 is large enough, such that no q component of the state experiences the edge of the lattice, defines a lower threshold for the next-nearest neighbor interaction

$$V_{\mathrm{NNN}} \gtrsim \frac{2\Omega}{r_0}. \quad (5)$$

If this condition is satisfied, then perfect Bloch oscillations as shown in Fig. 2(c) are observed. To quantify the onset of Bloch oscillations and the concomitant periodic behavior, we define the autocorrelation function

$$\mathcal{A}(t) = |\langle\psi(0)|\psi(t)\rangle|^2, \quad (6)$$

which measures the overlap between the initial state and the state at time t. Figure 3(a) shows that there is a gradual passage from a regime of ballistic expansion to one with Bloch oscillations with an intermediate coexistence regime, indicated with the blue shaded area. As expected, one observes pronounced time-periodic behavior for sufficiently large values of V_{NNN}, with high-amplitude revivals at the Bloch period $T_{\mathrm{Bloch}} = 2\pi/V_{\mathrm{NNN}}$. Decreasing the next-nearest neighbor interaction strength reduces the amplitude of these revivals, which is due to certain c.m.

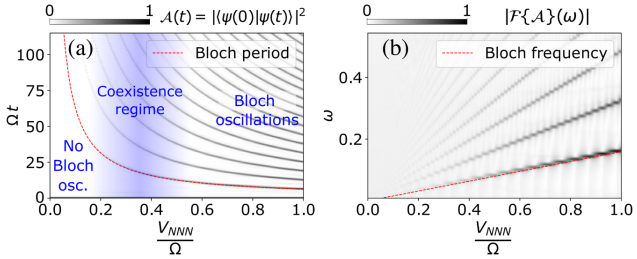

FIG. 3. Autocorrelation function and its Fourier transform. (a) Autocorrelation function, Eq. (6), as a function of the next-nearest neighbor interaction strength V_{NNN}. The red dashed line shows the expected Bloch oscillation period, $T_{\mathrm{Bloch}} = 2\pi/V_{\mathrm{NNN}}$. Bloch oscillations become visible through marked peaks only for sufficiently large V_{NNN}. In the coexistence regime, some wave packet components undergo ballistic expansion. (b) Fourier transform of the autocorrelation function. The red dashed line shows the expected Bloch oscillation frequency.

momentum components evolving ballistically. This behavior is also reflected in the Fourier transform of the autocorrelation function shown in Fig. 3(b), which displays a clear peak at the Bloch frequency (and higher harmonics) up to a threshold value of V_{NNN}.

Spin-orbit coupling of spin clusters.—So far, we have analyzed the evolution of an initial state that is composed of a single spin cluster with fixed size r_0 and c.m. position c_0. As can be seen from Eq. (4), such state has an equal weight (up to a phase factor) on all q components. This state is certainly the one that is most naturally prepared in experiment (see Supplemental Material [51]). However, to fully investigate how the (spin-orbit) coupling between the relative and c.m. motion affects the dynamics of spin clusters, it is instructive to study initial states in which the c.m. position is not fixed, but has the form of a Gaussian wave packet of finite width σ,

$$|\psi(0)\rangle = \left(\frac{1}{\mathcal{N}}\sum_c e^{-\frac{(c-c_0)^2}{4\sigma^2}} e^{-iq_0 c}|c\rangle\right) \otimes |r_0\rangle. \qquad (7)$$

Here $\mathcal{N}$ is a normalization constant and c_0 and q_0 are the average c.m. position and momentum. A possible protocol for creating such state is discussed in [63]. In order to get a first idea of what dynamical behavior to expect, we consider the band structure of the Hamiltonian H_q [Eq. (3)], which is depicted in Fig. 4(a). One observes a series of $N-1$ bands that govern the dynamics of the relative motion (spin cluster expansion and reduction) as a function of the c.m. momentum q, which is a direct manifestation of the coupling between those two degrees of freedom. Note that in case of an infinite lattice the bands would be flat and equally spaced forming the well-known Wannier-Stark ladder [59]. In a finite lattice, the eigenvalues of each Hamiltonian H_q are instead given by the zeros of the q-dependent Lommel polynomial of degree $N-1$ [64]. At $q = 0, \pm\pi$, and $\pm 2\pi$ the gradient of the bands is zero and the group velocity of a wave packet centered here vanishes. These points are thus well suited for an analysis in terms of the autocorrelation function, which otherwise would decay in time simply due to the linear motion of the wave packet. At $q = \pm\pi$, the hopping term in Eq. (3) vanishes and the Hamiltonian becomes diagonal in the $|r\rangle$ basis. This is seen in Fig. 4(b), which shows the projection of the initial spin domain state $|r_0\rangle$ (here with $r_0 = 6$) on the eigenstates of H_q. The plot also shows that for all other values of q the state $|r_0\rangle$ is not among the eigenstates but is formed by a superposition of them.

In Figs. 4(c) and 4(d), we show the autocorrelation function using the initial state (7) with $q_0 = 0$ and $q_0 = \pi$, respectively, as a function of σ. Both plots are obtained with the parameters of Fig. 2(b). For $\sigma = 0$, both situations correspond (up to a phase factor) to the one described by the state (4); i.e., we expect to observe a coexistence between Bloch oscillations and ballistic expansion. Indeed,

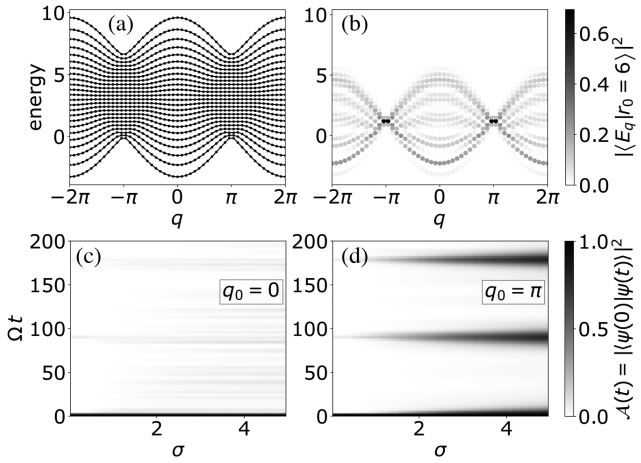

FIG. 4. Band structure and autocorrelation function. (a) Band structure given by the Hamiltonian H_q. Because of the presence of the linear potential introduced by the next-nearest neighbor interaction, the bands are locally flat and nondegenerate at $q = \pm\pi$. (b) Projection of the state $|r_0 = 6\rangle$ on the eigenstates of H_q, for different q. The overlap is larger for the low-energy eigenstates, and at $q = \pm\pi$ the state $|r_0 = 6\rangle$ is an eigenstate. (c) Autocorrelation function for an initial state centered on $q_0 = 0$. At $t = 0$, it has the value 1 and then decays rapidly. No periodic behavior is visible as σ increases. The faint features are due to finite size effects. (d) Autocorrelation function for an initial state centered on $q_0 = \pi$. Bloch oscillations appear as σ increases. (c),(d) We choose $V_{\mathrm{NNN}} = 0.07\Omega$ and $r_0 = 6$, which corresponds to the situation shown in Fig. 2(b).

here both Figs. 4(c) and 4(d) show the same faint signatures of Bloch oscillations. Upon an increase of σ, these are amplified for $q_0 = \pi$ and vanish for $q_0 = 0$. When $q_0 = \pi$, the initial state has support on the values of q that minimize the width of Bloch oscillations. Therefore, the initial spin cluster size r_0 is large enough not to see the boundary of the semi-infinite lattice. Conversely, when $q_0 = 0$, the width of the oscillations exceeds the initial cluster width r_0 and no Bloch oscillations appear. This result suggests that, for any given values of V_{NNN} and r_0, it is always possible to engineer an initial wave function sufficiently peaked around $q_0 = \pi$ that undergoes a periodic dynamics. This is a direct consequence of the spin-orbit coupling: Bloch oscillations are dynamical features of the relative spin cluster dynamics, but they can be controlled by the selection of specific c.m. momenta q.

Absence of relaxation in the many-body system.—Having understood the dynamics of a single spin cluster allows us to make statements on the dynamics in the many-body case: a general initial state can be decomposed into basis states containing m clusters. These shall be labeled with the coordinates $|c_i\rangle$ and $|r_i\rangle$, for $i = 1, 2, \ldots, m$. Such a state does not relax when each of the individual clusters performs Bloch oscillations without "touching" neighboring clusters. Such situation occurs when each of the m clusters has a length of at least $r_0 \simeq 2\Omega/V_{\mathrm{NNN}}$ and when the

distance between any two neighboring clusters is also at least r_0. The first requirement derives from Eq. (5) and ensures the emergence of Bloch oscillations within all m clusters. The second requirement comes from the fact that two neighboring clusters must not meet when oscillating with amplitude l_{Bloch}. A lower bound $\Gamma(N)$ for the number of many-body basis states that satisfy both conditions can be derived from the number $W(m)$ of ways m hard rods of length $2r_0$ can be arranged in a lattice of length N. With $W(m) = [(N - 2r_0m + m)!]/[(N - 2r_0m)!m!]$ and using that at most $N/(2r_0)$ rods can be inserted in a system of length N, we find that $\Gamma(N) = \sum_{m=1}^{N/2r_0} W(m) \sim C^N$, with $1 < C < 2$. Thus, the number of many-body states, whose dynamics is frozen due to spin cluster Bloch oscillations, scales exponentially with the lattice size. Therefore, nonrelaxing states are not rare in Hilbert space. This result is closely related to the fragmentation of Hilbert space observed in fractonic systems [48], characterized by a restricted mobility of elementary excitations. However, different from fractonic models, in our system there are no notions of charge and dipole moment conservation, and the emergence of disconnected Hilbert subspaces results from the restricted mobility of composite spin clusters.

Conclusions and outlook.—Observations related to ours have been made in quantum Ising chain systems [36,43,44], when an applied external longitudinal field penalizes the creation of extended spin clusters. In our case, however, confinement is created by interactions within the spin system itself, leading to emergent Bloch oscillations, whose dynamics is strongly dependent by the coupling between the internal and external dynamics of spin clusters. This shows that even weak interactions within constrained systems can have a dramatic impact on the ability to relax. In the future, it would be interesting to develop a scattering theory that describes collisions between two spin clusters and to generalize the study to kinetically constrained spin systems in two dimensions.

We acknowledge support from EPSRC (Grant No. EP/R04421X/1), the "Wissenschaftler-Rückkehrprogramm GSO/CZS" of the Carl-Zeiss-Stiftung and the German Scholars Organization e.V., as well as through the Deutsche Forschungsgemeinsschaft (DFG, German Research Foundation) under Project No. 428276754, through SPP 1929 (GiRyd), and under Germany's Excellence Strategy—EXC No. 2064/1—Project No. 390727645.

[1] C.-J. Lin and O. I. Motrunich, Out-of-time-ordered correlators in a quantum Ising chain, Phys. Rev. B **97**, 144304 (2018).
[2] C.-J. Lin and O. I. Motrunich, Exact Quantum Many-Body Scar States in the Rydberg-Blockaded Atom Chain, Phys. Rev. Lett. **122**, 173401 (2019).
[3] C. J. Turner, A. A. Michailidis, D. A. Abanin, M. Serbyn, and Z. Papic, Weak ergodicity breaking from quantum many-body scars, Nat. Phys. **14**, 745 (2018).
[4] M. Schecter and T. Iadecola, Weak Ergodicity Breaking and Quantum Many-Body Scars in Spin-1 XY Magnets, Phys. Rev. Lett. **123**, 147201 (2019).
[5] I. Lesanovsky and H. Katsura, Interacting Fibonacci anyons in a Rydberg gas, Phys. Rev. A **86**, 041601(R) (2012).
[6] V. Khemani, C. R. Laumann, and A. Chandran, Signatures of integrability in the dynamics of Rydberg-blockaded chains, Phys. Rev. B **99**, 161101(R) (2019).
[7] N. Shiraishi and T. Mori, Systematic Construction of Counterexamples to the Eigenstate Thermalization Hypothesis, Phys. Rev. Lett. **119**, 030601 (2017).
[8] F. M. Surace, P. P. Mazza, G. Giudici, A. Lerose, A. Gambassi, and M. Dalmonte, Lattice Gauge Theories and String Dynamics in Rydberg Atom Quantum Simulators, Phys. Rev. X **10**, 021041 (2020).
[9] M. Marcuzzi, M. Buchhold, S. Diehl, and I. Lesanovsky, Absorbing State Phase Transition with Competing Quantum and Classical Fluctuations, Phys. Rev. Lett. **116**, 245701 (2016).
[10] C. Ates, T. Pohl, T. Pattard, and J. M. Rost, Antiblockade in Rydberg Excitation of an Ultracold Lattice Gas, Phys. Rev. Lett. **98**, 023002 (2007).
[11] I. Lesanovsky and J. P. Garrahan, Out-of-equilibrium structures in strongly interacting Rydberg gases with dissipation, Phys. Rev. A **90**, 011603(R) (2014).
[12] M. Ostmann, M. Marcuzzi, J. P. Garrahan, and I. Lesanovsky, Localization in spin chains with facilitation constraints and disordered interactions, Phys. Rev. A **99**, 060101 (2019).
[13] M. Marcuzzi, J. Minar, D. Barredo, S. de Léséleuc, H. Labuhn, T. Lahaye, A. Browaeys, E. Levi, and I. Lesanovsky, Facilitation Dynamics and Localization Phenomena in Rydberg Lattice Gases with Position Disorder, Phys. Rev. Lett. **118**, 063606 (2017).
[14] J. P. Garrahan and D. Chandler, Geometrical Explanation and Scaling of Dynamical Heterogeneities in Glass Forming Systems, Phys. Rev. Lett. **89**, 035704 (2002).
[15] S. Moudgalya, B. A. Bernevig, and N. Regnault, Quantum many-body scars in a Landau level on a thin torus, Phys. Rev. B **102**, 195150 (2020).
[16] N. Pancotti, G. Giudice, J. I. Cirac, J. P. Garrahan, and M. C. Bañuls, Quantum East Model: Localization, Nonthermal Eigenstates, and Slow Dynamics, Phys. Rev. X **10**, 021051 (2020).
[17] M. M. Valado, C. Simonelli, M. D. Hoogerland, I. Lesanovsky, J. P. Garrahan, E. Arimondo, D. Ciampini, and O. Morsch, Experimental observation of controllable kinetic constraints in a cold atomic gas, Phys. Rev. A **93**, 040701(R) (2016).
[18] N. Lorenz, L. Festa, L.-M. Steinert, and C. Gross, Raman sideband cooling in optical tweezer arrays for Rydberg dressing, SciPost Phys. **10**, 052 (2021).
[19] A. Browaeys and T. Lahaye, Many-body physics with individually controlled Rydberg atoms, Nat. Phys. **16**, 132 (2020).
[20] S. Helmrich, A. Arias, G. Lochead, T. M. Wintermantel, M. Buchhold, S. Diehl, and S. Whitlock, Signatures of self-organized criticality in an ultracold atomic gas, Nature (London) **577**, 481 (2020).

[21] K. Singer, J. Stanojevic, M. Weidemüller, and R. Côté, Long-range interactions between alkali Rydberg atom pairs correlated to the *ns–ns*, *np–np* and *nd–nd* asymptotes, J. Phys. B **38**, S295 (2005).

[22] T. Pohl, H. Sadeghpour, and P. Schmelcher, Cold and ultracold Rydberg atoms in strong magnetic fields, Phys. Rep. **484**, 181 (2009).

[23] M. Aidelsburger, M. Lohse, C. Schweizer, M. Atala, J. T. Barreiro, S. Nascimbène, N. R. Cooper, I. Bloch, and N. Goldman, Measuring the Chern number of Hofstadter bands with ultracold bosonic atoms, Nat. Phys. **11**, 162 (2015).

[24] I. Bloch, J. Dalibard, and W. Zwerger, Many-body physics with ultracold gases, Rev. Mod. Phys. **80**, 885 (2008).

[25] I. Bloch, J. Dalibard, and S. Nascimbène, Quantum simulations with ultracold quantum gases, Nat. Phys. **8**, 267 (2012).

[26] Y.-Y. Jau, A. M. Hankin, T. Keating, I. H. Deutsch, and G. W. Biedermann, Entangling atomic spins with a Rydberg-dressed spin-flip blockade, Nat. Phys. **12**, 71 (2016).

[27] H. Bernien, S. Schwartz, A. Keesling, H. Levine, A. Omran, H. Pichler, S. Choi, A. S. Zibrov, M. Endres, M. Greiner *et al.*, Probing many-body dynamics on a 51-atom quantum simulator, Nature (London) **551**, 579 (2017).

[28] P. P. Mazza, R. Schmidt, and I. Lesanovsky, Vibrational Dressing in Kinetically Constrained Rydberg Spin Systems, Phys. Rev. Lett. **125**, 033602 (2020).

[29] C. Ates, J. P. Garrahan, and I. Lesanovsky, Thermalization of a Strongly Interacting Closed Spin System: From Coherent Many-Body Dynamics to a Fokker-Planck Equation, Phys. Rev. Lett. **108**, 110603 (2012).

[30] Z. Lan, M. van Horssen, S. Powell, and J. P. Garrahan, Quantum Slow Relaxation and Metastability Due to Dynamical Constraints, Phys. Rev. Lett. **121**, 040603 (2018).

[31] M. Ostmann, M. Marcuzzi, J. P. Garrahan, and I. Lesanovsky, Localization in spin chains with facilitation constraints and disordered interactions, Phys. Rev. A **99**, 060101(R) (2019).

[32] J. Sous and M. Pretko, Fractons from polarons, Phys. Rev. B **102**, 214437 (2020).

[33] D. A. Abanin, E. Altman, I. Bloch, and M. Serbyn, Colloquium: Many-body localization, thermalization, and entanglement, Rev. Mod. Phys. **91**, 021001 (2019).

[34] S. B. Rutkevich, Decay of the metastable phase in $d = 1$ and $d = 2$ Ising models, Phys. Rev. B **60**, 14525 (1999).

[35] S. B. Rutkevich, Kink confinement in the antiferromagnetic XXZ spin-$(1/2)$ chain in a weak staggered magnetic field, Europhys. Lett. **121**, 37001 (2018).

[36] M. Kormos, M. Collura, G. Takács, and P. Calabrese, Real-time confinement following a quantum quench to a non-integrable model, Nat. Phys. **13**, 246 (2017).

[37] P. P. Mazza, G. Perfetto, A. Lerose, M. Collura, and A. Gambassi, Suppression of transport in nondisordered quantum spin chains due to confined excitations, Phys. Rev. B **99**, 180302(R) (2019).

[38] A. Lerose, F. M. Surace, P. P. Mazza, G. Perfetto, M. Collura, and A. Gambassi, Quasilocalized dynamics from confinement of quantum excitations, Phys. Rev. B **102**, 041118(R) (2020).

[39] A. J. A. James, R. M. Konik, and N. J. Robinson, Nonthermal States Arising from Confinement in One and Two Dimensions, Phys. Rev. Lett. **122**, 130603 (2019).

[40] N. J. Robinson, A. J. A. James, and R. M. Konik, Signatures of rare states and thermalization in a theory with confinement, Phys. Rev. B **99**, 195108 (2019).

[41] G. Lagnese, F. M. Surace, M. Kormos, and P. Calabrese, Confinement in the spectrum of a Heisenberg-Ising spin ladder, J. Stat. Mech. (2020) 093106.

[42] F. B. Ramos, M. Lencsés, J. C. Xavier, and R. G. Pereira, Confinement and bound states of bound states in a transverse-field two-leg Ising ladder, Phys. Rev. B **102**, 014426 (2020).

[43] E. van Nieuwenburg, Y. Baum, and G. Refael, From Bloch oscillations to many-body localization in clean interacting systems, Proc. Natl. Acad. Sci. U.S.A. **116**, 9269 (2019).

[44] M. Schulz, C. A. Hooley, R. Moessner, and F. Pollmann, Stark Many-Body Localization, Phys. Rev. Lett. **122**, 040606 (2019).

[45] P. Sala, T. Rakovszky, R. Verresen, M. Knap, and F. Pollmann, Ergodicity Breaking Arising from Hilbert Space Fragmentation in Dipole-Conserving Hamiltonians, Phys. Rev. X **10**, 011047 (2020).

[46] V. Khemani, M. Hermele, and R. Nandkishore, Localization from Hilbert space shattering: From theory to physical realizations, Phys. Rev. B **101**, 174204 (2020).

[47] S. Moudgalya, A. Prem, R. Nandkishore, N. Regnault, and B. A. Bernevig, Thermalization and its absence within Krylov subspaces of a constrained Hamiltonian, arXiv: 1910.14048.

[48] R. M. Nandkishore and M. Hermele, Fractons, Annu. Rev. Condens. Matter Phys. **10**, 295 (2019).

[49] S. Pai and M. Pretko, Fractons from confinement in one dimension, Phys. Rev. Research **2**, 013094 (2020).

[50] D. A. Abanin, W. De Roeck, and F. Huveneers, Exponentially Slow Heating in Periodically Driven Many-Body Systems, Phys. Rev. Lett. **115**, 256803 (2015).

[51] See Supplemental Material at http://link.aps.org/supplemental/10.1103/PhysRevLett.126.103002 for details on the experimental parameters needed to observe Bloch oscillations and the preparation of the initial states, which includes Refs. [52–56].

[52] F. Nogrette, H. Labuhn, S. Ravets, D. Barredo, L. Béguin, A. Vernier, T. Lahaye, and A. Browaeys, Single-Atom Trapping in Holographic 2D Arrays of Microtraps with Arbitrary Geometries, Phys. Rev. X **4**, 021034 (2014).

[53] I. I. Beterov, I. I. Ryabtsev, D. B. Tretyakov, and V. M. Entin, Quasiclassical calculations of blackbody-radiation-induced depopulation rates and effective lifetimes of Rydberg nS, nP, and nD alkali-metal atoms with $n \leq 80$, Phys. Rev. A **79**, 052504 (2009).

[54] S. Weber, C. Tresp, H. Menke, A. Urvoy, O. Firstenberg, H. P. Büchler, and S. Hofferberth, Calculation of Rydberg interaction potentials, J. Phys. B **50**, 133001 (2017).

[55] J. Zeiher, R. van Bijnen, P. Schauß, S. Hild, J.-y. Choi, T. Pohl, I. Bloch, and C. Gross, Many-body interferometry of a Rydberg-dressed spin lattice, Nat. Phys. **12**, 1095 (2016).

[56] S. de Léséleuc, D. Barredo, V. Lienhard, A. Browaeys, and T. Lahaye, Optical Control of the Resonant Dipole-Dipole

Interaction between Rydberg Atoms, Phys. Rev. Lett. **119**, 053202 (2017).
[57] F. Bloch, Über die Quantenmechanik der Elektronen in Kristallgittern, Z. Phys. **52**, 555 (1929).
[58] C. Zener, A theory of the electrical breakdown of solid dielectrics, Proc. R. Soc. A **145**, 523 (1934).
[59] G. H. Wannier, Wave functions and effective Hamiltonian for Bloch electrons in an electric field, Phys. Rev. **117**, 432 (1960).
[60] G. H. Wannier, Dynamics of band electrons in electric and magnetic fields, Rev. Mod. Phys. **34**, 645 (1962).
[61] H. Fukuyama, R. A. Bari, and H. C. Fogedby, Tightly bound electrons in a uniform electric field, Phys. Rev. B **8**, 5579 (1973).
[62] T. Hartmann, F. Keck, H. J. Korsch, and S. Mossmann, Dynamics of Bloch oscillations, New J. Phys. **6**, 2 (2004).
[63] F. M. Surace and A. Lerose, Scattering of mesons in quantum simulators, arXiv:2011.10583.
[64] G. C. Stey and G. Gusman, Wannier-Stark ladders and the energy spectrum of an electron in a finite one dimensional crystal, J. Phys. C **6**, 650 (1973).

Second Publication

Phonon dressing of a facilitated one-dimensional Rydberg lattice gas

Matteo Magoni[1⋆], Paolo P. Mazza[1] and Igor Lesanovsky[1,2]

1 Institut für Theoretische Physik, Eberhard Karls Universität Tübingen, Auf der Morgenstelle 14, 72076 Tübingen, Germany
2 School of Physics and Astronomy and Centre for the Mathematics and Theoretical Physics of Quantum Non-Equilibrium Systems, The University of Nottingham, Nottingham, NG7 2RD, United Kingdom

⋆ matteo.magoni@uni-tuebingen.de

Abstract

We study the dynamics of a one-dimensional Rydberg lattice gas under facilitation (anti-blockade) conditions which implements a so-called kinetically constrained spin system. Here an atom can only be excited to a Rydberg state when one of its neighbors is already excited. Once two or more atoms are simultaneously excited mechanical forces emerge, which couple the internal electronic dynamics of this many-body system to external vibrational degrees of freedom in the lattice. This electron-phonon coupling results in a so-called phonon dressing of many-body states which in turn impacts on the facilitation dynamics. In our theoretical study we focus on a scenario in which all energy scales are sufficiently separated such that a perturbative treatment of the coupling between electronic and vibrational states is possible. This allows to analytically derive an effective Hamiltonian for the evolution of clusters of consecutive Rydberg excitations in the presence of phonon dressing. We analyze the spectrum of this Hamiltonian and show — by employing Fano resonance theory — that the interaction between Rydberg excitations and lattice vibrations leads to the emergence of slowly decaying bound states that inhibit fast relaxation of certain initial states.

Copyright M. Magoni *et al*.
This work is licensed under the Creative Commons Attribution 4.0 International License.
Published by the SciPost Foundation.

Received 28-04-2021
Accepted 29-07-2022
Published 23-08-2022
doi:10.21468/SciPostPhysCore.5.3.041

Contents

1 Introduction 1

2 One-dimensional Rydberg lattice gas 2

3 Facilitated Rydberg dynamics 4
3.1 Hamiltonian of a single Rydberg cluster 4
3.2 Decoupling the relative and center of mass motion of a Rydberg cluster 5
3.3 Effective Hamiltonian in the phonon dressing regime 6
3.4 Experimental considerations 7

4 Dynamics of a phonon dressed Rydberg cluster 9
4.1 Numerical results 9

5 Analytical results — Fano resonance theory 11

6 Conclusion 13

A Derivation of $H_{\text{eff},q}$ 14

B Derivation of the survival probability $p_d(t)$ 16

References 19

1 Introduction

In the past decades there has been a tremendous progress in the study of dynamical properties of complex quantum many-body systems with cold atoms [1–3]. A significant role has been played by Rydberg gases, in which atoms are excited to high-lying and strongly interacting states [4–19]. Thanks to the strong state-dependent interactions between Rydberg excitations, Rydberg gases constitute an ideal experimental platform for the implementation and simulation of so-called kinetically constrained quantum systems [20–23]. The phenomenology of such systems has been recently explored in several experiments involving bulk Rydberg gas clouds [24] or reconfigurable optical tweezer arrays [25–27]. The results observed in these experiments can be theoretically explained by the presence of a reduced connectivity between different configurations in the Hilbert space [28–31]. Being first introduced for the study of kinetic aspects in classical glassy systems [32], kinetically constrained systems have been shown to possess peculiar dynamical properties [33–36], in relation to nucleation and growth processes [37–39], the emergence of non-equilibrium phase transitions [40,41], localization [42–44] and the absence of relaxation and thermalization in general [45–48].

In this work we analyze the influence of lattice vibrations on the dynamics of a kinetically constrained one-dimensional Rydberg lattice gas. We focus on the so-called facilitation constraint, in which one Rydberg atom is favoured to (de)excite if only one neighboring Rydberg atom is already excited [49–52]. Being held in harmonic traps, the atoms are subject to lattice vibrations which couple to Rydberg excitations. This results in a phonon dressing [53] that affects the properties of the facilitation dynamics [54]. Throughout, we consider a parameter regime where the different energy scales involved in the problem are well separated. This allows us to employ a perturbative expansion in terms of the coupling constant between the Rydberg excitations (represented by effective spin degrees of freedom) and the phonon modes. By integrating out the phonon degrees of freedom, we derive an effective Hamiltonian describing the dynamics of phonon dressed clusters of consecutive Rydberg excitations. We investigate its energy spectrum and study the dynamics of phonon dressed Rydberg clusters. By using Fano resonance theory, we show that phonon dressing leads to a reduced mobility of some cluster configurations which is caused by the emergence of bound states. This effect can be observed in the dynamics of the (Rydberg atom) density making it detectable in experiments.

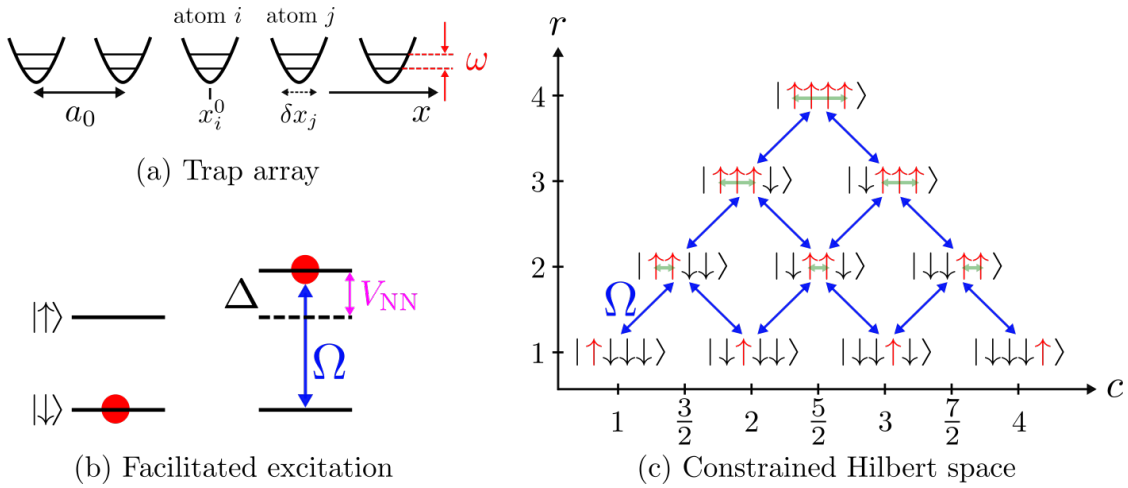

(a) Trap array

(b) Facilitated excitation

(c) Constrained Hilbert space

Figure 1: **Setting and structure of constrained Hilbert space**: (a) The system we consider consists of a one-dimensional lattice of N harmonic traps with harmonic frequency ω. The chain is orientated in x-direction and the spacing between adjacent traps is a_0. Each of the traps contains a single atom. The position of the center of the trap containing the i-th atom is denoted with x_i^0, while the displacement of the atom position from the respective trap center is δx_i. (b) Each atom is modeled as a two-level system, in which the states $|\downarrow\rangle$ and $|\uparrow\rangle$ represent the ground state and the (Rydberg) excited state, respectively. The atoms are excited with a laser with Rabi frequency Ω and detuning Δ. The facilitation constraint is established when $\Delta + V_{\mathrm{NN}} = 0$, where V_{NN} denotes the interaction between two adjacent atoms in their respective equilibrium positions. (c) For $\Omega \ll \Delta$, a kinetically constrained dynamics is implemented, which takes place between resonant states. The constraint manifests in a reduced connectivity between states in the Hilbert space: starting from an initial single excitation, clusters of adjacent Rydberg excitations are formed. Such states are described in terms of two coordinates, c and r, labeling the position of the center of mass and the number of excitations, respectively. Clusters containing at least two Rydberg excitations feature mechanical forces that act on the atoms on the edges of the excitation clusters (indicated by green arrows).

2 One-dimensional Rydberg lattice gas

We consider a one-dimensional chain of N traps, separated by a nearest-neighbor distance a_0 and each being loaded with a single atom, as shown in Fig. 1. The electronic structure of each atom is described via a two-level system (effective spin 1/2 particle), with the state $|\uparrow\rangle$ denoting the excited Rydberg state and the state $|\downarrow\rangle$ representing the ground state. Two atoms in the Rydberg state, located at sites j and k, interact via a power-law potential $V(\boldsymbol{r}_j, \boldsymbol{r}_k) = V(|\boldsymbol{r}_j - \boldsymbol{r}_k|) = V(r_{j,k}) = C_\gamma\, r_{j,k}^{-\gamma}$. Here $\gamma = \{3, 6\}$, depending on the type of interaction (dipole-dipole or van der Waals) [3]. The Hamiltonian of the full system is given by

$$H = \sum_{j=1}^{N} \left(\frac{\Omega}{2} \hat{\sigma}_j^x + \Delta \hat{n}_j + \sum_{k<j} V(\boldsymbol{r}_j, \boldsymbol{r}_k) \hat{n}_j \hat{n}_k + \omega a_j^\dagger a_j \right), \tag{1}$$

where Ω is the Rydberg excitation laser Rabi frequency, $\hat{\sigma}^x = |\uparrow\rangle\langle\downarrow| + |\downarrow\rangle\langle\uparrow|$ is the spin flip operator, $\hat{n} = |\uparrow\rangle\langle\uparrow|$ projects onto the up state, Δ is the laser detuning from the atomic transition frequency and ω is the trap frequency. The operators $a_j^\dagger$ and a_j are the phonon creation and annihilation operators at site j. These are defined with respect to the displacement of the

position $\boldsymbol{r}_j$ of the j-th atom, from the center of the respective trap $\boldsymbol{r}_j^0$: $\delta\boldsymbol{r}_j = \boldsymbol{r}_j - \boldsymbol{r}_j^0$. Although in principle $\delta\boldsymbol{r}_j$ is a vectorial quantity it is sufficient to consider only the phonon dynamics in x-direction, i.e. parallel to the chain. Then the fluctuations around the equilibrium positions are given in terms of bosonic operators as $\delta x_j = \sqrt{\frac{\hbar}{2m\omega}}(a_j^\dagger + a_j)$. This approximation relies on the fact that, if $|\delta\boldsymbol{r}_j| \ll a_0$, which we assume throughout, the potential can be expanded around the equilibrium positions and approximated to leading order as

$$V(\boldsymbol{r}_j, \boldsymbol{r}_k) \simeq V(\boldsymbol{r}_j^0, \boldsymbol{r}_k^0) + \nabla V(\boldsymbol{r}_j, \boldsymbol{r}_k)|_{(\boldsymbol{r}_j^0, \boldsymbol{r}_k^0)} \cdot (\delta\boldsymbol{r}_j, \delta\boldsymbol{r}_k) .$$

Since the interaction only depends on the relative distance between the atoms, $V(\boldsymbol{r}_j, \boldsymbol{r}_k) = C_\gamma\, r_{j,k}^{-\gamma}$, the gradient reads

$$\nabla\, V(\boldsymbol{r}_j, \boldsymbol{r}_k)\big|_{(\boldsymbol{r}_j^0, \boldsymbol{r}_k^0)} = -\frac{\gamma\, C_\gamma}{r_{j,k}^{\gamma+1}} (\hat{r}_{j,k}, -\hat{r}_{j,k})\Big|_{(\boldsymbol{r}_j^0, \boldsymbol{r}_k^0)} ,$$

where $\hat{r}_{j,k} = \frac{\boldsymbol{r}_j - \boldsymbol{r}_k}{|\boldsymbol{r}_j - \boldsymbol{r}_k|}$ is the unit vector connecting the atom k to the atom j. The gradient of the potential evaluated at $(\boldsymbol{r}_j^0, \boldsymbol{r}_k^0)$ has non-vanishing terms only in the x-components. Thus the only non zero component of the gradient is the one along the longitudinal direction. The expansion of the potential is then given by

$$\begin{aligned} V(\boldsymbol{r}_j, \boldsymbol{r}_k) &\simeq V(\boldsymbol{r}_j^0, \boldsymbol{r}_k^0) - \frac{\gamma\, C_\gamma}{|x_j^0 - x_k^0|^{\gamma+1}} (\delta x_j - \delta x_k) \\ &= V(\boldsymbol{r}_j^0, \boldsymbol{r}_k^0) - \frac{\gamma\, C_\gamma}{a_0^{\gamma+1}} \sqrt{\frac{\hbar}{2m\omega}} \left(a_j^\dagger + a_j - a_k^\dagger - a_k\right) . \end{aligned} \tag{2}$$

This expansion makes it evident that a simultaneous excitation of two atoms to the Rydberg state effectuates a coupling between the internal (electronic) and external (vibrational) degrees of freedom of the facilitated Rydberg chain.

3 Facilitated Rydberg dynamics

3.1 Hamiltonian of a single Rydberg cluster

We focus on the situation in which the dynamics of the system is subject to the facilitation constraint. This is achieved when the laser detuning Δ cancels out the interaction between two adjacent atoms, $V_{\mathrm{NN}} = V(\boldsymbol{r}_j^0, \boldsymbol{r}_{j+1}^0)$ in their respective equilibrium positions ($\Delta + V_{\mathrm{NN}} = 0$), as depicted in Fig. 1. Moreover, we assume that the next-nearest-neighbor interaction is small compared to the detuning, i.e. $V(\boldsymbol{r}_j^0, \boldsymbol{r}_{j+2}^0) \ll |\Delta|$, and that also the Rabi frequency of the laser is much smaller than the detuning $\Omega \ll |\Delta|$. These conditions lead to a constrained dynamics owed to the reduced connectivity between many-body states in the Hilbert space, which conserves the total number of clusters of consecutive Rydberg excitations in the lattice [55]. For example, when starting from a single excited Rydberg atom, the following states are connected (see also Fig. 1): $|{\downarrow}{\uparrow}{\downarrow}{\downarrow}{\downarrow}\ldots\rangle \Leftrightarrow |{\downarrow}{\uparrow}{\uparrow}{\downarrow}{\downarrow}\ldots\rangle \Leftrightarrow |{\downarrow}{\uparrow}{\uparrow}{\uparrow}{\downarrow}\ldots\rangle \Leftrightarrow |{\downarrow}{\downarrow}{\uparrow}{\uparrow}{\downarrow}\ldots\rangle \Leftrightarrow |{\downarrow}{\downarrow}{\uparrow}{\uparrow}{\uparrow}\ldots\rangle \Leftrightarrow \ldots$. This means that a cluster of consecutive excitations can expand or shrink, but cannot (dis)appear or split. When more than one cluster of consecutive Rydberg excitations is initially present, these clusters can also not merge.

Throughout this work we focus on a single cluster present in the lattice. In this case it is convenient to describe that state of a Rydberg cluster as a tensor product of its center of mass (CM) and relative coordinate

$$|\psi\rangle = |c\rangle \otimes |r\rangle \ . \tag{3}$$

Introducing these coordinates is particularly advantageous as they allow to reduce the complex many-body problem to a much simpler two-body problem, thanks to the kinetically constrained dynamics. Here c labels the position of the CM of the cluster and r denotes the number of excitations. In a lattice with N sites with periodic boundary conditions, the CM coordinate can take $2N$ different values, $c = \frac{1}{2}, 1, \ldots, N$ (in units of the lattice spacing a_0), where half-integer and integer values refer to CM positions at the middle of a lattice spacing or at a lattice site respectively. The coordinate r is an integer number between 1 and $N-1$, since a cluster with N excitations is not allowed. According to this notation, for instance, $|2\rangle\,|3\rangle = |\uparrow\uparrow\uparrow\downarrow\downarrow\ldots\rangle$ and $|\frac{5}{2}\rangle\,|2\rangle = |\downarrow\uparrow\uparrow\downarrow\downarrow\ldots\rangle$, as shown in Fig. 1c.

Given this representation, a state $|c\rangle\,|r\rangle$ is resonant with only four other states, provided that $1 < r < N-1$ (when $r = 1$ the cluster can only increase, when $r = N-1$ the cluster can only decrease). These are: $|c+\frac{1}{2}\rangle\,|r+1\rangle$ (the spin to the right of the rightmost excitation flips up), $|c-\frac{1}{2}\rangle\,|r+1\rangle$ (the spin to the left of the leftmost excitation flips up), $|c-\frac{1}{2}\rangle\,|r-1\rangle$ (the rightmost excitation flips down), $|c+\frac{1}{2}\rangle\,|r-1\rangle$ (the leftmost excitation flips down). Note, that the CM coordinate and the relative coordinate are not completely independent, as integer (half-integer) values of the CM position can be paired only with an odd (even) value for the relative coordinate. Such coupling between the relative and CM degrees of freedom of a cluster is a consequence of the discreteness of the lattice and does not appear in continuum space.

Using the expansion of the interaction potential, Eq. (2), and the representation in terms of the CM and relative coordinates, we can write the Hamiltonian of a single cluster of consecutive Rydberg excitations as

$$H = \Omega \sum_{c=\frac{1}{2}}^{N} \sum_{r=1}^{N-2} \left[\left| c+\frac{1}{2} \right\rangle \langle c| \otimes (|r+1\rangle \langle r| + \text{h.c.}) + \text{h.c.} \right] \tag{4}$$
$$- \kappa \sum_{c=\frac{1}{2}}^{N} \sum_{r=2}^{N-1} |c\rangle \langle c| \otimes |r\rangle \langle r| \left(a^{\dagger}_{c+\frac{r-1}{2}} + a_{c+\frac{r-1}{2}} - a^{\dagger}_{c-\frac{r-1}{2}} - a_{c-\frac{r-1}{2}} \right) + \omega \sum_{j=1}^{N} a^{\dagger}_j a_j \,.$$

The first term is the kinetic energy of the Rydberg cluster, while the second term contains the coupling between the degrees of freedom of the cluster and the phonons. The constant

$$\kappa = \sqrt{\frac{\hbar}{2m\omega}} \frac{\gamma\, C_\gamma}{a_0^{\gamma+1}} = \frac{x_0}{\sqrt{2}} \frac{\gamma\, C_\gamma}{a_0^{\gamma+1}} = \frac{\gamma}{\sqrt{2}} \frac{x_0}{a_0} V_{\text{NN}} \,, \tag{5}$$

quantifies the strength of this spin-phonon coupling. It depends on microscopic details, such as the gradient of the interaction potential (which for the power-law potential considered here can be expressed in terms of the nearest-neighbor interaction V_{NN}) and the harmonic oscillator length $x_0 = \sqrt{\hbar/(m\omega)}$. In case of a repulsive potential, that we consider in the following, $C_\gamma > 0$ and therefore κ is a positive constant.

Note that, if a cluster is composed of r consecutive excitations with the leftmost excitation at site i_l and the rightmost one at site $i_r = i_l + r - 1$, then only the phonon operators corresponding to the harmonic traps on sites i_l and i_r couple to the cluster degrees of freedom. Indeed, the sum over all neighboring sites of Eq. (2) gives rise to a telescoping series of the phonon operators, whose sum is the difference between the operator corresponding to the position of the rightmost excitation and the one at the leftmost excitation of the cluster, whose position coordinates can be expressed in terms of c and r.

3.2 Decoupling the relative and center of mass motion of a Rydberg cluster

In the next step we introduce phonon Fourier modes through $a_j = \frac{1}{\sqrt{N}} \sum_p A_p e^{ijp}$, with $p = \frac{2\pi}{N} k$ and $k = -\frac{N-1}{2}, \ldots, -1, 0, 1, \ldots, \frac{N-1}{2}$ (for odd N). Expressed in terms of the operators A_p, the

Hamiltonian reads

$$H = \Omega \sum_{c=\frac{1}{2}}^{N} \sum_{r=1}^{N-2} \left[\left| c + \frac{1}{2} \right\rangle \langle c| \otimes (|r+1\rangle \langle r| + \text{h.c.}) + \text{h.c.} \right] - \frac{\kappa}{\sqrt{N}} \sum_p \left[2i \sin\left(\frac{\hat{r}-1}{2} p \right) e^{i\hat{c}p} A_p + \text{h.c.} \right] + \omega \sum_p A_p^\dagger A_p \,, \tag{6}$$

where we have also introduced the operators $\hat{r} = \sum_{r=1}^{N-1} r \, |r\rangle \langle r|$ (the sum can start from $r = 1$ thanks to the presence of the sine function) and $\hat{c} = \sum_{c=\frac{1}{2}}^{N} c \, |c\rangle \langle c|$.

The CM degree of freedom and the phonon modes can now be decoupled by applying the so-called Lee-Low-Pines (LLP) transformation [56] to Eq. (6), which is implemented through the unitary operator

$$U = \exp\left\{ -i\hat{c} \sum_p p A_p^\dagger A_p - i \frac{\pi}{2} \sum_p A_p^\dagger A_p \right\}.$$

By introducing the Fourier transform of the CM coordinate, $|c\rangle = \frac{1}{\sqrt{2N}} \sum_q e^{iqc} |q\rangle$, where $q = -2\pi + \frac{2\pi}{N} k$ with $k = 0, 1, \ldots, 2N-1$, the Hamiltonian can be finally be written in a block-diagonal form as $U^\dagger H U = \sum_q H_q \, |q\rangle \langle q|$. Hence, after the LLP and the Fourier transform, the label q of the CM Fourier modes has become a good quantum number, and the Hamiltonian H_q governing the evolution within a given q sector is given by

$$H_q = 2\Omega \cos\left[\frac{1}{2} \left(q + \sum_p p A_p^\dagger A_p \right) \right] \sum_{r=1}^{N-2} |r+1\rangle \langle r| + \text{h.c.} - \frac{2\kappa}{\sqrt{N}} \sum_p \left[\sin\left(\frac{\hat{r}-1}{2} p \right) \left(A_p + A_p^\dagger \right) \right] + \omega \sum_p A_p^\dagger A_p \,. \tag{7}$$

3.3 Effective Hamiltonian in the phonon dressing regime

In the following we will integrate or trace out the phonons, in order to obtain an effective phonon dressed facilitation dynamics of a Rydberg cluster. To this end we apply the unitary displacement operator

$$\hat{D} = \exp\left(\sum_p \hat{S}_p A_p^\dagger - \hat{S}_p A_p \right) \tag{8}$$

to Hamiltonian (7). Here

$$\hat{S}_p = \frac{2\kappa}{\omega\sqrt{N}} \sin\left(\frac{\hat{r}-1}{2} p \right) \tag{9}$$

is an hermitian operator that depends on the phonon momentum p. Under the application of the unitary $\hat{D}$, each phonon annihilation operator gets shifted as $\hat{D}^\dagger A_p \hat{D} = A_p + \hat{S}_p$. The displaced Hamiltonian $\tilde{H}_q = D^\dagger H_q D$ reads

$$\tilde{H}_q = \hat{D}^\dagger \left\{ 2\Omega \cos\left[\frac{1}{2} \left(q + \sum_p p A_p^\dagger A_p \right) \right] \sum_{r=1}^{N-2} |r+1\rangle \langle r| \right\} \hat{D} + \text{h.c.} - \omega \sum_p \hat{S}_p^2 + \omega \sum_p A_p^\dagger A_p \,, \tag{10}$$

where $\hat{S}_p^2 = \frac{4\kappa^2}{\omega^2 N} \sin^2\left(\frac{\hat{r}-1}{2} p \right)$ and $\sum_p \hat{S}_p^2 = 2\frac{\kappa^2}{\omega^2} \sum_{r=2}^{N-1} |r\rangle \langle r|$. We did not explicitly evaluate here the displaced kinetic term. This is cumbersome, since $\hat{S}_p$ and $\sum_{r=1}^{N-2} |r+1\rangle \langle r|$ do not commute.

To make progress, nevertheless, we assume in the following that $\kappa \ll \omega$, i.e. that the interaction between the phonons and the Rydberg cluster dynamics is weak. We expand the

displaced kinetic term in powers of κ/ω and only retain terms up to order $(\kappa/\omega)^2$ (this is the same order as that of the term $\hat{S}_p^2$). To finally obtain the effective phonon dressed Hamiltonian, we project the displaced Hamiltonian onto the phonon vacuum, thus effectively tracing out the phonon degrees of freedom (see Appendix A for details). The effective "lattice-only" Hamiltonian for each CM mode q then becomes

$$\begin{aligned} H_{\mathrm{eff},q} &= 2\Omega\left(1-\frac{\kappa^2}{\omega^2}\right)\cos\left(\frac{q}{2}\right)\sum_{r=1}^{N-2}\left(|r+1\rangle\langle r|+|r\rangle\langle r+1|\right)-2\frac{\kappa^2}{\omega}\sum_{r=2}^{N-1}|r\rangle\langle r| \\ &= J_q(\kappa)\,\hat{T}+\alpha(\kappa)\,|1\rangle\langle 1|-2\frac{\kappa^2}{\omega}\,, \end{aligned} \tag{11}$$

where the last constant term will be neglected in the following. Here

$$\hat{T}=\sum_{r=1}^{N-2}\left(|r+1\rangle\langle r|+|r\rangle\langle r+1|\right)$$

is the kinetic energy (hopping) operator of the relative dynamics of the Rydberg cluster,

$$J_q(\kappa)=2\Omega\left(1-\frac{\kappa^2}{\omega^2}\right)\cos\left(\frac{q}{2}\right) \tag{12}$$

is the renormalized hopping rate and

$$\alpha(\kappa)=2\frac{\kappa^2}{\omega} \tag{13}$$

is a "repulsive" potential shift acting on a cluster of length 1, i.e. containing only a single Rydberg atom. This potential shift reflects the peculiarity of such cluster, as it is the only one in which there are no Rydberg-Rydberg interactions. Consequently, since there are no mechanical forces, it is completely decoupled from the phonons.

In order to assess the quality of the performed approximations we compare in the following the band structure of the effective phonon dressed Hamiltonian

$$H_{\mathrm{eff}}=\sum_q H_{\mathrm{eff},q}\,|q\rangle\langle q|\,, \tag{14}$$

with results from a numerical diagonalization of the full Hamiltonian (7). As can be seen in Fig. 2 the agreement is excellent for small values of κ/ω, which is the regime where perturbation theory is expected to be valid. This suggests that the obtained effective model correctly describes the physics of phonon dressed Rydberg clusters. Moreover, the two bottom panels show that, for increasing strength of the phonon dressing, the uppermost energy level separates from the rest of the band. This separation can be explained by the emergence of a bound state, which is caused by the presence of the repulsive potential $\alpha(\kappa)$ [Eq. (5)] and which will be discussed in detail further below. Also visible is the narrowing of the bands due to the factor $1-\kappa^2/\omega^2$ in the hopping rate, Eq. (12).

3.4 Experimental considerations

The perturbative expansion of the displacement operator in powers of κ/ω and the assumption of a coherent Rydberg cluster dynamics set certain constraints on the energy scales entering Hamiltonian (7) as well as the coherence time. In the following we will discuss whether these can be met in current experiments. Hamiltonian (7) is the sum of three terms, with Ω, κ and ω as the respective energy scales. A necessary condition for our perturbation theory to be

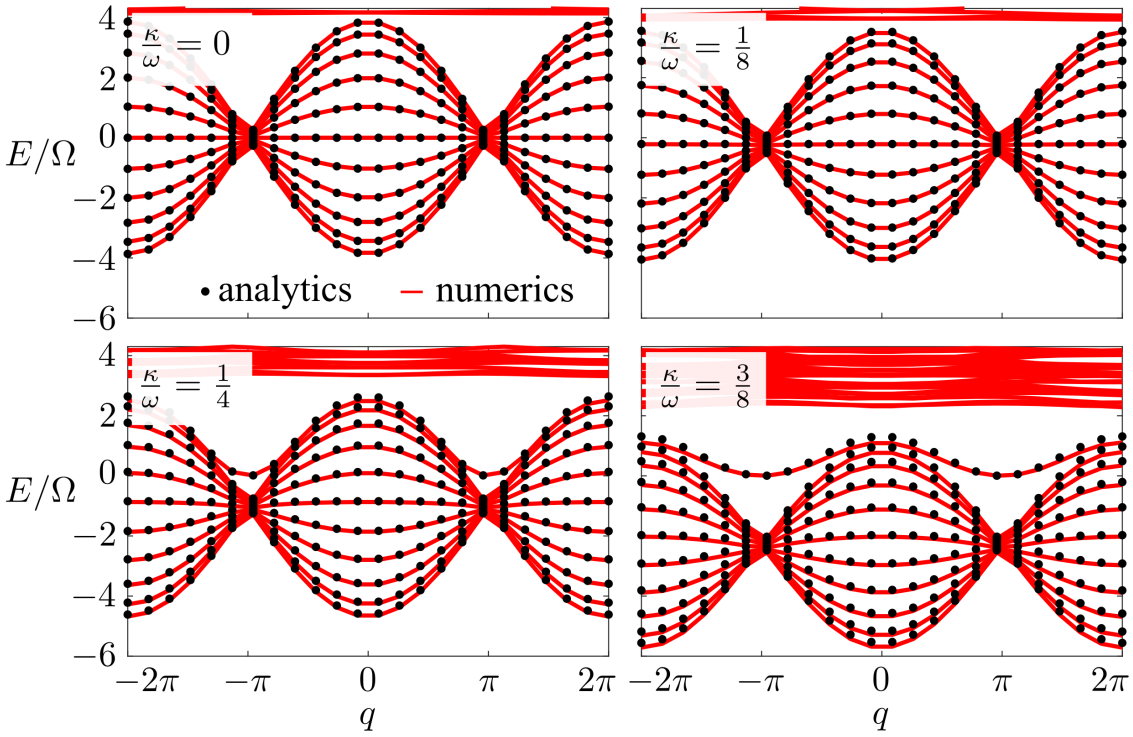

Figure 2: **Vibrationally dressed band structure of a single Rydberg cluster**: Energy bands in the free case ($\kappa = 0$) and with phonon dressing ($\kappa \neq 0$). Red lines are obtained through numerical diagonalization of Hamiltonian (7) with $N = 12$ sites and a truncation of the maximum number of phonons per site to 3. Black dots are the eigenvalues of the effective Hamiltonian (11) which has been obtained by integrating out the phonon degrees of freedom. The trap and Rabi frequencies are chosen such that $\omega = 8\Omega$. Note that, as κ/ω increases, the center of the band gets lower in energy. This is due to the presence of the constant term in Eq. (11) which is equal to $-2\kappa^2/\omega$ and is naturally included in the numerical diagonalization of Hamiltonian (7).

valid is that $\Omega, \kappa \ll \omega$, demanding that the trap frequency ω is much larger than the Rabi frequency Ω and the spin-phonon coupling constant κ. The trap frequency indeed measures the spacing between the zero-phonon band and the higher energy bands, while Ω determines the width of the zero-phonon band. The inequality $\Omega \ll \omega$ then ensures that the band with zero phonons remains well separated from the higher energy bands, avoiding undesired effects due to band mixing. The inequality involving κ and ω is on the other hand necessary for the perturbative expansion to be valid. Both Ω and κ are independent quantities, meaning that the derivation of the effective Hamiltonian (11) is rigorous in both situations where κ is larger or smaller than Ω. This is due to the fact that the displacement operator (8), that we expand perturbatively, depends on the ratio κ/ω, but not on Ω. Furthermore, in order to legitimately describe the coherent dynamics of phonon dressed Rydberg spin clusters with the effective Hamiltonian (11), the time scales involved therein must be considerably shorter than the Rydberg atom lifetime. Therefore — denoting with Γ the decay rate of the Rydberg state to other atomic states — the perturbative expansion turns out to be valid once

$$\omega \gg \Omega, \kappa \gg \Gamma \tag{15}$$

is satisfied. However, the perturbation treatment is found to be surprisingly accurate even when some of these conditions are not strictly met: as shown in Fig. 2, where the trap and

Rabi frequencies are chosen such that $\omega = 8\Omega$, the agreement between the numerical diagonalization of the Hamiltonian (7) and the eigenvalues of the effective Hamiltonian (11) is excellent even though the zero-phonon band is close to the higher energy bands.

Next, we estimate the magnitude of the spin-phonon coupling constant, Eq. (5), for a system of ^{87}Rb atoms. Assuming van der Waals interaction ($\gamma = 6$) among Rydberg atoms, this reduces to

$$\kappa = \frac{x_0}{\sqrt{2}} \frac{6\, C_6}{a_0^7} .$$

Choosing $a \simeq 5\,\mu m$ and $\omega \simeq 2\pi \times 300$ kHz, we obtain $x_0 \simeq 2 \times 10^{-2}\,\mu m$. The C_6 coefficient is proportional to n^{11}, where n is the principal quantum number of the Rydberg state. For $n \simeq 60$ Rydberg S-state, $C_6 \simeq 140$ GHz μm^6 [57]. We therefore obtain the estimate

$$\kappa \simeq 2\pi \times 25\,\text{kHz} .$$

The lifetime for a Rydberg excitation with $n \simeq 60$ at $T = 300\,\text{K}$ is $\tau \simeq 10^{-4} s$. So the decay rate is $\Gamma \simeq 2\pi \times 1.6$ kHz [58], which is indeed significantly smaller than the spin-phonon coupling. Noting furthermore that a Rabi frequency of the Rydberg excitation laser on the order of $\Omega = \omega/8 \simeq 2\pi \times 37.5$ kHz is experimentally achievable [59], we see that the condition (15) can indeed be satisfied with the above parameter choices. The assumption $\Omega \ll |\Delta|$ necessary for the facilitation condition is also fulfilled because $|\Delta| = V_{\text{NN}} = C_6/a_0^6 \simeq 10\,\text{MHz}$.

The most challenging condition is probably the assumption of a trap frequency of $\omega \simeq 2\pi \times 300$ kHz, which is larger than current typical values that are on the order of $\omega \simeq 2\pi \times 100$ kHz [60]. For this latter value one has $\kappa \simeq 2\pi \times 40\,\text{kHz}$, making the ratio $\kappa/\omega = 0.4$, close to the case depicted in the bottom right of Fig. 2. In this case the Rabi frequency evaluates to $\Omega = \omega/8 \simeq 2\pi \times 12.5$ kHz, which reduces the ratio Ω/Γ to about 8 and therefore limits the time interval over which coherent evolution can be observed.

We assumed throughout that atoms in both their ground state and Rydberg state are trapped in the lattice potential. The feasibility of this has been demonstrated in Ref. [61], however, this is not yet standard technology in Rydberg quantum simulator setups. Furthermore, for the parameters considered, the spin-phonon coupling constant is about 15 times larger than the Rydberg atom decay rate. However, given that κ depends on the gradient of the interaction potential, its value can be modified by tailoring the interaction potential between Rydberg states via microwave dressing, as theoretically discussed in Refs. [53, 62] and demonstrated in Ref. [63]. This may allow to push the ratio κ/ω in the region that is considered in Fig. 2.

We conclude this section by remarking that the parameter values discussed here represent the most ideal case in that they give rise to a scenario in which all energy scales are clearly separated. This is in fact very convenient for the theoretical analysis. In practice, it is reasonable to expect that also parameter choices that are less stringent will permit the experimental observation of signatures of phonon dressing in the dynamics of facilitated Rydberg clusters.

4 Dynamics of a phonon dressed Rydberg cluster

4.1 Numerical results

In this section we study the time evolution of a cluster initially prepared (at time $t = 0$) with a fixed CM position c_0 and a defined number of excitations r_0 as

$$|\psi(0)\rangle = |c_0\rangle \otimes |r_0\rangle .$$

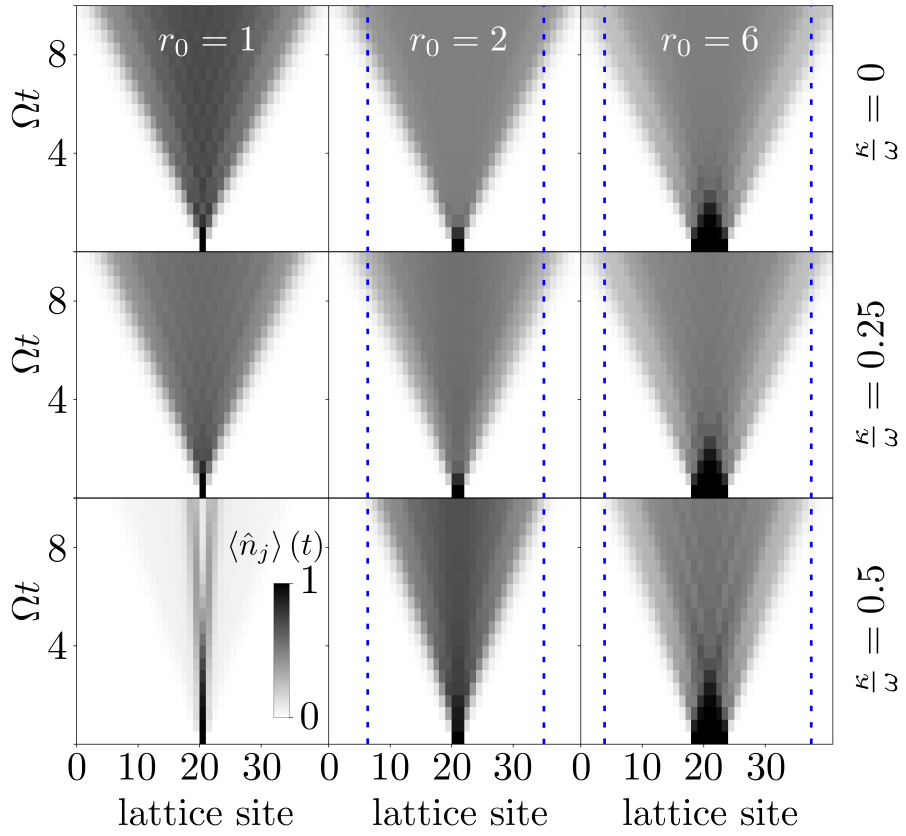

Figure 3: **Dynamics of a Rydberg cluster with r_0 consecutive initial excitations**: Time evolution of the Rydberg excitation density $\langle \hat{n}_j \rangle (t)$ for different values of the initial Rydberg cluster size, r_0, and spin-phonon coupling strength, κ/ω. Visible is a ballistic expansion, which becomes slower for large values of the spin-phonon coupling constant κ. An almost complete inhibition of expansion appears in the case $r_0 = 1$, as the strong repulsive potential makes transitions to propagating continuum states off-resonant. The propagation of the Rydberg clusters with $r_0 > 1$ also slows down with increasing spin-phonon interaction. This is due to the decrease of the hopping rate J_q. The dotted blue lines are used to enhance the visibility of this effect.

This state evolves according to

$$|\psi(t)\rangle = e^{-iH_{\text{eff}}t} |\psi(0)\rangle = \frac{1}{\sqrt{2N}} \sum_q e^{iqc_0} |q\rangle \otimes e^{-iH_{\text{eff},q}t} |r_0\rangle \,, \tag{16}$$

with each q mode of the wave function evolving independently through the effective Hamiltonian (11).

Figure 3 shows the time evolution of the site-resolved Rydberg excitation density — a quantity that can be experimentally measured [6] — for different values of r_0 and κ/ω. For $\kappa = 0$ (top three plots), the cluster undergoes ballistic expansion. This is indeed expected, as in this case the effective Hamiltonian is simply given by the hopping term. As the ratio κ/ω increases, the value of the effective hopping rate $J_q(\kappa)$ becomes smaller, leading to a slowdown of the ballistic expansion. The dashed blue lines, which are shown in the figure as a guide to the eye, indicate this effect: the time needed for the cluster excitations to reach a given distance from the initial location of the CM increases as the phonon dressing gets stronger. This effect is more pronounced when the initial state has only one Rydberg excitation ($r_0 = 1$). The reason

for this is that this initial configuration is subjected to the repulsive potential $\alpha(\kappa)$, which is given by Eq. (11). This brings transitions from this initial state to other states off resonance and therefore inhibits relaxation, thereby yielding a rather pronounced manifestation of the phonon dressing.

5 Analytical results — Fano resonance theory

In the following we focus more closely on the scenario in which an initial state is prepared, that contains only a single excitation ($r_0 = 1$). This case, which corresponds to the left column in Fig. 3 is interesting, because it can to a large extent be analytically treated via Fano resonance theory [64]. This theory describes the interaction between a discrete state and a set of continuum states, and in the following we will show that our problem can be indeed mapped onto such situation. Exploiting this connection will allow to derive an analytical expression for the survival probability of a Rydberg cluster containing a single excitation, which yields further insights into the inhibition of relaxation observed in Fig. 3.

We start by rewriting the effective Hamiltonian (11) as

$$\begin{aligned} H_{\mathrm{eff},q} &= J_q(\kappa)\sum_{r=2}^{N-2}\left(|r+1\rangle\langle r| + |r\rangle\langle r+1|\right) + \alpha(\kappa)\,|d\rangle\langle d| + J_q(\kappa)\left(|d\rangle\langle 2| + |2\rangle\langle d|\right) \\ &= \hat{H}_q^0 + \hat{V}_d + J_q(\kappa)\left(|d\rangle\langle 2| + |2\rangle\langle d|\right). \end{aligned} \tag{17}$$

Here, we use the state $|d\rangle$ to denote what we previously called state $|1\rangle$. It corresponds to the relative coordinate of a Rydberg cluster containing only a single excitation and will be identified as the discrete state in the framework of Fano theory. The energy of this state is $\alpha(\kappa)$ as given by Eq. (13) and the corresponding Hamiltonian is $\hat{V}_d$. This discrete state is coupled to one of the continuum states which interact through the Hamiltonian $\hat{H}_q^0$. The strength of this coupling $J_q(\kappa)$ is given by Eq. (12), which contains the dependence on the CM motion. For the sake of brevity we write in the following $J_q \equiv J_q(\kappa)$ and $\alpha \equiv \alpha(\kappa)$, leaving the dependence of these parameters on κ implicit.

The Hamiltonian $\hat{H}_q^0$ is easily diagonalized and its eigenvalues $\{E_q^0(k)\}_{k=1,\ldots,N-2}$ and normalized eigenvectors $|\bar{k}\rangle$, which satisfy $\hat{H}_q^0|\bar{k}\rangle = E_q^0(k)|\bar{k}\rangle$, are

$$E_q^0(k) = 2J_q\cos\left(\frac{\pi}{N-1}k\right), \qquad k = 1,\ldots,N-2$$

and

$$|\bar{k}\rangle = \sqrt{\frac{2}{N-1}}\sum_{r=2}^{N-1}\sin\left[\frac{\pi}{N-1}k(r-1)\right]|r\rangle\,. \tag{18}$$

Each eigenvector $|\bar{k}\rangle$ is therefore given as a superposition of the basis vectors $|r\rangle$ with which $\hat{H}_q^0$ was originally formulated [Eq. (17)]. We now proceed by choosing the vectors $\left\{|d\rangle, \{|\bar{k}\rangle\}_{k=1,\ldots,N-2}\right\}$ as the new basis. With this change of basis, the Hamiltonian (17) is partially diagonalized, i.e. all continuum states are now mutually orthogonal. The analogy with the Fano resonance scenario becomes apparent by plotting the diagonal elements of the Hamiltonian (17), as shown in Fig. 4a: a discrete (bound) state, which represents a Rydberg cluster containing a single excitation, is coupled to a set of uncoupled continuum states. We also show for comparison the spectrum of the fully diagonalized Hamiltonian (17) in Fig. 4b: for $\alpha < |J_q|$, the spectrum is continuous and extends over the same range as the eigenenergies

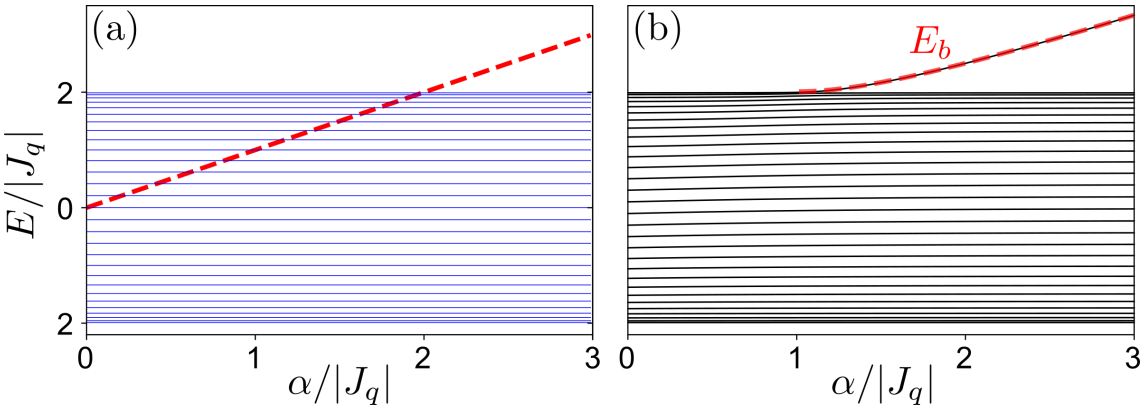

Figure 4: **Discrete state coupled to a continuum**: (a) Diabatic representation. Shown are the eigenvalues of $\hat{H}_q^0$ [see Eq. (17)] and the energy of the discrete state $|d\rangle$ (red dashed line). For $\alpha < 2|J_q|$, the discrete state is embedded inside the continuum. (b) Eigenvalues of the coupled Hamiltonian (17). When $\alpha > |J_q|$, a bound state possessing a large overlap with the state $|d\rangle$ emerges from the continuum. The red dashed line is the energy of the bound state, which is given by Eq. (19). Both panels are obtained with $N = 31$.

$E_q^0(k)$ of the uncoupled problem. For $\alpha > |J_q|$, a bound energy level with energy

$$E_b = \frac{\alpha^2 + J_q^2}{\alpha} \tag{19}$$

emerges (see derivation in Appendix B), which separates from the continuum band as α is increased. This bound state possesses a large overlap with the state $|d\rangle$. As shown below, the existence of such a bound state and the consequent modification of the spectrum of Hamiltonian (17) as a function of $\alpha/|J_q|$ are responsible for the strong inhibition of the expansion of a Rydberg cluster containing a single excitation (bottom left panel in Fig. 3).

Such cluster is represented by the state $|\psi(0)\rangle = |c_0\rangle \otimes |d\rangle$. Here c_0 denotes the initial CM position, which has to assume an integer number because it is paired with an odd value for the relative coordinate (Rydberg cluster of length 1, represented by $|d\rangle$), as discussed below Eq. (3). Each of the Fourier q modes contributing to the CM state $|c_0\rangle$ evolves under the effective Hamiltonian (17) according to Eq. (16).

In the following we compute the (survival) probability $p_d(t)$ for each Fourier component, i.e. the probability for the system to remain in the initial state $|d\rangle$ at time t. To start, we explicitly write the matrix elements of Hamiltonian (17) in the new basis $\left\{|d\rangle, \{|\bar{k}\rangle\}_{k=1,\ldots,N-2}\right\}$:

$$\begin{cases} \langle d|H_{\text{eff},q}|d\rangle = \alpha\,, \\ \langle d|H_{\text{eff},q}|\bar{k}\rangle = V(k)\,, \\ \langle \bar{k}|H_{\text{eff},q}|\bar{k'}\rangle = E_q^0(k)\,\delta_{k,k'}\,, \end{cases} \tag{20}$$

with the real valued function

$$V(k) = J_q \sqrt{\frac{2}{N-1}} \sin\left(\frac{\pi}{N-1}k\right) \tag{21}$$

describing the coupling between the discrete state and the continuum. A generic eigenstate of Hamiltonian (17) can be written as

$$|\psi_E\rangle = a(E)\,|d\rangle + \sum_{k=1}^{N-2} b_k(E)\,|\bar{k}\rangle\,, \tag{22}$$

where the amplitudes a and b_k depend on the corresponding eigenvalue E. Each eigenvalue E of course depends on q, but this dependence is left implicit in the notation for the sake of brevity. In order to obtain an expression for the survival probability, the key quantity to determine is the amplitude $a(E)$. This is because, according to Eq. (22), the survival probability is given by

$$p_d(t) = \left|\langle d|e^{-iH_{\mathrm{eff},q}t}|d\rangle\right|^2 = \left|\sum_E |a(E)|^2 e^{-iEt}\right|^2 . \tag{23}$$

Here, the sum runs over the eigenvalues of the coupled Hamiltonian (17), which actually are the energy levels shown in Fig. 4b. This sum hence contains the contribution coming from the energies in the continuum, but, when $\alpha > |J_q|$, also the bound state with energy E_b must be considered.

After some calculation detailed in Appendix B, one finds that the general expression for the survival probability is

$$p_d(t) = \left|\frac{\alpha^2 - J_q^2}{\alpha^2} e^{-iE_b t}\,\Theta(\alpha^2 - J_q^2) + \frac{2J_q^2}{\pi(\alpha^2 + J_q^2)}\int_0^\pi dx \frac{\sin^2 x}{1 - \frac{2\alpha J_q}{\alpha^2+J_q^2}\cos x} e^{-i2J_q t\cos x}\right|^2 , \tag{24}$$

where Θ is the Heaviside step function. This exact result is the squared of a sum of two terms. The second one is the contribution to the survival probability stemming from the coupling of the discrete state to the continuum. It involves an integration, which is convergent since $\left|2\alpha J_q/\left(\alpha^2 + J_q^2\right)\right| \leq 1$ for any value of α and J_q (the integral can also be expressed by a convergent series of Bessel functions). The first term appears only for Fourier modes for which $\alpha > |J_q|$, and depends on time only through a phase which involves the bound state energy E_b.

For sufficiently long times the integral in the second term vanishes, and hence the survival probability at late times is approximately given by $\left|(\alpha^2 - J_q^2)/\alpha^2\right|^2$. This value tends to 1 as the ratio $\alpha/|J_q|$ increases. This explains the restricted mobility of the single excitation cluster shown in the bottom left corner of Fig. 3. Indeed, as α gets larger, there are more modes q for which the condition $\alpha > |J_q|$ is satisfied, leading to a overall larger survival probability p_d at late times. This is explicitly illustrated in Fig. 5, where the survival probability obtained from the numerical evaluation of Eq. (23) is compared with the analytical result (24). The three panels are organized such that the spin-phonon coupling constant increases from left to right, while the considered three modes q are kept fixed. In the non-interacting case ($\alpha = 0$), the survival probability associated to all the modes q decays to 0 accordingly to Eq. (B.10) given in Appendix B. For increasing value of α, for more and more Fourier modes the inequality $\alpha > |J_q|$ is satisfied and the number of modes q for which p_d reaches a plateau at long times increases. This explains the inhibition of relaxation observed for a Rydberg cluster containing a single excitation.

6 Conclusion

We have considered a one-dimensional Rydberg lattice gas under facilitation conditions, which mimics the features of a kinetically constrained spin model. We have shown how the coupling between electronic and vibrational degrees of freedom — which is caused by the emergence of state-dependent forces — impacts on the dynamics of Rydberg excitations. This dressing of Rydberg excitations by phonons manifests in a reduction of the velocity with which facilitated clusters of consecutive Rydberg atoms grow over time. This becomes particularly apparent for

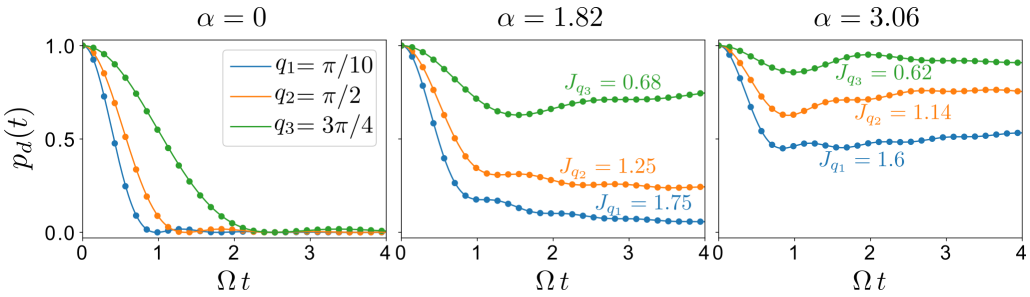

Figure 5: **Survival probability of a Rydberg cluster containing a single excitation**: The survival probability obtained from the numerical evaluation of Eq. (23) (plotted with dots) is exactly reproduced by the analytical result, Eq. (24), obtained from Fano theory and plotted with full lines. For $\alpha = 0$ the survival probability decays quickly to zero for all the three considered q values. As α increases, more q-modes acquire a non zero survival probability. This explains the strong inhibition of the spreading of a Rydberg cluster containing a single excitation, as observed in Fig. 3. The parameters chosen for the plots are $\omega = 8\Omega$ and $\kappa = \{0, 2.7\Omega, 3.5\Omega\}$.

clusters that initially contain only a single Rydberg excitation. Using a perturbative approach in the strength of the spin-phonon coupling constant, we obtain an effective Hamiltonian for the dynamics of dressed Rydberg excitations, which accurately reproduces the band structure of the full system. Using an approach inspired by Fano resonance theory, we analytically derive an exact expression for the survival probability of the Rydberg cluster containing a single excitation, providing an explanation for the observed inhibition of relaxation.

Signatures of the reported dynamical features should be observable on current quantum simulator platforms based on atomic arrays [6]. However, reaching a regime in which all energy scales are separated in a way which we exploited for our analytical calculations may be challenging. Nevertheless, basic features, such as an impact of the lattice vibration on the propagation of excitations are expected to manifest also in settings that are currently accessible. In the future it would be interesting to consider phonon dressing of Rydberg excitations in high-dimensional lattices. Here, the physics is expected to be significantly richer: for example, the interaction between electronic and vibrational degrees of freedom will depend on the shape of the Rydberg clusters. It would, moreover, be interesting to study situations in which clusters interact or scatter off one another [65, 66].

Acknowledgements

We are grateful for discussions with C. Groß, R. Eberhard, L. Steinert and P. Osterholz.

Funding information We acknowledge support from the "Wissenschaftler Rückkehrprogramm GSO/CZS" of the Carl-Zeiss-Stiftung and the German Scholars Organization e.V., as well as by the Deutsche Forschungsgemeinschaft through SPP 1929 (GiRyd), Grant No. 428276754.

A Derivation of $H_{\text{eff},q}$

Here we derive the effective displaced Hamiltonian given by Eq. (11) in the main text. The derivation requires the following steps. First, we expand the displaced hopping term in Eq. (10)

in powers of κ/ω. Secondly, we only keep the terms of the expansion up to order $(\kappa/\omega)^2$, to be consistent with the operator $\hat{S}_p^2$ which is also of order $(\kappa/\omega)^2$. Finally, the displaced Hamiltonian is projected onto the phonon vacuum state, which amounts to "integrating out" the phonons.

Let us rewrite the expression of the displaced hopping term present in Eq. (10) in the main text:

$$H_{\text{hop}} = \hat{D}^\dagger \left\{ 2\Omega \cos\left[\frac{1}{2}\left(q + \sum_p p A_p^\dagger A_p\right)\right]\right\} \hat{D}\,\hat{D}^\dagger \left\{\sum_{r=1}^{N-2} |r+1\rangle\langle r|\right\}\hat{D} + \text{h.c.}\,, \tag{A.1}$$

which, thanks to the identity $\hat{D}\hat{D}^\dagger = \mathbb{1}$, is given by a product of two displaced operators.

Now we proceed by computing the two factors separately. Since $\hat{D} = \prod_p e^{\hat{S}_p\left(A_p^\dagger - A_p\right)}$, the second displaced operator can be computed as

$$\begin{aligned}
D^\dagger \left\{\sum_{r=1}^{N-2} |r+1\rangle\langle r|\right\} D &= \prod_p e^{-\hat{S}_p\left(A_p^\dagger - A_p\right)} \left(\sum_{r=1}^{N-2} |r+1\rangle\langle r|\right) \prod_q e^{\hat{S}_q\left(A_q^\dagger - A_q\right)} \\
&= \sum_{r=1}^{N-2} \prod_p e^{-\frac{2\kappa}{\omega\sqrt{N}}\sin\left(\frac{r}{2}p\right)\left(A_p^\dagger - A_p\right)} \prod_q e^{\frac{2\kappa}{\omega\sqrt{N}}\sin\left(\frac{r-1}{2}q\right)\left(A_q^\dagger - A_q\right)} |r+1\rangle\langle r| \\
&= \sum_{r=1}^{N-2} \prod_p \left(e^{-\frac{2\kappa}{\omega\sqrt{N}}\sin\left(\frac{r}{2}p\right)\left(A_p^\dagger - A_p\right)} e^{\frac{2\kappa}{\omega\sqrt{N}}\sin\left(\frac{r-1}{2}p\right)\left(A_p^\dagger - A_p\right)}\right) |r+1\rangle\langle r| \\
&= \sum_{r=1}^{N-2} \prod_p e^{-\frac{2\kappa}{\omega\sqrt{N}}\left[\sin\left(\frac{r}{2}p\right) - \sin\left(\frac{r-1}{2}p\right)\right]\left(A_p^\dagger - A_p\right)} |r+1\rangle\langle r| \\
&= \sum_{r=1}^{N-2} e^{\sum_p -\frac{2\kappa}{\omega\sqrt{N}}\left[\sin\left(\frac{r}{2}p\right) - \sin\left(\frac{r-1}{2}p\right)\right]\left(A_p^\dagger - A_p\right)} |r+1\rangle\langle r|\,,
\end{aligned}$$

where from the 3rd to the 4th row we make use of the property of the displacement operators $D(\alpha)D(\beta) = e^{(\alpha\beta^* - \alpha^*\beta)/2} D(\alpha+\beta)$, where in our case $\alpha = \beta = \hat{S}_p = \hat{S}_p^\dagger$. For $\kappa \ll \omega$, the exponential can be expanded in powers of κ/ω and the previous expression can be approximated as

$$\begin{aligned}
&D^\dagger \left\{\sum_{r=1}^{N-2} |r+1\rangle\langle r|\right\} D \simeq \\
&\simeq \sum_{r=1}^{N-2} |r+1\rangle\langle r| + \sum_{r=1}^{N-2}\sum_p \left(A_p - A_p^\dagger\right)\left[S_p(r+1) - S_p(r)\right] |r+1\rangle\langle r| \\
&\quad + \frac{1}{2!}\sum_{r=1}^{N-2}\sum_p\sum_\nu \left(A_p - A_p^\dagger\right)\left[S_p(r+1) - S_p(r)\right]\left(A_\nu - A_\nu^\dagger\right)\left[S_\nu(r+1) - S_\nu(r)\right] |r+1\rangle\langle r|\,,
\end{aligned} \tag{A.2}$$

where $S_p(r) = \frac{2\kappa}{\omega\sqrt{N}}\sin\left(\frac{r-1}{2}p\right)$ is the eigenvalue of the operator $\hat{S}_p$ relative to the eigenstate $|r\rangle$.

Now let us focus on the first displaced operator in Eq. (A.1). We write

$$\hat{D}^\dagger \left\{ 2\Omega \cos\left[\frac{1}{2}\left(q + \sum_p p A_p^\dagger A_p\right)\right]\right\} \hat{D} = e^X Y e^{-X}\,,$$

where

$$X = \sum_p \hat{S}_p A_p - \hat{S}_p A_p^\dagger \quad \text{and} \quad Y = 2\Omega\cos\left[\frac{1}{2}\left(q + \sum_p p A_p^\dagger A_p\right)\right].$$

Using the Baker-Campbell-Hausdorff formula and truncating it at second order yields

$$e^X Y e^{-X} = Y + [X,Y] + \frac{1}{2!}[X,[X,Y]] + \dots$$
$$\simeq Y + (XY - YX) + \frac{1}{2!}(XXY + YXX - 2XYX)\,. \tag{A.3}$$

The idea now is to gather Eq. (A.3) and Eq. (A.2) to collect the terms of orders κ/ω and $(\kappa/\omega)^2$. We then project these terms on the subspace with no phonons by computing the braket $\langle 0_{\rm ph}|\text{Eq. (A.3)}\cdot\text{Eq. (A.2)}|0_{\rm ph}\rangle$. All the terms of order κ/ω are proportional to $\langle 0_{\rm ph}|A_p|0_{\rm ph}\rangle$ and $\langle 0_{\rm ph}|A_p^\dagger|0_{\rm ph}\rangle$ and therefore they vanish. The matrix element evaluated for the terms of order $(\kappa/\omega)^2$ is instead non zero and, using the relation $\hat{S}_p\sum_{r=1}^{N-2}|r+1\rangle\langle r| = \sum_{r=1}^{N-2} S_p(r+1)\,|r+1\rangle\langle r|$, is given by

$$\langle 0_{\rm ph}|\text{Eq. (A.3)}\cdot\text{Eq. (A.2)}|0_{\rm ph}\rangle =$$
$$= \Omega\sum_{r=1}^{N-2}\sum_p\left\{2\cos\left(\frac{q+p}{2}\right)S_p(r+1)S_p(r) - \cos\frac{q}{2}\left[S_p^2(r+1)+S_p^2(r)\right]\right\}|r+1\rangle\langle r|\,.$$

By computing explicitly the sums over p one obtains that $\sum_p \cos\left(\frac{q+p}{2}\right)S_p(r+1)S_p(r) = \cos\frac{q}{2}\,\frac{\kappa^2}{\omega^2}$ for $r>1$ (if $r=1$ it is equal to 0), $\sum_p S_p^2(r) = 2\,\frac{\kappa^2}{\omega^2}$ for $r>1$ (if $r=1$ it is equal to 0) and $\sum_p S_p^2(r+1) = 2\,\frac{\kappa^2}{\omega^2}\ \forall r$. This braket can thus be rewritten as $-2\,\Omega\,\frac{\kappa^2}{\omega^2}\cos\frac{q}{2}\sum_{r=1}^{N-2}|r+1\rangle\langle r|$. Taking also into account the zeroth order, $(\kappa/\omega)^0$, the displaced hopping term Eq. (A.1) finally reduces to

$$H_{\rm hop} = 2\Omega\left(1-\frac{\kappa^2}{\omega^2}\right)\cos\frac{q}{2}\sum_{r=1}^{N-2}|r+1\rangle\langle r|\,, \tag{A.4}$$

which is the first term of Eq. (11) in the main text.

B Derivation of the survival probability $p_d(t)$

We derive here the expression for the survival probability $p(t)$ given by Eq. (24). The derivation involves a sequence of steps which are detailed in the following: first, we derive the eigenvalue equation for $H_{{\rm eff},q}$ and obtain the expression of the bound state energy E_b. Then we calculate the general expression of $|a(E)|^2$ appearing in Eq. (23). This allows us to compute finally the survival probability $p_d(t)$.

Inserting Eq. (22) in the Schrödinger equation $H_{{\rm eff},q}|\psi_E\rangle = E|\psi_E\rangle$ and using Eq. (20), one obtains a system of equations in the unknowns $a = a(E)$ and $b_k = b_k(E)$ (the dependence on E will be indicated explicitly only where necessary):

$$\begin{cases} \alpha\, a + \sum_{k=1}^{N-2} V(k)\, b_k = E\, a\,, \\ V(k)\, a + E_q^0(k)\, b_k = E\, b_k\,, \end{cases} \tag{B.1}$$

where $V(k)$ is the interaction potential given by Eq. (21) of the main text. As shown in Fig. 4b, the eigenvalues E, except for the bound state energy E_b, extend over the same range to which the uncoupled energies $E_q^0(k)$ belong. For large N, the uncoupled energies $E_q^0(k)$ form a continuous band and the eigenvalues E included in this range degenerate to the energies $E_q^0(k)$. Therefore, in order to account for the occurrence of $E = E_q^0(k)$, the formal solution of the

second equation reads [67]

$$b_k = \left[\frac{1}{E - E_q^0(k)} + z(E)\,\delta(E - E_q^0(k))\right] V(k)\,a\,, \tag{B.2}$$

with the understanding that, when summed over k, one has to take the principal value (P.V.) of the sum over $(E - E_q^0(k))^{-1}$. The function $z(E)$ depends on energy, and for scattering problems one usually has conditions that imply $z = i\pi$ [68]. Here, instead, $z(E)$ is real and is determined by substituting the expression of b_k in the first equation of (B.1). After factoring out the coefficient a, this gives

$$\alpha + \text{P.V.}\sum_{k=1}^{N-2} \frac{V^2(k)}{E - E_q^0(k)} + z(E)\sum_{k=1}^{N-2} V^2(k)\,\delta(E - E_q^0(k)) = E\,. \tag{B.3}$$

This is the eigenvalue equation whose solutions E are the $N-1$ eigenvalues of $H_{\text{eff},q}$. By explicitly computing the two sums, one obtains the expression for $z(E)$. By noticing from Eq. (21) that

$$V^2(k) = \frac{4J_q^2 - E_q^0(k)^2}{2(N-1)}\,, \tag{B.4}$$

which expresses the interaction potential as a function of the energy in the continuum, the first sum can be computed as

$$\begin{aligned}
\text{P.V.}\sum_{k=1}^{N-2} \frac{V^2(k)}{E - E_q^0(k)} &= \frac{1}{2(N-1)}\text{P.V.}\sum_{k=1}^{N-2} \frac{4J_q^2 - E^2 + E^2 - E_q^0(k)^2}{E - E_q^0(k)} \\
&= \frac{1}{2(N-1)}\left[(N-2)E + (4J_q^2 - E^2)\text{P.V.}\sum_{k=1}^{N-2} \frac{1}{E - 2J_q\cos\left(\frac{\pi}{N-1}k\right)}\right].
\end{aligned}$$

The last principal value can be computed using

$$\begin{aligned}
\text{P.V.}\sum_{k=1}^{N-2} \frac{1}{E - 2J_q\cos\left(\frac{\pi}{N-1}k\right)} &\simeq \text{P.V.}\int_1^{N-2} \frac{1}{E - 2J_q\cos\left(\frac{\pi}{N-1}k\right)}dk \\
&= \frac{N-1}{\pi}\text{P.V.}\int_{\frac{\pi}{N-1}}^{\frac{\pi(N-2)}{N-1}} \frac{1}{E - 2J_q\cos x}dx \\
&= \frac{2(N-1)}{\pi}\text{P.V.}\int_{\tan\frac{\pi}{2(N-1)}}^{\tan\frac{\pi(N-2)}{2(N-1)}} \frac{1}{E - 2J_q + (E + 2J_q)t^2}dt \\
&= \begin{cases} \frac{N-1}{\sqrt{E^2 - 4J_q^2}} & \text{if} \quad E^2 - 4J_q^2 > 0\,, \\ 0 & \text{if} \quad E^2 - 4J_q^2 < 0\,, \end{cases}
\end{aligned}$$

where we have taken the large N limit and used the following substitutions:

$$x = \frac{\pi}{N-1}k, \qquad \cos x = \frac{1-t^2}{1+t^2}, \quad t = \tan\frac{x}{2}\,.$$

The second sum in Eq. (B.3) gives

$$\begin{aligned}
\sum_{k=1}^{N-2} V^2(k)\,\delta(E - E_q^0(k)) &= V^2(E)\,\rho(E)\,\Theta(4J_q^2 - E^2) \\
&= \frac{\sqrt{4J_q^2 - E^2}}{2\pi}\,\Theta(4J_q^2 - E^2),
\end{aligned}$$

where we have used Eq. (B.4) and defined

$$\rho(E) = \left| \frac{dk}{dE_q^0(k)} \right|_{k=(E_q^0)^{-1}(E)} = \frac{N-1}{\pi\sqrt{4J_q^2 - E^2}}$$

as the density of states of the continuum $\{|\bar{k}\rangle\}$. Collecting all the terms and taking the large N limit, the eigenvalue equation Eq. (B.3) now reads

$$\alpha + \frac{E}{2} - \frac{\sqrt{E^2-4J_q^2}}{2}\Theta(E^2-4J_q^2) + z(E)\frac{\sqrt{4J_q^2-E^2}}{2\pi}\Theta(4J_q^2-E^2) = E\,, \tag{B.5}$$

where Θ is the Heaviside step function. The energy of the bound state E_b, satisfying $E^2-4J_q^2>0$ and appearing only when $\alpha > |J_q|$, can be obtained by Eq. (B.5) as

$$E_b = \frac{\alpha^2+J_q^2}{\alpha}\,. \tag{B.6}$$

It is plotted in Fig. 4b of the main text. Eq. (B.5) also provides the expression for the function $z(E)$

$$z(E)\Theta(4J_q^2-E^2) = \pi\frac{E-2\alpha+\sqrt{E^2-4J_q^2}\Theta(E^2-4J_q^2)}{\sqrt{4J_q^2-E^2}}\,, \tag{B.7}$$

that is well defined only for $4J_q^2-E^2>0$, i.e. when the eigenvalue E is in the continuum. By enforcing the normalization condition

$$\langle\psi_E|\psi_{E'}\rangle = \delta_{E,E'}\,,$$

using Eqs. (B.2), (B.3) as well as the properties of the Dirac delta distribution and the principal value [64, 69], one finds

$$\begin{aligned}
|a(E)|^2 &= \frac{\Theta(E^2-4J_q^2)}{1-\frac{dF(E)}{dE}\Big|_{E=E_b}}\delta_{E,E_b} + \frac{\Theta(4J_q^2-E^2)}{V^2(E)\rho^2(E)\Theta(4J_q^2-E^2)[\pi^2+z^2(E)]} \\
&= \frac{\Theta(E^2-4J_q^2)}{1-\frac{dF(E)}{dE}\Big|_{E=E_b}}\delta_{E,E_b} + \frac{\Theta(4J_q^2-E^2)}{V^2(E)\rho^2(E)\left[\pi^2\Theta(4J_q^2-E^2)+z^2(E)\Theta(4J_q^2-E^2)\right]} \\
&= \frac{\Theta(E^2-4J_q^2)}{1-\frac{dF(E)}{dE}\Big|_{E=E_b}}\delta_{E,E_b} + \frac{\Theta(4J_q^2-E^2)}{V^2(E)\rho^2(E)\pi^2\left\{\Theta(4J_q^2-E^2)+\frac{\left[E-2\alpha+\sqrt{E^2-4J_q^2}\Theta(E^2-4J_q^2)\right]^2}{4J_q^2-E^2}\right\}} \\
&= \frac{\Theta(E^2-4J_q^2)}{1-\frac{dF(E)}{dE}\Big|_{E=E_b}}\delta_{E,E_b} + \frac{\Theta(4J_q^2-E^2)}{\frac{N-1}{2}\left\{\Theta(4J_q^2-E^2)+\frac{\left[E-2\alpha+\sqrt{E^2-4J_q^2}\Theta(E^2-4J_q^2)\right]^2}{4J_q^2-E^2}\right\}}\,,
\end{aligned} \tag{B.8}$$

where we denote

$$F(E) = \text{P.V.}\sum_{k=1}^{N-2}\frac{V^2(k)}{E-E_q^0(k)} = \frac{E}{2} - \frac{\sqrt{E^2-4J_q^2}}{2}\Theta(E^2-4J_q^2)\,,$$

for brevity. Since

$$\frac{dF(E)}{dE}\Big|_{E=E_b=\frac{\alpha^2+J_q^2}{\alpha}} = \frac{1}{2}\left(1-\frac{\alpha^2+J_q^2}{\sqrt{\left(\alpha^2-J_q^2\right)^2}}\right),$$

one finally obtains the expression for the survival probability by summing the factor $|a(E)|^2 e^{-iEt}$ over the $N-1$ eigenvalues E (the energies in the continuum and the eventual bound state). The Heaviside step functions in the numerators of Eq. (B.8) separates the sum into two contributions depending whether $E^2 \lessgtr 4J_q^2$. This leads to

$$\begin{aligned}
p_d(t) &= \left| \sum_E |a(E)|^2 e^{-iEt} \right|^2 \\
&= \left| \frac{\alpha^2 - J_q^2}{\alpha^2} e^{-iE_b t}\,\Theta(\alpha^2 - J_q^2) + \sum_{k=1}^{N-2} \frac{1}{\frac{N-1}{2}\left[1 + \frac{\left(E_q^0(k) - 2\alpha\right)^2}{4J_q^2 - E_q^0(k)^2}\right]} e^{-iE_q^0(k)t} \right|^2 \\
&= \left| \frac{\alpha^2 - J_q^2}{\alpha^2} e^{-iE_b t}\,\Theta(\alpha^2 - J_q^2) + \frac{2}{N-1} \sum_{k=1}^{N-2} \frac{1}{1 + \frac{\left[2J_q \cos\left(\frac{\pi}{N-1}k\right) - 2\alpha\right]^2}{4J_q \sin^2\left(\frac{\pi}{N-1}k\right)}} e^{-i2J_q \cos\left(\frac{\pi}{N-1}k\right)t} \right|^2 \\
&\simeq \left| \frac{\alpha^2 - J_q^2}{\alpha^2} e^{-iE_b t}\,\Theta(\alpha^2 - J_q^2) + \frac{2}{\pi} \int_0^\pi dx \frac{1}{1 + \frac{\left(J_q \cos x - \alpha\right)^2}{J_q \sin^2 x}} e^{-i2J_q t \cos x} \right|^2 \\
&= \left| \frac{\alpha^2 - J_q^2}{\alpha^2} e^{-iE_b t}\,\Theta(\alpha^2 - J_q^2) + \frac{2J_q^2}{\pi(\alpha^2 + J_q^2)} \int_0^\pi dx \frac{\sin^2 x}{1 - \frac{2\alpha J_q}{\alpha^2 + J_q^2}\cos x} e^{-i2J_q t \cos x} \right|^2 ,
\end{aligned} \tag{B.9}$$

which coincides with Eq. (24) of the main text.

Note that, when $\alpha = 0$ and $J_q \neq 0$, one recovers the simpler case where $H_{\text{eff},q}$ is merely a hopping Hamiltonian. Here, the survival probability reduces to

$$p_d(t) = \left| \frac{2}{\pi} \int_0^\pi dx \sin^2 x\, e^{-i2J_q t \cos x} \right|^2 = \frac{1}{J_q^2 t^2} \mathcal{J}_1^2(2J_q t), \tag{B.10}$$

where $\mathcal{J}_\alpha(x)$ is the Bessel function of the first kind. This result is in agreement with previous works [70, 71].

References

[1] I. Bloch, J. Dalibard and W. Zwerger, *Many-body physics with ultracold gases*, Rev. Mod. Phys. **80**, 885 (2008), doi:10.1103/RevModPhys.80.885.

[2] V. I. Balykin, V. G. Minogin and V. S. Letokhov, *Electromagnetic trapping of cold atoms*, Rep. Prog. Phys. **63**, 1429 (2000), doi:10.1088/0034-4885/63/9/202.

[3] M. Saffman, T. G. Walker and K. Mølmer, *Quantum information with Rydberg atoms*, Rev. Mod. Phys. **82**, 2313 (2010), doi:10.1103/RevModPhys.82.2313.

[4] K. Singer, J. Stanojevic, M. Weidemüller and R. Côté, *Long-range interactions between alkali Rydberg atom pairs correlated to the ns-ns, np-np and nd-nd asymptotes*, J. Phys. B: At. Mol. Opt. Phys. **38**, S295 (2005), doi:10.1088/0953-4075/38/2/021.

[5] M. T. Eiles and C. H. Greene, *Hamiltonian for the inclusion of spin effects in long-range Rydberg molecules*, Phys. Rev. A **95**, 042515 (2017), doi:10.1103/PhysRevA.95.042515.

[6] A. Browaeys and T. Lahaye, *Many-body physics with individually controlled Rydberg atoms*, Nat. Phys. **16**, 132 (2020), doi:10.1038/s41567-019-0733-z.

[7] T. Pohl, H. R. Sadeghpour and P. Schmelcher, *Cold and ultracold Rydberg atoms in strong magnetic fields*, Phys. Rep. **484**, 181 (2009), doi:10.1016/j.physrep.2009.10.001.

[8] I. Bloch, J. Dalibard and S. Nascimbène, *Quantum simulations with ultracold quantum gases*, Nat. Phys. **8**, 267 (2012), doi:10.1038/nphys2259.

[9] Y.-Y. Jau, A. M. Hankin, T. Keating, I. H. Deutsch and G. W. Biedermann, *Entangling atomic spins with a Rydberg-dressed spin-flip blockade*, Nat. Phys. **12**, 71 (2015), doi:10.1038/nphys3487.

[10] H. Bernien et al., *Probing many-body dynamics on a 51-atom quantum simulator*, Nature **551**, 579 (2017), doi:10.1038/nature24622.

[11] F. Letscher, O. Thomas, T. Niederprüm, M. Fleischhauer and H. Ott, *Bistability versus metastability in driven dissipative Rydberg gases*, Phys. Rev. X **7**, 021020 (2017), doi:10.1103/PhysRevX.7.021020.

[12] H. Kim, Y. Park, K. Kim, H.-S. Sim and J. Ahn, *Detailed balance of thermalization dynamics in Rydberg-atom quantum simulators*, Phys. Rev. Lett. **120**, 180502 (2018), doi:10.1103/PhysRevLett.120.180502.

[13] J. Han, T. Vogt, C. Gross, D. Jaksch, M. Kiffner and W. Li, *Coherent microwave-to-optical conversion via six-wave mixing in Rydberg atoms*, Phys. Rev. Lett. **120**, 093201 (2018), doi:10.1103/PhysRevLett.120.093201.

[14] O. Thomas, C. Lippe, T. Eichert and H. Ott, *Experimental realization of a Rydberg optical Feshbach resonance in a quantum many-body system*, Nat. Commun. **9**, 2238 (2018), doi:10.1038/s41467-018-04684-w.

[15] J. T. Wilson, S. Saskin, Y. Meng, S. Ma, R. Dilip, A. P. Burgers and J. D. Thompson, *Trapping alkaline earth Rydberg atoms optical tweezer arrays*, Phys. Rev. Lett. **128**, 033201 (2022), doi:10.1103/PhysRevLett.128.033201.

[16] C. S. Adams, J. D. Pritchard and J. P. Shaffer, *Rydberg atom quantum technologies*, J. Phys. B: At. Mol. Opt. Phys. **53**, 012002 (2019), doi:10.1088/1361-6455/ab52ef.

[17] F. Engel, T. Dieterle, F. Hummel, C. Fey, P. Schmelcher, R. Löw, T. Pfau and F. Meinert, *Precision spectroscopy of negative-ion resonances in ultralong-range Rydberg molecules*, Phys. Rev. Lett. **123**, 073003 (2019), doi:10.1103/PhysRevLett.123.073003.

[18] I. I. Beterov, D. B. Tretyakov, V. M. Entin, E. A. Yakshina, I. I. Ryabtsev, M. Saffman and S. Bergamini, *Application of adiabatic passage in Rydberg atomic ensembles for quantum information processing*, J. Phys. B: At. Mol. Opt. Phys. **53**, 182001 (2020), doi:10.1088/1361-6455/ab8719.

[19] S. Ebadi et al., *Quantum phases of matter on a 256-atom programmable quantum simulator*, Nature **595**, 227 (2021), doi:10.1038/s41586-021-03582-4.

[20] R. Blatt and C. F. Roos, *Quantum simulations with trapped ions*, Nat. Phys. **8**, 277 (2012), doi:10.1038/nphys2252.

[21] Y. O. Dudin and A. Kuzmich, *Strongly interacting Rydberg excitations of a cold atomic gas*, Science **336**, 887 (2012), doi:10.1126/science.1217901.

[22] H. Labuhn, D. Barredo, S. Ravets, S. de Léséleuc, T. Macrì, T. Lahaye and A. Browaeys, *Tunable two-dimensional arrays of single Rydberg atoms for realizing quantum Ising models*, Nature **534**, 667 (2016), doi:10.1038/nature18274.

[23] C. Gross and I. Bloch, *Quantum simulations with ultracold atoms in optical lattices*, Science **357**, 995 (2017), doi:10.1126/science.aal3837.

[24] A. Urvoy, F. Ripka, I. Lesanovsky, D. Booth, J. P. Shaffer, T. Pfau and R. Löw, *Strongly correlated growth of Rydberg aggregates in a vapor cell*, Phys. Rev. Lett. **114**, 203002 (2015), doi:10.1103/PhysRevLett.114.203002.

[25] N. Malossi, M. M. Valado, S. Scotto, P. Huillery, P. Pillet, D. Ciampini, E. Arimondo and O. Morsch, *Full counting statistics and phase diagram of a dissipative Rydberg gas*, Phys. Rev. Lett. **113**, 023006 (2014), doi:10.1103/PhysRevLett.113.023006.

[26] M. M. Valado, C. Simonelli, M. D. Hoogerland, I. Lesanovsky, J. P. Garrahan, E. Arimondo, D. Ciampini and O. Morsch, *Experimental observation of controllable kinetic constraints in a cold atomic gas*, Phys. Rev. A **93**, 040701 (2016), doi:10.1103/PhysRevA.93.040701.

[27] S. Helmrich, A. Arias, G. Lochead, T. M. Wintermantel, M. Buchhold, S. Diehl and S. Whitlock, *Signatures of self-organized criticality in an ultracold atomic gas*, Nature **577**, 481 (2020), doi:10.1038/s41586-019-1908-6.

[28] Z. Lan, M. van Horssen, S. Powell and J. P. Garrahan, *Quantum slow relaxation and metastability due to dynamical constraints*, Phys. Rev. Lett. **121**, 040603 (2018), doi:10.1103/PhysRevLett.121.040603.

[29] C. J. Turner, A. A. Michailidis, D. A. Abanin, M. Serbyn and Z. Papić, *Weak ergodicity breaking from quantum many-body scars*, Nat. Phys. **14**, 745 (2018), doi:10.1038/s41567-018-0137-5.

[30] C. J. Turner, A. A. Michailidis, D. A. Abanin, M. Serbyn and Z. Papić, *Quantum scarred eigenstates in a Rydberg atom chain: Entanglement, breakdown of thermalization, and stability to perturbations*, Phys. Rev. B **98**, 155134 (2018), doi:10.1103/PhysRevB.98.155134.

[31] W. Wei Ho, S. Choi, H. Pichler and M. D. Lukin, *Periodic orbits, entanglement, and quantum many-body scars in constrained models: Matrix product state approach*, Phys. Rev. Lett. **122**, 040603 (2019), doi:10.1103/PhysRevLett.122.040603.

[32] G. H. Fredrickson and H. C. Andersen, *Kinetic Ising model of the glass transition*, Phys. Rev. Lett. **53**, 1244 (1984), doi:10.1103/PhysRevLett.53.1244.

[33] J. P. Garrahan, *Aspects of non-equilibrium in classical and quantum systems: Slow relaxation and glasses, dynamical large deviations, quantum non-ergodicity, and open quantum dynamics*, Physica A: Stat. Mech. Appl. **504**, 130 (2018), doi:10.1016/j.physa.2017.12.149.

[34] J. P. Garrahan and D. Chandler, *Geometrical explanation and scaling of dynamical heterogeneities in glass forming systems*, Phys. Rev. Lett. **89**, 035704 (2002), doi:10.1103/PhysRevLett.89.035704.

[35] M. C. Bañuls and J. P. Garrahan, *Using matrix product states to study the dynamical large deviations of kinetically constrained models*, Phys. Rev. Lett. **123**, 200601 (2019), doi:10.1103/PhysRevLett.123.200601.

[36] C.-J. Lin and O. I. Motrunich, *Exact quantum many-body scar states in the Rydberg-blockaded atom chain*, Phys. Rev. Lett. **122**, 173401 (2019), doi:10.1103/PhysRevLett.122.173401.

[37] H. Schempp et al., *Full counting statistics of laser excited Rydberg aggregates in a one-dimensional geometry*, Phys. Rev. Lett. **112**, 013002 (2014), doi:10.1103/PhysRevLett.112.013002.

[38] I. Lesanovsky and J. P. Garrahan, *Out-of-equilibrium structures in strongly interacting Rydberg gases with dissipation*, Phys. Rev. A **90**, 011603 (2014), doi:10.1103/PhysRevA.90.011603.

[39] M. Mattioli, A. W. Glätzle and W. Lechner, *From classical to quantum non-equilibrium dynamics of Rydberg excitations in optical lattices*, New J. Phys. **17**, 113039 (2015), doi:10.1088/1367-2630/17/11/113039.

[40] M. Marcuzzi, M. Buchhold, S. Diehl and I. Lesanovsky, *Absorbing state phase transition with competing quantum and classical fluctuations*, Phys. Rev. Lett. **116**, 245701 (2016), doi:10.1103/PhysRevLett.116.245701.

[41] R. Gutiérrez, C. Simonelli, M. Archimi, F. Castellucci, E. Arimondo, D. Ciampini, M. Marcuzzi, I. Lesanovsky and O. Morsch, *Experimental signatures of an absorbing-state phase transition in an open driven many-body quantum system*, Phys. Rev. A **96**, 041602 (2017), doi:10.1103/PhysRevA.96.041602.

[42] M. Ostmann, M. Marcuzzi, J. Minár and I. Lesanovsky, *Synthetic lattices, flat bands and localization in Rydberg quantum simulators*, Quantum Sci. Technol. **4**, 02LT01 (2019), doi:10.1088/2058-9565/aaf29d.

[43] M. Marcuzzi, J. Minář, D. Barredo, S. de Léséleuc, H. Labuhn, T. Lahaye, A. Browaeys, E. Levi and I. Lesanovsky, *Facilitation dynamics and localization phenomena in Rydberg lattice gases with position disorder*, Phys. Rev. Lett. **118**, 063606 (2017), doi:10.1103/PhysRevLett.118.063606.

[44] M. Ostmann, M. Marcuzzi, J. P. Garrahan and I. Lesanovsky, *Localization in spin chains with facilitation constraints and disordered interactions*, Phys. Rev. A **99**, 060101 (2019), doi:10.1103/PhysRevA.99.060101.

[45] A. Lerose, F. M. Surace, P. P. Mazza, G. Perfetto, M. Collura and A. Gambassi, *Quasilocalized dynamics from confinement of quantum excitations*, Phys. Rev. B **102**, 041118 (2020), doi:10.1103/PhysRevB.102.041118.

[46] F. M. Surace, P. P. Mazza, G. Giudici, A. Lerose, A. Gambassi and M. Dalmonte, *Lattice gauge theories and string dynamics in Rydberg atom quantum simulators*, Phys. Rev. X **10**, 021041 (2020), doi:10.1103/PhysRevX.10.021041.

[47] R. Verdel, F. Liu, S. Whitsitt, A. V. Gorshkov and M. Heyl, *Real-time dynamics of string breaking in quantum spin chains*, Phys. Rev. B **102**, 014308 (2020), doi:10.1103/PhysRevB.102.014308.

[48] M. Magoni, P. P. Mazza and I. Lesanovsky, *Emergent Bloch oscillations in a kinetically constrained Rydberg spin lattice*, Phys. Rev. Lett. **126**, 103002 (2021), doi:10.1103/PhysRevLett.126.103002.

[49] C. Ates, T. Pohl, T. Pattard and J. M. Rost, *Antiblockade in Rydberg excitation of an ultracold lattice gas*, Phys. Rev. Lett. **98**, 023002 (2007), doi:10.1103/PhysRevLett.98.023002.

[50] T. Amthor, C. Giese, C. S. Hofmann and M. Weidemüller, *Evidence of antiblockade in an ultracold Rydberg gas*, Phys. Rev. Lett. **104**, 013001 (2010), doi:10.1103/PhysRevLett.104.013001.

[51] J. T. Young, T. Boulier, E. Magnan, E. A. Goldschmidt, R. M. Wilson, S. L. Rolston, J. V. Porto and A. V. Gorshkov, *Dissipation-induced dipole blockade and antiblockade in driven Rydberg systems*, Phys. Rev. A **97**, 023424 (2018), doi:10.1103/PhysRevA.97.023424.

[52] L. Festa, N. Lorenz, L.-M. Steinert, Z. Chen, P. Osterholz, R. Eberhard and C. Gross, *Blackbody-radiation-induced facilitated excitation of Rydberg atoms in optical tweezers*, Phys. Rev. A **105**, 013109 (2022), doi:10.1103/PhysRevA.105.013109.

[53] F. M. Gambetta, W. Li, F. Schmidt-Kaler and I. Lesanovsky, *Engineering nonBinary Rydberg interactions via phonons in an optical lattice*, Phys. Rev. Lett. **124**, 043402 (2020), doi:10.1103/PhysRevLett.124.043402.

[54] P. P. Mazza, R. Schmidt and I. Lesanovsky, *Vibrational dressing in kinetically constrained Rydberg spin systems*, Phys. Rev. Lett. **125**, 033602 (2020), doi:10.1103/PhysRevLett.125.033602.

[55] M. Ostmann, M. Marcuzzi, J. P. Garrahan and I. Lesanovsky, *Localization in spin chains with facilitation constraints and disordered interactions*, Phys. Rev. A **99**, 060101 (2019), doi:10.1103/PhysRevA.99.060101.

[56] T. D. Lee, F. E. Low and D. Pines, *The motion of slow electrons in a polar crystal*, Phys. Rev. **90**, 297 (1953), doi:10.1103/PhysRev.90.297.

[57] S. Weber, C. Tresp, H. Menke, A. Urvoy, O. Firstenberg, H. Peter Büchler and S. Hofferberth, *Calculation of Rydberg interaction potentials*, J. Phys. B: At. Mol. Opt. Phys. **50**, 133001 (2017), doi:10.1088/1361-6455/aa743a.

[58] I. I. Beterov, I. I. Ryabtsev, D. B. Tretyakov and V. M. Entin, *Quasiclassical calculations of blackbody-radiation-induced depopulation rates and effective lifetimes of Rydberg nS, nP, and nD alkali-metal atoms with $n \leq 80$*, Phys. Rev. A **79**, 052504 (2009), doi:10.1103/PhysRevA.79.052504.

[59] P. Schauß et al., *Observation of spatially ordered structures in a two-dimensional Rydberg gas*, Nature **491**, 87 (2012), doi:10.1038/nature11596.

[60] F. Nogrette, H. Labuhn, S. Ravets, D. Barredo, L. Béguin, A. Vernier, T. Lahaye and A. Browaeys, *Single-atom trapping in holographic 2D arrays of microtraps with arbitrary geometries*, Phys. Rev. X **4**, 021034 (2014), doi:10.1103/PhysRevX.4.021034.

[61] D. Barredo, V. Lienhard, P. Scholl, S. de Léséleuc, T. Boulier, A. Browaeys and T. Lahaye, *Three-dimensional trapping of individual Rydberg atoms in ponderomotive bottle beam traps*, Phys. Rev. Lett. **124**, 023201 (2020), doi:10.1103/PhysRevLett.124.023201.

[62] S. Sevinçli and T. Pohl, *Microwave control of Rydberg atom interactions*, New J. Phys. **16**, 123036 (2014), doi:10.1088/1367-2630/16/12/123036.

[63] C. Zhang, F. Pokorny, W. Li, G. Higgins, A. Pöschl, I. Lesanovsky and M. Hennrich, *Submicrosecond entangling gate between trapped ions via Rydberg interaction*, Nature **580**, 345 (2020), doi:10.1038/s41586-020-2152-9.

[64] U. Fano, *Effects of configuration interaction on intensities and phase shifts*, Phys. Rev. **124**, 1866 (1961), doi:10.1103/PhysRev.124.1866.

[65] F. M. Surace and A. Lerose, *Scattering of mesons in quantum simulators*, New J. Phys. **23**, 062001 (2021), doi:10.1088/1367-2630/abfc40.

[66] P. I. Karpov, G.-Y. Zhu, M. P. Heller and M. Heyl, *Spatiotemporal dynamics of particle collisions in quantum spin chains*, Phys. Rev. Research **4**, L032001 (2022), doi:10.1103/PhysRevResearch.4.L032001.

[67] P. A. M. Dirac, *Über die Quantenmechanik der Stoßvorgänge*, Z. Physik **44**, 585 (1927), doi:10.1007/BF01451660.

[68] P. A. M. Dirac, *The principles of quantum mechanics*, Clarendon Press, Oxford, UK, ISBN 9780198512080 (1958).

[69] G. D. Mahan, *Many-particle physics*, Springer US, Boston, Massachusetts, US, ISBN 9781441933393 (2000), doi:10.1007/978-1-4757-5714-9.

[70] G. C. Stey and G. Gusman, *Absence of decay and eigenvector localization in a soluble one-dimensional system*, Phys. Lett. A **39**, 393 (1972), doi:10.1016/0375-9601(72)90110-7.

[71] S. Longhi, *Nonexponential decay via tunneling in tight-binding lattices and the optical Zeno effect*, Phys. Rev. Lett. **97**, 110402 (2006), doi:10.1103/PhysRevLett.97.110402.

Third Publication

Rydberg tweezer molecules: Spin-phonon entanglement and Jahn-Teller effect

Matteo Magoni,[1] Radhika Joshi,[1] and Igor Lesanovsky[1,2]

[1] *Institut für Theoretische Physik, Universität Tübingen, Auf der Morgenstelle 14, 72076 Tübingen, Germany*

[2] *School of Physics and Astronomy and Centre for the Mathematics and Theoretical Physics of Quantum Non-Equilibrium Systems, The University of Nottingham, Nottingham, NG7 2RD, United Kingdom*

(Dated: June 12, 2023)

Atoms confined in optical tweezer arrays constitute a platform for the implementation of quantum computers and simulators. State-dependent operations are realized by exploiting electrostatic dipolar interactions that emerge, when two atoms are simultaneously excited to high-lying electronic states, so-called Rydberg states. These interactions also lead to state-dependent mechanical forces, which couple the electronic dynamics of the atoms to their vibrational motion. We explore these vibronic couplings within an artificial molecular system — a Rydberg tweezer molecule — in which Rydberg states are excited under so-called facilitation conditions. This system, which is not necessarily self-bound, undergoes a structural transition between an equilateral triangle and an equal-weighted superposition of distorted triangular states (Jahn-Teller regime) exhibiting spin-phonon entanglement on a micrometer distance. This highlights the potential of Rydberg tweezer arrays for the study of molecular phenomena at exaggerated length scales.

Introduction — Recent progress in controlling ultra cold atomic gases allows the preparation of atomic arrays with virtually arbitrary geometry [1, 2]. This technological advance is at the heart of recent breakthroughs in the domains of quantum simulation and quantum computation [3–16]. Key for the latter applications is the utilization of atomic Rydberg states in which atoms interact via electrostatic dipolar interactions [17–20]. This mechanism underlies the experimental implementation of many-body spin Hamiltonians with variable interaction range and geometry [21–29]. By building on this capability, a number of recent works have studied the dynamics of quantum correlations in many-body systems [30, 31], critical behavior near phase transitions [32, 33] and novel manifestations of ergodicity breaking [34].

Concomitant with the strong dipolar interactions among Rydberg atoms are mechanical forces, which owed to their state-dependent nature couple the internal atomic degrees of freedom with the external motional ones [35, 36]. On the one hand, in quantum simulators and processors this mechanism causes decoherence of the electronic dynamics [37–40]; and in the extreme case they may even lead to a rapid "explosion" of ensembles of Rydberg atoms [41]. On the other hand, this vibronic coupling can be exploited to implement coherent many-body interactions [42] and cooling protocols [43], and may also enable the exploration of polaronic physics in Rydberg lattice gases dressed by phonons [44–46]. Beyond that, it enables the realization of dynamical processes that bear close resemblance to those found in molecules, but on exaggerated micrometer length scales [47]. The viability of this idea has been recently investigated in a theoretical work on conical intersections in an artificial molecule realized with two trapped Rydberg ions [48]. Other examples of exotic types of molecules involving Rydberg states include ultralong-range Rydberg molecules reported in Refs. [49, 50] and Rydberg macrodimers investigated in Refs. [51–55].

In this work we introduce and theoretically investigate an artificial molecular system — a Rydberg tweezer molecule — which is realized in a small two-dimensional tweezer array in which atoms can be flexibly arranged. We focus on a simple setting where three trapped atoms, forming an equilateral triangle, are excited to Rydberg states under facilitation conditions. Our study, which is closely related to the physics of Rydberg aggregates [56–58], establishes how the molecular spectrum is affected by vibronic couplings. It moreover reveals the emergence of a Jahn-Teller regime where the molecule exhibits spin-phonon entanglement on micrometer distances. This highlights the vast possibilities offered by Rydberg arrays for studying complex dynamical processes involving coherent molecular dynamics near intersecting potential energy surfaces. Our findings also connect to recent research concerning the creation and exploitation of macroscopic quantum superposition of states in mechanical systems [59, 60].

Model — The Rydberg tweezer molecule we consider here is shown in Fig. 1a. The atoms form an equilateral triangle where the distance between neighboring atoms is d. The trapping potential within each tweezer shall be approximated by a two-dimensional (we consider the third dimension to be frozen out) isotropic harmonic trap with frequency $\omega_x = \omega_y = \omega$. Moreover, the trapping potential is assumed to be the same no matter whether an atom is in its ground state or Rydberg state. Such state-independent trapping can, for example, be achieved by operating the trapping laser at a so-called magic frequency [61–65]. Each atom is modeled as a two-level system (see Fig. 1b), where $|\downarrow\rangle$ denotes

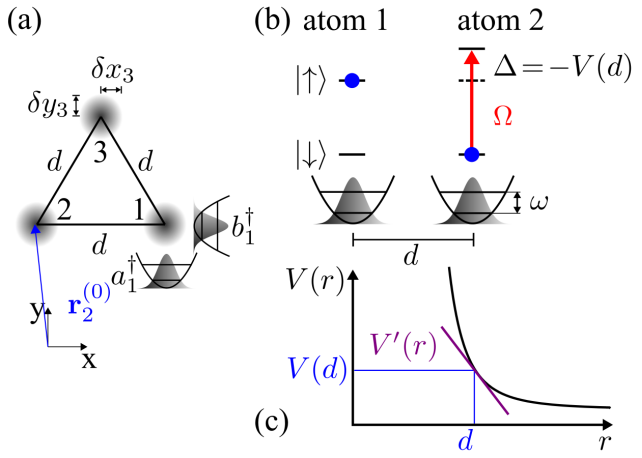

FIG. 1. **Rydberg tweezer molecule.** (a) The system under consideration is formed by atoms confined in harmonic optical tweezer traps (trap frequency ω) forming an equilateral triangle with side length d. The center of the respective traps is located at position $\mathbf{r}_j^{(0)}$. We consider motion in the xy-plane around the trap centers. The corresponding degrees of freedom are δx_j (δy_j) which can be represented in terms of phonon creation operators $a_j^\dagger$ ($b_j^\dagger$). (b) Atoms are modelled as two-level systems, where $|\downarrow\rangle$ is the ground state and $|\uparrow\rangle$ the Rydberg state. Both states are coupled by a laser with Rabi frequency Ω and detuning Δ with respect to the single-atom transition frequency. When one atom is excited into a Rydberg state, the simultaneous excitation of the neighboring one requires an additional energy. This energy shift is given by the interaction potential V, which depends on their distance d. The atoms are confined in a harmonic potential with trap frequency ω, which we assume to be state-independent. (c) When two atoms are simultaneously in the Rydberg state they interact with the potential $V(r)$. The gradient of the potential $V'(r)$ at the interatomic distance d gives rise to a force which leads to a coupling between the electronic degrees of freedom of the atoms and the vibrational dynamics within the tweezers.

the atomic ground state and $|\uparrow\rangle$ denotes the Rydberg excited state. These two states are coupled through a laser with Rabi frequency Ω and detuning Δ. Two atoms (at positions $\boldsymbol{r}_j, \boldsymbol{r}_k$) in the Rydberg state interact via a distance-dependent potential, typically of dipolar or van der Waals type $V(\boldsymbol{r}_j, \boldsymbol{r}_k) = V(|\boldsymbol{r}_j - \boldsymbol{r}_k|)$, as depicted in Fig. 1c. The Hamiltonian of the system is therefore given by ($\hbar = 1$)

$$H_{\text{full}} = \sum_{j=1}^{3}\left[\Omega\hat{\sigma}_j^x + \Delta\hat{n}_j + \omega(\hat{a}_j^\dagger\hat{a}_j + \hat{b}_j^\dagger\hat{b}_j)\right] + \sum_{j=1}^{3}\sum_{k<j} V(\boldsymbol{r}_j, \boldsymbol{r}_k)\hat{n}_j\hat{n}_k, \quad (1)$$

where $\hat{\sigma}_j^x = |\uparrow\rangle_j\langle\downarrow|_j + |\downarrow\rangle_j\langle\uparrow|_j$ is the spin flip operator and $\hat{n}_j = |\uparrow\rangle_j\langle\uparrow|_j$ is the projector onto the Rydberg state of atom j. The operators $\hat{a}_j$ and $\hat{b}_j$ are the annihilation operators along the x and y directions of the two-dimensional trap holding atom j. The displacement of the position of atom j from the center of the trap $\boldsymbol{r}_j^{(0)}$ is given by $\delta\boldsymbol{r}_j = \boldsymbol{r}_j - \boldsymbol{r}_j^{(0)} = (\delta x_j, \delta y_j)$. Assuming that the position fluctuations are small compared to the interatomic distance, $|\delta\boldsymbol{r}_j| \ll d$, we can expand the interaction potential around the equilibrium positions as

$$V(\boldsymbol{r}_j, \boldsymbol{r}_k) \simeq V(d) + \nabla V(\boldsymbol{r}_j, \boldsymbol{r}_k)|_{(\boldsymbol{r}_j^{(0)}, \boldsymbol{r}_k^{(0)})} \cdot (\delta\boldsymbol{r}_j, \delta\boldsymbol{r}_k). \quad (2)$$

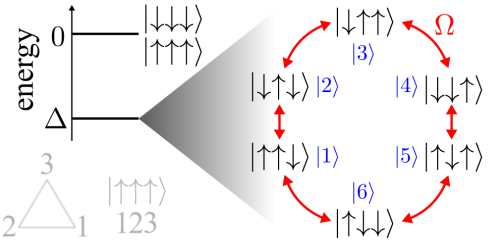

FIG. 2. **Tight-binding model of near-resonant states.** Under facilitation conditions, the Hilbert space of the internal dynamics of the Rydberg triangle separates into two manifolds. We are interested here in the manifold that is composed by atomic configurations of energy Δ. Its basis states are coupled with Rabi frequency Ω. The emerging structure corresponds to a tight-binding Hamiltonian with six sites, $|k\rangle$ with $k = 1, ..., 6$, and periodic boundary conditions. The order of the spins appearing in the kets is indicated in the bottom left.

In the following we consider the situation in which Rydberg atoms are excited under facilitation conditions [66–70] as depicted in Fig. 1b. Here the energy shift induced by the interaction among adjacent Rydberg atoms is cancelled by the laser detuning: $\Delta + V(d) = 0$. Under these conditions, the Hilbert space splits into disconnected sectors that contain states with the same energy, as shown in Fig. 2. The most interesting sector is the one including the states with one or two Rydberg excitations, which have energy Δ. These six near-resonant states, $|k\rangle$, belonging to this Hilbert subspace form the fictitious lattice sites of a tight-binding Hamiltonian with periodic boundary conditions, as depicted in Fig. 2. They are labeled as: $|1\rangle = |\uparrow\uparrow\downarrow\rangle$, $|2\rangle = |\downarrow\uparrow\downarrow\rangle$, $|3\rangle = |\downarrow\uparrow\uparrow\rangle$, $|4\rangle = |\downarrow\downarrow\uparrow\rangle$, $|5\rangle = |\uparrow\downarrow\uparrow\rangle$, $|6\rangle = |\uparrow\downarrow\downarrow\rangle$. To formulate the vibronic Hamiltonian on this subspace, we introduce the phonon operators $\delta x_j = x_{\text{ho}}(\hat{a}_j + \hat{a}_j^\dagger)/\sqrt{2}$ and $\delta y_j = x_{\text{ho}}(\hat{b}_j + \hat{b}_j^\dagger)/\sqrt{2}$, with $x_{\text{ho}} = 1/\sqrt{m\omega}$ being the harmonic oscillator length. This yields

$$H_{\text{res}} = \omega\sum_{j=1}^{3}(\hat{a}_j^\dagger\hat{a}_j + \hat{b}_j^\dagger\hat{b}_j) + \Omega\sum_{k=1}^{6}(|k+1\rangle\langle k| + \text{h.c.}) + \kappa\sum_{j=1}^{3}\left[\hat{d}_j^a(\hat{a}_j + \hat{a}_j^\dagger) + \hat{d}_j^b(\hat{b}_j + \hat{b}_j^\dagger)\right]. \quad (3)$$

The first term in the first line represents the free evolu-

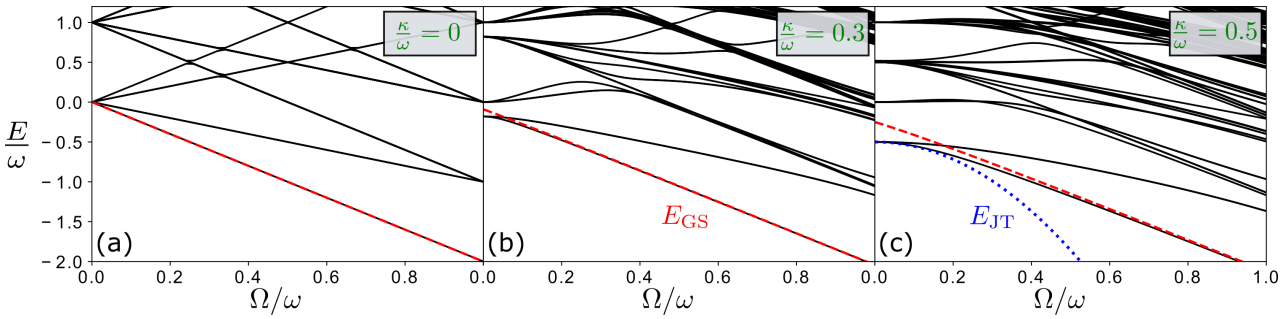

FIG. 3. **Energy spectrum.** Low-lying molecular energy levels as a function of the laser Rabi frequency Ω for different values of the electron-phonon coupling strength κ. The red dashed lines show the ground state energy obtained by second order perturbation theory: $E_{\rm GS} = E^{(0)}_{\rm GS} + E^{(2)}_{\rm GS}$. Note, that this perturbative result is valid only in the limit $\Omega \gg |\kappa|$. The blue dotted line shows the ground state energy obtained by second order perturbation theory in Ω: $E_{\rm JT} = E^{(0)}_{\rm JT} + E^{(2)}_{\rm JT}$. The energy levels are obtained by exact diagonalization of Hamiltonian (3), where we have truncated the maximum occupation number of each of the six oscillator modes at 3.

tion of the vibrations of the atoms in the x and y directions. The second term, proportional to Ω, governs the tight-binding dynamics in the electronic Hilbert space (see Fig. 2). The second line represents the coupling Hamiltonian between the vibrational and electronic dynamics. This coupling is parameterized by the constant

$$\kappa = \frac{x_{\rm ho}}{\sqrt{2}} \frac{\partial V(r)}{\partial r}\bigg|_{r=d}, \tag{4}$$

which is proportional to the gradient of the interaction potential at the equilibrium distance d. This mechanical force, which arises from the Rydberg interaction, displaces the atoms from the centers of the traps. The displacement is state-dependent which is manifest through the operators $\hat{d}^{a/b}_j$, which depend on the projectors $P_m = |m\rangle\langle m|$: $\hat{d}^a_1 = P_1 + \frac{1}{2}P_5$, $\hat{d}^a_2 = -(P_1 + \frac{1}{2}P_3)$, $\hat{d}^a_3 = \frac{1}{2}(P_3 - P_5)$ as well as $\hat{d}^b_1 = -\frac{\sqrt{3}}{2}P_5$, $\hat{d}^b_2 = -\frac{\sqrt{3}}{2}P_3$ and $\hat{d}^b_3 = \frac{\sqrt{3}}{2}(P_3 + P_5)$.

Energy spectrum — In the following we consider the case $|\kappa| \ll \omega, \Omega$, which can be studied within a perturbative analysis. The unperturbed eigenstates are products of the Fock states $|n^x_1, n^x_2, n^x_3; n^y_1, n^y_2, n^y_3\rangle$, with occupation numbers n^α_k (corresponding to the number of quanta in each vibrational degree of freedom), and the eigenstates of the electronic tight-binding Hamiltonian. Specifically, the unperturbed ground state is $|{\rm GS}\rangle^{(0)} = |{\rm GS}_{\rm elec}\rangle\,|0,0,0;0,0,0\rangle$, with

$$|{\rm GS}_{\rm elec}\rangle = \frac{1}{\sqrt{6}} \sum_{m=1}^{6} (-1)^m\,|m\rangle\,, \tag{5}$$

and with eigenenergy $E^{(0)}_{\rm GS} = -2\Omega$. Using perturbation theory up to second order in κ, the correction to the ground state energy is given by

$$E^{(2)}_{\rm GS} = -\frac{\kappa^2}{4}\left(\frac{1}{\omega} + \frac{1}{\omega+\Omega} + \frac{1}{\omega+3\Omega} + \frac{1}{\omega+4\Omega}\right), \tag{6}$$

which well captures the level repulsion between the non-degenerate ground state and the excited states, as shown by the red dashed lines in Fig. 3. Fixing the coupling constant κ, the full energy spectrum displays two distinct regimes: for $\Omega \ll \omega$, the spectrum is split into groups of energy levels, which are separated by gaps of energy ω. For $\Omega \gg \omega$, the spectrum is decomposed into groups in which each state possesses approximately the same eigenenergy with respect to the tight-binding Hamiltonian.

A second regime to consider is the one where $\Omega \ll \omega, |\kappa|$. Here the electronic tight-binding Hamiltonian can be treated as a perturbation. In this case, we diagonalize the unperturbed Hamiltonian by applying a unitary displacement operator

$$\hat{D} = \exp\left\{-\frac{\kappa}{\omega}\sum_{j=1}^{3}\left[\hat{d}^a_j(\hat{a}^\dagger_j - \hat{a}_j) + \hat{d}^b_j(\hat{b}^\dagger_j - \hat{b}_j)\right]\right\} \tag{7}$$

to Hamiltonian (3), thereby obtaining

$$\hat{D}^\dagger H_{\rm res}\hat{D} = H_0 + V, \tag{8}$$

where

$$H_0 = \omega\sum_{j=1}^{3}(\hat{a}^\dagger_j\hat{a}_j + \hat{b}^\dagger_j\hat{b}_j) - 2\frac{\kappa^2}{\omega}\,(P_1 + P_3 + P_5) \tag{9}$$

is diagonal in the product states $|k\rangle\,|n^x_1, n^x_2, n^x_3; n^y_1, n^y_2, n^y_3\rangle$, while

$$V = \Omega\hat{D}^\dagger\sum_{k=1}^{6}\left(|k+1\rangle\,\langle k| + {\rm h.c.}\right)\hat{D} \tag{10}$$

is a displaced hopping operator, whose explicit expression is derived in the Supplemental Material. The unperturbed Hamiltonian H_0 is characterized by the presence of three degenerate ground states, each with eigenvalue

$-2\kappa^2/\omega$, given by the phonon vacuum and the electronic states with two Rydberg excitations. This degeneracy is a manifestation of the invariance of the Hamiltonian under a 120° rotation around the center of mass of the equilateral triangle. By applying degenerate perturbation theory, one finds that the ground state degeneracy is partially lifted at second order in Ω, allowing to select the right ground state from the three-dimensional ground state manifold. This is given as

$$\begin{aligned}|\mathrm{JT}\rangle^{(0)} &= \frac{1}{\sqrt{3}}\Big(|1\rangle\left|-\frac{\kappa}{\omega},\frac{\kappa}{\omega},0;0,0,0\right\rangle \\ &+|3\rangle\left|0,\frac{\kappa}{2\omega},-\frac{\kappa}{2\omega};0,\frac{\sqrt{3}\kappa}{2\omega},-\frac{\sqrt{3}\kappa}{2\omega}\right\rangle \\ &+|5\rangle\left|-\frac{\kappa}{2\omega},0,\frac{\kappa}{2\omega};\frac{\sqrt{3}\kappa}{2\omega},0,-\frac{\sqrt{3}\kappa}{2\omega}\right\rangle\Big) \quad (11)\end{aligned}$$

and it has eigenenergy $E_{\mathrm{JT}}^{(0)} = -2\kappa^2/\omega$. It consists in a spin-phonon entangled state, where each of the three degenerate electronic states is coupled to a different set of motional coherent states. This state represents a neat manifestation of the Jahn-Teller effect [71, 72], as each motional coherent state represents a possible distortion of the triangular configuration. This state is fundamentally different from the product state $|\mathrm{GS}\rangle^{(0)}$, in which the atoms remain placed at the corners of an equilateral triangle. The energy shift of the ground state due to the Rabi coupling, computed by second order perturbation theory (see Supplemental Material), is given by

$$E_{\mathrm{JT}}^{(2)} = -2\frac{\Omega^2}{\omega}\left[\frac{\Gamma(\eta,0,-\eta)}{(-\eta e)^{\eta}}+\frac{\Gamma\left(\eta,0,-\frac{\eta}{4}\right)}{\left(-\frac{\eta e}{4}\right)^{\eta}}\right], \quad (12)$$

where $\Gamma(a,0,x) = \int_0^x t^{a-1}e^{-t}dt$ is the incomplete Gamma function and $\eta = 2\kappa^2/\omega^2$. It quantifies the curvature of the ground state energy for small Ω shown as the blue dotted line in Fig. 3c.

Born-Oppenheimer treatment — An instructive perspective on the structural properties of the triangular tweezer molecule is obtained by analyzing its lowest energy states within the Born-Oppenheimer approximation. To this end we neglect the kinetic energy of the atoms and write the Hamiltonian in terms of the normal modes q_m (see Supplemental Material), which are shown in Fig. 4a:

$$\begin{aligned}H_{\mathrm{BO}} &= \frac{\omega}{2}\sum_{m=1}^{6}\frac{q_m^2}{x_{\mathrm{ho}}^2}+\sqrt{2}\kappa(P_1+P_3+P_5)\frac{q_1}{x_{\mathrm{ho}}} \\ &-\frac{\kappa}{\sqrt{2}}(2P_1-P_3-P_5)\frac{q_2}{x_{\mathrm{ho}}}-\sqrt{\frac{3}{2}}\kappa(P_3-P_5)\frac{q_3}{x_{\mathrm{ho}}} \\ &+\Omega\sum_{k=1}^{6}\left(|k+1\rangle\langle k|+\mathrm{h.c.}\right). \quad (13)\end{aligned}$$

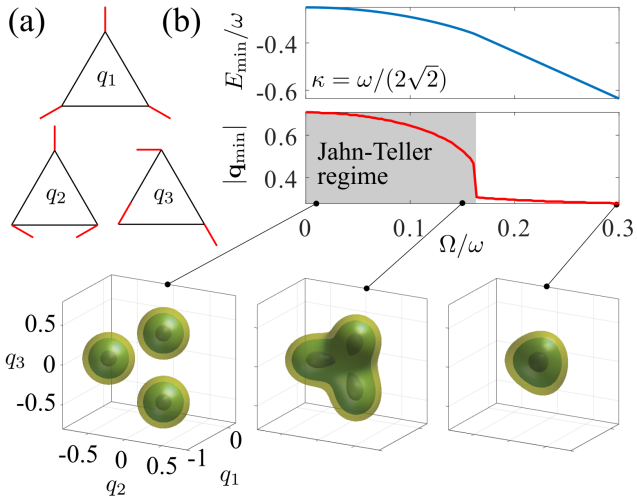

FIG. 4. **Born-Oppenheimer energy surfaces and structural transition.** (a) Sketch of the normal modes. The red lines indicate the distortion of the triangle associated with the q_m. (b) Minimum energy of the lowest Born-Oppenheimer surface $E_0(\mathbf{q})$ and position $|\mathbf{q}_{\mathrm{min}}|$ of the minimum. In the Jahn-Teller regime the minimum is three-fold degenerate as can be seen in the iso-energy surfaces. Lengths are given in units of the harmonic oscillator length $x_{\mathrm{ho}} = 1/\sqrt{m\omega}$. The axes labels are the same for all the panels in the bottom.

Calculation of the lowest eigenenergy of this Hamiltonian yields the ground state Born-Oppenheimer surface as a function of the normal coordinates $E_0(\mathbf{q})$. For sufficiently small values of Ω this surface has three degenerate minima, as can be seen in Fig. 4b. This is the Jahn-Teller regime [73–75], where the ground state of the full (quantum) problem is a superposition of three triangular configurations that have only one distorted side. When Ω increases the minima move towards each other until they collapse. From here onward the electronic and vibrational dynamics approximately factorise: the electronic state can by approximated by $|\mathrm{GS}_{\mathrm{elec}}\rangle$ and the external degrees of freedom arrange in way that leads to the minimization of the projected Hamiltonian $\langle\mathrm{GS}_{\mathrm{elec}}|H_{\mathrm{BO}}|\mathrm{GS}_{\mathrm{elec}}\rangle = \frac{\omega}{2}\sum_{m=1}^{6}q_m^2/x_{\mathrm{ho}}^2 + \frac{\kappa}{\sqrt{2}}q_1/x_{\mathrm{ho}} - 2\Omega$. Here only the mode q_1 gets displaced, while the other two modes remain at the origin, as shown in the rightmost panel of Fig. 4b. Since only $q_1 \neq 0$, the displaced atoms remain at the vertices of an equilateral triangle.

Experimental considerations — The molecular states can be prepared from the initial state $|\downarrow\downarrow\downarrow\rangle$ using an adiabatic ramp, which has been already demonstrated for substantially larger Rydberg atom arrays than discussed here [76–78]. In the Jahn-Teller regime the ground state (11) is a superposition of three states that minimize the energy. A measurement of the Rydberg density selects one of these states, corresponding to a configuration in which the atoms form a distorted trian-

gle. This distortion is given by $|\delta \boldsymbol{r}| = \frac{|V'(d)|}{m\omega^2}$, which is equal to the classical displacement of two interacting particles confined in a harmonic potential. To estimate the distortion, we consider ^{39}K atoms held in optical tweezers with trap frequency $\omega = 2\pi \times 70$ kHz at interatomic distance $d = 5\,\mu$m. With the van der Waals interaction between $60S$ Rydberg states one obtains $V'(d) = 6C_6/d^7 \simeq 6.76{\cdot}10^{-3}$ GHz μm^{-1} [79], which yields a Jahn-Teller distortion of $|\delta \boldsymbol{r}| \simeq 350$ nm. The position of Rydberg atoms and the transition into the Jahn-Teller regime with decreasing Ω can thus be detected by field ionization as the created ions can then be detected with high spatial resolution (~ 200 nm) as shown recently in Ref. [80], where the vibrational dynamics of Rydberg-ion molecules was probed. An alternative way to probe the Jahn-Teller distortion is through a reconstruction of the Wigner function, as recently demonstrated in the context of trapped neutral atoms in Ref. [81] with a direct approach and in Ref. [82] with time-of-flight imaging techniques. Note, that throughout we have assumed that we operate at zero temperature, which is currently still a challenge.

Summary and outlook — We studied the creation of molecular states formed in small Rydberg tweezer arrays. Their structure is dictated by the interplay between mechanical forces and coherent laser excitation, which gives rise to a crossover into a Jahn-Teller regime. Note, that throughout the paper, we have assumed that the atoms are trapped with a trap frequency that does not depend on their internal electronic state. We leave the analysis of this interesting scenario to future work. In the future it will also be interesting to investigate even more complex scenarios, such as conical intersections [83, 84]. This would enable the experimental probing of dynamical effects, such as the impact of geometric phases or non-adiabatic couplings among Born-Oppenheimer surfaces, in a molecular system on a micrometer length scale [48]. Moreover, as in the Jahn-Teller regime small external fields give rise to a measurable configuration change, tweezer molecules could potentially be utilized for sensing applications.

We are grateful for financing from the Baden-Württemberg Stiftung through Project No. BWST_ISF2019-23. We also acknowledge funding from the Deutsche Forschungsgemeinschaft (DFG, German Research Foundation) under Projects No. 428276754 and 435696605 as well as through the Research Unit FOR 5413/1, Grant No. 465199066. This project has also received funding from the European Union's Horizon Europe research and innovation program under Grant Agreement No. 101046968 (BRISQ). We thank C. Groß for discussions.

[1] M. Endres, H. Bernien, A. Keesling, H. Levine, E. R. Anschuetz, A. Krajenbrink, C. Senko, V. Vuletic, M. Greiner, and M. D. Lukin, Atom-by-atom assembly of defect-free one-dimensional cold atom arrays, Science **354**, 1024 (2016).

[2] D. Barredo, S. de Léséleuc, V. Lienhard, T. Lahaye, and A. Browaeys, An atom-by-atom assembler of defect-free arbitrary two-dimensional atomic arrays, Science **354**, 1021 (2016).

[3] D. Jaksch, J. I. Cirac, P. Zoller, S. L. Rolston, R. Côté, and M. D. Lukin, Fast Quantum Gates for Neutral Atoms, Phys. Rev. Lett. **85**, 2208 (2000).

[4] I. Bloch, J. Dalibard, and S. Nascimbène, Quantum simulations with ultracold quantum gases, Nat. Phys. **8**, 267 (2012).

[5] Y. Wang, A. Kumar, T.-Y. Wu, and D. S. Weiss, Single-qubit gates based on targeted phase shifts in a 3D neutral atom array, Science **352**, 1562 (2016).

[6] R. Han, H. K. Ng, and B.-G. Englert, Implementing a neutral-atom controlled-phase gate with a single Rydberg pulse, Europhys. Lett. **113**, 40001 (2016).

[7] S.-L. Su, E. Liang, S. Zhang, J.-J. Wen, L.-L. Sun, Z. Jin, and A.-D. Zhu, One-step implementation of the Rydberg-Rydberg-interaction gate, Phys. Rev. A **93**, 012306 (2016).

[8] C. Gross and I. Bloch, Quantum simulations with ultracold atoms in optical lattices, Science **357**, 995 (2017).

[9] D. Petrosyan, F. Motzoi, M. Saffman, and K. Mølmer, High-fidelity Rydberg quantum gate via a two-atom dark state, Phys. Rev. A **96**, 042306 (2017).

[10] X.-F. Shi and T. A. B. Kennedy, Annulled van der Waals interaction and fast Rydberg quantum gates, Phys. Rev. A **95**, 043429 (2017).

[11] A. Kumar, T.-Y. Wu, F. Giraldo, and D. S. Weiss, Sorting ultracold atoms in a three-dimensional optical lattice in a realization of Maxwell's demon, Nature **561**, 83 (2018).

[12] A. M. Kaufman and K.-K. Ni, Quantum science with optical tweezer arrays of ultracold atoms and molecules, Nat. Phys. **17**, 1324 (2021).

[13] S. R. Cohen and J. D. Thompson, Quantum Computing with Circular Rydberg Atoms, PRX Quantum **2**, 030322 (2021).

[14] S. Jandura and G. Pupillo, Time-Optimal Two- and Three-Qubit Gates for Rydberg Atoms, Quantum **6**, 712 (2022).

[15] T. M. Graham, Y. Song, J. Scott, C. Poole, L. Phuttitarn, K. Jooya, P. Eichler, X. Jiang, A. Marra, B. Grinkemeyer, M. Kwon, M. Ebert, J. Cherek, M. T. Lichtman, M. Gillette, J. Gilbert, D. Bowman, T. Ballance, C. Campbell, E. D. Dahl, O. Crawford, N. S. Blunt, B. Rogers, T. Noel, and M. Saffman, Multi-qubit entanglement and algorithms on a neutral-atom quantum computer, Nature **604**, 457 (2022).

[16] A. Pagano, S. Weber, D. Jaschke, T. Pfau, F. Meinert, S. Montangero, and H. P. Büchler, Error budgeting for a controlled-phase gate with strontium-88 Rydberg atoms, Phys. Rev. Res. **4**, 033019 (2022).

[17] M. Saffman, T. G. Walker, and K. Molmer, Quantum information with Rydberg atoms, Rev. Mod. Phys. **82**, 2313 (2010).

[18] C. S. Adams, J. D. Pritchard, and J. P. Shaffer, Rydberg atom quantum technologies, J. Phys. B: At. Mol. Opt. Phys. **53**, 012002 (2019).

[19] I. I. Beterov, D. B. Tretyakov, V. M. Entin, E. A. Yakshina, I. I. Ryabtsev, M. Saffman, and S. Bergamini, Application of adiabatic passage in Rydberg atomic ensembles for quantum information processing, J. Phys. B: At. Mol. Opt. Phys. **53**, 182001 (2020).

[20] X. Wu, X. Liang, Y. Tian, F. Yang, C. Chen, Y.-C. Liu, M. K. Tey, and L. You, A concise review of Rydberg atom based quantum computation and quantum simulation, Chin. Phys. B **30**, 020305 (2021).

[21] K. Singer, J. Stanojevic, M. Weidemüller, and R. Côté, Long-range interactions between alkali Rydberg atom pairs correlated to the ns–ns, np–np and nd–nd asymptotes, J. Phys. B: At. Mol. Opt. Phys. **38**, S295 (2005).

[22] T. Pohl, H. Sadeghpour, and P. Schmelcher, Cold and ultracold Rydberg atoms in strong magnetic fields, Phys. Rep. **484**, 181 (2009).

[23] Y.-Y. Jau, A. M. Hankin, T. Keating, I. H. Deutsch, and G. W. Biedermann, Entangling atomic spins with a Rydberg-dressed spin-flip blockade, Nat. Phys. **12**, 71 (2016).

[24] H. Labuhn, D. Barredo, S. Ravets, S. de Léséleuc, T. Macrì, T. Lahaye, and A. Browaeys, Tunable two-dimensional arrays of single Rydberg atoms for realizing quantum Ising models, Nature **534**, 667 (2016).

[25] F. Letscher, O. Thomas, T. Niederprüm, M. Fleischhauer, and H. Ott, Bistability Versus Metastability in Driven Dissipative Rydberg Gases, Phys. Rev. X **7**, 021020 (2017).

[26] O. Thomas, C. Lippe, T. Eichert, and H. Ott, Experimental realization of a Rydberg optical Feshbach resonance in a quantum many-body system, Nat. Comm. **9**, 2238 (2018).

[27] D. Ohl de Mello, D. Schäffner, J. Werkmann, T. Preuschoff, L. Kohfahl, M. Schlosser, and G. Birkl, Defect-Free Assembly of 2D Clusters of More Than 100 Single-Atom Quantum Systems, Phys. Rev. Lett. **122**, 203601 (2019).

[28] H. Kim, M. Kim, W. Lee, and J. Ahn, Gerchberg-Saxton algorithm for fast and efficient atom rearrangement in optical tweezer traps, Opt. Express **27**, 2184 (2019).

[29] L.-M. Steinert, P. Osterholz, R. Eberhard, L. Festa, N. Lorenz, Z. Chen, A. Trautmann, and C. Gross, Spatially tunable spin interactions in neutral atom arrays, arXiv:2206.12385 (2022).

[30] V. Lienhard, S. de Léséleuc, D. Barredo, T. Lahaye, A. Browaeys, M. Schuler, L.-P. Henry, and A. M. Läuchli, Observing the Space- and Time-Dependent Growth of Correlations in Dynamically Tuned Synthetic Ising Models with Antiferromagnetic Interactions, Phys. Rev. X **8**, 021070 (2018).

[31] D. Bluvstein, H. Levine, G. Semeghini, T. T. Wang, S. Ebadi, M. Kalinowski, A. Keesling, N. Maskara, H. Pichler, M. Greiner, V. Vuletić, and M. D. Lukin, A quantum processor based on coherent transport of entangled atom arrays, Nature **604**, 451 (2022).

[32] A. Keesling, A. Omran, H. Levine, H. Bernien, H. Pichler, S. Choi, R. Samajdar, S. Schwartz, P. Silvi, S. Sachdev, P. Zoller, M. Endres, M. Greiner, V. Vuletić, and M. D. Lukin, Quantum Kibble–Zurek mechanism and critical dynamics on a programmable Rydberg simulator, Nature **568**, 207 (2019).

[33] R. Samajdar, W. W. Ho, H. Pichler, M. D. Lukin, and S. Sachdev, Quantum phases of Rydberg atoms on a kagome lattice, Proc. Natl. Acad. Sci. U.S.A. **118** (2021).

[34] D. Bluvstein, A. Omran, H. Levine, A. Keesling, G. Semeghini, S. Ebadi, T. T. Wang, A. A. Michailidis, N. Maskara, W. W. Ho, S. Choi, M. Serbyn, M. Greiner, V. Vuletić, and M. D. Lukin, Controlling quantum many-body dynamics in driven Rydberg atom arrays, Science **371**, 1355 (2021).

[35] C. Ates, A. Eisfeld, and J. M. Rost, Motion of Rydberg atoms induced by resonant dipole–dipole interactions, New J. Phys. **10**, 045030 (2008).

[36] S. Wüster, C. Ates, A. Eisfeld, and J. M. Rost, Newton's Cradle and Entanglement Transport in a Flexible Rydberg Chain, Phys. Rev. Lett. **105**, 053004 (2010).

[37] M. Roghani, H. Helm, and H.-P. Breuer, Entanglement Dynamics of a Strongly Driven Trapped Atom, Phys. Rev. Lett. **106**, 040502 (2011).

[38] T. Keating, R. L. Cook, A. M. Hankin, Y.-Y. Jau, G. W. Biedermann, and I. H. Deutsch, Robust quantum logic in neutral atoms via adiabatic Rydberg dressing, Phys. Rev. A **91**, 012337 (2015).

[39] F. Robicheaux, T. M. Graham, and M. Saffman, Photon-recoil and laser-focusing limits to Rydberg gate fidelity, Phys. Rev. A **103**, 022424 (2021).

[40] Y. Chew, T. Tomita, T. P. Mahesh, S. Sugawa, S. de Léséleuc, and K. Ohmori, Ultrafast energy exchange between two single Rydberg atoms on a nanosecond timescale, Nat. Photonics **16**, 724 (2022).

[41] R. Faoro, C. Simonelli, M. Archimi, G. Masella, M. M. Valado, E. Arimondo, R. Mannella, D. Ciampini, and O. Morsch, van der Waals explosion of cold Rydberg clusters, Phys. Rev. A **93**, 030701 (2016).

[42] F. M. Gambetta, W. Li, F. Schmidt-Kaler, and I. Lesanovsky, Engineering NonBinary Rydberg Interactions via Phonons in an Optical Lattice, Phys. Rev. Lett. **124**, 043402 (2020).

[43] R. Belyansky, J. T. Young, P. Bienias, Z. Eldredge, A. M. Kaufman, P. Zoller, and A. V. Gorshkov, Nondestructive Cooling of an Atomic Quantum Register via State-Insensitive Rydberg Interactions, Phys. Rev. Lett. **123**, 213603 (2019).

[44] M. Płodzień, T. Sowiński, and S. Kokkelmans, Simulating polaron biophysics with Rydberg atoms, Sci. Rep. **8**, 9247 (2018).

[45] P. P. Mazza, R. Schmidt, and I. Lesanovsky, Vibrational Dressing in Kinetically Constrained Rydberg Spin Systems, Phys. Rev. Lett. **125**, 033602 (2020).

[46] M. Magoni, P. P. Mazza, and I. Lesanovsky, Phonon dressing of a facilitated one-dimensional Rydberg lattice gas, SciPost Phys. Core **5**, 041 (2022).

[47] J. P. Shaffer, S. T. Rittenhouse, and H. R. Sadeghpour, Ultracold Rydberg molecules, Nat. Commun. **9**, 1965 (2018).

[48] F. M. Gambetta, C. Zhang, M. Hennrich, I. Lesanovsky, and W. Li, Exploring the Many-Body Dynamics Near a Conical Intersection with Trapped Rydberg Ions, Phys. Rev. Lett. **126**, 233404 (2021).

[49] C. H. Greene, A. S. Dickinson, and H. R. Sadeghpour, Creation of Polar and Nonpolar Ultra-Long-Range Rydberg Molecules, Phys. Rev. Lett. **85**, 2458 (2000).

[50] V. Bendkowsky, B. Butscher, J. Nipper, J. P. Shaffer, R. Löw, and T. Pfau, Observation of ultralong-range Rydberg molecules, Nature **458**, 1005 (2009).

[51] C. Boisseau, I. Simbotin, and R. Côté, Macrodimers: Ultralong Range Rydberg Molecules, Phys. Rev. Lett. **88**, 133004 (2002).

[52] K. R. Overstreet, A. Schwettmann, J. Tallant, D. Booth, and J. P. Shaffer, Observation of electric-field-induced Cs Rydberg atom macrodimers, Nat. Phys. **5**, 581 (2009).

[53] M. Kiffner, H. Park, W. Li, and T. F. Gallagher, Dipole-dipole-coupled double-Rydberg molecules, Phys. Rev. A **86**, 031401 (2012).

[54] H. Saßmannshausen and J. Deiglmayr, Observation of Rydberg-Atom Macrodimers: Micrometer-Sized Diatomic Molecules, Phys. Rev. Lett. **117**, 083401 (2016).

[55] S. Hollerith, J. Zeiher, J. Rui, A. Rubio-Abadal, V. Walther, T. Pohl, D. M. Stamper-Kurn, I. Bloch, and C. Gross, Quantum gas microscopy of Rydberg macrodimers, Science **364**, 664 (2019).

[56] H. Schempp, G. Günter, M. Robert-de Saint-Vincent, C. S. Hofmann, D. Breyel, A. Komnik, D. W. Schönleber, M. Gärttner, J. Evers, S. Whitlock, and M. Weidemüller, Full Counting Statistics of Laser Excited Rydberg Aggregates in a One-Dimensional Geometry, Phys. Rev. Lett. **112**, 013002 (2014).

[57] M. M. Aliyu, A. Ulugöl, G. Abumwis, and S. Wüster, Transport on flexible Rydberg aggregates using circular states, Phys. Rev. A **98**, 043602 (2018).

[58] S. Wüster and J.-M. Rost, Rydberg aggregates, J. Phys. B **51**, 032001 (2018).

[59] F. Fröwis, P. Sekatski, W. Dür, N. Gisin, and N. Sangouard, Macroscopic quantum states: Measures, fragility, and implementations, Rev. Mod. Phys. **90**, 025004 (2018).

[60] T. Weiss, M. Roda-Llordes, E. Torrontegui, M. Aspelmeyer, and O. Romero-Isart, Large Quantum Delocalization of a Levitated Nanoparticle Using Optimal Control: Applications for Force Sensing and Entangling via Weak Forces, Phys. Rev. Lett. **127**, 023601 (2021).

[61] S. Zhang, F. Robicheaux, and M. Saffman, Magic-wavelength optical traps for Rydberg atoms, Phys. Rev. A **84**, 043408 (2011).

[62] J. Lampen, H. Nguyen, L. Li, P. R. Berman, and A. Kuzmich, Long-lived coherence between ground and Rydberg levels in a magic-wavelength lattice, Phys. Rev. A **98**, 033411 (2018).

[63] D. Barredo, V. Lienhard, P. Scholl, S. de Léséleuc, T. Boulier, A. Browaeys, and T. Lahaye, Three-Dimensional Trapping of Individual Rydberg Atoms in Ponderomotive Bottle Beam Traps, Phys. Rev. Lett. **124**, 023201 (2020).

[64] I. S. Madjarov, J. P. Covey, A. L. Shaw, J. Choi, A. Kale, A. Cooper, H. Pichler, V. Schkolnik, J. R. Williams, and M. Endres, High-fidelity entanglement and detection of alkaline-earth Rydberg atoms, Nat. Phys. **16**, 857 (2020).

[65] J. T. Wilson, S. Saskin, Y. Meng, S. Ma, R. Dilip, A. P. Burgers, and J. D. Thompson, Trapping Alkaline Earth Rydberg Atoms Optical Tweezer Arrays, Phys. Rev. Lett. **128**, 033201 (2022).

[66] C. Ates, T. Pohl, T. Pattard, and J. M. Rost, Antiblockade in Rydberg Excitation of an Ultracold Lattice Gas, Phys. Rev. Lett. **98**, 023002 (2007).

[67] T. Amthor, C. Giese, C. S. Hofmann, and M. Weidemüller, Evidence of Antiblockade in an Ultracold Rydberg Gas, Phys. Rev. Lett. **104**, 013001 (2010).

[68] S.-L. Su, Y. Gao, E. Liang, and S. Zhang, Fast Rydberg antiblockade regime and its applications in quantum logic gates, Phys. Rev. A **95**, 022319 (2017).

[69] M. Marcuzzi, J. Minar, D. Barredo, S. de Léséleuc, H. Labuhn, T. Lahaye, A. Browaeys, E. Levi, and I. Lesanovsky, Facilitation Dynamics and Localization Phenomena in Rydberg Lattice Gases with Position Disorder, Phys. Rev. Lett. **118**, 063606 (2017).

[70] M. Magoni, P. P. Mazza, and I. Lesanovsky, Emergent Bloch Oscillations in a Kinetically Constrained Rydberg Spin Lattice, Phys. Rev. Lett. **126**, 103002 (2021).

[71] H. A. Jahn and E. Teller, Stability of Polyatomic Molecules in Degenerate Electronic States. I. Orbital Degeneracy, Proc. Roy. Soc. A **161**, 220 (1937).

[72] H. A. Jahn, Stability of Polyatomic Molecules in Degenerate Electronic States. II. Spin Degeneracy, Proc. Roy. Soc. A **164**, 117 (1938).

[73] V. Kokoouline and C. H. Greene, Unified theoretical treatment of dissociative recombination of D_{3h} triatomic ions: Application to H_3^+ and D_3^+, Phys. Rev. A **68**, 012703 (2003).

[74] I. Honda and K. Terao, Exchange and Spin Jahn–Teller Distortions for Triangular Cluster of Spin-1/2, J. Phys. Soc. Jpn. **75**, 044704 (2006).

[75] D. Porras, P. A. Ivanov, and F. Schmidt-Kaler, Quantum Simulation of the Cooperative Jahn-Teller Transition in 1D Ion Crystals, Phys. Rev. Lett. **108**, 235701 (2012).

[76] P. Schauß, J. Zeiher, T. Fukuhara, S. Hild, M. Cheneau, T. Macrì, T. Pohl, I. Bloch, and C. Gross, Crystallization in Ising quantum magnets, Science **347**, 1455 (2015).

[77] S. Ebadi, T. T. Wang, H. Levine, A. Keesling, G. Semeghini, A. Omran, D. Bluvstein, R. Samajdar, H. Pichler, W. W. Ho, S. Choi, S. Sachdev, M. Greiner, V. Vuletić, and M. D. Lukin, Quantum phases of matter on a 256-atom programmable quantum simulator, Nature **595**, 227 (2021).

[78] P. Scholl, M. Schuler, H. J. Williams, A. A. Eberharter, D. Barredo, K.-N. Schymik, V. Lienhard, L.-P. Henry, T. C. Lang, T. Lahaye, A. M. Läuchli, and A. Browaeys, Quantum simulation of 2D antiferromagnets with hundreds of Rydberg atoms, Nature **595**, 233 (2021).

[79] N. Šibalić, J. Pritchard, C. Adams, and K. Weatherill, ARC: An open-source library for calculating properties of alkali Rydberg atoms, Comput. Phys. Commun. **220**, 319 (2017).

[80] Y.-Q. Zou, M. Berngruber, V. S. V. Anasuri, N. Zuber, F. Meinert, R. Löw, and T. Pfau, Observation of Vibrational Dynamics of Orientated Rydberg-Atom-Ion Molecules, Phys. Rev. Lett. **130**, 023002 (2023).

[81] F.-R. Winkelmann, C. A. Weidner, G. Ramola, W. Alt, D. Meschede, and A. Alberti, Direct measurement of the Wigner function of atoms in an optical trap, J. Phys. B: At. Mol. Opt. Phys. **55**, 194004 (2022).

[82] M. O. Brown, S. R. Muleady, W. J. Dworschack, R. J. Lewis-Swan, A. M. Rey, O. Romero-Isart, and C. A. Regal, Time-of-flight quantum tomography of an atom in an optical tweezer, Nat. Phys. **19**, 569 (2023).

[83] S. Wüster, A. Eisfeld, and J. M. Rost, Conical Intersections in an Ultracold Gas, Phys. Rev. Lett. **106**, 153002 (2011).

[84] F. Hummel, M. T. Eiles, and P. Schmelcher, Synthetic Dimension-Induced Conical Intersections in Rydberg Molecules, Phys. Rev. Lett. **127**, 023003 (2021).

Fourth Publication

Letter

Designing nonequilibrium states of quantum matter through stochastic resetting

Gabriele Perfetto,[1] Federico Carollo,[1] Matteo Magoni,[1] and Igor Lesanovsky[1,2]

[1]*Institut für Theoretische Physik, Eberhard Karls Universität Tübingen, Auf der Morgenstelle 14, 72076 Tübingen, Germany*

[2]*School of Physics and Astronomy and Centre for the Mathematics and Theoretical Physics of Quantum Non-Equilibrium Systems, The University of Nottingham, Nottingham NG7 2RD, United Kingdom*

(Received 14 July 2021; revised 29 September 2021; accepted 18 October 2021; published 2 November 2021)

We consider closed quantum many-body systems subject to stochastic resetting. This means that their unitary time evolution is interrupted by resets at randomly selected times. When a reset takes place, the system is reinitialized to a state chosen from a set of reset states conditionally on the outcome of a measurement taken immediately before resetting. We construct analytically the resulting nonequilibrium stationary state, thereby establishing an explicit connection between quantum quenches in closed systems and the emergent open system dynamics induced by stochastic resetting. We discuss as an application the paradigmatic transverse-field quantum Ising chain. We show that signatures of its ground-state quantum phase transition are visible in the steady state of the reset dynamics as a sharp crossover. Our findings show that a controlled stochastic resetting dynamics allows one to design nonequilibrium stationary states of quantum many-body systems, where uncontrolled dissipation and heating can be prevented. These states can thus be created on demand and exploited, e.g., as a resource for quantum enhanced sensing on quantum simulator platforms.

DOI: 10.1103/PhysRevB.104.L180302

Introduction. Deterministic or stochastic dynamics interspersed with stochastic resetting leads to the emergence of a nonequilibrium steady state (NESS). This concept has been put forward in the classical realm in Refs. [1–5], where it has been established that a particle undergoing Brownian motion reaches a NESS when its diffusive time evolution is *reset* at constant rate γ (Poissonian reset) to its initial position. Using the renewal equation approach [1,2,6–13], it has been further shown that stochastic resetting can improve the efficiency of search processes in terms of their mean first passage time [1,2,14–24]. In contrast to the case of classical systems, much less is known about the effect of stochastic resetting on quantum systems, either closed or open. In the latter case, the Markovian Lindblad equation [25,26] describing the evolution in the presence of Poissonian resetting has been analyzed in Refs. [27–32]. Closed quantum systems which are reinitialized to their initial state after Poissonian resetting have been, instead, analyzed without reference to the Lindblad equation in Ref. [33]. Using the renewal equation approach, it was shown in the latter work that the reached NESS differs from the diagonal ensemble for any finite, nonzero value of γ. For $\gamma \to \infty$, instead, one recovers the quantum Zeno effect [34,35], where the system does not evolve in time due to frequent reset projections. Resetting in closed quantum systems has also been studied in Refs. [36–41] for first detection problems. These recent works suggest that there is a direct link between the dynamics of closed quantum systems subject to stochastic resetting and an effective open system dynamics. However, the precise nature of this relation, and of possible connections between the NESS emerging from the resetting, unitary dynamics, and nonequilibrium signatures of quantum phase transitions [42–44], is not fully understood.

In this work, we establish such a connection by developing a general theory based on semi-Markov processes [30,45]. We prove analytically that by averaging the microscopic unitary time evolution over the reset distribution, an effective non-Markovian open dynamics, governed by a generalized Lindblad equation, emerges. The ensuing NESS can be constructed analytically and its structure establishes a transparent connection to quantum quenches in closed systems, which can display signatures of equilibrium quantum phase transitions [46–53]. Our results for the NESS recover the quantum Zeno effect in the limit of infinite resetting rate. We illustrate our ideas using, as an example, the quantum Ising chain in a transverse field (TFIC). The ground-state quantum phase transition of the model is signaled in the NESS by a crossover, whose sharpness is controlled by the distribution of the reset time. Our analysis establishes stochastic resetting as a tool to generate complex stationary many-body quantum states without detrimental processes, such as heating, that typically occur when coherent dynamics is competing with dissipative processes.

Reset protocol. The results we are going to develop in the following hold for a general many-body quantum system made of N particles or spin degrees of freedom, but for concreteness we will base our discussion mostly on the paradigmatic TFIC with Hamiltonian

$$H = -J \sum_{n=1}^{N} \left(\sigma_n^x \sigma_{n+1}^x + h \sigma_n^z \right). \tag{1}$$

Here, $\sigma_n^{x,y,z}$ are the Pauli matrices acting on site n, $J > 0$ is the ferromagnetic coupling constant, and h is the strength of a transverse magnetic field. This model exhibits a quantum

 ©2021 American Physical Society

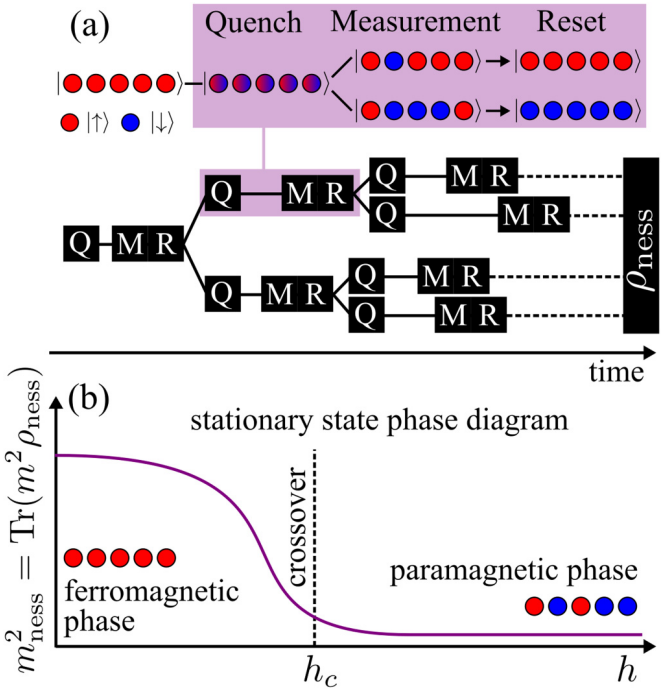

FIG. 1. Conditional reset protocol. (a) The time evolution is obtained upon alternating the quench-unitary dynamics, schematized by the "Q" boxes, and measurement-reset events, schematized by the "M-R" boxes, which happen at randomly selected times from a waiting time distribution. The average over all the ensuing "reset trajectories" generates the NESS density matrix $\rho_{\rm ness}$. In the inset (purple rectangle), the time evolution ensuing in a single quench dynamics and reset is shown. Conditioned on the measured value of the magnetization being positive or negative, the system is reinitialized either in a reset state completely polarized upwards ($|1\rangle = |\uparrow\uparrow \ldots \uparrow\rangle$) or downwards ($|2\rangle = |\downarrow\downarrow \ldots \downarrow\rangle$), respectively. (b) Sketch of the squared magnetization density $m^2_{\rm ness}$ in the NESS as a function of the transverse field h [see Eqs. (1) and (9)]. It displays remnants of the equilibrium quantum phase transition at $h_c = 1$ through a sharp crossover between a ferromagnetic and a paramagnetic stationary phase.

phase transition in its ground state at the critical field strength $h = h_c = 1$, which can be characterized by using the magnetization density $m = \sum_{n=1}^{N} \sigma_n^x/N$ as the order parameter.

We envisage a "conditional reset" protocol, which is sketched in Fig. 1(a): Starting from a given initial state (in the figure, the state $|\psi_0\rangle = |\uparrow\uparrow \ldots \uparrow\rangle$ [54]), the system is evolved unitarily under its many-body Hamiltonian H, e.g., Eq. (1) for the TFIC. After a randomly selected time, an observable is measured; in the figure, we measure the magnetization, and the many-body state is *reset* to a state chosen within a set of "reset states" *conditionally* on the outcome of the measurement. In our example, the reset states are $|1\rangle = |\uparrow\uparrow \ldots \uparrow\rangle$ and $|2\rangle = |\downarrow\downarrow \ldots \downarrow\rangle$ [with $|\uparrow\rangle$ and $|\downarrow\rangle$ referring to the longitudinal-x direction in Eq. (1)]. Our motivation to investigate the two aforementioned reset states is twofold: first, they are simple product states easy to prepare experimentally; second, they allow one to establish a connection between the NESS of the reset dynamics and quantum quenches in the Ising chain. The two reset states can be indeed identified with the two degenerate ground states $|{\rm GS}(h=0)\rangle_\pm$ of H in Eq. (1) for $h = 0$, namely, $|1\rangle = |{\rm GS}(h=0)\rangle_+$ and $|2\rangle = |{\rm GS}(h=0)\rangle_-$. The unitary dynamics from the reset state $|j\rangle$ ($j = 1, 2$), $|\psi_j(\tau)\rangle = \exp(-iH\tau)\,|j\rangle$ (setting $\hbar = 1$) between consecutive resets stems therefore from a quench of the transverse field from the prequench $h_0 = 0$ to the postquench value h [46–53,55–63]. The experimental motivation behind the conditional reset protocol comes from recent results on Rydberg quantum simulators [64], which allow one to experimentally implement Ising models with transverse and longitudinal fields [65–72] and permit, at the same time, the spatially resolved detection of the spin state upon which the reset is conditioned. Such measurement has been indeed implemented in Rydberg atom experiments on quantum quenches of the Ising model [73–76].

After the reset, the system evolves again under the quench dynamics up to the time at which the next measurement is performed. The time between consecutive measurements is drawn from a *waiting time probability density*, $p(\tau)$, which is normalized as $\int_0^\infty d\tau\, p(\tau) = 1$. Repeating this procedure leads at long times to a NESS, which in the case of the TFIC exhibits a sharp crossover between two stationary phases, as sketched in Fig. 1(b). Resetting can thus be interpreted as a dissipative process which leads to an effective open-system evolution.

The reset protocol also allows one to suppress naturally occurring dissipative processes, e.g., spontaneous photon emission or scattering in cold-atom experiments. This is achieved by choosing the probability $p(\tau)$ such that the reset must occur before a finite *maximum reset time* $t_{\rm max}$, which is shorter than the dissipation timescale. This may allow one to reduce decoherence and heating and thus enable one to tailor states of matter with robustness and long-term stability. In the following, we will develop the theory for deriving the form of this NESS and we discuss specifically the case of the TFIC. Note, however, that although the present discussion is based on two reset states, our derivations can be generalized to the case of an arbitrary number of reset states (see Supplemental Material [77]).

Nonequilibrium stationary state. When a reset takes place, the system is reinitialized in the reset state $|k\rangle$ ($k = 1, 2$) dependently on the sign of the measured magnetization; see Fig. 1(a). Which reset state is chosen depends only on the time τ elapsed since the previous reset event and on its outcome $|j\rangle$ ($j = 1, 2$), but, fundamentally, not on the previous history of the dynamics. The conditional reset dynamics can be therefore understood as a semi-Markov process [30,45], which is characterized by the transition probabilities $P_{jk}(\tau)$ [obeying $\sum_k P_{jk}(\tau) = 1$] from the previous reset state $|j\rangle$ to the following reset state $|k\rangle$, given that a time τ has elapsed between the two resets. The formalism of semi-Markov processes has been applied in Ref. [30] to Markovian open quantum systems. Here we consider, instead, the case of an underlying unitary time evolution and, for the conditional reset dynamics sketched in Fig. 1, we write

$$P_{jk}(\tau) = \langle \psi_j(\tau)\,|\,\mathcal{P}_k\,|\,\psi_j(\tau)\rangle, \tag{2}$$

where $\mathcal{P}_k$ denotes the projector onto the set of states of the Hilbert space with positive ($k = 1$) or negative ($k = 2$) magnetization [78].

To describe the time evolution of the density matrix $\rho(t)$, we exploit the fact that the resetting protocol induces a *renewal structure*, in the sense that the dynamics after a certain reset does not depend on what happened before that reset. This observation allows one to derive "renewal equations" which express the dynamics of the state $\rho(t)$ in the presence of resets, in terms of the state $\rho_{\text{free},j}(t) = |\psi_j(t)\rangle\langle\psi_j(t)|$ which evolves under a dynamics where resets are absent. We stress that in our analysis, the resetting is coupled to the underlying unitary dynamics via Eq. (2). This makes the conditional reset dynamics fundamentally different with respect to resets to a single state, first analyzed in Ref. [33] for closed quantum systems, where the reset is independent from the underlying dynamics, which significantly simplifies the analysis.

We consider the observation time t to be fixed and calculate the average density matrix $\rho_n(t)$ over all the "reset trajectories" that have exactly $n \geqslant 0$ resets within the interval $[0, t]$. The density matrix is then given by accounting for all the reset trajectories with an arbitrary number of resets $\rho(t) = \sum_{n=0}^{\infty} \rho_n(t)$, as shown pictorially in Fig. 1(a). The previous expression can be resummed by taking the Laplace transform $\widehat{\rho}(s)$ of $\rho(t)$. The average density matrix $\widehat{\rho}_n(s)$ is, indeed, obtained starting from the initial state, similarly as in Markov chains, by considering n reset transitions $\widehat{R}^n(s)$, with the transition matrix $\widehat{R}_{jk}(s)$:

$$\widehat{R}_{jk}(s) = \int_0^{\infty} d\tau\, P_{jk}(\tau) p(\tau) e^{-s\tau}. \tag{3}$$

In the previous equation, $R_{jk}(\tau) = P_{jk}(\tau)p(\tau)$ is the probability density that the system is reinitialized in the reset state $|k\rangle$ in the time interval $(\tau, \tau + d\tau)$ since the previous reset to the reset state $|j\rangle$. Note that $\widehat{R}_{jk}(s = 0)$ is a Markov matrix since $\sum_k \widehat{R}_{jk}(s = 0) = 1$. The resulting expression for $\widehat{\rho}(s)$ is (see Supplemental Material [77])

$$\widehat{\rho}(s) = \widehat{\rho}_{01}(s) + \widehat{\rho}_{01}(s)\widehat{r}_{11}(s) + \widehat{\rho}_{02}(s)\widehat{r}_{12}(s), \tag{4}$$

with

$$\widehat{\rho}_{01}(s) = \int_0^{\infty} d\tau\, q(\tau)\rho_{\text{free},1}(\tau)e^{-s\tau}, \tag{5}$$

and analogously for $\widehat{\rho}_{02}(s)$ in terms of $\rho_{\text{free},2}(t)$. In Eq. (5), we have introduced the *survival probability* $q(\tau) = \int_{\tau}^{\infty} d\tau'\, p(\tau')$, which is the probability that no reset happens before time τ.

The case of Poissonian resetting with constant rate γ corresponds to $p(\tau) = p_\gamma(\tau) = \gamma \exp(-\gamma\tau)$ and $q(\tau) = q_\gamma(\tau) = \exp(-\gamma\tau)$. The derivations in this Letter apply, however, to arbitrary distributions $p(\tau)$.

The first term in Eq. (4), involving $\widehat{\rho}_{01}(s)$, accounts for trajectories where no reset takes place and it is therefore given by the unitary time evolution from the initial state $|\psi_0\rangle = |1\rangle$ over the interval $[0, t]$. The coefficients $r_{11}(t) \geqslant 0$ and $r_{12}(t) \geqslant 0$, which are obtained from the inverse Laplace transform of $\widehat{r}_{11}(s) = \sum_{n=1}^{\infty}[\widehat{R}^n(s)]_{11}$ and $\widehat{r}_{12}(s) = \sum_{n=1}^{\infty}[\widehat{R}^n(s)]_{12}$ in Eq. (4), can be interpreted as two *effective time-dependent* rates of jumping into the reset states $|1\rangle$ and $|2\rangle$, respectively. Crucially, $r_{11}(t)$ and $r_{12}(t)$ are determined both by the resetting distribution $p(\tau)$ and by the Hamiltonian dynamics, which are coupled due to the conditional protocol. The calculation of the NESS density matrix ρ_{ness} can then be directly performed from Eq. (4) as $\rho_{\text{ness}} = \lim_{t\to\infty} \rho(t) = \lim_{s\to 0} s\,\widehat{\rho}(s)$, which gives

$$\rho_{\text{ness}} = \frac{\widehat{R}_{21}(0)}{\widehat{R}_{21}(0) + \widehat{R}_{12}(0)} \frac{1}{\widehat{q}(0)} \int_0^{\infty} d\tau\, \rho_{\text{free},1}(\tau) q(\tau) + \frac{\widehat{R}_{12}(0)}{\widehat{R}_{21}(0) + \widehat{R}_{12}(0)} \frac{1}{\widehat{q}(0)} \int_0^{\infty} d\tau\, \rho_{\text{free},2}(\tau) q(\tau). \tag{6}$$

This equation is the first main result of this work. It expresses ρ_{ness} as a statistical mixture of the unitary (reset-free) time evolution ensuing from the reset states $|1\rangle$ and $|2\rangle$. Fundamentally, both the weights of the terms in the sum couple the Hamiltonian dynamics with the reset via Eqs. (2) and (3). One can further check (see Supplemental Material [77]), as noted also in Ref. [33] for resets to a single state, that ρ_{ness} has nonvanishing off-diagonal matrix elements in the basis of the eigenstates of the Hamiltonian H. This shows that ρ_{ness} is a genuinely nonequilibrium density matrix since it is different from the diagonal ensemble, which describes the relaxation at long times of closed quantum systems [33,79].

A complementary way to the renewal equation approach is to construct an evolution equation for $\rho(t)$, which for classical systems has been done in Ref. [5]. This perspective is useful as it sheds light on the effective open-system dynamics which emerges upon superimposing resetting to the unitary time evolution of the system. For our conditional reset protocol, we find (see Supplemental Material [77]), from Eq. (4), the *generalized Lindblad equation*,

$$\frac{d\rho(t)}{dt} = \mathcal{L}[\rho(t)] + r_{11}(t)\,|1\rangle\langle 1| + r_{12}(t)\,|2\rangle\langle 2| - \int_0^t dt' r(t-t') e^{(t-t')\mathcal{L}} \rho(t'), \tag{7}$$

with the time-dependent rates $r_{1k}(t)$, with $k = 1, 2$, written in terms of the density matrix (see Supplemental Material [77]) as

$$r_{1k}(t) = \int_0^t dt' r(t-t') \text{Tr}[\mathcal{P}_k e^{(t-t')\mathcal{L}} \rho(t')]. \tag{8}$$

In Eq. (7), $\mathcal{L}[\rho] = -i[H, \rho]$ is the generator of the unitary time evolution and $r(t)$ satisfies $r_{11}(t) + r_{12}(t) = \int_0^t dt' r(t')$, which ensures a trace-preserving dynamics.

Equations (7) and (8) are our second main result. They show that stochastic resetting is generating an engineered dissipative process which leads to an emergent open dynamics for the system without an actual environment being present. The dynamics in Eqs. (7) and (8) is, in general, non-Markovian because of the presence of the integral over the complete time history of the process. This is a consequence, as in the classical case of Ref. [5], of the fact that for non-Poissonian distributions $p(\tau)$, one has to keep track of the time elapsed since the last reset. Only in the Poissonian case, $p_\gamma(\tau)$, resetting occurs at constant rate γ, independently of the time elapsed since the last reset. In this case, one verifies that $r(t) = \gamma\delta(t)$ in Eq. (7), which gives back a Markovian-Lindblad dynamics [27–29,31,32,77].

The quantum Ising chain in a transverse field. We particularize, in this section, our theory to the TFIC introduced above [see Eq. (1)]. Periodic boundary conditions will be henceforth assumed. The quantum critical point at $h = h_c = 1$ separates [80–83], at zero temperature and in the thermodynamic

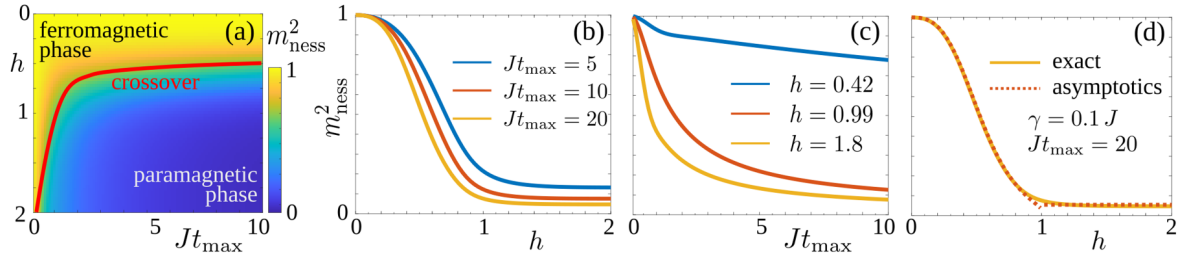

FIG. 2. NESS phase diagram. (a) Squared magnetization density $m^2_{\rm ness}$ in the TFIC as a function of transverse field h and (scaled) maximum reset time $Jt_{\rm max}$. The red line is a guide for the eye showing the region where the crossover from the ferromagnetic to the paramagnetic stationary phase takes place. (b) Plot of $m^2_{\rm ness}$ as a function of h for fixed values of $Jt_{\rm max} = 5, 10, 20$ (from top to bottom). As the maximum reset time increases, the crossover becomes sharper and resembles more and more the equilibrium quantum phase transition behavior. (c) Plot of $m^2_{\rm ness}$ as a function of $Jt_{\rm max}$ for different fixed values of $h = 0.42, 0.99, 1.8$ (from top to bottom). (d) Comparison between the result for $m^2_{\rm ness}$ as a function of h from the exact evaluation of Eq. (9) with $\langle\sigma^x(\tau)\rangle$ obtained from the clustering property of the two-point function (yellow solid line), and the result obtained using the asymptotic expression of $\langle\sigma^x(\tau)\rangle$ valid for large τ (red dashed line). In the figure, $\gamma = 0.1J$.

limit $N \to \infty$, the paramagnetic ($h > 1$) from the ferromagnetic ($h < 1$) phase. In the latter, because of the spontaneous breaking of the $\mathbb{Z}_2$ symmetry, the ground-state expectation value of the magnetization density m becomes nonzero ${}_\pm\langle {\rm GS}(h)\,|\,m\,|\,{\rm GS}(h)\rangle_\pm = \pm(1-h^2)^{1/8}$, where $|{\rm GS}(h)\rangle_\pm$ are the two degenerate ground states for $h < 1$.

Because of the $\mathbb{Z}_2$ symmetry, the matrices $P_{jk}(\tau)$ and $\widehat{R}_{jk}(s)$ in Eqs. (2) and (3) are symmetric. This, in turn, implies that the magnetization density in the NESS in Eq. (6) is identically zero: ${\rm Tr}(m\,\rho_{\rm ness}) = 0$ (and the same for all the odd operators under the $\mathbb{Z}_2$ symmetry; see Supplemental Material [77]). The natural order parameter to distinguish between the ordered and the disordered phase is then the squared magnetization density $m^2_{\rm ness} = {\rm Tr}(m^2\rho_{\rm ness})$. For the latter, one can derive, in the thermodynamic limit $N \to \infty$, the expression (see Supplemental Material [77])

$$m^2_{\rm ness} = \frac{1}{\widehat{q}(0)} \int_0^\infty d\tau\, q(\tau)\langle\sigma^x(\tau)\rangle^2, \tag{9}$$

which directly connects the NESS expectation value of $m^2_{\rm ness}$ in the presence of reset with the magnetization density quench dynamics $\langle m(\tau)\rangle = \langle\sigma^x(\tau)\rangle$ (with the last equality coming from the choice of periodic boundary conditions). Equation (9) can be evaluated exactly in the thermodynamic limit upon extracting $\langle\sigma^x(\tau)\rangle$ from the cluster decomposition principle of the two-point function $\langle\sigma^x_n\sigma^x_{n+l}\rangle(\tau)$ at large separation l (see Supplemental Material [77]), as outlined first in [84–87] for the equilibrium correlation function and in [49–51] for the nonequilibrium quench dynamics. In the latter case, it is known [49–51,63] that $\langle\sigma^x(\tau)\rangle \propto \exp(-t\,\Lambda(h,h_0))$ relaxes exponentially to zero at long times with a characteristic timescale $\Lambda(h,h_0)^{-1} > 0$ set by the quench (see Supplemental Material [77]).

In Fig. 2, we evaluate Eq. (9) for the waiting time distribution $p(\tau) = p_{\gamma,t_{\rm max}}(\tau) = \gamma e^{-\gamma\tau}/(1-e^{-\gamma t_{\rm max}})\Theta(t_{\rm max}-\tau)$, which represents a "chopped Poissonian distribution" with rate γ and maximum reset time $t_{\rm max}$ [$\Theta(\tau)$ denotes the Heaviside step function]. The NESS reflects the equilibrium quantum phase transition through a sharp crossover due to the competition between the maximum reset time $t_{\rm max}$ and the order parameter decay time $\Lambda(h,h_0)^{-1}$. Upon increasing $Jt_{\rm max}$ with fixed γ/J (or, vice versa, decreasing γ/J with $Jt_{\rm max}$ fixed), the crossover becomes very sharp, as shown in Fig. 2(b) for $\gamma = 0.1J$ and $Jt_{\rm max} = 20$. We emphasize that $m^2_{\rm ness}$ is always different from zero, even for large values of h deep in the paramagnetic phase, for any finite value of $Jt_{\rm max}$ or γ/J. This means that $\rho_{\rm ness}$, thanks to the resetting protocol, retains part of the long-range order stored in the reset states $|1\rangle$ and $|2\rangle$. For the reset-free quench time evolution, indeed, the diagonal ensemble predicts a vanishing expectation value of m^2 and therefore a complete loss of the order of $|1\rangle$ and $|2\rangle$. As $Jt_{\rm max} \to 0$, one encounters the quantum Zeno effect [34,35] since the initial state does not evolve in time due to very frequent resets and therefore the squared magnetization density remains close to 1. In the limit of large $Jt_{\rm max}$ (small γ/J), when the crossover gets sharp and it closely resembles the equilibrium quantum phase transition, a large time, on average, elapses between consecutive resets. As a consequence, one can evaluate Eq. (9) using the asymptotics of $\langle\sigma^x(\tau)\rangle \propto \exp(-t\,\Lambda(h,h_0))$ for long times $\tau \to \infty$, which has been analytically derived in Refs. [49–51,77]. The result is shown in Fig. 2(d) (see Supplemental Material [77]). We can see that the asymptotics of the order parameter is in excellent agreement with the exact numerical evaluation of Eq. (9). Only for values of $h \gtrsim 0.9$ are discrepancies visible. This is caused by the fact that when h becomes large, the order parameter $\langle\sigma^x(\tau)\rangle$ quickly relaxes to zero as a function of τ and the integral in Eq. (9) is therefore no longer dominated by the behavior of $\langle\sigma^x(\tau)\rangle$ at large times.

Outlook. We have presented a general protocol for constructing the NESS of a unitary many-body dynamics interspersed by random resets. Using the TFIC as an exemplary case, we have shown that this NESS is intimately connected to the dynamics following a quantum quench, and that it embodies the ground-state quantum phase transition of the TFIC through a sharp crossover. NESS with sharp crossovers can be exploited here to design collectively enhanced sensing protocols, where a small change of the parameter (external perturbation) driving the quantum phase transition translates into an easy-to-detect macroscopic response, as, e.g., discussed in Refs. [88,89]. A possible advantage of our protocol is, however, that the establishment of the NESS relies on stochastic resetting, which diminishes the impact of uncontrolled dissipative effects such as heating.

Acknowledgments. We acknowledge support from the "Wissenschaftler Rückkehrprogramm GSO/CZS" of the Carl-Zeiss-Stiftung and the German Scholars Organization e.V., from the European Union's Horizon 2020 research and innovation program under Grant Agreement No. 800942 (ErBeStA), as well as from the Baden-Württemberg Stiftung through Project No. BWST_ISF2019-23.

[1] M. R. Evans and S. N. Majumdar, Phys. Rev. Lett. **106**, 160601 (2011).
[2] M. R. Evans and S. N. Majumdar, J. Phys. A: Math. Theor. **44**, 435001 (2011).
[3] M. R. Evans and S. N. Majumdar, J. Phys. A: Math. Theor. **47**, 285001 (2014).
[4] S. N. Majumdar, S. Sabhapandit, and G. Schehr, Phys. Rev. E **91**, 052131 (2015).
[5] S. Eule and J. J. Metzger, New J. Phys. **18**, 033006 (2016).
[6] A. Pal, A. Kundu, and M. R. Evans, J. Phys. A: Math. Theor. **49**, 225001 (2016).
[7] A. Pal and S. Reuveni, Phys. Rev. Lett. **118**, 030603 (2017).
[8] A. Chechkin and I. M. Sokolov, Phys. Rev. Lett. **121**, 050601 (2018).
[9] M. R. Evans and S. N. Majumdar, J. Phys. A: Math. Theor. **51**, 475003 (2018).
[10] J. Masoliver and M. Montero, Phys. Rev. E **100**, 042103 (2019).
[11] A. S. Bodrova, A. V. Chechkin, and I. M. Sokolov, Phys. Rev. E **100**, 012119 (2019).
[12] A. S. Bodrova, A. V. Chechkin, and I. M. Sokolov, Phys. Rev. E **100**, 012120 (2019).
[13] M. Magoni, S. N. Majumdar, and G. Schehr, Phys. Rev. Research **2**, 033182 (2020).
[14] S. Redner, *A Guide to First-passage Processes* (Cambridge University Press, Cambridge, 2001).
[15] A. J. Bray, S. N. Majumdar, and G. Schehr, Adv. Phys. **62**, 225 (2013).
[16] M. R. Evans, S. N. Majumdar, and K. Mallick, J. Phys. A: Math. Theor. **46**, 185001 (2013).
[17] M. Montero and J. Villarroel, Phys. Rev. E **87**, 012116 (2013).
[18] C. Christou and A. Schadschneider, J. Phys. A: Math. Theor. **48**, 285003 (2015).
[19] D. Campos and V. Méndez, Phys. Rev. E **92**, 062115 (2015).
[20] M. Montero, A. Masó-Puigdellosas, and J. Villarroel, Eur. Phys. J. B **90**, 1 (2017).
[21] A. Masó-Puigdellosas, D. Campos, and V. Méndez, Phys. Rev. E **99**, 012141 (2019).
[22] G. Tucci, A. Gambassi, S. Gupta, and E. Roldán, Phys. Rev. Research **2**, 043138 (2020).
[23] M. R. Evans, S. N. Majumdar, and G. Schehr, J. Phys. A: Math. Theor. **53**, 193001 (2020).
[24] D. M. Busiello, D. Gupta, and A. Maritan, New J. Phys. **23**, 103012 (2021).
[25] G. Lindblad, Commun. Math. Phys. **48**, 119 (1976).
[26] V. Gorini, A. Kossakowski, and E. C. G. Sudarshan, J. Math. Phys. **17**, 821 (1976).
[27] L. Hartmann, W. Dür, and H.-J. Briegel, Phys. Rev. A **74**, 052304 (2006).
[28] N. Linden, S. Popescu, and P. Skrzypczyk, Phys. Rev. Lett. **105**, 130401 (2010).
[29] D. C. Rose, H. Touchette, I. Lesanovsky, and J. P. Garrahan, Phys. Rev. E **98**, 022129 (2018).
[30] F. Carollo, R. L. Jack, and J. P. Garrahan, Phys. Rev. Lett. **122**, 130605 (2019).
[31] A. Tavakoli, G. Haack, N. Brunner, and J. B. Brask, Phys. Rev. A **101**, 012315 (2020).
[32] A. Riera-Campeny, J. Ollé, and A. Masó-Puigdellosas, arXiv:2011.04403.
[33] B. Mukherjee, K. Sengupta, and S. N. Majumdar, Phys. Rev. B **98**, 104309 (2018).
[34] B. Misra and E. G. Sudarshan, J. Math. Phys. **18**, 756 (1977).
[35] C. B. Chiu, E. C. G. Sudarshan, and B. Misra, Phys. Rev. D **16**, 520 (1977).
[36] Y. Aharonov, L. Davidovich, and N. Zagury, Phys. Rev. A **48**, 1687 (1993).
[37] D. A. Meyer, J. Stat. Phys. **85**, 551 (1996).
[38] H. Friedman, D. Kessler, and E. Barkai, J. Phys. A: Math. Theor. **50**, 04LT01 (2016).
[39] H. Friedman, D. A. Kessler, and E. Barkai, Phys. Rev. E **95**, 032141 (2017).
[40] F. Thiel, E. Barkai, and D. A. Kessler, Phys. Rev. Lett. **120**, 040502 (2018).
[41] F. Thiel, I. Mualem, D. A. Kessler, and E. Barkai, Phys. Rev. Research **2**, 023392 (2020).
[42] S. L. Sondhi, S. M. Girvin, J. P. Carini, and D. Shahar, Rev. Mod. Phys. **69**, 315 (1997).
[43] M. Vojta, Rep. Prog. Phys. **66**, 2069 (2003).
[44] S. Sachdev, *Quantum Phase Transitions* (Cambridge University Press, Cambridge, 2011).
[45] J. Janssen and R. Manca, *Applied Semi-Markov Processes* (Springer Science & Business Media, New York, 2006).
[46] K. Sengupta, S. Powell, and S. Sachdev, Phys. Rev. A **69**, 053616 (2004).
[47] P. Calabrese and J. Cardy, Phys. Rev. Lett. **96**, 136801 (2006).
[48] P. Calabrese and J. Cardy, J. Stat. Mech.: Theory Exp. (2007) P06008.
[49] P. Calabrese, F. H. L. Essler, and M. Fagotti, Phys. Rev. Lett. **106**, 227203 (2011).
[50] P. Calabrese, F. H. L. Essler, and M. Fagotti, J. Stat. Mech.: Theory Exp. (2012) P07016.
[51] P. Calabrese, F. H. L. Essler, and M. Fagotti, J. Stat. Mech.: Theory Exp. (2012) P07022.
[52] M. Heyl, A. Polkovnikov, and S. Kehrein, Phys. Rev. Lett. **110**, 135704 (2013).
[53] M. Heyl, Rep. Prog. Phys. **81**, 054001 (2018).
[54] The NESS does not depend on the specific choice of the initial state. The latter influences only the transient dynamics.
[55] F. H. Essler and M. Fagotti, J. Stat. Mech.: Theory Exp. (2016) 064002.
[56] F. Iglói and H. Rieger, Phys. Rev. Lett. **106**, 035701 (2011).
[57] H. Rieger and F. Iglói, Phys. Rev. B **84**, 165117 (2011).
[58] A. Silva, Phys. Rev. Lett. **101**, 120603 (2008).
[59] F. H. L. Essler, S. Evangelisti, and M. Fagotti, Phys. Rev. Lett. **109**, 247206 (2012).

[60] L. Foini, L. F. Cugliandolo, and A. Gambassi, J. Stat. Mech.: Theory Exp. (2012) P09011.
[61] F. Meinert, M. J. Mark, E. Kirilov, K. Lauber, P. Weinmann, A. J. Daley, and H.-C. Nägerl, Phys. Rev. Lett. **111**, 053003 (2013).
[62] L. Bucciantini, M. Kormos, and P. Calabrese, J. Phys. A: Math. Theor. **47**, 175002 (2014).
[63] C. B. Dağ and K. Sun, Phys. Rev. B **103**, 214402 (2021).
[64] A. Browaeys and T. Lahaye, Nat. Phys. **16**, 132 (2020).
[65] M. Kormos, M. Collura, G. Takács, and P. Calabrese, Nat. Phys. **13**, 246 (2017).
[66] A. J. A. James, R. M. Konik, and N. J. Robinson, Phys. Rev. Lett. **122**, 130603 (2019).
[67] N. J. Robinson, A. J. A. James, and R. M. Konik, Phys. Rev. B **99**, 195108 (2019).
[68] P. P. Mazza, G. Perfetto, A. Lerose, M. Collura, and A. Gambassi, Phys. Rev. B **99**, 180302(R) (2019).
[69] A. Lerose, F. M. Surace, P. P. Mazza, G. Perfetto, M. Collura, and A. Gambassi, Phys. Rev. B **102**, 041118(R) (2020).
[70] G. Lagnese, F. M. Surace, M. Kormos, and P. Calabrese, J. Stat. Mech.: Theory Expt. (2020) 093106.
[71] R. Verdel, F. Liu, S. Whitsitt, A. V. Gorshkov, and M. Heyl, Phys. Rev. B **102**, 014308 (2020).
[72] F. B. Ramos, M. Lencsés, J. C. Xavier, and R. G. Pereira, Phys. Rev. B **102**, 014426 (2020).
[73] J. F. Sherson, C. Weitenberg, M. Endres, M. Cheneau, I. Bloch, and S. Kuhr, Nature (London) **467**, 68 (2010).
[74] P. Schauß, M. Cheneau, M. Endres, T. Fukuhara, S. Hild, A. Omran, T. Pohl, C. Gross, S. Kuhr, and I. Bloch, Nature (London) **491**, 87 (2012).
[75] J. Zeiher, P. Schauß, S. Hild, T. Macrì, I. Bloch, and C. Gross, Phys. Rev. X **5**, 031015 (2015).
[76] H. Labuhn, D. Barredo, S. Ravets, S. De Léséleuc, T. Macrì, T. Lahaye, and A. Browaeys, Nature (London) **534**, 667 (2016).
[77] See Supplemental Material at http://link.aps.org/supplemental/10.1103/PhysRevB.104.L180302 for the details of the calculations.
[78] For an even number N of spins, $\mathcal{P}_k$ is not a projector since one has to account for states with zero total magnetization. This does not spoil our general theory since the fundamental property $\sum_k P_{jk}(\tau) = 1$ still holds [77].
[79] L. D'Alessio, Y. Kafri, A. Polkovnikov, and M. Rigol, Adv. Phys. **65**, 239 (2016).
[80] E. Lieb, T. Schultz, and D. Mattis, Ann. Phys. **16**, 407 (1961).
[81] S. A. Pikin and V. M. Tsukernik, Zh. Eksp. Teor. Fiz. **50**, 1377 (1966) [Sov. Phys. JETP **23**, 914 (1966)].
[82] P. Pfeuty, Ann. Phys. **57**, 79 (1970).
[83] J. B. Kogut, Rev. Mod. Phys. **51**, 659 (1979).
[84] E. Barouch, B. M. McCoy, and M. Dresden, Phys. Rev. A **2**, 1075 (1970).
[85] E. Barouch and B. M. McCoy, Phys. Rev. A **3**, 786 (1971).
[86] E. Barouch and B. M. McCoy, Phys. Rev. A **3**, 2137 (1971).
[87] B. M. McCoy, E. Barouch, and D. B. Abraham, Phys. Rev. A **4**, 2331 (1971).
[88] M. Raghunandan, J. Wrachtrup, and H. Weimer, Phys. Rev. Lett. **120**, 150501 (2018).
[89] C. G. Wade, M. Marcuzzi, E. Levi, J. M. Kondo, I. Lesanovsky, C. S. Adams, and K. J. Weatherill, Nat. Commun. **9**, 3567 (2018).

Fifth Publication

Emergent quantum correlations and collective behavior in noninteracting quantum systems subject to stochastic resetting

Matteo Magoni [1], Federico Carollo [1], Gabriele Perfetto [1], and Igor Lesanovsky [1,2]

[1]*Institut für Theoretische Physik, Eberhard Karls Universität Tübingen, Auf der Morgenstelle 14, 72076 Tübingen, Germany*

[2]*School of Physics and Astronomy and Centre for the Mathematics and Theoretical Physics of Quantum Non-Equilibrium Systems, The University of Nottingham, Nottingham NG7 2RD, United Kingdom*

(Received 7 March 2022; accepted 31 October 2022; published 16 November 2022)

We investigate the dynamics of a noninteracting spin system, undergoing coherent Rabi oscillations, in the presence of stochastic resetting. We show that resetting generally induces long-range quantum and classical correlations both in the emergent dissipative dynamics and in the nonequilibrium stationary state. Moreover, for the case of conditional reset protocols—where the system is reinitialized to a state dependent on the outcome of a preceding measurement—we show that in the thermodynamic limit, the spin system can feature collective behavior which results in a phenomenology reminiscent of that occurring in nonequilibrium phase transitions. The discussed reset protocols can be implemented on quantum simulators and quantum devices that permit fast measurement and readout of macroscopic observables, such as the magnetization. Our approach does not require the control of coherent interactions and may therefore highlight a route towards a simple and robust creation of quantum correlations and collective nonequilibrium states, with potential applications in quantum enhanced metrology and sensing.

DOI: 10.1103/PhysRevA.106.052210

I. INTRODUCTION

Understanding and exploiting the interplay between coherent unitary evolution and measurement in quantum systems has been a central topic since the early days of quantum mechanics [1,2]. Recent research in this direction is closely linked to the physics of open quantum systems [3–6], where interactions among quantum particles compete with the coupling to the surrounding environment. Modern experiments allow one to externally control and even artificially engineer open system dynamics. This can, e.g., be achieved through so-called feedback protocols [7–12], which rely on the continuous monitoring of a system followed by some action conditioned on the output of a detector. This procedure can generate nonequilibrium steady states (NESS) that feature nontrivial quantum correlations [13–16]. Another approach that relies on externally imposed interventions in order to create effectively open system dynamics is *stochastic resetting* [17]. In its simplest form, it amounts to resetting a system to its initial state at random times. This procedure has been originally studied for classical diffusive systems [18–21], search processes [18,19,22–25], and active systems [26–32], and also here interesting NESS have been shown to emerge [33–44]. Similar observations have been made recently in the context of quantum systems [45–55]. However, it remains an open question whether resetting can induce nontrivial NESS, which may display emergent quantum correlations or even nonequilibrium phase transition behavior.

In this manuscript, we fill this gap by investigating the interplay between stochastic resetting and many-body quantum coherent evolution in the simplest—yet surprisingly nontrivial—case of noninteracting spin systems; see Fig. 1(a). We show that despite the absence of interactions in the coherent dynamics, resetting induces quantum correlations as well as a critical (nonanalytic) behavior in the NESS. We demonstrate this by envisaging three distinct protocols, named henceforth Protocol I, II, and III, in increasing order of complexity [see Figs. 1(b) and 1(c)]. Protocol I amounts to the aforementioned simple stochastic resetting of the system to a fixed state, while Protocols II and III include a measurement step whose outcome determines to which state the system is reset.

In *all three* cases, we find that resetting induces long-range correlations, although the system's reset-free dynamics is noninteracting. These correlations, emerging from the global operations associated with the reset events, are not exclusively of a statistical nature, but also have a quantum origin. Moreover, Protocols II and III induce stationary collective behavior, which manifests in nonanalyticities in an appropriate order parameter. While reminiscent of a nonequilibrium phase transition, the phenomenology we observe here is rather different in nature. Standard phase transitions take place between phases with short-range correlations and finite susceptibility parameter. Here, instead, due to the reset process, the system features strong long-range correlations and a divergent susceptibility throughout the whole phase diagram and not only at the critical point. The collectively enhanced response of the system to external parameter variations may be exploited for high-density quantum sensing, as discussed, e.g., in Refs. [56–58]. The fact that such property emerges even within a simple noninteracting system readily realizable with neutral atoms highlights a novel and simple way for creating

 ©2022 American Physical Society

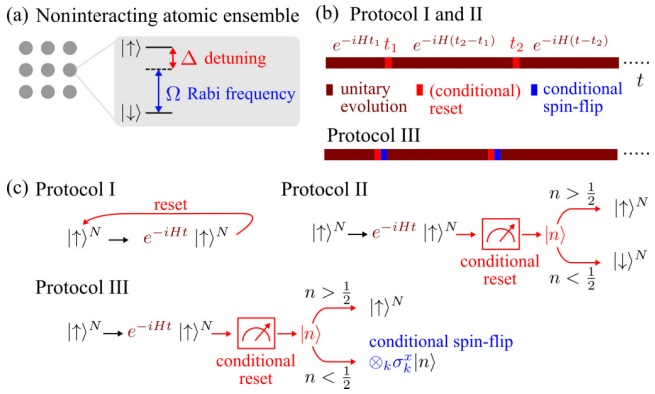

FIG. 1. Noninteracting spins subject to resetting. (a) Noninteracting spin system subject to a (laser) field with Rabi frequency Ω and detuning Δ. (b) The unitary time evolution according to Hamiltonian (1) is interspersed by randomly distributed reset events, which reinitialize the system to a specific state depending on the adopted reset protocol. In the figure, t denotes the observation time and t_k the time when the kth reset event takes place. (c) Details of the reset protocols. In Protocol I, the system is unconditionally reset to the state $|\uparrow\rangle^N$. In Protocols II and III, the reset is preceded by a measurement of the excitation density n, which selects a product configuration state $|n\rangle$, with density n. In Protocol II, the value of n determines the choice between two fixed reset states. In Protocol III, when $n < 1/2$, the reset state is determined by a spin-flip operation applied to the state obtained from the projective measurement.

and exploiting correlated many-body states on quantum simulators [59–63].

II. DYNAMICS AND RESET STATES

We consider a system of N spins with Hamiltonian

$$H = \Omega \sum_{i=1}^{N} \sigma_i^x + \Delta \sum_{i=1}^{N} \sigma_i^z, \tag{1}$$

describing, for instance, noninteracting atoms subject to an external laser field. Here, $\sigma_i^{x,y,z}$ are the Pauli matrices of the ith spin, Ω is the Rabi frequency, and Δ is the laser detuning. The two basis states of each spin, $|\uparrow\rangle$ and $|\downarrow\rangle$, are chosen as the eigenstates of σ^z and represent the excited state and the ground state, respectively [see Fig. 1(a)]. These can be, for example, two hyperfine levels of an atom or of an ion.

Before turning to the discussion of the reset protocols, it is useful to first characterize the dynamical properties of the system during its coherent evolution. Since Hamiltonian (1) is the sum of single-body terms, we can focus on the time evolution of single-body operators. For example, the local excitation density at site j, defined as $n_j = (1+\sigma_j^z)/2$, evolves as $n_j^F(t) = e^{iH_j t} n_j e^{-iH_j t}$, with $H_j = \Omega\sigma_j^x + \Delta\sigma_j^z$ and F indicating evolution under the Hamiltonian reset-free dynamics. Without loss of generality, we fix the initial state to be $|\uparrow\rangle^N = \otimes_{i=1}^N |\uparrow\rangle_i$. With this choice, one finds $\langle n_j^F(t)\rangle_\uparrow = 1 - (\Omega^2/\overline{\Omega}^2)\sin^2(\overline{\Omega}t)$, where $\overline{\Omega} = \sqrt{\Omega^2+\Delta^2}$ is the effective Rabi frequency and the arrow in the subscript indicates the initial state.

The reset protocols are depicted in Figs. 1(b) and 1(c). All have in common that the system evolves coherently with Hamiltonian (1) in between consecutive reset events. In Protocol I, we employ stochastic resetting, i.e., the system is reinitialized to the state $|\uparrow\rangle^N$ unconditionally to any measurement. In Protocols II and III, instead, the reset state is chosen conditionally on a measurement taken right before resetting, as pictured in Fig. 1(c). A natural choice for the quantity to be measured is the excitation density $n = (1/N)\sum_{i=1}^N n_i$. In particular, in Protocol II, first proposed in Ref. [51], two reset states are present, $|\uparrow\rangle^N$ and $|\downarrow\rangle^N$, which correspond to the two completely polarized states with excitation density 1 and 0, respectively. The outcome of the measurement determines the reset state: if the measured excitation density exceeds a certain threshold, which is fixed to be $1/2$, then the system is reset to $|\uparrow\rangle^N$; otherwise it is reset to $|\downarrow\rangle^N$. In Protocol III, the system is reset to $|\uparrow\rangle^N$ if the measured density exceeds the threshold. Otherwise, the coherent dynamics resumes from the state obtained by flipping all the spins in the postmeasurement configuration, as sketched in Fig. 1(c).

III. PROTOCOL I: UNCONDITIONAL RESET

In this simple case, the coherent dynamics of the system is interrupted at random times at which the system is reset to state $|\uparrow\rangle^N$. Resets happen at a constant rate γ. The time τ between consecutive reset is therefore distributed according to the Poisson waiting time distribution $f(\tau) = \gamma e^{-\gamma\tau}$ (see Appendix E for a different waiting time distribution). The survival probability, i.e., the probability that no reset happens for a time τ, is given by $q(\tau) = \int_\tau^\infty f(s)ds = e^{-\gamma\tau}$. This, together with the reset-free time-evolved density matrix $\rho_\uparrow^F(t)$, determines the quantum state of the system $\rho_\uparrow(t)$ in the presence of resetting through the *last renewal* equation derived in Ref. [48],

$$\rho_\uparrow(t) = e^{-\gamma t}\rho_\uparrow^F(t) + \gamma\int_0^t dt' e^{-\gamma t'}\rho_\uparrow^F(t'). \tag{2}$$

The first term in the above equation corresponds to having no reset up to time t. The second term accounts for realizations of the stochastic resetting process where the last reset has been at a previous time $t - t'$ and the system has then evolved without reset events up to time t via the Hamiltonian (1).

The average excitation density in state (2) is given by $\langle n(t)\rangle_\uparrow = \mathrm{Tr}[n\rho_\uparrow(t)]$ and its stationary value reads

$$\langle n\rangle_{\uparrow,\mathrm{ness}} = \lim_{t\to\infty}\langle n(t)\rangle_\uparrow = 1 - 2\frac{\Omega^2}{\gamma^2+4\overline{\Omega}^2}, \tag{3}$$

which is shown in Fig. 2(a). This expression smoothly varies with Ω/Δ, contrary to what we will show for Protocols II and III. Equation (3) is equal to 1, i.e., the excitation density of the initial state, for $\Omega = 0$ (no coupling between single spin states), $\gamma\to\infty$ (the infinitely frequent resets induce a quantum Zeno effect [64,65] which freezes the system to its initial state), and $\Delta\to\infty$ (transitions between the two spins states are highly off-resonant). Note, finally, that the limit $\gamma\to 0$ corresponds to a stationary state with extremely rare reset events.

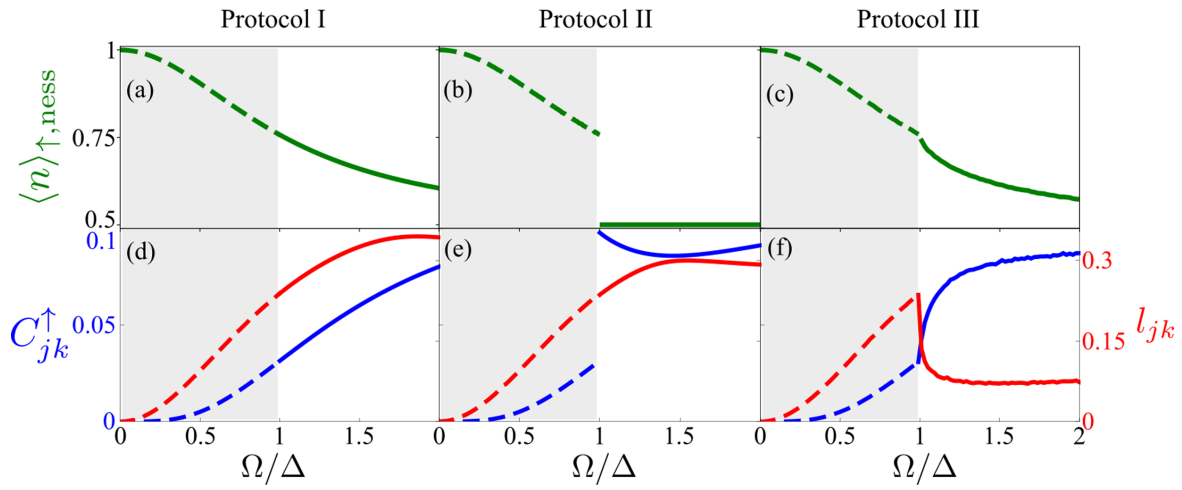

FIG. 2. Collective behavior and quantum correlations induced by reset. First row: stationary excitation density as a function of Ω/Δ for the three protocols. (a) For Protocol I, the order parameter (excitation density) is given by Eq. (3). For Protocols (b) II and (c) III, the order parameter displays a nonanalyticity at the critical point $\Omega_c = \Delta$, which is discontinuous or continuous, respectively. For Protocol III, the order parameter behaves as a power law when approaching the critical point from the right with an exponent close to 0.5. Second row: Connected correlation function (in blue, left axis) and quantum discord (in red, right axis), computed from the two-spin reduced density matrix ρ_{jk}, as a function of Ω/Δ. In contrast to (d) Protocol I, where both quantities are continuous, (e) Protocol II leads to a discontinuity of both quantities at the critical point $\Omega_c = \Delta$. Note that the discontinuity of the quantum discord is imperceptible on the scale shown. (f) For reset Protocol III, both the connected correlation function and the quantum discord feature power-law behavior in a right neighborhood of the critical point. The characteristic exponent is approximately 0.5 for the connected correlation function and 0.2 for the quantum discord. The dashed parts of the curves in all panels highlight the fact that when $\Omega < \Delta$, the three protocols become equivalent. All data are obtained analytically, except for (c) and (f) where numerical simulations are necessary. The reset rate is chosen to be $\gamma = \Delta/2$.

Rather surprisingly, although in each realization of the process the system is in a product state at all times, the reset mechanism introduces long-range correlations. This is due to the *global* character of the resetting procedure: all the individual spins are reset to the same single-spin state. This becomes evident when looking at the stationary two-spin connected correlation function $C^{\uparrow}_{jk} = [\langle n_j n_k \rangle_{\uparrow,\mathrm{ness}} - \langle n_j \rangle_{\uparrow,\mathrm{ness}} \langle n_k \rangle_{\uparrow,\mathrm{ness}}]$, which is equal to

$$C^{\uparrow}_{jk} = 4\Omega^4 \frac{5\gamma^2 + 8\overline{\Omega}^2}{(\gamma^2 + 4\overline{\Omega}^2)^2(\gamma^2 + 16\overline{\Omega}^2)}, \tag{4}$$

showing that correlations do not depend on the considered spins. This is reminiscent of what happens in fully connected models (see, e.g., [66] for an example in dissipative settings). However, in our case, these correlations are *strong* in the sense that they do not vanish in the thermodynamic $N \to \infty$ limit. As such, contrary to the case of fully connected models [67], the stationary state of our reset process is not clustering, i.e., it does not possess Gaussian fluctuations, as shown by the fact that the susceptibility is diverging: $\chi = \lim_{N\to\infty} 1/N \sum_{j,k=1}^{N} C^{\uparrow}_{jk} = \infty$. Note that the correlations (4) can also be computed from suitable single-spin trajectory correlations, following, e.g., Ref. [68]. This is, however, not possible for Hamiltonians with interactions among the spins or for the Protocols II and III discussed further below.

In addition to these strong classical density-density correlations, the NESS, in fact, also contain correlations of quantum origin. This aspect can be shown by computing the local quantum uncertainty (LQU), defined in Ref. [69], which is a type of bipartite quantum discord [70,71]. It quantifies the extent of the fluctuations of a local measurement due to the noncommutativity between the state and the measured local observable. The LQU isolates the fluctuations that are caused only by the coherence of the state and not by its mixedness. Despite being a fairly common feature in quantum states [72], quantum discord is proved to be a useful quantity for metrology and sensing applications [73–75]. Here we compute the LQU for the stationary two-spin reduced density matrix ρ_{jk}; see Appendix C. It is given by $l_{jk} = 1 - \lambda_{\max}\{W_{jk}\}$, where $\lambda_{\max}\{W_{jk}\}$ is the largest eigenvalue of the 3×3 matrix W_{jk} with elements $(W_{jk})_{ab} = \mathrm{Tr}[\sqrt{\rho_{jk}}(\sigma^a_j \otimes \mathbb{1})\sqrt{\rho_{jk}}(\sigma^b_j \otimes \mathbb{1})]$, with $a, b = x, y, z$. As for the classical correlations, the LQU also does not depend on the distance between sites. In Fig. 2(d), we show the connected correlation function (4) (left axis) together with the quantum discord quantified via the LQU (right axis) for Protocol I. Both quantities possess qualitatively the same shape and smoothly vary with Ω/Δ.

IV. PROTOCOL II: CONDITIONAL RESET TO TWO STATES

This protocol exploits two reset states: $|\uparrow\rangle^N$ and $|\downarrow\rangle^N$. At each reset event, the local density at each site is measured and the total excitation density n is computed. The system is reinitialized to the reset state $|\uparrow\rangle^N$ if the majority of the spins is found in the excited state, i.e., $n > 1/2$. On the contrary, if $n < 1/2$, the reset state is chosen as $|\downarrow\rangle^N$. For large N, the probability distribution for measuring a certain value of n after a time t since the last reset is a Gaussian distribution centered on the average, $\langle n^F(t) \rangle_{\uparrow/\downarrow}$, with variance

$\sigma_n^2 \propto 1/N$. This means that at each reset event, the system can, in principle, be reinitialized in both reset states, albeit with different probabilities. This aspect, together with the fact that the Hamiltonian dynamics of the average density satisfies the relation $\langle n^F(t)\rangle_\uparrow = 1 - \langle n^F(t)\rangle_\downarrow$, makes the stationary excitation density exactly equal to $1/2$, i.e., the average between the density of the two reset states; see Appendix B.

A different phenomenology takes place in the thermodynamic limit $N \to \infty$. In this case, as a consequence of the *law of large numbers* applied to the operator n, the probability distribution to measure a certain value for n becomes a δ function peaked around the average $\langle n^F(t)\rangle_{\uparrow/\downarrow}$. This self-averaging property makes the measurement of the excitation density fully deterministic with outcome equal to its average value. As a consequence, for $\Omega < \Delta$, given the initial condition and the fact that $\langle n^F(t)\rangle_\uparrow > 1/2 \ \ \forall t$, the system can only be reset to the state $|\uparrow\rangle^N$ and, therefore, the average density in the process is always larger than $1/2$. For $\Omega > \Delta$, instead, both reset states can be reached so that the stationary excitation density is equal to $1/2$; see Appendix B. The stationary excitation density, acting as an order parameter, then displays a jump discontinuity at the critical point $\Omega_c = \Delta$, as shown in Fig. 2(b). This is a consequence of an abrupt change in the dynamics: for $\Omega > \Delta$, the system can reset to both states, while for $\Omega < \Delta$, the dynamics is effectively that of Protocol I, with the stationary excitation density coinciding with Eq. (3) (see, also, Fig. 2).

As shown in Fig. 2(e), the connected correlation function and the quantum discord display a behavior that is qualitatively different from that of Protocol I. They are both discontinuous at the critical point even though the discontinuity of the LQU is tiny on the scale of the figure.

V. PROTOCOL III: CONDITIONAL RESET TO THE INITIAL STATE

In the third protocol, the system is reset to its initial state $|\uparrow\rangle^N$ only if the measured excitation density exceeds $1/2$. If not, the system resumes its dynamics from the state generated by the projective measurement after a subsequent flip of all its spins is performed [see Figs. 1(b) and 1(c)]. This means that if the state after the projective measurement possesses an excitation density equal to $n' < 1/2$, the reset state will have excitation density $1 - n' > 1/2$. This protocol is still conditioned on the measured excitation density, but, in contrast to Protocol II, any state with $n > 1/2$ can be considered as a reset state according to the parameter regime. The resulting nonequilibrium phase diagram [see Fig. 2(c)] exhibits a continuous nonanalytic behavior at the critical point $\Omega_c = \Delta$.

We note that without the additional spin-flip operation, the stationary behavior of the density would be discontinuous also for this protocol. Indeed, when $\Omega > \Delta$, each realization of the reset process would spend, on average, half of the time in configurations with n smaller than $1/2$ and half of the time in configurations with n larger than $1/2$. The stationary state, obtained by averaging over trajectories, would therefore be very different from the one attained when $\Omega < \Delta$, where trajectories maintain a positive magnetization, $n > 1/2$, throughout the whole reset process. This substantial dissimilarity between the two regimes would result in a jump discontinuity of the order parameter at Ω_c. On the contrary, with the introduction of the spin-flip operation, the order parameter is continuous, but still nonanalytic since its first derivative has a jump discontinuity at Ω_c. This can be understood by noticing that in this case, for $\Omega \gtrsim \Delta$, each trajectory of the reset process spends only an infinitesimal time in states with $n < 1/2$ since after a reset the system restarts the dynamics from a state with $n > 1/2$.

In the vicinity of Ω_c, the order parameter displays a power-law behavior $\sim (\Omega - \Omega_c)^\beta$, for $\Omega \to \Omega_c^+$, with a static exponent $\beta \approx 0.5$. This seems to indicate the emergence of a second-order phase transition in the NESS. However, looking at the behavior of the correlation function reveals a rather unexpected phenomenology. Indeed, in second-order phase transitions, upon approaching the critical point, the correlation length of the system increases, giving rise to a power-law divergence of the susceptibility at criticality. Here, instead, as already mentioned when discussing Protocol I, the system features strong long-range correlations which determine a divergence of the susceptibility parameter χ for any value of Ω/Δ and not only at criticality. Despite this divergence, we can still analyze the two-spin correlation function $C^\uparrow_{jk}$. This quantity, displayed in Fig. 2(f), interestingly also obeys a power-law behavior $\sim(\Omega - \Omega_c)^\beta$ close to the critical point, with the same static exponent β of the order parameter. Also, the quantum discord, as measured by the LQU, follows a power law with exponent $\delta \approx 0.2$.

VI. CONCLUSIONS AND OUTLOOK

We have shown that combining a noninteracting quantum dynamics with an externally imposed reset process can lead to surprisingly rich nonequilibrium stationary states. Even the simplest possible protocol results in a state with nontrivial classical and quantum correlations. More involved protocols lead to the emergence of a phase-transition behavior in an initially noninteracting system, which may be relevant for the implementation of quantum sensing and metrology applications [56,76–78]. The nonanalyticities characterizing such collective behavior emerge since the reset state is completely determined, in the thermodynamic limit, by the average value of the density as a consequence of the *law of large numbers*. For any finite system, fluctuations in the measurement outcomes inhibit the emergence of the observed nonanalyticities. We have shown how this occurs in the case of a noninteracting unitary dynamics. However, one would observe a similar phenomenology in the case of Hamiltonian dynamics with short-range interactions, for which the time evolution only builds up exponentially decaying correlations which do not invalidate the convergence of the operator n to its average value, in the large-N limit. Conceptually, this mechanism underlying collective behavior may appear simpler than the creation of strong coherent interactions. However, one requires the ability to rapidly read out and initialize the spin ensemble [79]. For the results discussed in Fig. 2, we have assumed a reset rate $\gamma = \Delta/2$, which in some settings may be impractical (it could be of the order of MHz for cold atoms). However, our findings do not change qualitatively for smaller values of the reset rate. The key quantity is indeed the ratio Ω/Δ, while the value of γ simply provides the timescale for the approach to stationarity.

ACKNOWLEDGMENTS

We acknowledge support from the "Wissenschaftler Rückkehrprogramm GSO/CZS" of the Carl-Zeiss-Stiftung and the German Scholars Organization e.V., from the European Union's Horizon 2020 research and innovation program under Grant Agreement No. 800942 (ErBeStA), as well as from the Baden-Württemberg Stiftung through Project No. BWST_ISF2019-23. We also acknowledge funding from the Deutsche Forschungsgemeinschaft through SPP 1929 (GiRyd), Grant No. 428276754, as well as through the Research Unit FOR 5413/1, Grant No. 465199066. G.P. acknowledges support from the Alexander von Humboldt Foundation through a Humboldt research fellowship for postdoctoral researchers.

APPENDIX A: GENERAL EXPRESSION OF THE STATIONARY DENSITY MATRIX FOR PROTOCOL II

The resetting dynamics described in Protocols I and II allows one to write the exact form of the stationary density matrix $\rho_{\rm ness}$ in terms of the waiting time distribution and the reset-free dynamical properties of the system. In particular, for Protocol II, the expression of the stationary density matrix $\rho_{\rm ness}$ has been determined in Ref. [51] and it reads

$$\rho_{\rm ness} = \frac{c_\uparrow}{\widehat{q}} \int_0^\infty dt' q(t') \rho_\uparrow^F(t') + \frac{c_\downarrow}{\widehat{q}} \int_0^\infty dt' q(t') \rho_\downarrow^F(t'), \tag{A1}$$

where

$$c_\uparrow = \frac{R_{\downarrow\uparrow}}{R_{\downarrow\uparrow} + R_{\uparrow\downarrow}}, \quad c_\downarrow = \frac{R_{\uparrow\downarrow}}{R_{\downarrow\uparrow} + R_{\uparrow\downarrow}}, \tag{A2}$$

and

$$\widehat{q} = \int_0^\infty dt' q(t'), \quad R_{ij} = \gamma \int_0^\infty dt' e^{-\gamma t'} P_{ij}(t'), \quad i, j = \uparrow, \downarrow . \tag{A3}$$

In the previous equation, $P_{ij}(t)$ is the probability that the system, starting its reset-free evolution from the reset state $|i\rangle$ ($|\uparrow\rangle^N$ or $|\downarrow\rangle^N$), in the occurrence of a reset event after a time t, is reinitialized to the reset state $|j\rangle$ ($|\uparrow\rangle^N$ or $|\downarrow\rangle^N$). Equation (A1) expresses $\rho_{\rm ness}$ as a statistical mixture of the unitary time evolutions ensuing from the reset states $|\uparrow\rangle^N$ and $|\downarrow\rangle^N$. Fundamentally, both weights $c_\uparrow$ and $c_\downarrow$ couple the Hamiltonian dynamics with the reset via Eqs. (A2) and (A3). In particular, since the probabilities $P_{ij}(t)$ depend on Ω, the weights $c_{\uparrow/\downarrow}$ also depend on Ω.

In the main text and further below in Appendices B–D, for the sake of simplicity, we consider the case of Poissonian resetting, with survival probability $q(t) = \exp(-\gamma t)$, while we comment in Appendix E about the non-Poissonian case.

For Protocol III, any state with excitation density $n > 1/2$ can be considered as a reset state. The generalization of Eq. (A1) is therefore of no practical utility since it involves a summation over all the reset states, whose number is exponentially large in the system size. In order to obtain the stationary values of different properties such as the excitation density, the two-point correlation function, and the quantum discord, in Protocol III, we shall therefore resort to Monte Carlo simulations and use combinatorial properties (see Appendix D).

We finally note that the expression in Eq. (A1) does not apply in the regime $\Omega < \Delta$, when considering the noninteracting spin system in the thermodynamic limit $N \to \infty$. Indeed, as we discuss below, for $\Omega < \Delta$, the magnetization of the spin ensemble can never change sign so that whether $n < 1/2$ or $n > 1/2$ throughout the whole dynamics solely depends on the value of n in the initial state. This implies that the system cannot visit all the reset states, as witnessed, for instance, by the fact that $P_{\uparrow\downarrow} = P_{\downarrow\uparrow} = 0$ for Protocol II (similar relations would apply to Protocol III). As such, the quantities $c_{\uparrow/\downarrow}$ become, in principle, ill defined. In any case, it is straightforward to see that starting from the state with all spins pointing up, in the regime $\Omega < \Delta$ and in the thermodynamic limit $N \to \infty$, the system can only reset to its initial state. As such, in this regime, the stationary density matrix is the one given in Eq. (A1) with $c_\uparrow = 1$ and $c_\downarrow = 0$. Note that in this limit, the stationary density matrix in Eq. (A1) reduces to the stationary limit of Eq. (2) in the main text, as expected. This applies to both Protocol II and Protocol III.

APPENDIX B: STATISTICAL PROPERTIES OF THE EXCITATION DENSITY IN A FINITE SYSTEM

From Appendix A, it is evident that once the probabilities $P_{ij}(t)$ in Eq. (A3) are computed, one can then easily obtain the stationary density matrix defined in Eq. (A1), which is valid for Protocol II. Exploiting the fact that the spins do not interact, it is indeed possible to compute those probabilities. Let us therefore focus on Protocol II, where the measurement of the excitation density n determines the reset state to choose. In particular, if the outcome of the measurement exceeds the threshold $1/2$, the selected reset state is $|\uparrow\rangle^N$; otherwise it is $|\downarrow\rangle^N$. It would therefore be beneficial to have an expression for the probability to measure a certain value of n which, at a given time t, is above or below this threshold. To compute this probability, it is of course sufficient to consider only the properties of the reset-free dynamics. The fact that the system is noninteracting reduces the computation to a simple combinatorial problem. Since the threshold is $1/2$, a sort of majority rule applies in the sense that the threshold is exceeded whenever there are more up spins than down spins.

As an example, let us show how to compute $P_{\uparrow\downarrow}^{(N)}(t)$, which is defined to be the probability that the system, being initialized in $|\uparrow\rangle^N$ (appearing as first subscript), is found after a time t to have an excitation density $n < 1/2$ (appearing as the second subscript). In the notation of Appendix A, it would be $P_{ij}(t)$, with $i = \uparrow$ and $j = \downarrow$. Following the majority rule, this amounts to the probability of having, after a time t, more down spins than up spins. Assuming, for simplicity, that the total number of spins, N, is odd and denoting with $p^{\uparrow\downarrow}(t) = (\Omega^2/\overline{\Omega}^2)\sin^2(\overline{\Omega} t)$ the probability that a single spin, initialized in the state $|\uparrow\rangle$, is found after a time t in the state $|\downarrow\rangle$,

$$P_{\uparrow\downarrow}^{(N)}(t) = \sum_{k=0}^{\frac{N-1}{2}} \binom{N}{k} [1 - p^{\uparrow\downarrow}(t)]^k [p^{\uparrow\downarrow}(t)]^{N-k}, \tag{B1}$$

which takes into account all the possible spin configurations with, at most, $(N-1)/2$ spins in the excited state. By using

the normal approximation of the binomial distribution, which is valid for large N (see, e.g., Ref. [80]),

$$\binom{N}{k}(1-p)^k p^{N-k} \simeq \frac{1}{\sqrt{2\pi N p(1-p)}} \exp\left[-\frac{[k-N(1-p)]^2}{2Np(1-p)}\right], \tag{B2}$$

and approximating the discrete sum with an integral, Eq. (B1) gets simplified to

$$P^{(N)}_{\uparrow\downarrow}(t) \simeq \frac{1}{\sqrt{2\pi N p^{\uparrow\downarrow}(t)[1-p^{\uparrow\downarrow}(t)]}} \int_0^{\frac{N}{2}} dx \exp\left\{-\frac{[x-N(1-p^{\uparrow\downarrow}(t))]^2}{2Np^{\uparrow\downarrow}(t)[1-p^{\uparrow\downarrow}(t)]}\right\}. \tag{B3}$$

We can therefore write the probability $P^{(N)}_{\uparrow\downarrow}(t)$ as a difference between two error functions as

$$P^{(N)}_{\uparrow\downarrow}(t) = \frac{1}{2}\left[\mathrm{erf}\left(\frac{-\frac{N}{2}+Np^{\uparrow\downarrow}(t)}{\sqrt{2Np^{\uparrow\downarrow}(t)[1-p^{\uparrow\downarrow}(t)]}}\right) - \mathrm{erf}\left(\frac{-N+Np^{\uparrow\downarrow}(t)}{\sqrt{2Np^{\uparrow\downarrow}(t)[1-p^{\uparrow\downarrow}(t)]}}\right)\right]. \tag{B4}$$

With the explicit expression for the probabilities $P_{ij}(t)$, of which Eq. (B4) is an example, one can obtain the stationary density matrix (A1). Note that thanks to the fact that the single-spin transition probabilities satisfy $p^{\uparrow\downarrow}(t) = p^{\downarrow\uparrow}(t)$,

$$P^{(N)}_{\uparrow\downarrow}(t) = P^{(N)}_{\downarrow\uparrow}(t) \qquad \text{and} \qquad P^{(N)}_{\uparrow\uparrow}(t) = P^{(N)}_{\downarrow\downarrow}(t), \tag{B5}$$

so the symmetry in the reset-free dynamics is not restricted to the average value of the excitation density operator through $\langle n^F(t)\rangle_\uparrow = 1 - \langle n^F(t)\rangle_\downarrow$, but it is also extended to the probabilities.

In the thermodynamic limit, Eq. (B4) can be further simplified. Indeed, for $N \to \infty$, the second term tends to 1 because $p^{\uparrow\downarrow}(t) \leqslant 1$. On the other hand, the first term tends to $+1$ if $p^{\uparrow\downarrow}(t) > 1/2$ or to -1 if $p^{\uparrow\downarrow}(t) < 1/2$. Note that the number $1/2$ comes from the chosen threshold. As a consequence, the probability $P^{(N)}_{\uparrow\downarrow}(t)$ simply reduces to a Heaviside step function with a time-dependent argument,

$$P^{(\infty)}_{\uparrow\downarrow}(t) = \lim_{N\to\infty} P^{(N)}_{\uparrow\downarrow}(t) = \Theta\left[p^{\uparrow\downarrow}(t) - \frac{1}{2}\right]. \tag{B6}$$

Importantly, this result shows that $P^{(\infty)}_{\uparrow\downarrow}(t)$ can be either 1 or 0, meaning that in the thermodynamic limit, the excitation density $n = (1/N)\sum_{i=1}^N n_i$, when measured, takes deterministically a certain value, which turns out to be equal to the average value of the single-spin excitation density. This self-averaging property shows indeed that the fluctuations of n around its average value are suppressed, in accordance with the *law of large numbers*.

It is also interesting to see how the previous results change if N is assumed to be large but finite. In particular, given the large x expansion of the error function as $\mathrm{erf}x \simeq 1 - e^{-x^2}/(\sqrt{\pi}x)$, Eq. (B6) gets modified by a correction of the order of $e^{-N}/\sqrt{N}$ as

$$P^{(N)}_{\uparrow\downarrow}(t) \simeq \frac{\sqrt{2p^{\uparrow\downarrow}(t)[1-p^{\uparrow\downarrow}(t)]}}{2\sqrt{\pi N}}\left(\frac{e^{-N\frac{[\frac{1}{2}-p^{\uparrow\downarrow}(t)]^2}{2p^{\uparrow\downarrow}(t)[1-p^{\uparrow\downarrow}(t)]}}}{\frac{1}{2}-p^{\uparrow\downarrow}(t)} - \frac{e^{-N\frac{[1-p^{\uparrow\downarrow}(t)]^2}{2p^{\uparrow\downarrow}(t)[1-p^{\uparrow\downarrow}(t)]}}}{1-p^{\uparrow\downarrow}(t)}\right) \qquad \text{if } p^{\uparrow\downarrow}(t) < \frac{1}{2}, \tag{B7}$$

and

$$P^{(N)}_{\uparrow\downarrow}(t) \simeq 1 - \frac{\sqrt{2p^{\uparrow\downarrow}(t)[1-p^{\uparrow\downarrow}(t)]}}{2\sqrt{\pi N}}\left(\frac{e^{-N\frac{[\frac{1}{2}-p^{\uparrow\downarrow}(t)]^2}{2p^{\uparrow\downarrow}(t)[1-p^{\uparrow\downarrow}(t)]}}}{\frac{1}{2}-p^{\uparrow\downarrow}(t)} + \frac{e^{-N\frac{[1-p^{\uparrow\downarrow}(t)]^2}{2p^{\uparrow\downarrow}(t)[1-p^{\uparrow\downarrow}(t)]}}}{1-p^{\uparrow\downarrow}(t)}\right) \qquad \text{if } p^{\uparrow\downarrow}(t) > \frac{1}{2}. \tag{B8}$$

Note that for $N \to \infty$, one recovers the result in Eq. (B6).

Figure 3 investigates the behavior of the order parameter in Protocol II as a function of Ω/Δ for various numbers N of particles. The plotted curves are obtained with Monte Carlo simulations. In particular, we fix a large observation time T and we simulate several realizations of the reset process within this time interval by drawing the times between consecutive resets from the waiting time distribution $f(\tau)$. The average of the computed excitation density at time T over the many independent realizations of the reset process gives the numerical estimate of $\langle n\rangle_{\uparrow,\mathrm{ness}}$. This procedure is repeated for different values of Ω/Δ, leading to the result in Fig. 3. The discontinuous nonanalytic behavior of the order parameter occurring in Protocol II, and shown in Fig. 2(b) of the main text, becomes a continuous crossover when N is finite. The reason for the observed smoothening is due to the fact that for finite N, the measurement of n is no longer deterministic and does not coincide with its average value because of the statistical fluctuations encoded in Eqs. (B7) and (B8). As a consequence, even for $\Omega < \Delta$, the probability to measure $n < 1/2$ is nonzero and the system can be reset to the state $|{\downarrow}\rangle^N$. Because of the symmetry relation between the transition probabilities given by Eq. (B5), both coefficients $c_\uparrow$ and $c_\downarrow$ in Eq. (A1) would be equal to $1/2$, leading to a stationary value of the excitation density, computed as $\mathrm{Tr}[n\rho_{\mathrm{ness}}]$, equal to $1/2$ for any value of Ω/Δ. This is only partly captured in Fig. 3 because the exponentially small correction (B7) and (B8) to Eq. (B6) due to finite-size effects would require an

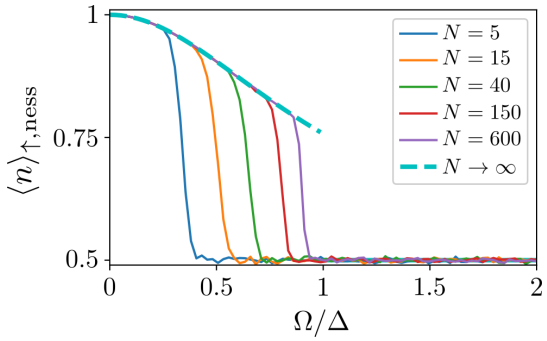

FIG. 3. Phase diagram of the (quasi)stationary excitation density in Protocol II in a finite system. The first-order phase transition that takes place in the thermodynamic limit becomes a crossover in a finite system. In this latter case, the stationary excitation density would be a constant function equal to 1/2. Due to the exponentially small finite-size corrections to Eq. (B6), only a (quasi)stationary state can be obtained numerically, which displays the expected plateau up to a certain value of Ω/Δ. The plots are obtained numerically averaging over 10 000 trajectories of the reset process. The reset rate is $\gamma = \Delta/2$ and the observation time is $T = 2000$ in units of $1/\Delta$. The dashed line, valid in the thermodynamic limit, is Eq. (3) of the main text.

exponentially long simulation to make this effect visible. In other words, obtaining numerically the stationary state for finite N becomes challenging because an exponentially large value of T is needed. Nevertheless, for small values of N, the aforementioned correction becomes larger, making the predicted plateau more visible as the crossover tends to take place at smaller values of Ω/Δ. However, since these long timescales are hardly reached in current experiments due to dissipative and incoherent effects, the curves of Fig. 3 resemble what can be realistically observed in the laboratory.

A change from the continuous nonanalytic behavior to a smooth crossover is also expected to happen in Protocol III, although the stationary excitation density would not be equal to 1/2, but would remain a decreasing function of Ω/Δ because all the possible reset states possess a positive magnetization ($n > 1/2$) and the reasoning that makes use of the symmetric relation (B5) cannot be exploited.

APPENDIX C: COMPUTATION OF THE QUANTUM DISCORD

In the main text, we compute the quantum discord of the stationary two-spin reduced density matrix, defined as

$$\rho_{jk} = \lim_{t\to\infty} \rho_{jk}(t), \tag{C1}$$

where $\rho_{jk}(t)$ is the two-spin reduced density matrix at time t. In Protocol I, it is possible to explicitly compute $\rho_{jk}(t)$ which, from Eq. (2) of the main text, is given by

$$\rho_{jk}(t) = e^{-\gamma t}\rho^F_{jk,\uparrow}(t) + \gamma \int_0^t dt' e^{-\gamma t'} \rho^F_{jk,\uparrow}(t'), \tag{C2}$$

where $\rho^F_{jk,\uparrow}(t) = \rho^F_{j,\uparrow}(t) \otimes \rho^F_{k,\uparrow}(t) = (e^{-iH_j t}\,|\uparrow\rangle_j\,\langle\uparrow|_j\, e^{iH_j t}) \otimes (e^{-iH_k t}\,|\uparrow\rangle_k\,\langle\uparrow|_k\, e^{iH_k t})$, with $H_j = \Omega\sigma^x_j + \Delta\sigma^z_j$. The stationary reduced density matrix is therefore obtained by taking the infinite time limit,

$$\rho_{jk} = \gamma \int_0^\infty dt' e^{-\gamma t'} \rho^F_{jk,\uparrow}(t'), \tag{C3}$$

which suppresses the first term of Eq. (C2). In Protocol II, instead, ρ_{jk} has two different expressions for $\Omega < \Delta$ and $\Omega > \Delta$. In particular, as also mentioned in the main text about the observable n, when $\Omega < \Delta$, its expression is the same of Eq. (C3) due to the equivalence between the two protocols. When $\Omega > \Delta$, instead, ρ_{jk} takes its most general form from Eq. (A1) and is given by two contributions, referring to the reset-free evolution from the two reset states, weighted by the coefficients $c_\uparrow$ and $c_\downarrow$ as [51]

$$\rho_{jk} = \gamma\left[c_\uparrow \int_0^\infty dt' e^{-\gamma t'} \rho^F_{jk,\uparrow}(t') + c_\downarrow \int_0^\infty dt' e^{-\gamma t'} \rho^F_{jk,\downarrow}(t')\right]. \tag{C4}$$

Because of the symmetric relation $\langle n(t)\rangle_\uparrow = 1 - \langle n(t)\rangle_\downarrow$, one has from Eq. (B5) that $c_\uparrow$ and $c_\downarrow$ in Eq. (A1) simplify as $c_\uparrow = c_\downarrow = 1/2$. This implies that the two contributions are equally weighted. This is also the reason why, for $\Omega > \Delta$, $\langle n\rangle_{\uparrow,\mathrm{ness}} = 1/2$, as explained in Appendix B.

The reduced density matrices in Eqs. (C3) and (C4) are used to compute the quantum discord for Protocol I (and Protocol II for $\Omega < \Delta$) and Protocol II (only for $\Omega > \Delta$), respectively. As mentioned in the main text, the quantum discord is quantified via the LQU, which is defined according to Ref. [69] as $l_{jk} = 1 - \lambda_{\max}\{W_{jk}\}$, where $\lambda_{\max}\{W_{jk}\}$ is the largest eigenvalue of the 3×3 matrix W_{jk} with elements $(W_{jk})_{ab} = \mathrm{Tr}[\sqrt{\rho_{jk}}(\sigma^a_j \otimes \mathbb{1})\sqrt{\rho_{jk}}(\sigma^b_j \otimes \mathbb{1})]$, with $a, b = x, y, z$.

APPENDIX D: COMPUTATION OF THE CONNECTED CORRELATION FUNCTION

In the main text, we also compute the connected correlation function between spins at sites j and k. Its stationary value is defined as

$$C^{\uparrow}_{jk} = \langle n_j n_k\rangle_{\uparrow,\mathrm{ness}} - \langle n_j\rangle_{\uparrow,\mathrm{ness}}\langle n_k\rangle_{\uparrow,\mathrm{ness}}\,. \tag{D1}$$

For Protocols I and II when $\Omega < \Delta$, its value is given by Eq. (4) of the main text. For Protocol II when $\Omega > \Delta$, its expression can also be exactly computed using the stationary density matrix (C4) and is given by

$$C^{\uparrow}_{jk} = \frac{1}{4} - 2\Omega^2 \frac{\gamma^2 - 12\Omega^2 + 16\overline{\Omega}^2}{\gamma^4 + 20\gamma^2\overline{\Omega}^2 + 64\overline{\Omega}^4}. \tag{D2}$$

This function is plotted in Fig. 2(e) of the main text.

As mentioned in Appendix A, for Protocol III, we resort to numerical Monte Carlo simulations to efficiently compute the connected correlation function and the quantum discord. We adopt the same numerical procedure described in Appendix B by simulating 80 000 independent realizations of the reset process up to the observation time $T = 30$ (in units of $1/\Delta$). The average over the reset realizations of the connected correlation function at time T is plotted, as a function of Ω/Δ, in Fig. 2(f) of the main text. Note that contrary to what has been previously observed for the estimate of $\langle n\rangle_{\uparrow,\mathrm{ness}}$, now there is no need for a very large value of T because the simulations are done in the thermodynamic limit and, therefore, one does not need a long time to reach the stationary state. What

is needed is just the dynamics of $\langle n_j^F(t) n_k^F(t)\rangle$ between two consecutive resets. In Protocol III, every state with positive magnetization ($n > 1/2$) can be considered as a reset state. Therefore, we need an expression for the reset-free dynamics of the two-point correlation function for any possible initial state with $n_0 > 1/2$. The dynamics of the order parameter is readily obtained as

$$\langle n^F(t)\rangle_{n_0} = n_0 \langle n^F(t)\rangle_{\uparrow} + (1-n_0)\langle n^F(t)\rangle_{\downarrow} \tag{D3}$$

because $N_0 = N n_0$ spins evolve starting from the $|\uparrow\rangle$ state and the remaining $N - N_0$ from the $|\downarrow\rangle$ state. For the two-point correlation function, the computation is slightly more complicated because, given an initial state with excitation density n_0, both spins at sites j and k can be initialized to $|\uparrow\rangle$ or $|\downarrow\rangle$, so four different combinations are possible. Moreover, although the probability that a *single* spin is initialized to $|\uparrow\rangle$ is exactly n_0, an analog reasoning cannot naively be applied for two spins because the event that one spin is in the excited state is clearly not independent from the state of the other spin. As a consequence, one has to follow another procedure through direct counting. In particular, since the spin pair at sites j and k can be initialized in four possible ways, given an initial state with excitation density n_0, the dynamics of the two-point correlation function until the next reset event is given by

$$\begin{aligned}\left\langle n_j^F(t) n_k^F(t)\right\rangle_{n_0} = {} & c_{\uparrow\uparrow}\langle n_j(t)^F n_k(t)^F\rangle_{\uparrow\uparrow} + c_{\uparrow\downarrow}\langle n_j(t)^F n_k(t)^F\rangle_{\uparrow\downarrow} \\ & + c_{\downarrow\uparrow}\langle n_j(t)^F n_k(t)^F\rangle_{\downarrow\uparrow} \\ & + c_{\downarrow\downarrow}\langle n_j(t)^F n_k(t)^F\rangle_{\downarrow\downarrow},\end{aligned} \tag{D4}$$

where the coefficients c_{ab} are the probabilities to find the spin at site j initialized in the state $|a\rangle$ and the spin at site k initialized in the state $|b\rangle$, given that the system has excitation density n_0. In order to compute these probabilities, let us first count the number of possible spin configurations which give a total excitation density equal to $n_0 = N_0/N$. This is given by $\binom{N}{N_0}$. The number of configurations in which both spins at sites j and k are in the excited state is obtained by counting the possible ways to arrange the remaining $N_0 - 2$ up spins among the remaining $N - 2$ sites. Since this number is simply given by $\binom{N-2}{N_0-2}$, the first coefficient entering Eq. (D4) reads

$$c_{\uparrow\uparrow} = \binom{N-2}{N_0-2}\Big/\binom{N}{N_0} = \frac{N_0(N_0-1)}{N(N-1)}. \tag{D5}$$

Analogously, the other coefficients are given by

$$\begin{aligned} c_{\uparrow\downarrow} &= \binom{N-2}{N_0-1}\Big/\binom{N}{N_0} = \frac{N_0(N-N_0)}{N(N-1)}, \\ c_{\downarrow\uparrow} &= c_{\uparrow\downarrow}, \\ c_{\downarrow\downarrow} &= \binom{N-2}{N_0}\Big/\binom{N}{N_0} = \frac{(N-N_0)(N-N_0-1)}{N(N-1)}. \end{aligned} \tag{D6}$$

One can check that the coefficients normalize to 1, i.e., $c_{\uparrow\uparrow} + c_{\uparrow\downarrow} + c_{\downarrow\uparrow} + c_{\downarrow\downarrow} = 1$. By taking the thermodynamic limit $N \to \infty$, their dependence on N disappears and they reduce to

$$\begin{aligned} c_{\uparrow\uparrow} &= n_0^2, \\ c_{\uparrow\downarrow} &= c_{\downarrow\uparrow} = n_0(1-n_0), \\ c_{\downarrow\downarrow} &= (1-n_0)^2, \end{aligned} \tag{D7}$$

showing that the thermodynamic limit eliminates the statistical dependence between the state of the spin at site j and the one of the spin at site k. One can then easily obtain the dynamics of the correlation function by inserting these coefficients in Eq. (D4) and exploiting the factorization $\langle n_j^F(t) n_k^F(t)\rangle = \langle n_j^F(t)\rangle \langle n_k^F(t)\rangle$ as a result of the fact that the spins do not interact. The quantum discord, plotted in Fig. 2(f) of the main text as a function of Ω/Δ, is obtained numerically in an analogous way by simulating 20 000 independent realizations of the reset process up to the observation time $T = 30$ (in units of $1/\Delta$). Specifically, one needs the dynamics $\rho_{jk}^F(t)_{n_0}$ of the two-spin reduced density matrix between two consecutive resets. The dynamics $\rho_{jk}^F(t)_{n_0}$ is then written analogously as in Eq. (D4) in terms of the reset-free dynamics $\rho_{jk}^F(t)_{ab}$, where the spins j and k are initialized in the state $|a\rangle$ and $|b\rangle$, respectively. The coefficients c_{ab} of the four terms in the sum are again given in Eq. (D7).

APPENDIX E: NON-POISSONIAN RESETTING

In the main text and in the previous sections, we focus on the Poissonian resetting, where the waiting time distribution is an exponential function. To account for the finite coherence time attained in cold-atom systems, a more suitable waiting time distribution would, however, be of the form of a "chopped exponential" [51],

$$f(t) = \frac{\gamma}{1 - e^{-\gamma t_{\max}}} e^{-\gamma t}\,\Theta(t_{\max} - t), \tag{E1}$$

where $t_{\max}$ is the maximum reset time. The survival probability then reads

$$q(t) = \frac{e^{-\gamma t} - e^{-\gamma t_{\max}}}{1 - e^{-\gamma t_{\max}}}\,\Theta(t_{\max} - t). \tag{E2}$$

The non-Poissonian case of Eqs. (E1) and (E2) does not bear any additional conceptual difficulty with respect to the Poissonian one and it can be analyzed along the same lines using Eq. (A1) [which is indeed valid for an arbitrary waiting time distribution $f(t)$ and survival probability $q(t)$]. For Protocol I, the stationary density matrix $\rho_{\rm ness}$ is obtained from the limiting form of Eq. (A1) with $c_\uparrow = 1$ and $c_\downarrow = 0$, as explained in Appendix A.

The results remain qualitatively the same as in the Poissonian case, with the appearance of a discontinuous and a continuous nonanalytic behavior of the order parameter at the same critical point $\Omega_c = \Delta$ in Protocols II and III, respectively. This is, in particular, true as long as $t_{\max}$ is large enough compared to Ω^{-1} to allow for the magnetization to change sign in the regime $\Omega > \Delta$. If this is not the case, then all the protocols reduce to Protocol I. The properties of the correlation function and the quantum discord also remain unchanged. As an example, here we report the expression of

the stationary excitation density $\langle n\rangle_{\uparrow,\mathrm{ness}}$ for $\Omega < \Delta$ as

$$\langle n\rangle_{\uparrow,\mathrm{ness}} = 1 - \frac{\Omega^2}{2\overline{\Omega}^2(\gamma^2+4\overline{\Omega}^2)}\left\{4\overline{\Omega}^2 - \frac{\gamma^2}{e^{\gamma t_{\max}}-1-\gamma t_{\max}}\left[2\sin^2(\overline{\Omega}t_{\max}) - \frac{\gamma}{\overline{\Omega}}\sin(\overline{\Omega}t_{\max})\cos(\overline{\Omega}t_{\max}) + \gamma t_{\max}\right]\right\}, \quad \text{(E3)}$$

which reduces to Eq. (3) of the main text for $t_{\max} \to \infty$.

[1] M. Born, Quantenmechanik der Stoßvorgänge, Z. Phys. **38**, 803 (1926).

[2] N. Bohr, The quantum postulate and the recent development of atomic theory, Nature (London) **121**, 580 (1928).

[3] G. Lindblad, On the generators of quantum dynamical semigroups, Commun. Math. Phys. **48**, 119 (1976).

[4] V. Gorini, A. Kossakowski, and E. C. G. Sudarshan, Completely positive dynamical semigroups of *N*-level systems, J. Math. Phys. **17**, 821 (1976).

[5] C. Gardiner and P. Zoller, *Quantum Noise: A Handbook of Markovian and non-Markovian Quantum Stochastic Methods with Applications to Quantum Optics*, Springer Series in Synergetics (Springer, New York, 2004).

[6] H.-P. Breuer and F. Petruccione, *The Theory of Open Quantum Systems* (Oxford University Press, Oxford, 2007).

[7] H. M. Wiseman, Quantum theory of continuous feedback, Phys. Rev. A **49**, 2133 (1994).

[8] H. M. Wiseman and G. J. Milburn, *Quantum Measurement and Control* (Cambridge University Press, Cambridge, 2009).

[9] K. Jacobs, *Quantum Measurement Theory and its Applications* (Cambridge University Press, Cambridge, 2014).

[10] J. Lammers, H. Weimer, and K. Hammerer, Open-system many-body dynamics through interferometric measurements and feedback, Phys. Rev. A **94**, 052120 (2016).

[11] H. Nurdin and N. Yamamoto, *Linear Dynamical Quantum Systems: Analysis, Synthesis, and Control* (Springer International, New York, 2017).

[12] K. Kroeger, N. Dogra, R. Rosa-Medina, M. Paluch, F. Ferri, T. Donner, and T. Esslinger, Continuous feedback on a quantum gas coupled to an optical cavity, New J. Phys. **22**, 033020 (2020).

[13] D. A. Ivanov, T. Y. Ivanova, S. F. Caballero-Benitez, and I. B. Mekhov, Feedback-Induced Quantum Phase Transitions Using Weak Measurements, Phys. Rev. Lett. **124**, 010603 (2020).

[14] G. Buonaiuto, F. Carollo, B. Olmos, and I. Lesanovsky, Dynamical Phases and Quantum Correlations in an Emitter-Waveguide System with Feedback, Phys. Rev. Lett. **127**, 133601 (2021).

[15] D. A. Ivanov, T. Y. Ivanova, S. F. Caballero-Benitez, and I. B. Mekhov, Tuning the universality class of phase transitions by feedback: Open quantum systems beyond dissipation, Phys. Rev. A **104**, 033719 (2021).

[16] J. T. Young, A. V. Gorshkov, and I. B. Spielman, Feedback-stabilized dynamical steady states in the Bose-Hubbard model, Phys. Rev. Res. **3**, 043075 (2021).

[17] M. R. Evans, S. N. Majumdar, and G. Schehr, Stochastic resetting and applications, J. Phys. A: Math. Theor. **53**, 193001 (2020).

[18] M. R. Evans and S. N. Majumdar, Diffusion with Stochastic Resetting, Phys. Rev. Lett. **106**, 160601 (2011).

[19] M. R. Evans and S. N. Majumdar, Diffusion with optimal resetting, J. Phys. A: Math. Theor. **44**, 435001 (2011).

[20] M. R. Evans and S. N. Majumdar, Diffusion with resetting in arbitrary spatial dimension, J. Phys. A: Math. Theor. **47**, 285001 (2014).

[21] S. N. Majumdar, S. Sabhapandit, and G. Schehr, Dynamical transition in the temporal relaxation of stochastic processes under resetting, Phys. Rev. E **91**, 052131 (2015).

[22] L. Kusmierz, S. N. Majumdar, S. Sabhapandit, and G. Schehr, First Order Transition for the Optimal Search Time of Lévy Flights with Resetting, Phys. Rev. Lett. **113**, 220602 (2014).

[23] A. Pal and S. Reuveni, First Passage under Restart, Phys. Rev. Lett. **118**, 030603 (2017).

[24] A. Chechkin and I. M. Sokolov, Random Search with Resetting: A Unified Renewal Approach, Phys. Rev. Lett. **121**, 050601 (2018).

[25] M. Radice, Diffusion processes with Gamma-distributed resetting and non-instantaneous returns, J. Phys. A: Math. Theor. **55**, 224002 (2022).

[26] M. R. Evans, S. N. Majumdar, and K. Mallick, Optimal diffusive search: Nonequilibrium resetting versus equilibrium dynamics, J. Phys. A: Math. Theor. **46**, 185001 (2013).

[27] C. Christou and A. Schadschneider, Diffusion with resetting in bounded domains, J. Phys. A: Math. Theor. **48**, 285003 (2015).

[28] A. B. Slowman, M. R. Evans, and R. A. Blythe, Jamming and Attraction of Interacting Run-and-Tumble Random Walkers, Phys. Rev. Lett. **116**, 218101 (2016).

[29] M. R. Evans and S. N. Majumdar, Run and tumble particle under resetting: A renewal approach, J. Phys. A: Math. Theor. **51**, 475003 (2018).

[30] V. Kumar, O. Sadekar, and U. Basu, Active Brownian motion in two dimensions under stochastic resetting, Phys. Rev. E **102**, 052129 (2020).

[31] I. Santra, U. Basu, and S. Sabhapandit, Run-and-tumble particles in two dimensions under stochastic resetting conditions, J. Stat. Mech. (2020) 113206.

[32] P. C. Bressloff, Modeling active cellular transport as a directed search process with stochastic resetting and delays, J. Phys. A: Math. Theor. **53**, 355001 (2020).

[33] S. Gupta, S. N. Majumdar, and G. Schehr, Fluctuating Interfaces Subject to Stochastic Resetting, Phys. Rev. Lett. **112**, 220601 (2014).

[34] S. Eule and J. J. Metzger, Non-equilibrium steady states of stochastic processes with intermittent resetting, New J. Phys. **18**, 033006 (2016).

[35] V. Méndez and D. Campos, Characterization of stationary states in random walks with stochastic resetting, Phys. Rev. E **93**, 022106 (2016).

[36] P. Grange, Non-conserving zero-range processes with extensive rates under resetting, J. Phys. Commun. **4**, 045006 (2020).

[37] M. Magoni, S. N. Majumdar, and G. Schehr, Ising model with stochastic resetting, Phys. Rev. Res. **2**, 033182 (2020).
[38] C. Aron and M. Kulkarni, Nonanalytic nonequilibrium field theory: Stochastic reheating of the Ising model, Phys. Rev. Res. **2**, 043390 (2020).
[39] W. Wang, A. G. Cherstvy, H. Kantz, R. Metzler, and I. M. Sokolov, Time averaging and emerging nonergodicity upon resetting of fractional Brownian motion and heterogeneous diffusion processes, Phys. Rev. E **104**, 024105 (2021).
[40] V. Stojkoski, T. Sandev, L. Kocarev, and A. Pal, Geometric Brownian motion under stochastic resetting: A stationary yet nonergodic process, Phys. Rev. E **104**, 014121 (2021).
[41] I. Santra, S. Das, and S. K. Nath, Brownian motion under intermittent harmonic potentials, J. Phys. A: Math. Theor. **54**, 334001 (2021).
[42] F. Huang and H. Chen, Random walks on complex networks with first-passage resetting, Phys. Rev. E **103**, 062132 (2021).
[43] K. Goswami and R. Chakrabarti, Stochastic resetting and first arrival subjected to Gaussian noise and Poisson white noise, Phys. Rev. E **104**, 034113 (2021).
[44] P. Chełminiak, Non-linear diffusion with stochastic resetting, J. Phys. A: Math. Theor. **55**, 384004 (2022).
[45] L. Hartmann, W. Dür, and H.-J. Briegel, Steady-state entanglement in open and noisy quantum systems, Phys. Rev. A **74**, 052304 (2006).
[46] N. Linden, S. Popescu, and P. Skrzypczyk, How Small Can Thermal Machines Be? The Smallest Possible Refrigerator, Phys. Rev. Lett. **105**, 130401 (2010).
[47] A. Tavakoli, G. Haack, N. Brunner, and J. B. Brask, Autonomous multipartite entanglement engines, Phys. Rev. A **101**, 012315 (2020).
[48] B. Mukherjee, K. Sengupta, and S. N. Majumdar, Quantum dynamics with stochastic reset, Phys. Rev. B **98**, 104309 (2018).
[49] D. C. Rose, H. Touchette, I. Lesanovsky, and J. P. Garrahan, Spectral properties of simple classical and quantum reset processes, Phys. Rev. E **98**, 022129 (2018).
[50] F. Carollo, R. L. Jack, and J. P. Garrahan, Unraveling the Large Deviation Statistics of Markovian Open Quantum Systems, Phys. Rev. Lett. **122**, 130605 (2019).
[51] G. Perfetto, F. Carollo, M. Magoni, and I. Lesanovsky, Designing nonequilibrium states of quantum matter through stochastic resetting, Phys. Rev. B **104**, L180302 (2021).
[52] A. Riera-Campeny, J. Ollé, and A. Masó-Puigdellosas, Measurement-induced resetting in open quantum systems, arXiv:2011.04403.
[53] X. Turkeshi, M. Dalmonte, R. Fazio, and M. Schirò, Entanglement transitions from stochastic resetting of non-Hermitian quasiparticles, Phys. Rev. B **105**, L241114 (2022).
[54] D. Das, S. Dattagupta, and S. Gupta, Quantum unitary evolution interspersed with repeated non-unitary interactions at random times: The method of stochastic Liouville equation, and two examples of interactions in the context of a tight-binding chain, J. Stat. Mech. (2022) 053101.
[55] G. Perfetto, F. Carollo, and I. Lesanovsky, Thermodynamics of quantum-jump trajectories of open quantum systems subject to stochastic resetting, SciPost Phys. **13**, 079 (2022).
[56] M. Raghunandan, J. Wrachtrup, and H. Weimer, High-Density Quantum Sensing with Dissipative First Order Transitions, Phys. Rev. Lett. **120**, 150501 (2018).
[57] L.-P. Yang and Z. Jacob, Quantum critical detector: Amplifying weak signals using discontinuous quantum phase transitions, Opt. Express **27**, 10482 (2019).
[58] Y. Chu, S. Zhang, B. Yu, and J. Cai, Dynamic Framework for Criticality-Enhanced Quantum Sensing, Phys. Rev. Lett. **126**, 010502 (2021).
[59] I. M. Georgescu, S. Ashhab, and F. Nori, Quantum simulation, Rev. Mod. Phys. **86**, 153 (2014).
[60] M. Endres, H. Bernien, A. Keesling, H. Levine, E. Anschuetz, A. Krajenbrink, C. Senko, V. Vuletic, M. Greiner, and M. Lukin, Atom-by-atom assembly of defect-free one-dimensional cold atom arrays, Science **354**, 1024 (2016).
[61] D. Barredo, S. Léséleuc, V. Lienhard, T. Lahaye, and A. Browaeys, An atom-by-atom assembler of defect-free arbitrary 2D atomic arrays, Science **354**, 1021 (2016).
[62] C. Robens, J. Zopes, W. Alt, S. Brakhane, D. Meschede, and A. Alberti, Low-Entropy States of Neutral Atoms in Polarization-Synthesized Optical Lattices, Phys. Rev. Lett. **118**, 065302 (2017).
[63] L. Henriet, L. Beguin, A. Signoles, T. Lahaye, A. Browaeys, G.-O. Reymond, and C. Jurczak, Quantum computing with neutral atoms, Quantum **4**, 327 (2020).
[64] B. Misra and E. C. G. Sudarshan, The Zeno's paradox in quantum theory, J. Math. Phys. **18**, 756 (1977).
[65] C. B. Chiu, E. C. G. Sudarshan, and B. Misra, Time evolution of unstable quantum states and a resolution of Zeno's paradox, Phys. Rev. D **16**, 520 (1977).
[66] F. Benatti, F. Carollo, R. Floreanini, and H. Narnhofer, Quantum spin chain dissipative mean-field dynamics, J. Phys. A: Math. Theor. **51**, 325001 (2018).
[67] F. Benatti, F. Carollo, R. Floreanini, and H. Narnhofer, Non-Markovian mesoscopic dissipative dynamics of open quantum spin chains, Phys. Lett. A **380**, 381 (2016).
[68] M. Buchhold, Y. Minoguchi, A. Altland, and S. Diehl, Effective Theory for the Measurement-Induced Phase Transition of Dirac Fermions, Phys. Rev. X **11**, 041004 (2021).
[69] D. Girolami, T. Tufarelli, and G. Adesso, Characterizing Nonclassical Correlations via Local Quantum Uncertainty, Phys. Rev. Lett. **110**, 240402 (2013).
[70] H. Ollivier and W. H. Zurek, Quantum Discord: A Measure of the Quantumness of Correlations, Phys. Rev. Lett. **88**, 017901 (2001).
[71] L. Henderson and V. Vedral, Classical, quantum and total correlations, J. Phys. A: Math. Gen. **34**, 6899 (2001).
[72] A. Ferraro, L. Aolita, D. Cavalcanti, F. M. Cucchietti, and A. Acín, Almost all quantum states have nonclassical correlations, Phys. Rev. A **81**, 052318 (2010).
[73] K. Modi, H. Cable, M. Williamson, and V. Vedral, Quantum Correlations in Mixed-State Metrology, Phys. Rev. X **1**, 021022 (2011).
[74] D. Girolami, A. M. Souza, V. Giovannetti, T. Tufarelli, J. G. Filgueiras, R. S. Sarthour, D. O. Soares-Pinto, I. S. Oliveira, and G. Adesso, Quantum Discord Determines the Interferometric Power of Quantum States, Phys. Rev. Lett. **112**, 210401 (2014).
[75] A. Sone, Q. Zhuang, and P. Cappellaro, Quantifying precision loss in local quantum thermometry via diagonal discord, Phys. Rev. A **98**, 012115 (2018).
[76] C. G. Wade, M. Marcuzzi, E. Levi, J. M. Kondo, I. Lesanovsky, C. S. Adams, and K. J. Weatherill, A terahertz-driven nonequi-

librium phase transition in a room temperature atomic vapour, Nat. Commun. **9**, 3567 (2018).

[77] Y.-Y. Jau and T. Carter, Vapor-Cell-Based Atomic Electrometry for Detection Frequencies below 1 kHz, Phys. Rev. Appl. **13**, 054034 (2020).

[78] L. A. Downes, A. R. MacKellar, D. J. Whiting, C. Bourgenot, C. S. Adams, and K. J. Weatherill, Full-Field Terahertz Imaging at Kilohertz Frame Rates Using Atomic Vapor, Phys. Rev. X **10**, 011027 (2020).

[79] S. Hollerith, J. Zeiher, J. Rui, A. Rubio-Abadal, V. Walther, T. Pohl, D. M. Stamper-Kurn, I. Bloch, and C. Gross, Quantum gas microscopy of Rydberg macrodimers, Science **364**, 664 (2019).

[80] W. Feller, *An Introduction to Probability Theory and its Applications* (Wiley, New York, 1968).